Fundamentals and Catalytic Applications of CeO_2-Based Materials

Tiziano Montini, Michele Melchionna, Matteo Monai, and Paolo Fornasiero*

Department of Chemical and Pharmaceutical Sciences, University of Trieste and ICCOM-CNR and INSTM Trieste Research Units Via L. Giorgieri 1, 34127 Trieste, Italy

ABSTRACT: Cerium dioxide (CeO_2, ceria) is becoming an ubiquitous constituent in catalytic systems for a variety of applications. 2016 sees the 40th anniversary since ceria was first employed by Ford Motor Company as an oxygen storage component in car converters, to become in the years since its inception an irreplaceable component in three-way catalysts (TWCs). Apart from this well-established use, ceria is looming as a catalyst component for a wide range of catalytic applications. For some of these, such as fuel cells, CeO_2-based materials have almost reached the market stage, while for some other catalytic reactions, such as reforming processes, photocatalysis, water-gas shift reaction, thermochemical water splitting, and organic reactions, ceria is emerging as a unique material, holding great promise for future market breakthroughs. While much knowledge about the fundamental characteristics of CeO_2-based materials has already been acquired, new characterization techniques and powerful theoretical methods are deepening our understanding of these materials, helping us to predict their behavior and application potential. This review has a wide view on all those aspects related to ceria which promise to produce an important impact on our life, encompassing fundamental knowledge of CeO_2 and its properties, characterization toolbox, emerging features, theoretical studies, and all the catalytic applications, organized by their degree of establishment on the market.

CONTENTS

1. INTRODUCTION

Cerium is the most abundant of the so-called rare earth elements (about 0.0046 wt % of the Earth's crust, Figure 1), which are utilized today in many fields of application, such as magnetics, phosphors, alloys, and catalysis. Given to its large natural reserves, China has been for more than a decade the biggest producer of rare earths, with over 90% of the global production. The perspectives of the use of cerium are therefore mostly related to geopolitical matters, together with environmental concerns about mining practices used for rare earths extraction. Nonetheless, the progressive adoption of more restrictive regulations on greener methodologies may inevitably lead to cuts in the production and, as a consequence, to price spikes.

Despite these adverse market factors and in contrast with most of the other rare earth elements, cerium's price has consistently dropped over the last years, reaching a value of

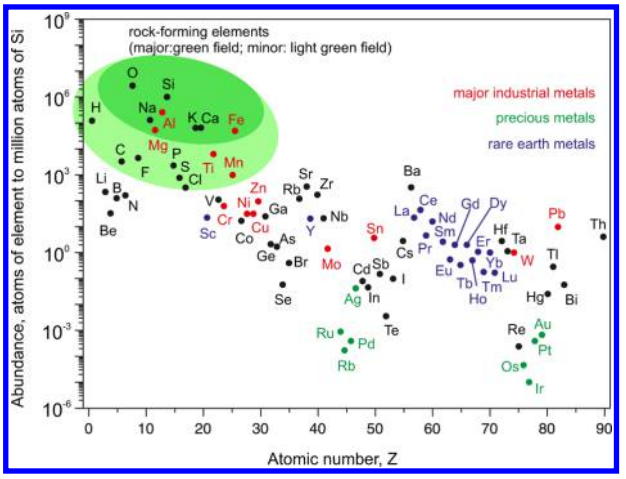

Figure 1. Relative abundance of elements in the Earth's upper continental crust in function of the atomic number. Rare earth elements are in blue. Adapted from ref 1 (Source: United States Geological Survey, 2002).

about 6.0 USD/kg in December 2015 (http://www.metalprices.com/). Even more interestingly, cerium oxide cost has enjoyed a steeper descend, and it is notably going below the price of lanthanum oxide.

When ranked in terms of value versus risk in the supply (Figure 2), cerium does not fall into what is called "critical rare earths" category, which denotes those elements with scarcity as compared to their utilization. Therefore, it is a highly exploitable element, whose potential in the short-to-medium term is projected to be relatively high.

Cerium dioxide (CeO_2), a pale yellow/white powder, is a very well-known cerium compound, formed by the calcination of cerium oxalate or hydroxide. CeO_2 is most commonly used as a catalyst or as a non-inert support for catalysts, and above all, it is of critical importance in the construction of three way catalysts (TWCs).

CeO_2 has long been the subject of a plethora of studies both in academia and in industry. The number of publications with the field "CeO_2" or "ceria" from 1950 to 2015 exceeds 26000, and an analysis over the years since 1994 indicates a constant increase of interest in this subject (Figure 3). The number of papers on ceria associated with the field of "catalysis" is notably following a similar trend.

The years 2014 and 2015 have been the most prolific years in terms of publications recording more than 2300 papers on ceria materials; noteworthy is the fact that the papers concerning catalytic applications have for the first time become 50% of the total, with 1301 publications in 2015, a sign of the ever-growing interest in applying CeO_2 to catalysis. All this vast literature on ceria comprises a number of excellent reviews, which encompasses several specific aspects of this intriguing compound.[3−10] Many of the original publications, on the other hand, refer to energy and environmental processes, spanning from the most traditional topics to the more cutting edge research based on nanostructured systems. However, it is worth mentioning the appearance of studies on the employment of ceria within new scientific areas such as biology and medicine. For example, CeO_2 has been used as a vehicle for intracellular drug delivery[11] or as a support for stem cells cultured in vitro.[12] Another remarkable investigation showed how CeO_2 nanoparticles could reduce ischemic brain damage by disruption of the blood−brain barrier after ischemia.[13] Although fascinating, these brand new themes will only be briefly treated at the end of this review, as we believe that they deserve to be discussed in a dedicated comprehensive review. Photocatalysis by ceria-based compounds is emerging as a new and challenging research topic while the utilization of CeO_2 in solar reactors for the thermal splitting of H_2O and CO_2 for fuel generation is another rising field which merits special mention.[14−16]

The goal of the present review is to provide the reader with a general and ample view on the properties of ceria-based materials and their applications ranging from the most well-established ones such as TWCs to those which have started to make tangible breakthroughs, even though they still suffer from some drawbacks that hamper marketing.

After discussing the main fundamental aspects related to the structural features of pure CeO_2 and of its solid solutions with other metal oxides, the review will outline the characteristics of redox chemistry and the derived properties, such as, above all, the so-called oxygen storage capacity (OSC). Given their widespread integral part into application-focused reports, some of the most representative theoretical studies will be presented, followed by two sections dedicated to nanostructured ceria and model catalysts. Finally, all the most widespread applications in catalysis will be reviewed, with selected examples provided. Given the vast number of examples, the list is far from being

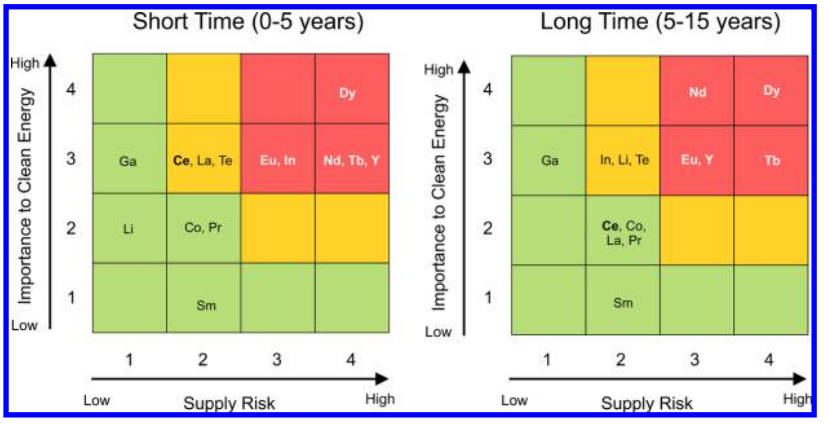

Figure 2. Charts illustrating value vs risk assessments on short-term and long-term ranges for rare earth elements. Adapted from ref 2 (Source: U.S. Department of Energy, 2011).

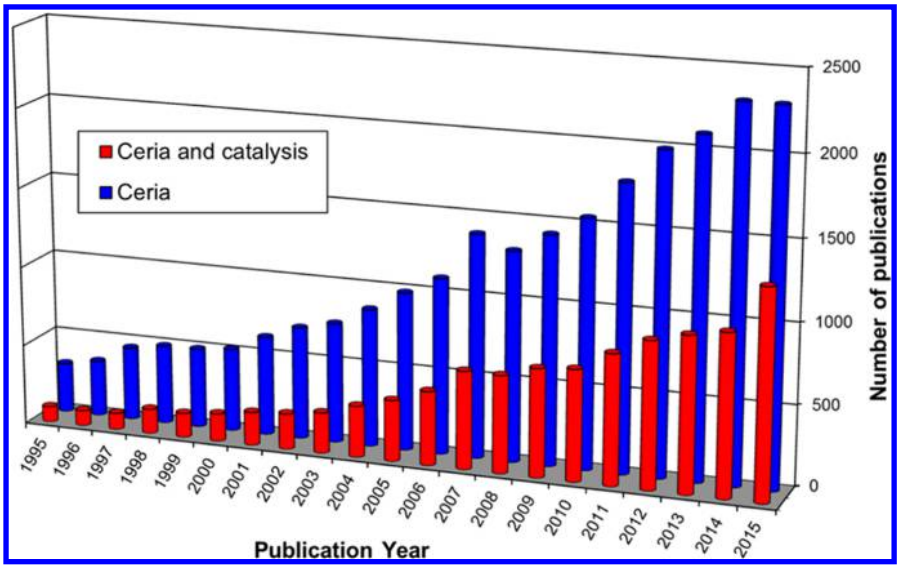

Figure 3. Histogram of number of publications on ceria (blue bars) and publications on ceria associated with catalysis (red bars) from 1994 to 2015 (Source: Web of Science, Jan 9, 2016).

exhaustive, but it aims at incorporating the most prominent research efforts that could be illustrative for the discussion.

2. STRUCTURAL PROPERTIES OF CeO_2-BASED MATERIALS

2.1. Structural and Non-Stoichiometric Properties of CeO_2

Many different phases can be formed by oxidation of metal Ce with O_2, depending on temperature and oxygen pressure. Considering the possible oxidation states of Ce (III and IV), the extreme compositions of the oxides are Ce_2O_3 and CeO_2. The formation of these compounds from metal Ce is spontaneous with $\Delta G^0_{298} = -1796$ and -1089 kJ mol^{-1}, respectively, expressed per mole of compound.

CeO_2 crystallizes in the fluorite structure, with a face-centered cubic (f.c.c.) unit cell within the space group $Fm\bar{3}m$ (a = 0.541134 nm, JCPDS 34-394). In this structure, eight equivalent nearest-neighbor oxygen anions are coordinated around each Ce cation at the corners of a cube, with each anion coordinated by four cations forming a tetrahedron.

Non-stoichiometric CeO_{2-y} can be formed by oxygen release and reduction of Ce(IV) to Ce(III), with the concomitant formation of oxygen vacancies within the crystal structure. The reaction can be expressed, following the Kröger-Vink notation (eq 1) as

$$2Ce_{Ce} + O_O \rightarrow V_O^{\bullet\bullet} + 2Ce'_{Ce} + \frac{1}{2}O_2 \quad (1)$$

Many different CeO_{2-y} phases have been identified depending on the amount of oxygen lost by the starting material and on the symmetry assumed by the oxygen vacancies, as can be deduced from the Ce_2O_3-CeO_2 phase diagram.[17] It must be emphasized that conventional powder X-ray diffraction (XRD) have some constraints in the determination of the structural parameters of non-stoichiometric CeO_{2-y} oxides because of the low scattering power of oxygen. Considering this, the biggest part of the work reported in the literature for the identification of the different phases in the Ce_2O_3-CeO_2 phase diagram have been performed using neutron or electron diffraction techniques.[18−20] Moreover, it must be underlined that the studies presented in this section mainly concern well-crystallized materials, while the properties of powders commonly employed in catalysis could be considerably different.

At elevated temperatures (above 685 °C) and low oxygen pressures, CeO_2 is reduced forming a continuum of oxygen-deficient non-stoichiometric oxides, the so-called α phase, with compositions in the range of $0 < y < 0.286$ for CeO_{2-y}. The α phase presents a disordered non-stoichiometric fluorite-related structure.[18,19] High-temperature XRD patterns do not show superstructures, and the lattice parameter a of the cubic phase increases linearly with the content of Ce(III),[21] in agreement with the larger ionic radius of Ce(III) compared to Ce(IV) (0.114 nm vs 0.097 nm).[22] After thermal treatment, the α phase forms fluorite-related phases with general formula Ce_nO_{2n-2m} characterized by an ordered arrangement of the oxygen vacancies.[20,23−26] Relevant examples of these phases are Ce_6O_{11} (the β phase, monoclinic),[24] $Ce_{11}O_{20}$ (the δ phase, triclinic),[25] and Ce_7O_{12} (rhombohedral).[23,25,27] The most important features of the Ce-O phase diagram are presented in Figure 4, with detail on the Ce_nO_{2n-2m} phases.

As the amount of oxygen vacancies in CeO_{2-y} increases to $y > 0.286$, the high-temperature part of the Ce_2O_3−CeO_2 phase diagram is dominated by the presence of σ phase, with a non-stoichiometric, body-centered cubic (b.c.c.) structure. The compositional end member of the σ phase, the C-type sesquioxide Ce_2O_3 crystallizes in the bixbyite structure (space group $Ia\bar{3}$), that is closely related to the f.c.c. structure of CeO_2. The two cation arrays are almost identical, with oxygen anions occupying all the tetrahedral sites in the f.c.c. structure, while only three-quarters are occupied in the b.c.c. structure in a perfectly ordered array. For this reason, the cell parameter of C-type Ce_2O_3 is almost twice that of CeO_2: a value of 1.121 nm can be calculated by extrapolation from the cell parameters of the C-type sesquioxide of the other lanthanides or from the Vegard's law for the Ce_2O_3-CeO_2 systems.[28] The σ phase, commonly represented as $Ce_2O_{3+\delta}$, is difficult to distinguish from the C-type sesquioxide. By reduction of high surface area CeO_2, materials with composition $Ce_2O_{3+\delta}$ with $\delta = 0.2-0.33$ have been obtained[21,29,30] and recognized as the σ phase from the cell parameter (1.112−1.113 nm), which is significantly lower than that expected for the C-type sesquioxide. In

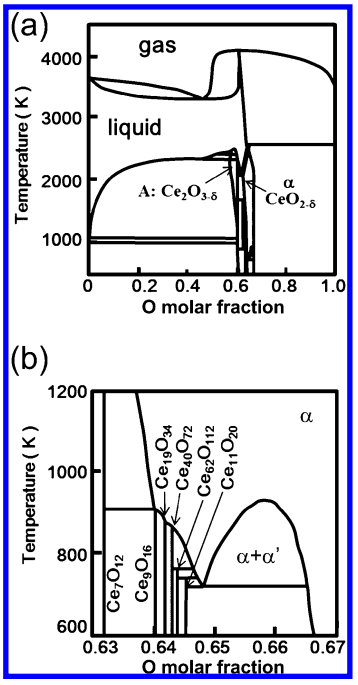

Figure 4. Calculated phase diagrams of the Ce−O system: (a) O molar fraction = 0.0 − 1.0, T = 50 − 4500 K; (b) O molar fraction = 0.63 − 0.67, T = 600 − 1200 K. Adapted with permission from ref 23. Copyright 2006 Elsevier.

agreement with this, neutron diffraction on a single crystal of $CeO_{1.68}$ ($Ce_2O_{3.36}$) gives a cell parameter of 1.1111 nm.[25]

Finally, the A-type sesquioxide Ce_2O_3 (the so-called θ phase) possesses an hexagonal structure belonging to the $P32/m$ space group (a = 0.389 nm, c = 0.607 nm; JCPDS 23-1048).[31] It was suggested that the preferred formation of the A-type Ce_2O_3 instead of the C-type material is not related to the thermodynamic stability of the hexagonal phase[32] but to the higher reactivity of the sesquioxide with cubic structure with atmospheric oxygen.[30]

2.2. Solid Solutions Containing CeO_2

The literature suggests that the fluorite structure of CeO_2 is able to form solid solutions with a large variety of oxides. The lattice parameter of the solid solution usually follows the Vegard's rule (i.e., a linear lattice parameter dependence on the solute concentration), although some deviation from this rule has been reported (see below).

It is important to emphasize that the term "dopant" should be strictly used for situations in which a foreign cation is part of the ceria lattice, in contrast to those cases in which simple physical mixtures of two oxides (with one of the two consisting only of a minor percentage) are discussed.

An empirical relation between the lattice parameter of the solid solution and the ionic radius and charge of a cation (dopant) dissolved into CeO_2 (and other fluorite-structured oxides) has been reported by Kim (eq 2):[33]

$$a = 0.5413 + \sum_k (0.0220\Delta r_k + 0.00015\Delta z_k)m_k \quad (2)$$

where a (in nm) is the cell parameter of doped CeO_2, $\Delta r_k = r_k - r_{Ce(IV)}$ (in nm) is the difference between the ionic radii of the kth dopant and Ce(IV), $\Delta z = z_k - z_{Ce(IV)}$ (in nm) is the difference between the charge of the kth dopant and Ce(IV), and m_k is the molar fraction of the kth dopant. In the same work, Kim argued that the solubility of an oxide into the fluoritic lattice of CeO_2 is governed by the elastic energy per substituted ion introduced in the lattice because of the difference in ionic radius: the larger the Δr_k, the larger the elastic energy and the lower the solubility limit. The maximum in solubility is achieved for the dopant cations having a radius correspondent to the matching radius, r_m, that is the ionic radius resulting in Vegard's slope = 0. Following the calculations of Kim,[33] r_m assumes the value of 0.097 nm for tetravalent dopants, 0.1038 nm for trivalent dopants, and 0.1106 nm for divalent dopants. Similar values have been obtained by other authors.[4,34]

Deviations from the Vegardian behavior have been occasionally observed. Nakamura rationalized the non-Vegardianity observed in MO_2-$LnO_{1.5}$ [M (IV) = Ce, Th; Ln (III) = lanthanide] solid solutions with a model comprising non-random distribution of defects within the crystal structure, with oxygen vacancies preferentially associated with the smallest cations.[35,36] In the case of nanostructured CeO_2-ZrO_2 (the most relevant for catalytic applications), a significant increase of the cell parameters has been observed for both cubic and tetragonal structures having crystallite size below 12−15 nm.[37] This deviation from the Vegard's law has been related to relaxation of the outermost layers of the crystallites. Because of surface strain, these layers can be expanded or compressed, leading to significant modification of the "apparent lattice parameters" measured on the basis of XRD analysis.[37]

It must be emphasized that the maximum amount of dopant tolerated by the fluorite structure is strongly influenced by the temperature. For oxides with a cationic radius close to r_m, a solubility limit of 15−25% of substitution of Ce(IV) is commonly observed for materials prepared around 1000 °C. This limit can increase above 40% for materials treated at 1500 °C.[38]

Above the solubility limit for solid solutions, the preparation conditions are crucial to determine the structural properties of the obtained materials. The increases in the treatment temperature and time favor the formation of equilibrium phases by diffusional transformation. This requires the diffusion of cations until equilibrium is reached, resulting in the formation of the phases with the highest thermodynamic stability. Usually, a large miscibility gap is present in the phase diagram for CeO_2-dopant oxide systems, and intermediate compositions are obtained as mixtures of the CeO_2-rich and dopant oxide-rich phases. If temperature is not high enough to allow a significant cation diffusion, partitionless phase transition can take place producing bulk homogeneous, metastable materials with crystalline structure intermediate between the cubic fluorite-type structure of CeO_2 and the crystal structure of the dopant oxides.

The most important structural features of solid solutions containing CeO_2 will be summarized in this section, with particular attention to the materials with the wider catalytic application.

2.2.1. CeO_2-ZrO_2 Solid Solutions. CeO_2-ZrO_2 mixed oxides are certainly the best known because of their widespread use in TWCs, and as a consequence, they are probably the most investigated from a structural point of view. The ionic radius of Zr(IV) (0.084 nm for a 8-fold coordination)[22] differs by ∼15% to that of Ce(IV) (0.097 nm).

The equilibrium phase diagram of the CeO_2-ZrO_2 system has been studied experimentally by many researchers,[39−42] and reviews summarizing the key results have become recently

available.[43] Yashima et al. studied the evolution of the CeO_2-ZrO_2 system by annealing in $Na_2B_2O_7$-NaF flux. The XRD analysis of the products allowed for the determination of the behavior of the system at temperatures lower than 1000 °C, presenting the complete equilibrium phase diagram of the CeO_2-ZrO_2 system, which is presented in Figure 5.[42] A CeO_2-

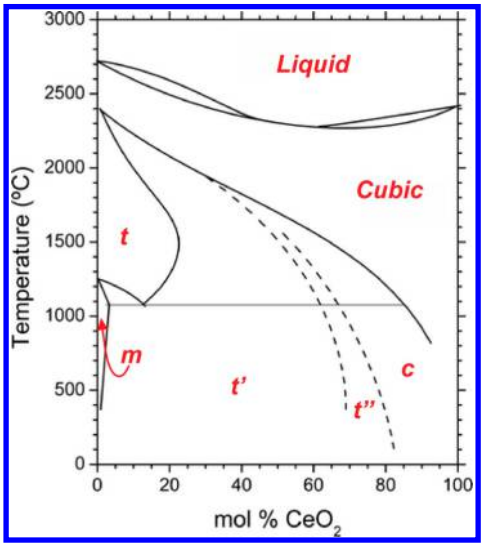

Figure 5. CeO_2-ZrO_2 phase diagram. Adapted with permission from ref 45. Copyright 1994 Wiley-VCH.

rich phase with cubic structure (c) has been recognized in equilibrium with a ZrO_2-rich phase with tetragonal (t) or monoclinic (m) structure, depending on temperature.[42] At 1055 °C, an eutectoid reaction from t to (m + c) takes place, with equilibrium compositions of the t, m, and c phases of x = 0.112, 0.009, and 0.84 in $Ce_xZr_{1-x}O_2$, respectively.[42] Notably, a consistent phase diagram was reported by Du et al.[44] following the CALPHAD (calculation of phase diagram) method.

Despite the fact that the equilibrium phase diagram of the CeO_2-ZrO_2 system is known with high reliability, the identification of the crystal structure and composition of the bulk homogeneous, metastable solid solutions was a difficult task. These phases are the most important from the point of view of the catalytic application, since they are formed at moderate temperatures (below 1055 °C). Various phases have been identified by a combination of XRD, Raman spectroscopy, differential scanning calorimetry (DSC), neutron diffraction, and high-resolution transmission electron microscopy (HR-TEM) studies.[45−49] The most important phases identified are summarized in Table 1, presenting their main structural characteristics.

Pure ZrO_2 and $Ce_xZr_{1-x}O_2$ with $x < 0.12$ possess a monoclinic structure belonging to the $P2_1/c$ space group. As the CeO_2 content increases, the a_m value approaches b_m, the angle β_m decreases (indicating a decrease of the monoclinic distortion) and all positional parameters of the monoclinic $Ce_xZr_{1-x}O_2$ approach those of the tetragonal structure.[48,49] The phase boundary, around x = 0.12, is strongly dependent on the preparation of the sample and on the grain size, these being the factors that mainly influence the nucleation, growth, and kinetics of the transformation.[54]

Above a CeO_2 content of x = 0.12, three phases with tetragonal structure have been identified.[45−49] The t phase is stable at high temperature and for the lower CeO_2 contents. As

Table 1. Most Relevant Metastable, Bulk Homogeneous Phases Identified for the $Ce_xZr_{1-x}O_2$ Materials below 1055°C

composition (x)	crystal system and phases	space group	unit-cell parameters	refs
$0.90 \le x \le 1$	cubic (c)	$Fm\bar{3}m$	$c/a = 1$	45−47
$0.65 \le x < 0.90$[a]	tetragonal (t″)	$P4_2/nmc$	$c/a = 1$	45−47
$0.20 \le x < 0.65$[a]	tetragonal (t′)	$P4_2/nmc$	$c/a > 1$	45−47
$0.12 \le x < 0.20$[a]	tetragonal (t)	$P4_2/nmc$	$c/a > 1$	48 and 49
$0 \le x < 0.12$[a]	monoclinic (m)	$P2_1/c$	$a_m \neq b_m \neq c_m$, $\beta > 90°$	48 and 49
$x = 0.5$, $Ce_2Zr_2O_{7+y}$	pyrochlore	$Fd\bar{3}m$	$c/a = 1$	50 and 51
$x = 0.5$, $Ce_2Zr_2O_8$	phase κ (cubic)	$P2_13$	a = 1.05270 nm	52
$x = 0.5$, $Ce_2Zr_2O_8$	phase t* (tetragonal)	$P4_2/nmc$	$c/a > 1$	53

[a]The compositional ranges are dependent on the processing and grain size.

the value of x increases, the t′ and t″ phases are formed as metastable, non-equilibrium phases observed at lower temperature. The c/a ratio is slightly higher than 1 for the t and t′ phases, while it is equal to 1 in the t″ form. The t″ phase belongs to the $P4_2/nmc$ space group because the oxygen ions are displaced along the c axis from the atomic position of the cubic structure. The existence of the t″ phase was confirmed by a combination of diffraction and spectroscopic techniques. In bulk $Ce_xZr_{1-x}O_2$ samples with $x = 0.65 - 0.70$, no splitting was detected by synchrotron XRD between the reflection 004_F and 400_F of the pseudofluorite lattice, indicating a cubic order in the cation sublattice.[47] At the same time, Raman spectra of the same samples showed the typical bands of a tetragonal phase, providing evidence that there is a displacement of the O sublattice from the position of the cubic fluorite-type structure.[45] Notably, neutron diffraction shows a detectable signal corresponding to the 112_F reflection,[47] which is present for the $P4_2/nmc$ space group but is forbidden for the cubic structure. As the CeO_2 content increases, the unit-cell parameters and the cell volume increase, as a result of the larger ionic radius of Ce(IV) compared to Zr(IV). The c/a_F ratio and the oxygen displacement decreases as x increases in $Ce_xZr_{1-x}O_2$ tetragonal phases. A discontinuity is observed for the c/a_F ratio around 0.6, corresponding to the t′-t″ transition.[47] Raman bands attributable to the tetragonal distortion disappeared at around x = 0.9, indicating the t″-c transition.[45,47]

The local structure of CeO_2-ZrO_2 solid solutions has been deeply studied by extended x-ray absorption fine structure (EXAFS) spectroscopy.[55,56] For an intermediate composition such as $Ce_{0.5}Zr_{0.5}O_2$, a significant distortion of O sublattice is evidenced especially around the Zr atoms. The best model describing the local environment around Zr involves 4 O atoms at 0.2115 nm, 2 O atoms at 0.2324 nm, and other 2 O atoms probably placed at a distance larger than 0.26 nm, while 8 O atoms at the distance of 0.2312 nm were detected around Ce (similarly to the case of pure CeO_2).[55] The longer Zr-O distances observed for some oxygen ions and the consequent weakness of the bond have been used to interpret the easier diffusion of these O atoms in these materials (also called oxygen mobility) and finally their catalytic properties.[55−57]

Together with these phases recognized in the non-equilibrium phase diagram of CeO_2-ZrO_2 materials, particular structures have been identified for solid solutions with a Ce:Zr 1:1 molar ratio. Of particular importance is the non-stoichiometric phase related to the pyrochloric structure, obtained by reduction of the $Ce_{0.5}Zr_{0.5}O_2$ compounds at high temperature.[50,51,53,58] The pyrochlore $Ce_2Zr_2O_7$ belongs to the $Fd\bar{3}m$ space group: the Ce and Zr cations are arranged in an ordered face-centered cubic sublattice and, compared to the fluorite structure, 1/8 of the anions are absent in a systematic way, producing an ordered defect structure. For this reason, the unit-cell parameter of the pyrochloric structure is double as compared to the unit-cell in the fluorite phase. Considering the fact that the materials obtained by reduction of $Ce_{0.5}Zr_{0.5}O_2$ are usually not fully stoichiometric, the pyrochlore structure in the $Ce_xZr_{1-x}O_2$ system is often reported as $Ce_2Zr_2O_{7+y}$.[50,51] Controlled oxidation at moderate temperature (600 °C) of the pyrochlore $Ce_2Zr_2O_{7+y}$ leads to the formation of the κ phase with formula $Ce_2Zr_2O_8$: this phase maintains the ordered arrangement of the cations with all the positions of anions occupied by oxide ions.[52,53] The κ phase has been recognized as the $Ce_xZr_{1-x}O_2$ material that releases and stores oxygen at the lower temperature.[53] Increasing the oxidation temperature, a new phase, named t*, is formed with a tetragonal structure.

Considering the large number of non-equilibrium phases identified in the CeO_2-ZrO_2 system, major problems have been encountered in the determination of the exact crystallographic phase in nanocrystalline materials, which are the most interesting for catalytic applications. The broadening of powder XRD reflections often does not allow a reliable identification of the overlapping of patterns deriving from materials with similar composition and/or the splitting of particular reflections. Useful information could be obtained combining diffraction results with the analysis using Raman spectroscopy. Nevertheless, less common techniques could provide useful information.

Analysis of a sample with composition $Ce_{0.5}Zr_{0.5}O_2$ by neutron diffraction revealed that the material was constituted by nanodomains of $Ce_{0.4}Zr_{0.6}O_2$ with mean dimension of 2.5–3.0 nm within a matrix of $Ce_{0.7}Zr_{0.3}O_2$. Conventional XRD was ineffective for the determination of this structure.[50]

The presence on nanodomains in samples that appeared homogeneous from XRD and Raman analysis has been revealed by luminescence spectroscopy, using Eu(III) ions as structural probe to investigate the local structure of the materials.[59,60] Eu(III) was introduced into the bulk during the synthesis or by impregnation of the surface of the materials. Bulk-doped $Ce_xZr_{1-x}O_2$ samples with thermally stable compositions (x = 0.2 and 0.8) show Eu(III) luminescence spectra compatible with the symmetry of the cationic sites of the tetragonal and cubic phases, respectively.[59] In particular, the analysis of the $^5D_0 \rightarrow {}^7F_0$ transition provides evidence for bands attributable to Eu(III) hosted in bulk and surface sites (Figure 6).[59] On the other hand, metastable $Ce_{0.5}Zr_{0.5}O_2$ treated at 1000 °C appears homogeneous by XRD and Raman, belonging to the t″ phase, while Eu(III) luminescence shows a complex feature resembling that of a mixture of different phases.[59] Moreover, a more detailed study combining emission and excitation spectroscopies demonstrated that CeO_2-ZrO_2 materials could be formed by nanodomains after treatment at lower temperature (750 °C).[60,61] Finally, luminescence spectroscopy was also able to evidence the diffusion of Eu(III) ions between surface and bulk of the materials[62,63] and the presence and

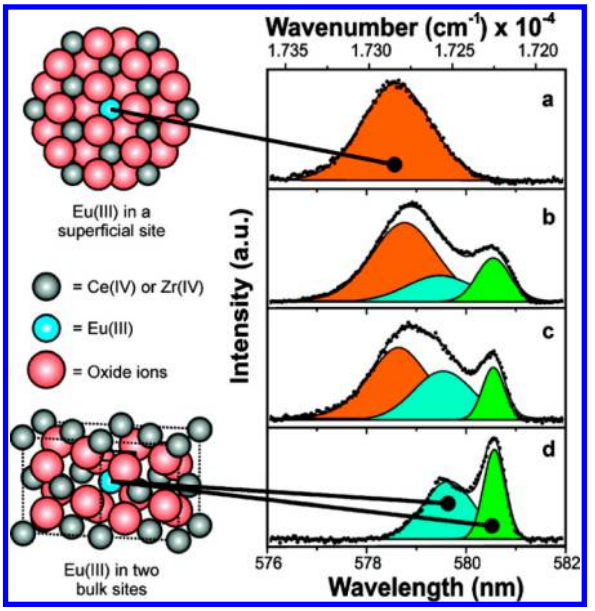

Figure 6. Eu(III) emission spectra of the thermodynamically stable tetragonal CZE-20 samples with the schematic representation of the Eu surface site located on the stable (101) surface of tetragonal $Ce_{0.2}Zr_{0.8}O_2$ and of the two Eu bulk sites of $Ce_{0.2}Zr_{0.8}O_2$ as indicated by EXAFS data.[55] The details of the $^5D_0 \rightarrow {}^7F_0$ transition are reported for both surface and bulk Eu(III) doped materials after different thermal treatments: (a) surface-doped CZE-20 heated at 500 °C for 5 h, (b) bulk-doped CZE-20 calcined at 500 °C for 5 h, (c) bulk-doped CZE-20 calcined at 1000 °C for 5 h, and (d) bulk-doped CZE-20 calcined at 1400 °C for 5 h. In accordance with XRD pattern and Raman spectra, all materials show Eu(III) emission spectra consistent with the presence of a single tetragonal t′ phase. Reprinted from ref 59. Copyright 2009 American Chemical Society.

location of oxygen vacancies inside the nanocrystals of CeO_2-ZrO_2 materials,[64,65] as well as the interaction between different lanthanide ions codoping the materials.[64] These results highlight the potential power of the luminescence technique in evidencing the structure of mixed oxides at the nanometric level, helping in discriminating bulk homogeneous materials from nanocomposites. Finally, luminescence spectra can be useful to ascertain the presence of lanthanides impurities.[66]

2.2.2. Other CeO_2-Based Solid Solutions. Doped-CeO_2 incorporating many other metal oxides has been reported in literature. Despite their wide use in catalysis, no detailed studies on the real structural characteristics of doped-CeO_2 materials treated at moderate temperature (400–600 °C) have been reported, and generally, the possible formation of nanodomains cannot be ruled out.

Tetravalent dopants have been considered, comprising of both IVa and IVb groups on the periodic table. On the basis of the defect formation energy calculated following a DFT approach for materials with a dopant amount of ~ 3 mol%, IVb metals (Ti, Zr, and Hf) seem likely to remain dispersed in the bulk on CeO_2, while IVa elements (C, Si, Ge, Sn, and Pb) should be preferentially segregated on the surface.[67] The defect formation energy decreases as the size of the dopant increases, as a result of the better size-match with Ce(IV) ions.[67] Despite suggestions from theoretical calculations, the synthesis of Ti-doped CeO_2 materials has been reported up to 25 mol % of Ti only for materials prepared at low temperatures.[68] It must be taken into account that, differently from the case of CeO_2-ZrO_2 solid solutions, the possible formation of nanodomains in

CeO_2-TiO_2 materials calcined at low temperatures has not been investigated up to now. After treatment at high temperature (usually above 800 °C), the low solubility of TiO_2 into CeO_2 leads to composite materials.[69,70] Moreover the formation of stoichiometric cerium titanates have been observed: Ce_2TiO_5, $Ce_2Ti_2O_7$, and $Ce_4Ti_9O_{24}$ for Ce(III) and $CeTiO_4$ and $CeTi_2O_6$ for Ce(IV).[71] Similarly, the formation of many cerium silicates have been observed in the CeO_2/Ce_2O_3-SiO_2 systems,[72−74] although the information on Si-doped CeO_2 materials are scarce.[75,76]

Samples in the CeO_2-HfO_2 system have a structural evolution which is very similar to that observed for CeO_2-ZrO_2 materials. Stable solid solutions of $Ce_xHf_{1-x}O_2$ are formed with cubic fluoritic structure for $x > 0.85$ (CeO_2-rich materials) and with monoclinic structure for the $x < 0.15$ (HfO_2-rich materials), as revealed by XRD analysis on samples treated at 1400 °C for 48 h, followed by slowly cooling.[77] Metastable tetragonal phases (t′ as well as t″) have been observed for quenched samples by a combination of high-resolution XRD and Raman spectroscopy.[78] CeO_2-HfO_2 materials prepared by adopting relatively low calcination temperatures are usually reported as materials with cubic structure, although they should be often recognized as t″ phase.[79−81] Thermodynamic redox properties of the mixed oxides were also defined by coulometric titration, evidencing how for ceria-hafnia the similarities with ceria-zirconia are remarkable. These findings are of relevance to catalytic applications given the more marked weakness of the oxygen bonding.[82] Moreover, ceria-terbia and ceria-praseodymia displayed an interesting phase stability, in particular Tb and Pr preserved their phase stability for a calcination temperature of 1100 °C.[82]

Solid solutions of CeO_2 with Y_2O_3 and oxide of lanthanides in the 3+ oxidation state have been widely investigated for their possible application as electrolyte or mixed ionic electronic conductors for the electrodes of solid oxide fuel cells (SOFCs). The solubility limits of many M_2O_3 oxides into CeO_2 lattice have been reviewed by Etsell and Flengas.[38] Particular attention has been given to the data reported for systems after reaching the thermodynamic equilibrium following treatment at high temperature, for uses in SOFCs. In samples calcined at 1400 °C, complete miscibility with CeO_2 have been reported for M = Y, Sm, Eu, Gd, and Dy,[38,83,84] while maximum solubility around 25 − 50 mol % are reported for M = La, Pr, Nd, and Yb.[83,85,86] This is in agreement with the ionic radius of these elements in the 3+ oxidation state,[22] with the first group having the best correspondence with the matching radius reported by Kim to minimize the elastic energy induced by the introduction of the *k*th dopant.[33] Increasing the temperature treatment to 1600 °C, the maximum amounts of M_2O_3 miscible into CeO_2 lattice significantly decreases for all the trivalent dopants considered.[38] The anion vacancy model has been confirmed for these solid solutions by both density and X-ray intensity analysis.[85,86] In some cases, a certain long-range ordering of the anion vacancies, resulting in the formation of C-type rare earth oxide structure, has been observed, with ordering favored for the smaller trivalent metal cations.[87,88] The formation of oxygen vacancies within the structure of M_2O_3-doped CeO_2 is a key factor to promote oxygen diffusion in the materials, allowing hopping of O^{2-}anions from one position to the next empty one.[89] Among the ceria-rare earth oxide systems, Sm(III) and Gd(III) have been shown to cause the highest increase of electrical conductivity given their ionic radii, which are very close to that of Ce(IV). Moreover, both cationic dopants, in particular Sm, result in higher ionic conductivity of the doped ceria, which also has important implications for the assembly of low-temperature SOFCs.[89]

Some data are reported in the literature for CeO_2 doped with divalent alkaline-earth ions (Mg, Ca, Sr, and Ba). Solubility limits of 2, 15, and 9 mol % have been recognized for Mg, Ca, and Sr, respectively, in doped-CeO_2 materials prepared at 1600 °C.[90] Samples prepared at 700 °C show the formation of CaO-CeO_2 solid solutions (on XRD basis) up to 30 mol % of Ca.[91] Increasing the preparation temperature, the solubility limit decreases to ∼20 mol% of Ca at 1000 °C and becomes even lower at 1200 °C, with the formation of a secondary phase recognized as Ce-doped CaO.[92,93] Alkaline-earths elements have been tested as codopants in Sm-doped CeO_2 electrolytes for SOFCs, forming solid solutions and with the best conductivity at 800 °C for Ca and Sr.[94] Notably, in the case of Sr and Ba, ternary compounds have been identified: doped-$SrCeO_3$ and doped-$BaCeO_3$ show potential application such as high-temperature proton conductors for SOFCs[95] and electrolyzers,[96] while Sr_2CeO_4 is a luminescent material with blue-white emission.[97]

3. REDOX PROPERTIES AND OXYGEN STORAGE CAPACITY (OSC)

The wide use of ceria and ceria-based mixed oxides as active component for catalytic oxidation in exhaust converters,[98,99] in hydrocarbons reforming[100,101] and water gas shift reaction (WGSR)[102] has been traditionally associated with the unique excellent ability of these oxides to shuttle between Ce(III) and Ce(IV) states. This property is known as oxygen storage capacity (OSC),[98,103] the quantification of which has seen a tremendous improvement in the adopted methodologies up to recent re-evaluation of its importance under reaction conditions.

Early investigation of ceria oxygen storage properties was triggered by the introduction of TWCs in automotive converters.[98,104,105] Since the purpose of TWC is to promote the simultaneous oxidation of CO and HCs and the reduction of NO_x, the catalyst has to work around specific air-to-fuel (A/F) stoichiometric ratios to achieve optimal efficiency for all reactions. This is accomplished by coupling the engine with an A/F electronic control system and introducing an oxygen buffering material, such as ceria, or more recently ceria-zirconia.[104]

OSC measurements were introduced to evaluate and compare redox properties. Simple temperature programmed reductions (TPR) and reoxidations give information on total-OSC, while more sophisticated methods include monitoring the effect of alternating an oxidant atmosphere with a reducing one under transient conditions. CO,[106−108] H_2,[109] and HCs[110] are the most common reductants used, while O_2 and NO are used as oxidants.[111]

In their pioneering work, Yao and Yao[98] studied the transient oxidation of CO by ceria using pulse chromatographic systems. The OSC values of ceria range around 50−100 μmolO g^{-1}, and they are strongly dependent on surface area, and therefore on particle size, thermal or chemical pretreatment, and synthetic procedure.

In general, OSC of ceria is improved by incorporation of Zr[106,112,113] or other additives (e.g., Ni and Cu)[114] with optimum OSC for $Ce_xZr_{1-x}O_2$ in the region of $0.6 < x < 0.8$. Simple calculations indicate that while oxygen storage in CeO_2 is restricted to the surface, for Ce-Zr mixed oxides, there is

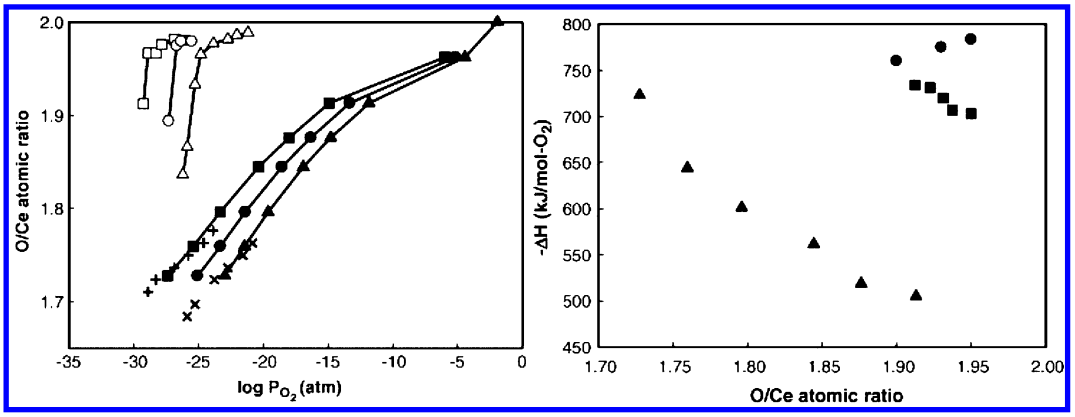

Figure 7. (Left) Oxidation isotherms for pure ceria (open symbols) and 30 wt % ceria/LA (filled symbols) at selected temperatures (■, 600 °C; ●, 650 °C; ▲, 700 °C). (Right) $-\Delta H$ of oxidation at 700 °C for (▲) 30 wt % ceria/LA, (■) $Ce_{0.8}Sm_{0.2}O_{1.9}$, and (●) pure ceria as a function of extent of reduction. LA = lanthanium-alumina. Reprinted with permission from ref 131. Copyright 2007 Elsevier.

participation of bulk oxygen in the storage process.[106] Structural defects and local compound formation have been proposed to be the cause of such changes in OSC properties and redox thermodynamics, as discussed later.[55,115] Supported metals greatly promote OSC of ceria and ceria-zirconia, both directly participating through redox cycling of metal/metal oxide (M/MO) and activating oxygen species of the support.[116−118] For example, OSC at 400 °C can increase 3−4 times for $Ce_xZr_{1-x}O_2$ in the presence of supported noble metals (e.g., Ru, Ir, Pd, and Pt).[118]

Different experimental setups can be used to study oxygen storage kinetics, such as in high-frequency OSC measurements[117] and in oxygen buffering capacity (OBC) measurements, indicating the capability of a material to attenuate fast oscillation in O_2 pressure.[119]

Oxygen isotopic-exchange measurements, based on $^{18}O_2$ labeling and mass spectroscopic analysis, are very powerful in giving insights into the processes and kinetics at the basis of OSC.[120] Oxygen activation process was studied,[121,122] as well as oxygen diffusivities on the surface and bulk of the material.[123] Oxygen species involved in OSC were identified by coupling oxygen exchange with FT-IR: superoxide species were observed to form on $Ce_xZr_{1-x}O_2$ during oxygen adsorption at room temperature, and a correlation between the population in O_2^- species and OSC at 400 °C was found.[124] Moreover, a simultaneous exchange of $^{16}O_2^-$ with $^{18}O_2^-$ during isotopic exchange experiments strongly suggests that binuclear oxygen species may be involved in oxygen mobility on ceria-based materials.

The influence of alumina supports on the redox properties of ceria entities was investigated through several analytical techniques, including XRD, Raman, UV−vis DRS, TEM-EDS, XANES, and EPR to establish a solid model. In the study, two types of ceria entities were found, namely three-dimensional (3D) aggregated crystalline species and two-dimensional (2D) patches, both exhibiting different redox properties than free-standing ceria, thus highlighting the importance to consider the support for evaluating redox characteristics.[125]

OSC and related measurements have paved the way toward a better understanding of redox properties of ceria-based materials and the development of more efficient catalysts. However, the role of ceria in catalytic converters is actually more complex than that of a simple oxygen capacitor, and OSC measurements are often not representative of catalytic activity in exhaust after treatments.

For instance, catalysts showing comparable OSC performed much differently from each other in transient conditions on a vehicle.[126]

Catalysts deactivation is also tentatively followed through OSC measurements, both in poisoning (e.g., phosphorus poisoning of real and model TWC[127−129]) or sintering and thermal aging.[119] However, generally there is no simple and direct relationship between OSC values and deactivation extent, even if a common trend may be extrapolated. In certain cases, OSC measurements can be misleading, as it was reported that ceria-based catalysts OSC values increased after exposure to SO_2, while the loss of catalytic activity due to SO_2 poisoning is well-documented.[130]

Redox properties of materials can be investigated at equilibrium using different approaches. Regarding ceria, by measuring equilibrium data at different temperatures for the reaction (eq 3),

$$CeO_2 \rightarrow CeO_{2-y} + \frac{y}{2}O_2 \qquad (3)$$

reliable oxidation enthalpies can be determined.

Since the activities of the solid phases are unity, the equilibrium constant for (eq 3) is equal to $P(O_2)^{1/2}$. The oxygen partial pressure can be controlled by exposing the material to equilibrium mixtures of H_2-H_2O or $CO-CO_2$ or via coulometric titration, controlling the oxygen chemical potential electrochemically.[131,132]

Figure 7 shows isotherm data and differential oxidation enthalpies for bulk ceria and for 30 wt % ceria on La-modified alumina.

Notably, supported ceria reduction begins at significantly higher $P(O_2)$ compared to bulk ceria. Also, the oxidation enthalpies of the two samples are quite different: for bulk ceria values of −750 and −800 kJ mol^{-1} O_2, almost independent from stoichiometry, were calculated, while for the supported catalyst, the oxidation enthalpy varies from −500 kJ mol^{-1} O_2 for low extent of reduction to values comparable to bulk ceria at higher extents.

Ceria-zirconia mixed oxides oxidation enthalpies were also found to be around −500 kJ mol^{-1} O_2 but did not change with variation in oxygen stoichiometry or Ce:Zr ratio.[132−134] This observation was ascribed to the formation of ordered pyrochlore-type $Ce_2Zr_2O_7$ structure, whose local formation in the mixed oxides would cause the appearance of a plateau in the oxidation isotherms.[132]

An explanation of pure ceria oxidation enthalpies variation with the extent of reduction and thermal treatment would be ascribed to the stabilization of Ce(IV) state by ordered fluorite structure, which is broken by defects in supported or low-temperature calcined ceria. This hypothesis is supported by some general considerations but still lacks experimental evidence.

After almost 50 years of research, redox properties of ceria-based materials remain puzzling, and their understanding requires new techniques and the knowledge coming from emerging fields of application of these materials. In this context, it is worth mentioning the combination of CeO_2 with other forefront materials in nanotechnology such as graphene. It was proven for instance that deposition of CeO_{2-y} on a layer of graphene on Ru {111} causes irreversible intercalation of oxygen under the graphene layer, emphasizing the excellent oxygen storage-release capacity of CeO_x and the potential to give access to intriguing nanodevices.[135]

One final point that needs to be highlighted concerns the definition of OSC. Despite its traditional definition, which we have used herein, studies have shown that under real working conditions (namely in the real engine components), the presence of water can alter the reducibility of the CeO_2 phase.[115,136] Thus it is claimed that a redefinition of the OSC of ceria should be given, with the calculation of OSC done under real conditions.

4. COMPUTATIONAL STUDIES

Many theoretical studies have been devoted to providing a fundamental understanding of the properties of CeO_2 to different levels of detail. Indeed, computational studies have become an essential part in the design of ceria-based materials in most application-driven research.

Several aspects have been theoretically investigated using different approaches and methods. Very recently, Sauer et al. reviewed the surface chemistry of CeO_2,[3] particularly focusing on oxygen-defect formation, which has been subject of extensive and sometimes contradictory investigations. For instance, the once believed reduction of the Ce ions which are nearest neighbors (NN) to the oxygen defects has been more recently revisited through a number of density-functional theory (DFT) calculations. Thus, DFT with the HSE06 (Heyd-Scuseria-Ernzerhof hybrid functional) and the DFT+U approach (U = Hubbard-like term describing the on-site Coulomb interactions) suggest that the Ce cations neighboring the oxygen vacancies might be still in 4+ oxidation state, and that the O vacancy-induced two excess electrons might not necessarily sit on NN cations. The explanation is based on the fact that the lattice structure can relax into a global minimum energy with electrons localizing on ions further away from the vacancy (next nearest neighbors, NNN).[137,138] More detailed DFT analysis combined with scanning tunneling microscopy (STM) imaging afforded a more accurate (although still not precise) positioning of the two excess electrons, which appear to be always confined in two different coordination spheres around the defect.[138,139]

These examples testify to the great debate on the important issue of the relative stability of surface and subsurface oxygen vacancies and are somehow in contrast with earlier reports, in which LDA+U results combined with STM images of materials subject to annealing at 900 °C and cooling to 300 °C led to interpretation of the Ce(III) ion localized in NN position.[140] On the basis of DFT calculations, Kullgren et al.[141] recently claimed that those observations are to be explained as originating from fluorine impurities that are often present in specific ceria crystals.[142] While a critical assessment of the influence of such impurities is certainly relevant, the study neglects several important issues: (i) discussion of multiple defects such as triple protrusions, (ii) adequate consideration that the O vacancy does break the symmetry of the hexagon formed by the O atoms NN to the vacancy, or (iii) discussion of the thermodynamic stability of the F dimer on the basis of tiny calculated binding energies. More recently, the presence of neighboring hydroxyls has been indicated to significantly stabilize the thermodynamically unstable oxygen vacancy clusters, and the behaviors of oxygen vacancies become largely consistent with the STM observations.[143]

The examples given above tacitly introduce the two main approaches employed to overcome shortcomings arising in the calculation of total energies for Ce compounds. The first approach is based on the use of a so-called Hubbard-like functional, which models the on-site correlation of the 4f electrons of cerium by favoring their localization. For integral values of the occupation numbers, this procedure does not change the total energy; on the other hand, it allows us to capture the essential features of the cerium ion if the 4f states are occupied to some extent. A striking example of this is Ce_2O_3, which is described as a metallic conductor by conventional DFT methods, while it becomes an insulator, in agreement with the experimental evidence, when an Hubbard term is included in the Hamiltonian.[144] It is noteworthy that the calculated energies and structural parameters are not dependent on the U parameter if this is defined in terms of maximally localized Wennier functions.[144] The second approach relies on the use of hybrid functionals, in which a fraction of the Fock exchange energy is added to the gradient-corrected DFT exchange energy.[145] The two approaches have their own weaknesses, and it is convenient at times to carry out a cross-check investigation using both methods. Common consensus places a warning on the use of DFT+U because of its non-universality (dependence on band gap, lattice constants, etc.), therefore, very careful interpretation of the results needs to be conducted. For instance, Branda et al.[146] reported the study of electronic structure and oxidation state of atomic Au deposited on CeO_2 {111} by means of periodic DFT-based calculation using the LDA+U, GGA+U, as well as the HSE06 exchange-correlation potentials. Thus, the authors highlighted the difficulty to univocally predict the oxidation state of Au, as the results are strongly affected by the method chosen and, in the case of the DFT+U approach, by the chosen U.[146]

Doping of ceria is a common strategy to tune the properties of the final material, and it has been the subject of several theoretical investigations. As an example, praseodymium[147] and gadolinium[148] doping have been simulated using kinetic lattice Monte Carlo methods. Study of Ti doping of CeO_2 nanoparticles, nanorods, and framework architectures provided a general atomistic model by means of a simulated synthesis of the various nanostructured shapes. This theoretically confirms previous experimental observations[149] on how the Ti ions are able to "smooth" the ceria surface, converting the {111} and {100} facets of the hexagonal prism-shaped nanorods into more cylindrical morphologies and the framework architectures from facetted pores and channels with well-defined {111} and {100} surfaces to "smooth" pores and channels (Figure 8).[150]

Given the importance of the noble metals-cerium oxide electronic interaction (i.e., electron transfer from a reduced

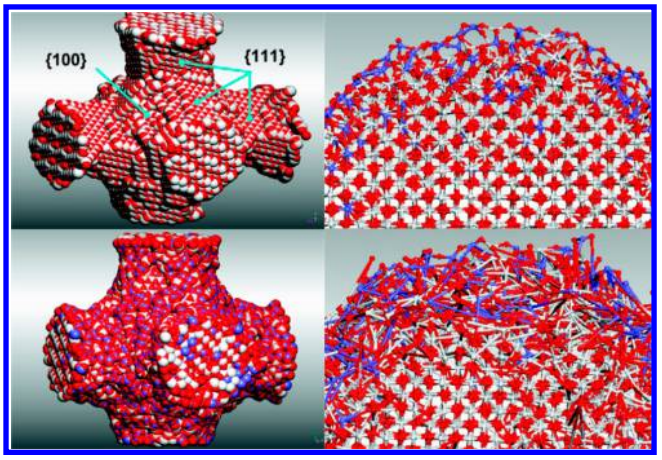

Figure 8. Low-temperature nanoporous framework architectures for CeO_2 (top left) and Ti-doped CeO_2 (bottom left). Ball and stick model of the Ti-doped CeO_2 nanocrystal taken after 1000 ps (top right) and after 1050 ps (bottorm right) of molecular dynamic simulation around 3500 °C. Ce is colored white, Ti blue, and O red. Adapted from ref 150. Copyright 2007 American Chemical Society.

cerium oxide to a metal), in catalytic applications, numerous calculations have been carried out in order to understand the synergy between the two components. Au-CeO_2 represents a special system that has been most widely investigated, and exhaustive examples of computational studies have been recently reviewed.[151] In general, most authors agree that deposition of Au clusters on CeO_2 results in an oxidation of the Au and reduction of the ceria in defect-free surfaces.[151] On the other hand, a much stronger binding occurs at O-vacancies, but it is associated with an electron transfer from one of its Ce(III) ions to the Au atom, which becomes negatively charged, as demonstrated by density of states projected onto stets with f symmetry.[152]

In comparison with Au, a higher adsorption energy for the other two coinage metals Ag and Cu has been reported; in this case, the two metals turn out to be always oxidized due to the lower ionization potential.[153] In another report, a DFT approach (with LDA+U and GGA+U) has been used as a robust method to complement STM and X-Ray Photoelectron Spectroscopy (XPS) analysis of Ag nanoparticles deposited on CeO_2 films, suggesting that the O transfer from the CeO_2 to the Ag particles is an energetically unfavored process, thus ruling out an earlier hypothesis of oxygen diffusion on the surface of the Ag nanoparticles leading to a CeO_{2-x}/Ag_nO_m system with partially oxidized Ag nanoparticles supported on partially reduced ceria; conversely, the direct electron transfer from Ag to the ceria is shown to be an energetically more favorable process.[154]

As far as other noble metals are concerned, DFT+U studies on Pd-doped CeO_2 showed that the noble metal affects the oxygen vacancy formation energy by introducing gap states above the valence band and below the empty Ce 4f states.[155] Similar conclusions were drawn for a system consisting of platinum clusters (Pt_8) on ceria nanoparticles with different shapes and sizes, for which lowering the vacancy formation energy was shown to be dependent upon the size of the nanoparticle and location of Pt cluster relative to the vacancy, and it determines the oxygen spillover from the support to the metal.[156] Upon comparison of the adsorption energies of Pd and Pt on both ceria and zirconia through periodic DFT analysis within GGA Hamiltonian, higher energies for Pt deposition (400 kJ mol^{-1} vs 200 kJ mol^{-1} for Pd) were found. Moreover, it was observed that the thermodynamically more favored Pt-Pt interactions in comparison with Pd-Pd are the determining factor for the resulting cluster shapes and metal growth modes.[157]

An important perspective to understand the role of CeO_2 in catalysis is to study the mechanism of activation of small molecules that are involved in a specific catalytic process. For example, DFT+U analysis of the catalytic activity of Ce-supported Au nanoparticles (NPs) for CO oxidation suggested that this reaction proceeds via three possible mechanistic pathways, all crucially relying on the rich presence of oxygen vacancies on the CeO_2 surface (Figure 9),[158] while two major mechanisms for the Au/CeO_2-catalyzed water-gas shift reaction were proposed based on DFT calculations, although the

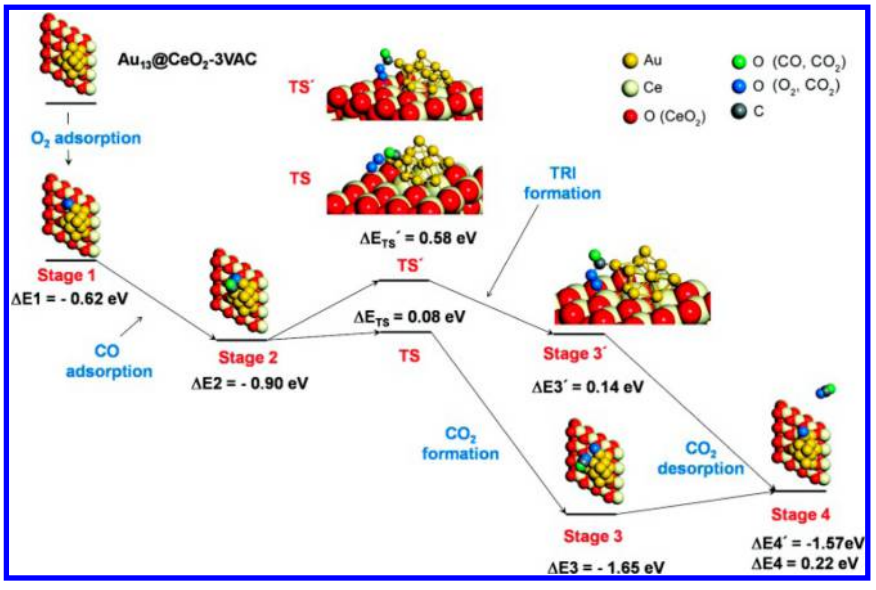

Figure 9. Possible pathways for CO oxidation following the coadsorption mechanism calculated by Kim et al. on Au_{13}@CeO_2-3VAC (Au nanoparticle in contact with partially reduced CeO_2 with three vacancies). Reprinted from ref 158. Copyright 2012 American Chemical Society.

common shortcoming of surface oxygen atom reproduction was identified in both mechanisms.[159] The methanation of CO_2 by a Ru-doped ceria catalyst was studied via a PAW approach, employing the LDA+U(5.5) method, and a segregation of the Ru at the surface was proposed; moreover, the calculations ruled out the possible formation of CO as intermediate in the catalytic sequence.[160]

Computational studies are available in literature where the exclusive interaction between the small molecule and the CeO_2 is considered. As an example, the (GGA-type) PW91 xc functional was applied to explore the adsorption of CO on {111} and {110} planes, finding that adsorption on the former is weaker (energy = 16.4 kJ mol^{-1}) than that on the {110} surface (ranging from 17.4 to 189 kJ mol^{-1}) due to the formation in the latter of a carbonate species following chemisorption on a O-bridging atom.[161] Other computational reports on CO adsorption convey toward the weak adsorption of CO on facets other than {110} an {100}, over which a chemisorption phenomenon occurs with formation of CO_3^{2-} species. Other typical molecules that have been computationally evaluated are H_2O and H_2S. Adsorption of water on both ceria and reduced ceria, typically on the {111} facet, proceeds molecularly or via a dissociative mechanism.[162,163] Although it has been demonstrated that H_2O can strongly bind the CeO_2 surface on O vacancies, there is still a gap of knowledge as regards to the two adsorption states. On the other hand, H_2S can adsorb on the {111} facet in a similar fashion to the water molecule; however, in this case it is clearer that the reduction of CeO_2 can occur more readily.[164,165] Interaction of ceria with several other small molecules such as NO_2,[166,167] N_2O,[168] SO_2,[169] Cl_2, Br_2, and CH_4[170] have been computationally assessed. Not long ago, formation of the paramagnetic superoxide O^{2-} radical, an elusive species evolving from exposing reduced ceria to molecular oxygen, was shown to form by direct interaction of O_2 with low-coordinated Ce(III) ions on reduced ceria nanoparticles, and a full atomistic model of this system was presented.[171] The conversion from methanol to formaldehyde or syngas was thoroughly studied through DFT+U calculations, unraveling the dependence of the reaction on the inherent stoichiometries of the different surfaces of CeO_2.[172]

5. NANOSTRUCTURES

An ever growing converging tendency toward the fabrication of materials with nanodimensions has contributed to the advent of what has been symbolically termed "nanotechnology revolution". The term is justified by the incredible expansion of applicative options that nanomaterials may offer. Indeed, the decrease of particle size to the nanometer scale is in most cases accompanied by a distinct change of the physical and chemical properties as compared to bulk materials. This also translates into a different catalytic behavior. For instance, nanosized CuO/CeO_2 composite were shown to behave much more efficiently in the decomposition of N_2O as compared to bulk analogues.[173] Moreover, tailoring the shape of the nanoparticles has emerged as an equally important aspect as it may lead to further changes of such properties. Thus, considerable attention is being given to the preparation of ceria nanostructured materials with defined size and morphology. Doping with other metals or metal oxides represents an additional attractive possibility in relation to the well-documented improved characteristics of the doped bulk material analogues in several applications.

In a work by Li et al., the influence of the morphology of CeO_2 nanoparticles in catalysis was investigated, comparing traditional irregularly shaped CeO_2 nanoparticles with single crystalline CeO_2 nanorods in the catalytic oxidation of CO.[174] Despite the smaller size and higher surface areas of the former, the nanorods displayed a 3-times higher activity, which according to the authors originates by the exposure of the unusually reactive facets {001} and {110} instead of the more stable {111} facets exposed by the nanoparticles (Figure 10).

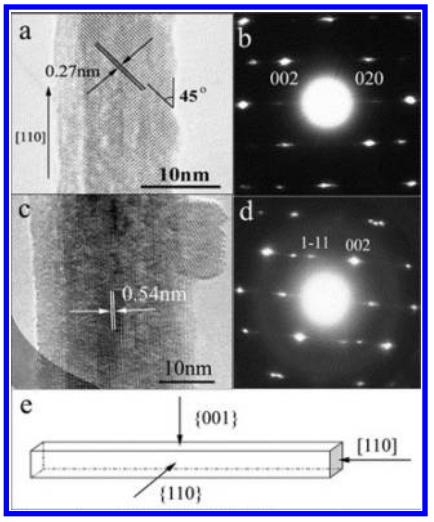

Figure 10. (a) Representative HR-TEM of a CeO_2 nanorod view along [001]; (b) selected area electron diffraction (SAED) pattern of (a); (c) representative HRTEM of a CeO_2 nanorod view along [110]; (d) the SAED pattern of (c); and (e) the structural models of CeO_2 nanorods. Reprinted with permission from ref 174. Copyright 2005 Elsevier.

The example is a milestone for the recognition of the importance of morphology/activity relationship. However, a number of studies in conjunction with advanced characterization techniques such as HR-TEM have evidenced that there are still uncertainties on the actual morphology/exposed facet correlation and, therefore, on the mechanism of crystal growth.[175,176] Some light is being shed through TEM and surface reactivity experiments,[177] but this area still requires further elucidation. Never-the-less, Zhou's work paved the way to the proliferation of synthetic methodologies that allow control over the morphology, size, and faceting of nanostructured ceria. Today it is possible to control the final architecture of CeO_2-based materials to obtain zero-, one-, two-, and three-dimensional structures, classified based on the number of dimensions which are not confined to the nanoscale range (<100 nm).

Zero-dimensional (0D) nanostructured ceria can be regarded as a stand-alone case due to the isotropic cubic phase of the fluorite structure. As a result, there is absence of a preferential growth direction of the seeding crystals, thus 0D nanostructures synthesis are the most straightforward. The simplest preparative approach for CeO_2 nanopolyhedra is to apply the standard protocols traditionally used for other material nanoparticles. The coprecipitation method takes advantage of the very low solubility of ceria and because of its simplicity is the method of choice for commercial production. Alkaline solutions of NaOH,[178] urea,[179] ammonia,[180] etc. can be used as precipitating agents. The relationship between the specific

polyhedron, its size, and the dominance of a particular crystallographic plane was also systematically studied via high-resolution TEM.[181] An extra requirement is often the use of a surfactant such as cetyltrimethylammonium bromide (CTAB)[182] or polyvinylpyrrolidone (PVP)[183] to avoid the problem associated with the quick precipitation of too small-sized crystals and to allow for a better tuning of the final nanoparticle dimensions and shape.

The use of different capping agents often results in variation of the final morphology. By adopting a certain range of concentrations of PVP and reaction time, spheres of CeO_2 could be selectively prepared after calcination at 500 °C from the hydrothermally formed $Ce(OH)CO_3$. By selecting a different value of the two parameters, disk-like morphologies were obtained instead.[184] On the other hand, oleic acid[185] and oleate anion[186] lead to the formation of small nanocubes, whose dimensions could be tailored by varying the Ce precursor.

For lower-order symmetry nanoparticles [one-dimensional (1D), 2D, and 3D], synthetic protocols require a more demanding evaluation of the suitable reaction conditions, as the crystal growth has to be kinetically controlled and appropriately fine-tuned in order to diverge from the thermodynamically favored structures. The typical strategy relies on two general approaches, which are (i) use of capping agents and (ii) template-assisted method.

The former method exploits the distinct interaction of the capping agent with a specific crystallographic plane, which alters the facet surface energies and favors growth along some preferred directions. For example, several anions were investigated as mediators in the CeO_2 nanocrystals growth, and it turned out that NO_3^- was effective in the synthesis of nanocubes, while halides and SO_4^- favored the assembly of nanorods (Figure 11).[187] This finding is explained in terms of

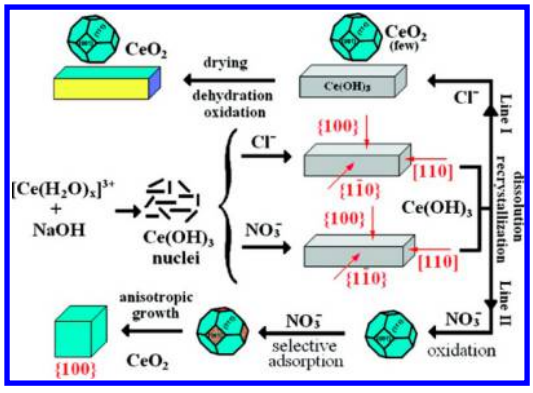

Figure 11. Schematic illustration for the conversion from nanorods to nanocubes depending on the presence of chloride or nitrate ions. Reprinted with permission from ref 187. Copyright 2008 American Chemical Society.

the preferential interaction of the nitrate ion with the {100} plane; thus, the initially formed nanorods can convert to cubes by anisotropic growth of the {110} plane as already reported by Mai et al.[188] More recently, a comparative study of the catalytic activity for carbon dioxide reforming of methane and coke resistance of nickel deposited on CeO_2 nanorods (NRs) and nanopolyhedra (NPs) (prepared via hydrothermal method in the presence of NaOH) showed the superior performance of the monodimensional Ni/CeO_2 NRs system.[189]

The second general synthetic methodology is based on the use of a template that restricts growth either through Ostwald ripening mechanism (soft template) or by spatial confinement (hard template). Soft templates are typically surfactants, and the strategy has already been illustrated earlier for the morphology-controlled synthesis of nanospheres and nanodiscs by applying critical concentrations of PVP.

CeO_2 nanotubes have been accessed through micellar nanoparticle formation and aging in a double microemulsion system consisting of bis(2-ethylhexyl)sulfosuccinate sodium salt (AOT), toluene, and water.[190] Similarly, nanowires consisting of many interconnected nanocrystallites of about 7 nm in size have been synthesized via a solution-phase route using sodium bis(2-ethylhexyl) sulfosuccinate as a structure-directing agent.[191] Many parameters such as pH, solvent, surfactant type, and ratio to cerium precursor, temperature, etc. can play a pivotal role in determining the resulting final architecture.[192]

Ethylene glycol-mediated synthesis can lead to nanorods, nanospindles and nanospheres according to the experimental reaction time and concentration of the cerium precursor.[193]

Hard templates such as anodic aluminum oxide (AAO) or polycarbonate membrane filters represent an effective alternative to the soft-template methodology for the assembly of 1D motifs. For instance, the Ce precursor can diffuse through capillary force into the hexagonally ordered AAO channels and form the dioxide species upon hydrolysis and/or heating.[194] The surge of carbon nanostructures into material chemistry has opened interesting opportunities in the assembly of inorganic–organic hybrid systems in a broad array of diverse applications. Carbon nanotubes (CNTs) have been predominantly explored as rigid scaffold to template the fabrication of 1D nanostructures.[195] The possibility of removing the carbonaceous scaffold by heat treatment after coating with CeO_2, leaving all-inorganic hollow tubes, is of particular interest. To overcome the problems associated with the hydrophobicity of the carbon support and guarantee an adequate interaction with the Ce precursor, it is a standard prerequisite to treat the carbon nanotubes with strong oxidizing acids in order to introduce polar functionalities (hydroxyl and carboxyl groups) or alternatively by adsorbing appropriate negatively charged organic entities on the CNT sidewalls; by this means, solubility in polar solvents is enhanced, and the scaffold are endowed with anchor points for the Ce salt, which is adsorbed through metal–oxygen bonds or electrostatic forces. Final hydrolysis results in the deposition of CeO_2 layers along the CNTs framework. Calcination treatment of the hybrid removes the CNTs, leaving the hollow CeO_2 tubular structure.[196,197] However, the common choice is to retain the carbon support because of the beneficial effects arising from the carbon nanostructure chemical and physical properties.[198] For example, retaining the multi-wall carbon nanotubes (MWCNTs) scaffold after the synthesis of a MWCNTs/Pd@CeO_2 hybrid catalyst resulted in a higher stability for the low-temperature water-gas shift reaction (LT-WGSR) as compared to the analogue catalyst where CNTs had been removed.[199]

In another report, ZnO has been successfully employed as hard template for CeO_2 nanorods. The ZnO nanorods were prepared with high precision on cordierite or glass substrates and instantaneously removed by dissolution assisted by the protons released during precipitation of the CeO_2.[200]

Electrochemical methods turn out to be convenient strategies for the preparation of CeO_2 nanoparticles of different geometries and suitable for photo- or electro-catalytic screening

in several transformations. One-dimensional oriented hexagonal CeO_2 nanorods (NRs) mainly exposing the {110} planes were prepared through template-free electrochemical growth on a Ti substrate and showed excellent activity in the photocatalytic hydrogen evolution, with H_2 productivity reaching 741 mmol g^{-1}.[201]

Given the peculiar properties and huge prospects of monodimensional (1D) CeO_2 nanoparticles, they have been more explored than 2D and 3D architectures, and a wide variety of preparative protocols are available. However, 2D and 3D architectures are emerging as intriguing alternatives in several catalytic and energy applications, and their preparation is drawing significant attention.

In general, for 2D and 3D morphologies, the template-assisted method appears to be the inevitable choice, given that controlling the crystal growth rate along two or more facets is considerably challenging. One of the very few examples of a template-free method for preparing disklike structures is based on a solvothermal method.[202] In another recent contribution, hydrothermal synthesis was applied for the preparation of disk- and triangle-shaped cobalt-doped CeO_2 nanostructures; the selectivity of the resulting morphology is determined by the doping amount of cobalt nitrate during the reaction.[203] Ultrathin ceria nanoplates were prepared through soft surfactant-assisted (oleic acid or oleylamine) synthesis in the presence of mineralizers (sodium diphosphate or sodium oleate). Several parameters could be adjusted to tune the morphology of the final products. Depending on the synthetic conditions, the nanoplates had a squared or elongated geometry (e.g., increasing the amount of surfactant resulted in circular shapes, while decreasing the reaction time gave access to less elongated plates).[204] Comparison of the OSC of the different 2D structures with that for 3D counterparts prepared by hydrothermal and combustion method, underlined the considerable higher reducibility of the former.

Electrochemical methods have also been employed to access 2D structures. Synthesis of nanosheets and nanobelts was reported via electro-deposition of Ce(III) in solution of NH_4NO_3. The final geometry was determined by the applied current density.[205]

As with the case of 1D structures, removable templates can direct the assembly of hollow 2D or 3D architectures. Carbon spheres have emerged as particularly useful scaffolds in the facile assembly of hollow spherical morphology. One typical approach is to generate the carbon spheres by hydrothermal treatment of aqueous solutions of glucose and polysaccharides, followed by adsorption of the metal precursor and calcination, which removes the carbon template and forms the hollow oxide spherical framework. The protocol can be applied to various metal oxides.[206] Alternatively, silica spheres could be adopted as hard templates, and after precipitation of the CeO_2 nanocrystals, they were removed by alkaline etching leaving hollow oxide structures.[207]

A similar concept was adopted to construct a spongy mesoporous CeO_2 microspheres, exploiting the in situ formation of the removable template by graft polymerization reaction between acrylamide and glucose (Figure 12).[208] The obtained CeO_2 microspheres have open 3D porous and hollow structures consisting of nanosheets as the petals. The method has also been generalized to prepare a series of pure and element-doped CeO_2 microspheres.[208−210] Large surface area endows these materials with high reactivity and stability in CO oxidation[209,210] and ethanol steam reforming.[210,211] Moreover,

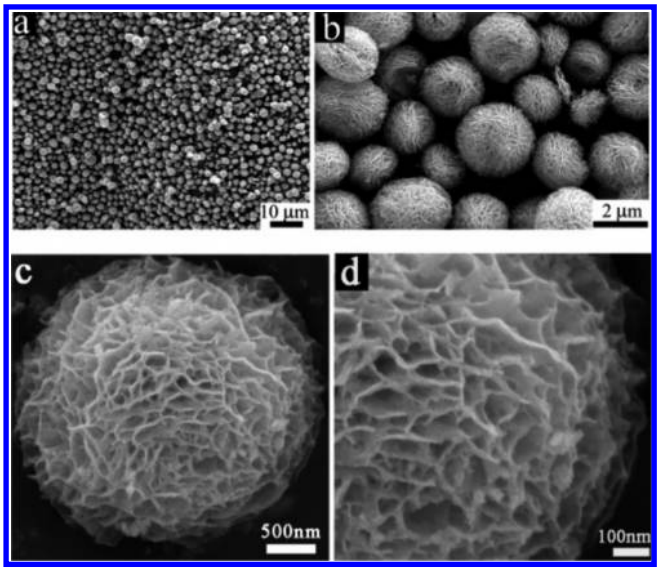

Figure 12. Representative SEM images of the CeO_2 microspheres. (a and b) Overall morphology of the products; (c and d) high-magnification SEM image of an individual microspheres, revealing the detailed spongelike substructure of the microspheres. Reprinted from ref 208. Copyright 2006 American Chemical Society.

they were successfully applied in SOFC as reforming catalytic layer on the anode side[212] and as a component of the cathode.[213]

Several other methods have been reported for spherical nanostructures.[181,214−216] The spherical structure has proven to be particularly suitable for bearing doping cations. For example, $Ce_{1-x}Ti_xO_2$ ($0 < x < 0.25$) nanospheres were prepared by liquid-phase flame spray pyrolysis of cerium and titanium alcoholic (or other flammable solvents) solutions,[149] while Cu-doped CeO_2 hollow nanospheres were obtained through soft surfactant-assisted hydrothermal method.[217]

Other 3D shapes have been accessed through various protocols. For example, prism-shaped mesocrystals were obtained via hydrothermal methods using suitable concentrations of OH^-,[218] while tadpole structures were isolated in the sol−gel synthesis using cerium(III) nitrate, diphenyl ether, and appropriate surfactants.[219]

As far as catalytic applications are concerned, the synthesis of ceria nanoparticles requires in most cases the combination with metal nanoparticles that function as the catalytically active sites. Strategies exploiting metal nanoparticles to dictate assembly of nanoceria with specific geometries or high-ordered hierarchical arrangements are an interesting approach which is increasing in popularity. As a representative example, formation of core−shell systems, in which a CeO_2 porous shell enwraps a noble metal nanoparticle core can be prepared via a simple sol−gel method. The layering of Ce alkoxide precursor is harnessed by a ligand-exchange reaction with a bifunctional capping agent such as mercapto-undecanoic acid (MUA). Hydrolysis and calcination lead to isolation of nanosized M@CeO_2 (M = Pd, Pt) core−shells, in which, in addition to participation into the catalysis, the CeO_2 shell provides protection of the metal NPs toward aggregation.[220] The stability can be further enhanced by immobilizing the core−shells on modified alumina, which results in exceptional activity in the oxidation of methane under dry conditions,[221] while some deactivation was observed under wet conditions.[222] Recently, in situ high-temperature TEM observation shows that these systems undergoes structural

evolutions.[223] While the alkoxide ligand has been used for the assembly of these core−shell structures, it is interesting to speculate that by using different Ce metal complex precursors with ad-hoc designed ligands, it would be possible to tune the redox properties of the final CeO_2, particularly if the ligand remains coordinated to the oxide surface. For instance, in one latest report, Schelter and co-workers prepared a 1,3-bis[(20-tertbutyl)hydroxyaminophenyl]-benzene Ce complex, in which the ligand was proved to influence the stability of the Ce(III)/Ce(IV) redox couple.[224]

Core−shell systems based on other precious metal cores have also been prepared. Ag@CeO_2 was synthesized by reverse micelle/redox reaction,[225] while Au@CeO_2 have been recently prepared through a facile hydrothermal/calcination process.[226]

An emerging and attractive field of research is to deposit CeO_2 nanoparticles on a sheet of graphene to improve electronic characteristics and provide an enhanced dispersion of the nanocatalysts over a 2D plane. A CeO_2-ZrO_2 catalyst deposited on graphene oxide by continuous hydrothermal flow synthesis was assembled to successfully carry out the green synthesis of dimethyl carbonate from MeOH and CO_2.[227]

A hierarchical system, which is very active for the sequential two-step sequence (1) CH_3OH-decomposition to CO and H_2 followed by (2) hydroformylation of ethylene, was synthesized using CeO_2 nanocube building blocks, which were assembled on a 2D sheet of Pt nanocubes. The Pt cubes had been previously drop-casted onto a SiO_2 substrate, and after removal of the capping agents by ultraviolet/ozone treatment, a ternary system composed of Pt/CeO_2 bilayers on SiO_2 was attained, with effective interfacing of the three components.[228]

6. MODEL CATALYSTS

Given the complexity of CeO_2-based systems, many model catalysts have been prepared and studied in order to gain a deeper understanding of general or specific catalytic phenomena. A typical approach has been the synthesis of thin films (thickness in the order of 20Å), which allows the possibility of an atomic scale study (as opposed to bulk materials) and is a strategy used not only for ceria but for many other metal oxides.[229] In practical terms, thin films offer the double advantage of (1) a more straightforward application of analysis techniques involving charge transfers between the ceria and the probed sample as a result of the increased charge carrier mobility, (2) an easier investigation of the ceria/metal interactions, and (3) the possibility to tune the structural and electronic properties of the supported films by appropriate selection of the supporting substrate. There are several methods to prepare thin films. One versatile method is the electrodeposition, which was for example used to prepare a CeO_2 thin film on a highly oriented pyrolytic graphite. The thickness could be tailored by changing the Ce^{3+} concentration in solution and the deposition time.[230] In another example, anodic electrodeposition from Ce(III) ions suitably complexed by organic ligands allowed the deposition of thin films of CeO_2 onto several types of substrates. Tuning of the temperature and current density also results in a preferential crystallographic facet orientation.[231] Mechanistic studies of the anodic electrodeposition of CeO_2 films under several conditions have also been reported.[231] Recently, a careful control of the electrochemical parameters afforded the growth of porous films of isotropic CeO_2 nanoparticles on copper surfaces for application in condensate microdrop self-propelling (CMDSP) surfaces (Figure 13). The synthesis of the porous films made use of small bubbles generated through the hydrogen evolution reaction which functioned as pore-making templates.[232]

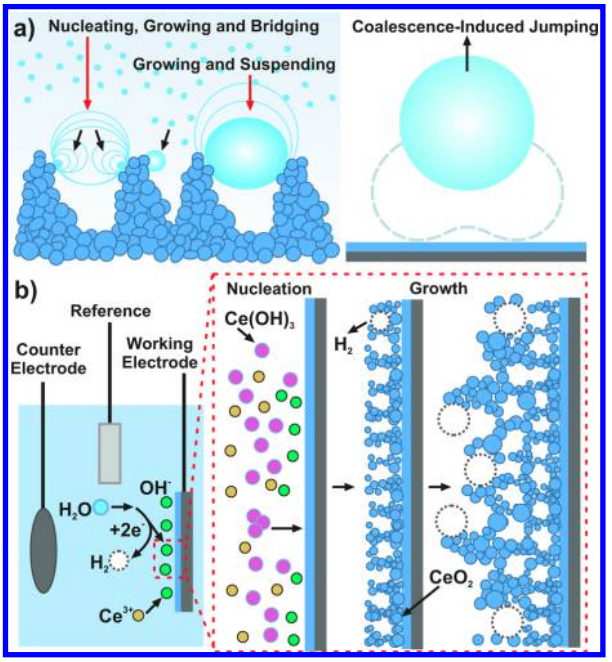

Figure 13. (a) Schematic diagrams of utilizing rugged, porous, nanoparticle films to endow copper surfaces with a condensate microdrop self-propelling function. (b) Schematic diagrams of synthesizing porous films of cerium oxide nanoparticles by the control of the preferential growth of isotropic nanoparticles and the synergistic utilization of tiny bubbles, released by the hydrogen-evolution reaction, as pore-making templates. Sky blue H_2O, green OH^- ions, orange Ce(III) ions, pink $Ce(OH)_3$, blue CeO_2, and white H_2. Reprinted with permission from ref 232. Copyright 2015 Wiley-VCH.

Atomic force microscopy (AFM) is a very powerful and popular technique that is applied to the study of ultrathin films and is often performed under ultrahigh vacuum conditions. Despite the fact that the adopted experimental conditions are significantly far from those of real catalytic applications (especially in the early studies), very relevant information of the interaction of model surfaces with small molecules and with water in particular can be obtained. The so-called non-contact mode (nc-AFM) was employed to outline the structural features of stoichiometric, slightly reduced, and contaminated terraces formed on the CeO_2(111) surface, and it turned out that water readily adsorbs on the ceria surfaces provided that oxygen vacancies are present.[233] In a more recent report, water adsorption and dissociation was evaluated for oxidized and reduced CeO_2(111) and CeO_2(100) surfaces. Adsorption occurs both molecularly and dissociatively, and in accord with theoretical calculations,[234] dissociation was more favorable on the reduced surface compared to the oxidized surface for the CeO_2(100); however, the effect is far more significant in the case of CeO_{2-y}(111).[235] Interaction with water was also studied for systems based on the deposition of CeO_2(111) films on Cu(111). The analysis was conducted by photoelectron spectroscopy (PES), STM, and temperature-programmed desorption (TPD), revealing the molecular adsorption of water at $T < -153$ °C on stoichiometric CeO_2(111) surfaces and a partially dissociative adsorption on surface reduced by ion bombardment.[236] The same authors also compared stoichiometric CeO_2(111)/Cu(111), partially reduced CeO_{2-y}/Cu-

(111), and Pt/CeO_2/Cu(111) model catalysts by synchrotron−radiation photoelectron spectroscopy (SRPES), resonant photoemission spectroscopy (RPES), infrared reflection absorption spectroscopy (IRAS), and DFT calculations.[237] Due to the surge of bioderived hydrocarbons as potential feedstock for hydrogen production, the same investigation was carried out for the adsorption and reactions of formic acid. Depending on the system and the operative temperature, the percentages and rates of formation of a number of possible products were evaluated.[238]

A series of studies on the adsorption/reactivity of several other molecules such as CO_2,[239] CO,[240] CH_4,[241] and SO_2[242] by similar model catalysts was reported, while an alternative synthetic method for reduced thin films involving the physical vapor deposition of metallic Ce onto a stoichiometric CeO_2(111) film on Cu(111) was more recently accomplished. Here, it was proposed that the as-obtained highly ordered films of Ce_2O_3 were formed through the interfacial reaction of the CeO_2 with metallic Ce at high temperatures, and the strategy allows for the presence of ordered oxygen vacancy clusters both on the surface and subsurface.[243]

Acetone was shown to weakly chemisorb on oxidized CeO_2(111) in a η_1 configuration (η term refers to the number of atoms of a molecule coordinated with the surface, in this case one) while adsorption on reduced CeO_{2-y}(111) is much stronger and it occurs through formation of the ketone carbanion.[244] Other than small organic molecules, the interaction of metals with CeO_2 has also been studied, being of high relevance for the assembly of catalytic metal systems. The adsorption of Cu onto slightly reduced CeO_2 (111) surfaces was investigated through calorimetric and surface spectroscopy techniques, highlighting that at lower temperature (−173 °C) with respect to a previous study (27 °C),[245] there is formation of isolated Cu adatoms onto CeO_2 (111) terraces, which are accompanied by a higher Cu chemical potential as compared to Cu nanoparticles.[246]

An interesting variation was introduced by Rodriguez with the assembly of the so-called "inverse" catalysts[247] in which the ceria nanoparticles are deposited onto the catalytically active metal phase, rather than the other way round. The interaction between the metal and the nanostructured support alters the electronic states of the oxide support resulting in different chemical properties which give rise to new and enhanced catalytic properties.

For instance, an inverse model catalysts composed of 20−30% of CeO_{2-y} NPs covering Au(111) films was studied for the WGSR. While clean Au(111) was inert toward this reaction, the presence of the ceria (and titania) NPs allowed the H_2O dissociation onto the O vacancies, which was ensued by the reaction at the Au-CeO_2 interphase with Au-adsorbed CO, leading to moderate catalytic activity.[248] The same rationale was used to prepare CeO_x/Cu_2O/Cu(111) inverse systems (Figure 14) for the WGSR and the CO oxidation; for the latter reaction, the ceria NPs serve to achieve the crucial O_2 dissociation, which secures a considerable activity enhancement.[249]

By means of reactive deposition of Ce with use of molecular or atomic oxygen as the oxidizing gas, epitaxial growth of CeO_2 ultrathin films on Pt(111) surfaces was achieved, with stabilization provided by means of Pt oxidation (Figure 15).[250]

Very recently, Matolin et al. prepared an anode catalyst made of Pt-CeO_x thin films and evaluated the activity in a hydrogen proton exchange membrane fuel cell (PEMFC), showing

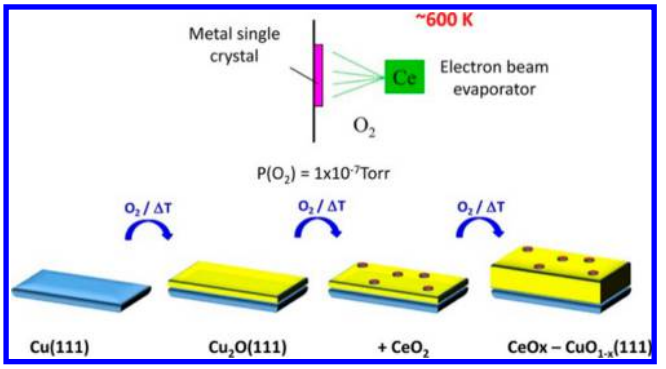

Figure 14. Scheme of evaporation process (top). Growth of CeO_x on a Cu(111) surface (bottom). Reprinted from ref 249. Copyright 2013 American Chemical Society.

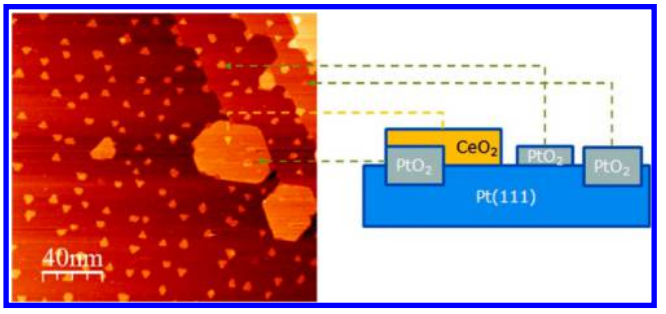

Figure 15. STEM image and schematic representation of epitaxially grown CeO_2 film on Pt. Reprinted from ref 250. Copyright 2011 American Chemical Society.

comparable performance to that of commercial anodes, which implied a much higher specific power than that of conventional reference cells.[251]

Ceria-based thin films have also been prepared in combination with other oxides. Inverse CeO_2-TiO_2 opals with a core−shell structure obtained via a combination of colloidal crystal template and atomic layer deposition (ALD) were screened as model catalysts for the photodegradation of methylene blue (MB), which could be degraded under UVA light with moderate activity.[252] Ordered mesoporous CeO_2-ZrO_2 thin films were assembled in order to study the size dependence of the reactivity driven by defects. Given the considerable conductivity deviation from classical point defect models for binary oxides upon changing of the oxygen partial pressure, a new "surface" defect model was suggested, which considered the effective charges of the lattice ions near the surface not necessarily similar to those of the bulk phase.[253]

In general, the presence of a metal boosts the activity of ceria catalysts for most processes. Therefore, many efforts are being made to develop model catalysts able to provide insights into kinetics, mechanisms, and energetics occurring at the surface. Noble metal nanoparticles are surely the most prominent and investigated class of catalysts.

The intimate contact between Pt and CeO_2 often results in a considerable increase of activity. Two types of important interactions were identified by means of DFT and RPES on well-defined Pt-ceria, namely (1) electron transfer from the Pt nanoparticle to the support, and (2) oxygen transfer from ceria to Pt. These two events require a close contact between the noble metal and the ceria, which in turn relies on the nanosize effect of the oxide support.[254] In another report, the relevance of such contact was demonstrated under the working

conditions, showing the involvement of ceria lattice oxygen in the oxidation of CO. The length of the ceria-metal interface could be tailored because of the use of monodisperse nickel, palladium, and platinum nanocrystals.[255] The CO oxidation performance was also set as model reaction for a shape-activity dependence investigation with three different ceria nanocrystal morphologies: octahedra, rods, and cubes,[256] while a shape-dependency was reported for the total oxidation of polycyclic aromatic hydrocarbons.[257] The importance of the nanoscale structure was also highlighted in an electrochemical study of mesoporous ceria films exhibiting a periodic nanoscale porosity prepared by a template-assisted method. Nanoporosity favored Li^+ intercalation and could be of better potential for application requiring charge storage.[258] Recently, it has been shown that nanostructured cerium oxide films expose $\{100\}_c$ nanofacets, which can stabilize Pt atoms in the form of Pt(II) ions.[259] This is particularly interesting as there is a growing attention toward the design of stable atomically dispersed supported noble metal catalysts as a new generation of cost-effective catalytic materials.

Another consideration that needs to be looked into is that the chosen film support plays very often a non-innocent role onto the CeO_2 properties. For example, Gorte et al. compared the properties of CeO_2 films supported onto yttria-stabilized zirconia (100) (YSZ 100) and α-Al_2O_3(0001) single crystals and found a much decreased reducibility when the latter support was used, with ceria being stable for temperatures as high as 727 °C. In contrast, when the YSZ was employed, reduction to Ce_2O_3 took place already at 552 °C. The two supports also behaved differently under oxidation conditions, with CeO_2 reacting with α-Al_2O_3(0001) at 1000 °C to form $CeAlO_3$, while with the YSZ system agglomeration of ceria occurs at $T > 552$ °C, leading to oriented bar-shaped structures. For temperatures below 552 °C, the CeO_2 turns out to be stable toward oxidation.[260]

7. APPLICATIONS

7.1. Well-Established Applications

7.1.1. Three Way Catalysts (TWCs). The most diffused and known application of CeO_2-based materials is as promoter in the automotive TWCs. Mounted after an internal combustion engine, the TWCs role is to remove the pollutant produced by the combustion of gasoline, promoting at the same time the oxidation of CO and unburnt hydrocarbons (HC) and the reduction of nitrogen oxides (NO_x). Catalytic converters generally consist of a monolithic support (usually made of cordierite) with honeycomb structure with the inner surface of the channels covered by the catalytic material. This comprises of a thermally stable support (usually doped Al_2O_3), the active phase made by noble metals, and a CeO_2-based promoter (usually $Ce_xZr_{1-x}O_2$). The oxidation reactions are promoted by Pt and/or Pd, while some Rh is essential to catalyze the reduction of NO_x.[261]

Figure 16 presents the conversion efficiency of the three classes of pollutants as a function of A/F. A good removal of all the pollutants is obtained only in a narrow window around the stoichiometric value, which is near 14.6.[262] This is achieved by a continuous control of the oxygen pressure in the gas stream and the modulation of the air and fuel flows by the electronic system of the car (the so-called λ-sensor). Nevertheless, the required tight stoichiometry requirements are not easily attainable in a randomly (to the driving features) oscillating dynamic combustion, and the gas phase coming out of the engine rapidly fluctuates between lean ($A/F > 14.6$) to rich conditions ($A/F < 14.6$) and vice versa.

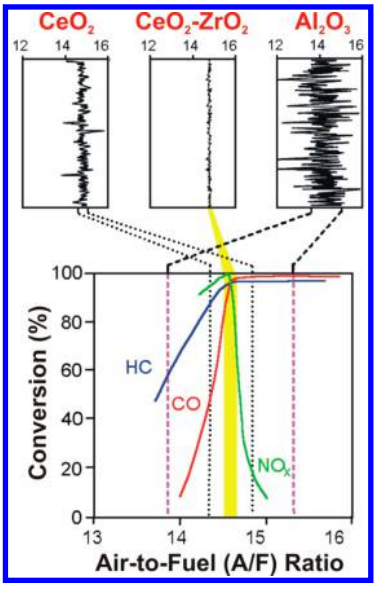

Figure 16. Conversion efficiency of HC, CO, and NO_x, with the control of the A/F ratio depending on different supports used in TWCs. Adapted from ref 262. Copyright 2000 Elsevier.

The principal role of CeO_2 in TWCs is to act as oxygen buffer, extending the three-way "window" of operation of the TWC (Figure 16).[262] Reduced ceria (CeO_{2-y}) is able to store oxygen during lean-to-rich transients, promoting the reduction of NO_x. On the other hand, CeO_2 is able to provide the oxygen needed for CO and HC oxidation during rich-to-lean transients. As described in a previous section, the maximum amount of oxygen that the CeO_2/CeO_{2-y} composite is able to provide/accept to/by the gas stream is the so-called OSC.

During 1970s−1980s, the preparation of TWC consisted essentially in the coimpregnation of the noble metals and CeO_2 precursors on doped Al_2O_3 support. Even if this preparation method is very simple, the performance of TWC was dramatically improved.[263]

Since the mid-1980s, a second generation of CeO_2-containing TWCs was developed, known as "high tech" catalysts. The improvements in the performance of these catalysts have been achieved mainly through the developments in the preparation technology in order to increase the CeO_2 content but, at the same time, optimizing the CeO_2 dispersion on the doped-Al_2O_3 support, although preventing formation of undesirable $CeAlO_3$ and the interaction between CeO_2 and the noble metals. Also in this case, a dramatic enhancement in the performance of TWCs has been observed. Nevertheless, the high-tech catalysts were not able to meet the stricter requirements introduced in the USA and Europe for car pollution control, such as lower emission limits and longer durability of the converters. The most problematic aspect was the thermal stability of the TWCs, because the trend was to move the catalyst close-coupled to the exhaust manifold to obtain faster light-off. The loss of performance on the high-tech TWC were associated with the decrease of OSC due to CeO_2 sintering and to the loss of contact between CeO_2 and the noble metals.[264]

Nowadays, the efficient control of pollutant emission is realized by the use of the so-called advanced TWCs. They use CeO_2-ZrO_2 solid solution instead of pure CeO_2.[99] As described

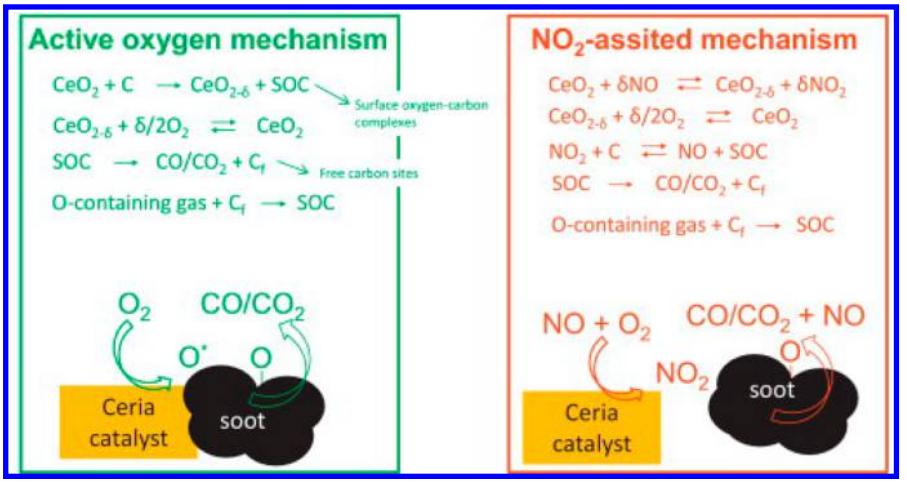

Figure 17. Schemes of the two main mechanisms accepted for CeO_2-catalyzed soot combustion. SOC = surface oxygen complexes, C_f = free carbon site, O* = oxygen atom transferred to the carbon particle. Reprinted from ref 271. Copyright 2014 Elsevier.

previously, the introduction of ZrO_2 into the CeO_2 lattice enhances the OSC of the materials involving also bulk oxygen ions in the redox cycles, improving the activity of the catalyst and reducing emission at the start of the engine.

TWCs are exposed to high operative temperature, usually close or above 1000 °C, for very long periods (even more than 200000 km). For this reason, the catalytic components must be thermally stable. Sintering of the active components results in loss of "active oxygen", in a reduction of the exposed metal surface area, and in loss of the contact between noble metal particles and the CeO_2-based promoter. Although sintering phenomena cannot be completely avoided, the use of CeO_2-ZrO_2 in advanced TWC instead of CeO_2 helps to overcome the detrimental effects of long high temperature treatments. First, CeO_2-ZrO_2 solid solutions are more resistant to sintering compared with bare CeO_2.[265] Moreover, the controlled deposition of CeO_2-ZrO_2 on the doped Al_2O_3 support enhances the sintering resistance of the composite, preventing the transformation of Al_2O_3 into the α form characterized by a very low surface area.[266,267] In addition, undesirable fixation of Ce(III) in the stable $CeAlO_3$ is hindered.[267]

OSC and surface area are not strictly correlated in CeO_2-ZrO_2 materials and "active oxygen" is available also after severe sintering of the materials. Mamontov et al. ascribed this effect to the presence of Frenkel defects (vacancy-interstitial pairs) in CeO_2-based materials with high surface area.[268,269] By neutron diffraction analysis, the amount of these defects significantly decreases in CeO_2 above 800 °C while they remain almost unaffected at higher temperature in CeO_2-ZrO_2 materials, despite the collapse of the surface area of the materials.

7.1.2. Diesel Engines. Together with NO_x, CO, and unburned hydrocarbons, soot is one of the main pollutants emitted by diesel engines, and its proven adverse effects on human health impose stringent regulations on the limits of emission. Several strategies have been proposed to reduce the soot emission levels, with catalytic filters surely representing one of the most advocated techniques.[270] It is based on the filtering and subsequent catalytic oxidation of the particulates. Some of the drawbacks reside in the complex filter regeneration and the limited soot-catalyst contact efficiency. Moreover, the catalyst is required to be active and stable in a wide temperature range.

Ceria is among the best catalyst for soot combustion, as it has recently been reviewed.[271,272] It can considerably lower the temperature of combustion leading to less power-demanding filter regeneration. There are two main accepted mechanisms for the ceria-catalyzed soot combustion (Figure 17): (1) Active oxygen mechanism, in which there is direct oxygen exchange between the catalyst and the gas-phase O_2 and (2) NO_2-assisted mechanism, which exploits the higher temperature-induced oxidation of NO to NO_2, which is a better oxidant than O_2.

A great deal of formulations includes modification of the CeO_2 with other metal species. For example, ultrasonic-assisted incipient-wetness impregnation was used to produce a CeO_2-supported cobalt oxide which displayed a highly enhanced activity in comparison with the corresponding CeO_2 catalyst prepared by autocombustion. The CoO_x, which exists as CoO at low Co loadings and as spinel Co_3O_4 at medium and high loadings, favors the Ce(IV) ↔ Ce(III) process by means of its strong redox properties.[273] Rare earth-modified ceria $CeMO_x$ (M = La, Pr, Sm, Y) were compared with pure ceria prepared by calcination of a nitrate precursor, showing improved soot oxidation despite a decrease of the surface area, which is however compensated by an increase of the meso/macro pore volume. This last factor is one important parameter when O_2 is used as oxidant.[274] Trovarelli et al. reported on the promotion effect of alkali metals in ceria-catalyzed soot combustion, with an order of activity Cs > Rb ≈ K > Na. Moreover, the performance is sensitive to the amount of metal and the selected precursor, with chlorides being always nearly inactive. The activity was interpreted in terms of oxygen exchange mechanism in which carbon−oxygen complexes (C−O−M with M alkali metals) are the active sites (i.e., the M promote the oxidation of carbon located near the catalyst). The effect of alkali metals is to favor the chemisorption of molecular oxygen with the formation of carbon surface complexes that eventually reacts with soot.[275]

As for the TWC, many studies have been devoted to the replacement of pure ceria with ceria-zirconia-based catalyst. Parallel removal of soot and NO_x by a series of Ce-Zr mixed oxide was explored. The catalytic activity was found to be dependent on the chemical composition of the solid solutions, with $Ce_{0.76}Zr_{0.24}O_2$ showing an optimal performance, as the result of high thermal stability and efficient redox properties, in

contrast, to pure CeO_2, which provided lower activity and progressive deactivation with increase of temperature.[276] Potential benefits brought about by alkali metals have been explored for ceria-zirconia, too. $Ce_{0.65}Zr_{0.35}O_2$ and CeO_2 supported on cordierite monolith were impregnated with potassium, and the system was compared with K-free catalysts. Deactivation for $K/Ce_{0.65}Zr_{0.35}O_2$ and K/CeO_2 was found after 10 cycles of soot combustion, as opposed to the pure oxides, which became more active after the 10 cycles. However, the presence of NO/O_2 significantly improved the performance of the K-modified oxides.[277] Doping with rare earth metals (La, Pr, Sm, and Tb) was also reported to enhance textural properties as well as activity of the CeO_2-ZrO_2 catalysts.[278] A $Ce_{0.73-x}Zr_{0.27}Nd_xO_2$ mixed oxides (x = 0, 0.01, 0.05, 0.09, 0.2, and 0.3) was reported by Bueno-López et al. to be an active catalyst for the simultaneous oxidation of CO, propylene, benzene, and soot from a simulated diesel exhaust mixture. In this case, when in low amounts, the neodymium favors the formation of oxygen vacancies and the surface area reducibility, thus leading to improved performances. However, when present in amounts higher than 0.2, the final performance is worsened due to promotion of sintering and decrease of surface area.[279] An important investigation was carried out by Trovarelli et al. on the effect of the exposed ceria and ceria-zirconia crystal planes in soot combustion. Calcination conditions can drive the exposure of the more reactive {100} and {110} over the more stable and less reactive {111} planes,[280] although this preference becomes decreasingly important as the samples are enriched with Zr.[281] As a result, a correlation between soot combustion activity and exposed facets could be found for the ceria catalyst, while such correlation remains unclear for the corresponding CeO_2-ZrO_2.[281] As another example, functionalized Fe-Al-Cr alloy fibers covered with Pt/CeO_2-ZrO_2 oxidation catalyst, with concomitant high filtration capability were recently proposed.[282]

Temperature-programmed experiments are a powerful technique to clarify behavior of the catalysts under conditions which are comparable to those found in commercial applications.[283] The problem of the soot-ceria contact has been recently addressed using experimental microkinetics with temperature-programmed experiments on three mechanically mixed ceria-soot mixtures, in which the contact was varied from tight to loose.[284] In another paper, preparation of highly porous ceria nanofibers deposited on SiC diesel particulate filters (DPFs) led to a bigger number of contact points between the soot and the fiber, as the soot particles could penetrate into the nanofibers network. This translates into a higher activity for the loose contact mode, with combustion temperatures being sensibly lowered. However, the effects under tight contact conditions were not very significant.[285]

Several experiments addressed the stability of the CeO_2-based catalyst under thermal stress or other factors. For instance, the good activity of $Ba,K/CeO_2$ catalyst for soot combustion was retained at temperatures as high as 830 °C. A further increase of temperature determined formation of perovskite phase as $BaCeO_3$ and depletion of K content from the catalyst surface, with a resulting drop of activity.[286] Another factor that has recently been evaluated is the presence of CO_2, H_2O, and SO_2 in the diesel exhaust mixture, with the inhibition effects following the trend $SO_2 > H_2O > CO_2$.[287] As described in the section on ceria nanostructures, the controlled morphology of CeO_2 at the nanoscale level can produce considerable catalytic performance enhancement. Recently, CeO_2 nanocubes were reported to be excellent catalysts, especially after deposition of Co_3O_4 onto the ceria cubes, for the low-temperature diesel soot oxidation,[288] while Co_3O_4–CeO_2 supported via isovolumetric impregnation on a SBA-15 monolith turned out active in the NO_x-assisted soot combustion, with optimum Co/Ce ratio being 1:4.[289]

7.2. Prototypes and Niche Applications

7.2.1. Solid Oxide Fuel Cells. Solid oxide fuel cells (SOFCs) constitute an environmentally friendly and therefore very attractive class of fuel cells, with outputs in most cases being simply electricity, water (when H_2 is used as fuel), and heat. They offer the advantage of compatibility with several fuels without suffering from CO poisoning. The literature on the use of ceria in SOFCs is too vast to be comprehensively reviewed, so only a flavor is given herein through few representative examples.

There are three places where ceria is commonly used in SOFC: (1) doped ceria is used as an electrolyte in some designs, (2) CeO_2 is used as a barrier layer for cathodes to prevent reaction with the YSZ electrolyte, and (3) CeO_2 is sometimes added as a catalyst in both cathodes and anodes.[290,291] In the latter case, doping with other bi- (less common) or trivalent elements is a strategy to further improve the performances. A classic example is the Gd-doped ceria anode (CGO), for which the cell performance is increased as a consequence of the increased oxygen vacancy concentration arising from the doping.[292] The reported higher resistance of ceria-based ionic conductors to carbon deposition results in an extra asset, as hydrocarbon fuels can be directly supplied to the anodes.[293,294] Murray et al. fabricated an intermediate-temperature SOFC consisting of a thin (0.5 μm) yttria-doped ceria (YDC) anode which was deposited on porous $La_{0.8}Sr_{0.2}MnO_3$ (LSM) cathodes and combined with a Ni-ceramic composite thicker layer as current collector. The as-assembled cell stack could work with direct oxidation of methane, generating power densities of up to 0.37 W cm^{-2} at 650 °C.[295] The catalyst morphology is an aspect that is worth some special care during the electrode assembly stage. $Pd@CeO_2$ core–shell systems proved to be effective anodic catalysts with H_2 and CH_4 as fuels, with extra stabilization provided by the core–shell structure; the synthetic design included a silanization step of the YSZ (YSZ = yttria-stabilized zirconia) in order to have a uniform coverage of the electrode with the $Pd@CeO_2$ nanoparticles (Figure 18). Activities were retained at high temperature either during oxidative (calcination) or operative reduction conditions.[296]

Sun et al. improved the efficiency of a previously reported anode based on Ru-CeO_2 catalyst using iso-octane as fuel.[297] The enhanced performance originates from the porous flowerlike microsphere morphology of the CeO_2 support, reaching maximum power densities up to 654 mW cm^{-2} at 600 °C.[212]

An important aspect to take into consideration is the sulfur tolerance of the anode, as sulfur is often a detrimental poison for the cell. Cu can considerably improve such tolerance, with H_2-fueled SOFCs performance reportedly being maintained with H_2S impurity levels up to 445 ppm.[298] Similarly, when conventional Ni–YSZ anodes were infiltrated with ceria nanoparticles, the tolerance to sulfur was considerably enhanced, with the cathodic cell delivering a power density of 220–240 mW cm^{-2} for 500 h with H_2 fuel contaminated with

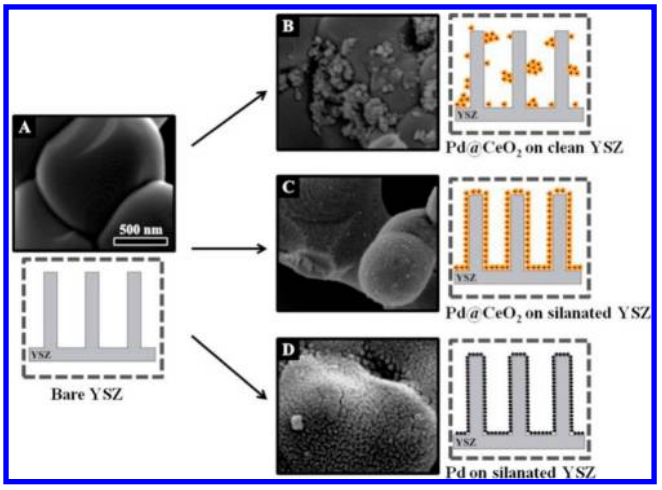

Figure 18. SEM images and schematic representations of (A) bare YSZ, (B) Pd@CeO_2 nanoparticles deposited on clean YSZ porous electrode, (C) Pd@CeO_2 nanoparticles deposited on silanated YSZ porous electrode, and (D) uncoated Pd nanoparticles deposited on silanated YSZ porous electrode. YSZ = yttria-stabilized zirconia. Reprinted from ref 296. Copyright 2013 American Chemical Society.

40 ppm of H_2S. In contrast, when ceria-free Ni-YSZ anodes were employed, the cathodic cell exhibited a much diminished performance, with power density dropping to 0 after 13 min under the same operating conditions.[299]

The variation of the anode thickness was set as a parameter for the evaluation of the long-term durability and performance in a SOFC working with humidified methane. Both Ni-YSZ and Ni-samaria-doped ceria (Ni-SDC) were employed as anodic components, and an improvement with the latter composite was observed, independent upon the thickness of the electrode. Such enhancement was attributed to the higher catalytic activity of the Ni-SDC and higher electronic conductivity of the SDC, in which the partial reduction of Ce(IV) to Ce(III) under reducing atmosphere plays a critical role.[300]

Another wide explored area in SOFCs development concerns the use of ceria-based composites as electrolytes, given the ionically conductive and electronically insulating properties of CeO_2.[301] The number of reports on doped ceria used as electrolyte in SOFCs is large, and recent literature provides a comprehensive list of composite electrolytes, their properties, and performance.[5] Gadolinium, samarium, yttrium, and calcium are typical dopants. In the case of nanostructures, the enhancement in conductivity is associated with a larger contribution of the grain-boundary conductivity in comparison with traditional polycrystalline solids. In this region, nano-electrolytes exhibit faster oxygen ions diffusion than in the bulk, in contrast with conventional microsized electrolytes.[302,303]

There has been a convergence to study two-phase electrolyte materials on account of the highly improved ionic conductivity arising from the binary conductive nature (O^{2-}/H^+),[304] and at present, the interest is predominantly focused on this type of electrolyte in which the doped-ceria is combined with other salts. Without doubt, the most explored and promising composite is obtained by combining ceria with carbonates,[305−310] although recently some skepticism has arisen for these systems that present several question marks. Ceria-carbonate composites are generally accessed by means of mechanical mixing or by infiltration techniques. The microstructure is typically of a core−shell type, where crystalline core ceria is enveloped in the amorphous shell of carbonate.[311]

Other than carbonates, oxides,[312−314] hydroxides,[315] sulfates,[316] and halides[317] are also becoming more and more popular electrolytes.

7.2.2. Polymer Exchange Membrane Fuel Cells (PEMFCs). Although to a lesser extent in comparison with SOFCs, polymer electrolyte-membrane fuel cells (PEMFCs) have also been explored in combination with ceria-based composites. Most of the studies focused on the half reaction of the cell, typically implying a reforming processes to produce H_2 which is then employed as PEMFC fuel, as discussed in the section dedicated to reforming.[318]

PEMFCs offer advantages such as absence of electrolyte leakages, lower corrosion, and simplicity of the stack design, although there is still much work to be done to improve the kinetics for the oxygen reduction reaction and the conveyance of protons and reagents toward the cathode.[319] Modification of a Pt/C catalyst with CeO_2 via sol−gel method resulted in an initial electrochemical reduction of ceria at the cathode, which was then oxidized by an intermediate product of oxygen reduction (i.e., hydrogen peroxide). This determines an enhancement of the PEMFCs performance, as the overall cyclic process promotes the rate for oxygen reduction.[320] Similarly, the ceria redox properties were exploited to assemble a highly durable catalyst in combination with mesoporous carbon-supported Pt nanoparticles; when integrated into a PEMFCs, an appreciable performance enhancement at low humidity compared with the conventional Pt/C catalyst was observed together with higher resistance to corrosion. One of the reasons for the improved performance was related to the water retention by the ceria component.[321]

One issue to be addressed in the use of CeO_2 in PEMFCs is its stability under acidic conditions, which are normally employed in PEMFCs. Given its solubility in acids, latest developments point to the assembly of ceria-based PEMFCs working under alkaline conditions, where ceria is more stable. Moreover, the use of basic pH would open the door to the exploration of other non-noble metals as catalyst, which are incompatible with acid solutions. We reported the first example of direct ethanol PEM fuel cell with an anode made of Pd supported on CeO_2/carbon black. The importance of the ceria component becomes evident as the analogue Pd catalyst supported only on carbon black has a half energy efficiency when tested; presumably, the ceria promotes formation of Pd-OH_{ads} species, which can decrease the onset energy (E_{onset}) of ethanol.[322]

In a recent and elegant work, Chueh et al. opened new perspectives to optimize the activity of ceria-based electrodes. The direct spectroscopic quantification of the samaria-doped ceria−gas interface revealed the surface oxygen-ion incorporation pathway during electrochemical hydrogen oxidation and water splitting. Facile reactivity of oxygen vacancies with water molecules was observed together with the rapid rates at which additional vacancies and polarons were transported between the bulk and the surface. On the basis of these operando observations, it was suggested that electron-transfer between cerium cations and hydroxyl ions is the rate-determining step.[323] The same group also studied the surface electrochemistry of CO_2 reduction and CO oxidation on Sm-doped CeO_{2-y}, proving that the reactions proceeds via a stable carbonate intermediate, the coverage of which is coupled to the surface Ce(III) concentration.[324]

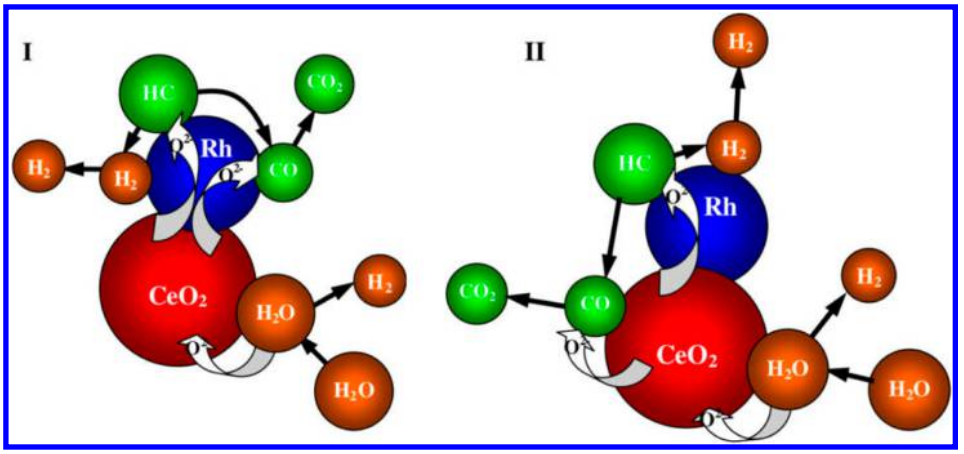

Figure 19. Scheme for hydrocarbon steam reforming and water-gas shift reaction on Rh/CeO_2 according to mechanisms I and II. Reprinted with permission from ref 338. Copyright 2009 Elsevier.

7.3. Emerging Applications

7.3.1. Reforming. In this section, steam, dry, and autothermal reforming of hydrocarbons or oxygenated compounds using CeO_2-based catalysts will be reviewed.

7.3.1.1. Steam Reforming. Steam methane reforming (SMR) is the method most widely applied by industry to produce hydrogen. Compared to other reforming processes, the theoretical H_2/CO ratio is higher (equals 3) but the reaction is thermodynamically unfavored, being overall endothermic. Therefore it must be conducted at high temperatures:[325]

$$CH_4 + H_2O \rightleftharpoons CO + 3H_2 \quad (\Delta H^0_{298} = 206.2 \text{ kJ mol}^{-1}) \tag{4}$$

Nevertheless, the number of reports on the use of CeO_2-catalyst for the SMR has enjoyed an exponential growth in the 2000−2010 decade, reaching a plateau in the last couple of years.

Similarly to other reforming processes, the most explored systems are based on ceria-zirconia mixed oxides, on account of their improved redox properties. CeO_2-ZrO_2 oxides typically serve as active supports for groups 8, 9, and 10 metal nanoparticles, which act as the catalytically active phase for the activation of hydrocarbons. For instance, Kusakabe and co-workers investigated the different SMR performances of Ni, Pt, Ru, and Rh catalysts prepared by the urea hydrolysis method, concomitantly varying the ceria-zirconia composition ($Ce_xZr_{1-x}O_2$, $0.5 < x < 1$). The catalysts were active at relatively low temperatures (500−600 °C), and the authors noticed that the Ni-supported cubic system with $Ce_{0.5}Zr_{0.5}O_2$ composition was more active than the corresponding tetragonal $Ni/Ce_{0.25}Zr_{0.75}O_2$ and $Ni/Ce_{0.75}Zr_{0.25}O_2$.[326] This finding somehow contrasts with a later report in which the superior activity of $Ce_{0.75}Zr_{0.25}O_2$ over other $Ce_xZr_{1-x}O_2$ phases for the SMR was observed,[327] highlighting an overarching mechanistic complexity that still eludes predictability despite the massive bulk of studies and information available today on CeO_2-ZrO_2-based materials. Kinetic and temperature programmed experiments for the SMR by a $Rh/Ce_{0.6}Zr_{0.4}O_2$ catalyst elucidated several mechanistic aspects and showed a non-linear dependence on CH_4 and steam partial pressures,[328] while the effect of the Ce/Zr ratio was tested for a 10% Ni-loaded support. In this latter case, the highest performance found for $Ni/Ce_{0.8}Zr_{0.2}O_2$ was put in relation with its higher thermal stability, higher redox capacity and smaller Ni crystallite size.[329]

A comparative study on two different preparation methods (impregnation and coprecipitation) for the same catalyst was also reported; the difference in the synthetic protocol is reflected in their SMR performance.[330]

Due to its comparatively lower cost, nickel has been a widely explored metal for the steam reforming process. The addition of ceria to the commercial $Ni/SiO_2/Al_2O_3$ catalyst resulted in a lower carbon deposition and thus better performance for the SMR when the water-to-methane ratios were kept low. The authors also varied the synthetic protocol for the ceria deposition, which led to different degrees of carbon inhibition.[331]

Doping with cations (usually trivalent) other than zirconium represents another commonly explored approach. Gadolinium, lanthanum, yttrium, and samarium have been successfully employed as dopants in ceria materials for several catalytic processes. For instance, $Ce_{0.9}Gd_{0.1}O_{2-y}$ has been shown to be an active catalyst for the SMR at 900 °C with reaction rates similar to those for the corresponding dry reforming, a fact explained in terms of a mechanism that is rate-controlled by the slow reaction of adsorbed CH_4 with oxygen.[332] However, it must be noted that the effect of the dopant is not always beneficial, and that, in some cases, it can lead to a decrease in the performance of the ceria-based material. A series of mixed oxide with Yb_2O_3, Y_2O_3, Sm_2O_3, Gd_2O_3, La_2O_3, Nb_2O_5, Ta_2O_5, and Pr_6O_{11} were prepared via sol−gel method, and it was found that all the mixtures were less active than pure CeO_2 in the oxidation of *n*-butane.[333] Hence, a merely structural effect by the dopants may also be the cause of variation in activity, with enhanced or decreased surface area playing the dominant role. This highlights how there are still unclear issues, and that more studies would be required in this area.

In general, for the most widely industrially utilized Ni-based catalysts, the use of higher hydrocarbons in the steam-reforming reactions is thwarted by the carbon deposition (coke) that leads to catalyst deactivation.[334] Nevertheless, higher hydrocarbons have also been investigated, albeit to a lesser extent. In a seminal work by Gorte and co-workers, stable reaction rates for the steam reforming of *n*-butane were reported with a Pd/ceria catalyst, while under the same conditions, an immediate coking occurred with a Ni/silica catalyst; the authors proposed a dual-function mechanism with alkane activation on the Pd phase followed by oxidation on the CeO_2.[101] The scope of the catalytic process was then extended

to hydrocarbons of several sizes subject to steam reforming by the same Pd/ceria system.[335] With the purpose of building low-cost reactors for solid oxide fuel cells, propane was investigated as reforming gas using a $Rh/Ce_{0.5}Zr_{0.5}O_2$ catalyst prepared by sol–gel method. The conversion of propane began at lower temperature (250 °C) than the corresponding alumina-supported Rh catalyst (320 °C), with a 3-fold enhancement of the overall conversion.[336]

Use of CeO_2 as dopant (14 wt %) in a Ni/Al_2O_3 catalytic system for the steam reforming (SR) of ethane and propane resulted in an improved resistance toward carbon formation at high temperature (900 °C).[337] More recently, the kinetics of hexadecane SR were investigated using microchannels coated with Rh/CeO_2. The experimental data were combined with numerical simulations to produce a model able to accurately predict not only hexadecane but also methane and ethane turnover frequencies.[338] Two possible pathways have been proposed (Figure 19) for steam reforming of hydrocarbons, involving hydrocarbon activation on Rh surface, water activation on CeO_2, and spillover of activated O from CeO_2 to Rh.[338] CO oxidation can take place on both the metal surface (mechanism I) or on the CeO_2 support (mechanism II).[338]

Methanol is the most investigated alcohol in reforming studies due to its high energy density (high hydrogen-to-carbon ratio), relatively lower temperatures of the reforming (200–300 °C) and easier storage. As for the case with alkanes, ceria-zirconia mixed oxides in combination with other metals, such as copper in particular, have been subjected to a number of investigations for the methanol steam reforming (SRMe). Pioneering work was carried out by Kumagai's group, who prepared a highly active SRMe catalyst composed of Cu/CeO_2,[339] while Oguchi et al. reported on a substantial acceleration of the conversion when ZrO_2 was added as promoter into a CuO/CeO_2 catalyst, unveiling the presence of Cu_2O traces together with metallic Cu in the ZrO_2-modified catalyst. This was evidence of the Cu stabilization provided by the ZrO_2 resulting in the observed longer durability. The system turned out to be rather sensitive to the CuO content, with 80 wt % being the optimum CuO amount.[340]

Excellent durability was also detected for a $Cu/CeO_2/ZrO_2$ composite prepared via coprecipitation and polymer template method, with Cu content in the range of 5–15 wt %; moreover, the catalyst showed little CO production. In this case, stability was not significantly enhanced by increasing the Cu loading, while reduction of CO was more pronounced in Cu-richer systems, presumably due to alteration of the microstructures (and therefore of the active Cu surfaces) when using higher concentrations of the Cu precursors in the synthetic protocol.[341] CeO_2-Gd_2O_3 mixed oxides have also been explored as supports for Cu catalysts in the SRMe process,[342] while a comparative study was carried out between Cu/CeO_2 and Cu/ZnO [and Cu/Zn(Al)O] that highlighted the superior performance of the CeO_2-based catalyst.[343]

Gold is emerging as a promising catalyst for the SRMe process in combination with CeO_2. Flytzani-Stephanopoulos et al. demonstrated the dependence on catalyst morphology of the SRMe for Au-ceria systems with different nanoshapes such as nanorods and nanocubes. They proposed a mechanism based on the cooperation between Au and ceria that, respectively, adsorb as-formed formaldehyde and oxygen to form methyl formate (Figure 20), which in turn is hydrolyzed to formic acid and eventually leads to release of CO_2 and H_2.[344,345]

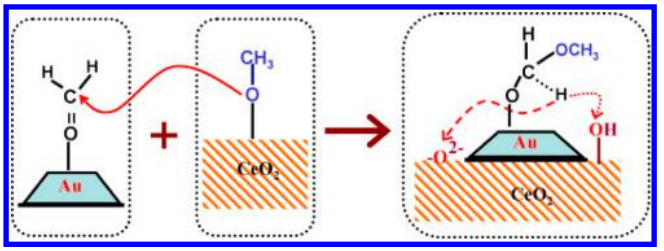

Figure 20. Schematic possible mechanism of steam reforming of methanol catalyzed by Au/CeO_2 systems. Reprinted with permission from ref 344. Copyright 2010 Elsevier.

Very recently, the effect of the support on Au-based catalysts for SRMe has been evaluated by changing the composition of $Ce_{1-x}Zr_xO_2$ oxides, with best activities obtained up to 25 wt % Zr. Calcination temperatures were also found to critically affect the performance, with CeO_2 agglomeration and ZrO_2 segregation occurring above 400 °C.[346]

Steam reforming of ethanol (SRE) is a promising and greener alternative route to H_2 production,[347] particularly in view of its use as biofuel (bioethanol) derived from renewable resources. As far as noble metals are concerned, several studies indicate a general Rh ≫ Pd > Pt = Ni trend in terms of activity and selectivity. High activities at low temperature (450 °C) were reported for $Rh/Ce_xZr_{1-x}O_2$, justified by the high oxygen transfer rate, which favors dehydrogenation of ethanol and reforming of acetaldehyde over methane production.[348] A simple synthetic protocol gave access to $Rh(1\%)@Ce_xZr_{1-x}O_2/Al_2O_3$ nanocomposites in which the porous metal oxide phase was grown around the Rh catalyst. Embedding of the active phase protects it from sintering, resulting in stable activities for the SRE, without compromising accessibility of the Rh nanoparticles to the reactive gas feed, as substantiated by chemisorption analysis.[349,350] Insights into the origins of large amounts of methane formation during the SRE with a $Rh/Ce_{0.5}Zr_{0.5}O_2$ prepared by wet impregnation were supplied by Duprez et al., who studied the $CO/CO_2/CH_4$ interconversion reactions and concluded that formation of methane occurs through CO hydrogenation, favored by the specific catalytic system, while no CO_2 hydrogenation was observed.[351] As a less expensive alternative to Rh, nickel has been the subject of several studies.[352,353] A very active $Ce_{0.8}Ni_{0.2}O_{2-y}$ synthesized through reverse-microemulsion method displayed no (or very minor) methane formation side-reaction, which was suppressed by the metal–ceria interaction that introduces a perturbation in the electronic structure of Ni.[354]

Ru, Pd, and Ag were investigated as catalytic active phases in SRE after wet impregnation on ceria-yttria stabilized zirconia supports. Despite some degree of sintering detected by combination of TEM, XRD, and chemisorption techniques, Ru and Pd displayed decent performances, while poor performances were observed for the Ag-based system.[355] Ce/Mn mixed oxides prepared by coprecipitation and added with SiO_2 were shown to have enhanced selectivity, with neither methane nor CO being detected under the used conditions.[356] A commercial bimetallic Pt-Ni catalyst supported on CeO_2 was very successfully utilized in SRE at temperatures above 300 °C due to the synergy between the two metals.[357] On the other hand, NiCo bimetallic particles on CeO_2-ZrO_2 displayed high activity above 530 °C with high H_2 yields; the basicity of ceria is responsible for limiting the undesirable formation of ethane as side products.[358]

In an interesting investigation, Davis and co-workers utilized ethanol as a steam reforming model alcohol compound in hydrogen-rich conditions to assess the effect of partially reduced ceria in a Pt/CeO_2 system. The experimental observations suggest that defect sites arising from reduction to Ce(III) are responsible for the activation of ethanol by dissociative adsorption to form ethoxy species, that in the presence of steam rapidly convert to acetate. The acetate intermediate eventually decomposes to CO_2 and CH_4, with the latter requiring additional energy to be activated for further H_2 production. The finding is important as it inherently conveys toward the perception that methanol is a better-suited alcohol for H_2 generation by Pt/ceria, as the hydrogen evolution does not take place through CH_4 formation.[359] Recent advances on Pt/ceria systems led to the discovery of an effect of improved stability of the catalytic ensemble by alloying Pt with Sn or by cofeeding the reactive gas with CO_2.[360]

Ozkan et al. carried out extensive investigations on Co/CeO_2-based systems as cost-effective alternative to Rh-based catalysts for the SRE, evidencing the importance of oxygen mobility,[361,362] morphology of the CeO_2 support,[363] and the Co precursor for the activity, stability, and selectivity of the catalytic system.[364] More recently, a study on the macro- versus nanosized-particle (MP vs NP) of the CeO_2 support confirmed the profound differences that the nanometer scale of CeO_2 imparts to the cobalt catalyst active phase and that this is associated with a considerable performance enhancement (Figure 21).[365]

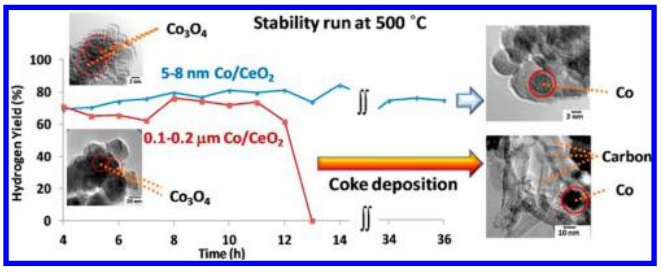

Figure 21. Time-on-stream performance of $CoCeO_2$(MP) and $CoCeO_2$(NP) during steam reforming of ethanol. Reprinted from ref 365. Copyright 2012 American Chemical Society.

More accurate insights on the role of oxygen mobility in Co/CeO_2 systems were provided by Noronha and co-workers, who demonstrated the correlation between a higher oxygen/OH group mobility in ceria having high surface area with the high stability of Co/CeO_2 catalysts.[366] They also proposed a mechanism of catalyst deactivation, which is dependent upon the nature of the carbon deposition and the reaction conditions.[367]

Although less attractive than cobalt, iridium has also drawn some attention as CeO_2-supported catalysts for SRE. A comparison in SRE activity by Co, Ir, and Ni on CeO_2 prepared via deposition-precipitation was carried out in the temperature range of 300−700 °C, revealing the better stability of the Ir-based species as a consequence of the strong metal−support interaction between Ir and CeO_2, which prevents sintering of the highly dispersed Ir particles.[368] In a more recent study, the influence of CeO_2 doping with PrO_x on the SRE catalysis was proved to be beneficial, thanks to the surface vacancies introduced by the PrO_x dopant.[369]

Steam reforming of bio oil derivatives is increasing in popularity for sustainability issues. However, given the complexity of the bio oil organic mixture, other oxygenated compounds have been explored mainly as model compounds for catalyst design and mechanistic studies.[370] Acetic acid was shown to lead to high rates of hydrogen evolution over ceria-zirconia-supported Rh and Ni catalysts,[371] while in a more recent study, the effects of Ni and Ce content, as well as those of the reaction temperature, steam-to-carbon ratio, and liquid hourly space velocity were screened.[372]

Recent advances in sustainability rely on the use of byproducts derived from biodiesel production, such as glycerol. One issue associated with glycerol steam reforming is the lower selectivity toward H_2 production arising from the formation of several byproduct intermediates that lead to catalyst deactivation and coke formation. However, a reported CeO_2-supported Ir (and to a less extent Co and Ni) catalyst could convert glycerol to H_2 with selectivity higher than 85%.[373] Recently, it was shown that addition of CeO_2 (and of La_2O_3) to Pt/Al_2O_3 composites reduces the acidity of the support, and in turn improves the stability of the catalyst, leading to complete conversion of glycerol to syngas at temperatures as low as 350 °C.[374] In another latest study, a nickel-ceria mixed oxide catalyst prepared by microemulsion exhibited excellent activity in glycerol steam reforming and, in contrast to standard Ni-based catalysts, largely improved long-time stability with no detected byproducts.[375] Some studies also deal with reforming of more complex and real renewable raw feedstocks, such as the steam reforming of bio-oil products (obtained from the fast pyrolysis of rice hull) over a series of Ni/CeO_2-ZrO_2 catalysts[376] or the steam reforming of palm fatty acid distilled (PFAD) and free fatty acids (palmitic, oleic, and linoleic acids) over CeO_2 and CeO_2-ZrO_2 based catalysts.[377]

7.3.1.2. Dry Reforming. The dry reforming process offers an attractive opportunity from the environmental point of view as it makes use of a greenhouse gas such CO_2 to generate syngas.

As far as fundamental dry-reforming studies by ceria-related catalysts are concerned, attention has almost exclusively been focused on methane. In the dry reforming of methane (DRM), the intrinsic higher endothermicity (in comparison with standard steam reforming) is counterbalanced by a CO-richer syngas formation, as a consequence of the accompanying reverse water-gas shift reaction (RWGS).

The study of the effect of the ceria surface area prepared by a surfactant-assisted method indicated that an increase in surface area considerably reduces thermal sintering and deactivation by carbon coke formation. Kinetic experiments are in agreement with a mechanism similar to that for the SR process and, therefore, with a rate governed by the methane adsorption step.[378] Use of ceria as dopant (8 wt %) in Ni/Al_2O_3 resulted in higher activities and stability, thanks to hindered carbon formation (Figure 22).[379] As expected, exploration of CeO_2-ZrO_2 mixed oxides as supports for DR has been a fruitful field. Small amounts of ceria (6 wt %) are sufficient to impart enhanced stability to Pt/ZrO_2 systems; the prevention of catalyst deactivation was related to the close contact between the CeO_2 and the Pt nanoparticles together with the higher oxygen mobility introduced by ceria, which accelerates gasification of coke deposited on Pt particles.[380] Comparable results were found under similar conditions using $Ru/Ce_{0.75}Zr_{0.25}O_2$.[381]

Worthy of note is the fact that nickel appears to be an interesting prospect due to its cost. As for SR, the main

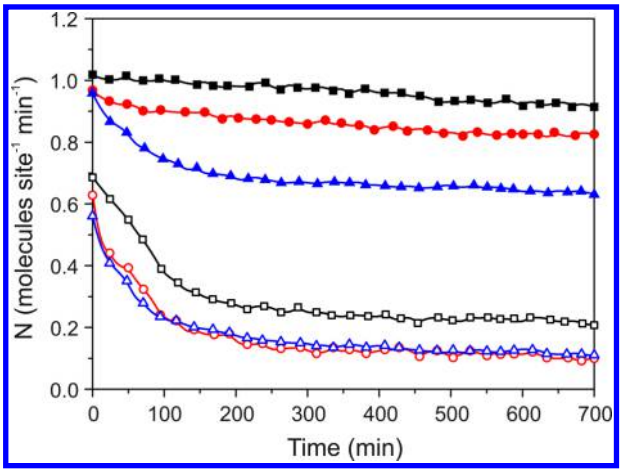

Figure 22. Dry reforming of methane at 900 °C for: Ce (8 wt%) Ni/Al_2O_3 (filled symbols) and Ni/Al_2O_3 (empty symbols); and various inlet CH_4/CO_2 ratios: 1.0:3.0 (black squares), 1.0:1.0 (red circles), 1.0:0.3 (blue triangles). Adapted with permission from ref 379. Copyright 2005 Elsevier.

drawback of Ni catalysts resides in the generally more pronounced coke deposition on the metal nanoparticles. An in-depth study on a series of catalysts based on Ni supported on several CeO_2-ZrO_2 with different Ce/Zr ratios was carried out for the DRM, and despite the complexity of the electronic alteration introduced by the zirconia could not be completely rationalized, the as-prepared materials displayed a higher activity trend for the reaction.[382] A series of Ni/CeO_2 catalysts with Ni loading ranging from 7 to 26 wt% were prepared via combustion synthesis, which allows good control of the final stoichiometry. The actual Ni phase was found to be NiO, and albeit the system had good stability and activity, some carbon nanofibers were deposited over the course of the catalysis.[383]

Bimetallic Co-Ni supported on ceria have been shown to lead to improvements in the DRM compared to the corresponding monometallic systems. Despite the larger size of the Ni-Co nanoparticles, the alloy catalyst presents a higher activity after activation with H_2 at 800 °C. Moreover, the presence of cobalt is effective in preventing coke deposition.[384] In a parallel study, the Ni-Co metal nanoparticles were dispersed on CeO_2-ZrO_2 and the effect of the variable loading of the two metals, the specific synthetic method and aging process, as well as the oxygen mobility was evaluated.[385] More recently, a Co-based catalyst, supported on CeO_2-ZrO_2, was successfully tested in DRM.[386]

Manganese was also tested as doping metal in a Co/CeO_2-ZrO_2 ensemble. It was claimed that the structural distortion induced by Mn favors the migration of the lattice oxygen and therefore the availability of oxygen on the surface and, as a consequence, leads to an enhanced activity toward the DRM.[387] However, the effective insertion of Mn into the CeO_2 lattice remains controversial, and the possibility that simple oxide mixtures Mn_2O_3-CeO_2 (in place of a real doping) are formed can also be invoked based on experimental evidence. In a report by Gorte et al., coulometric titration experiments indicated that the manganese oxide phase remains separated from the solid.[388] The open question of real doping versus simple physical oxide mixtures with CeO_2 can be extended to other metals, for which a real insertion of the metal into the CeO_2 lattice has not been unequivocally proven.

There are only very few investigations on the dry reforming of molecules other than methane by ceria-based materials, and most of them incorporate the dry-reforming process into the field of fuel cells assembly, which is discussed in a separate section. Two examples given here are the work by Noronha and co-workers, who prepared two types of Rh/CeO_2 catalysts by incipient wetness impregnation on low (14 m^2 g^{-1}) and high surface area (275 m^2 g^{-1}) ceria and tested them in the DR of ethanol. In comparison with the SR process by the same catalyst, the selectivity to CO was higher, while that to H_2 was lower due to the concomitant reverse water-gas shift reaction. When the CO_2/EtOH molar ratio was increased from 1 to 4, the stability of the catalyst turned out to be superior. In general, however, the performances were not exceptional.[389] Butane was studied as the model molecule in several syngas-producing processes, among which was dry reforming, over Rh/CeO_2-ZrO_2 catalysts to evaluate the advantages of employing a disk-shaped reactor, which appears to bring benefits in terms of both conversion and selectivity toward H_2 and CO.[390]

7.3.1.3. Autothermal Reforming. Autothermal reforming (ATR) integrates the SR with catalytic partial oxidation (CPO), and it has been proven to be a useful solution for small scale production of H_2 because of the fast start-up, small size, and a higher hydrogen purity.

Several metals supported on CeO_2 or CeO_2-based mixed oxides have been investigated as catalysts for autothermal reforming of methane (ATRM). Temperature treatments and CeO_2 loadings were correlated to the activity and stability of a Pd/CeO_2-Al_2O_3 catalytic systems for the ATRM. The performance critically depends on CeO_{2-y} species partially covering Pd, which, in addition to prohibiting CO adsorption in bridge carbonyl form, could promote coke gasification, leading to improved accessibility of the active sites to CH_4.[391] The favorable influence of La was proven in a Rh/CeO_2−ZrO_2−La_2O_3 catalyst and related to formation of "Rh−La interfacial species" which could promote catalytic activity and H_2 selectivity for ATR reactions but needed to be controlled to an optimum content of 15% in order not to compromise the amount of exposed Rh required by the catalytic process.[392] Hori et al. studied the effect of different metal promoters such as Pd, Pt, and Ag on Ni/CeO_2-ZrO_2 systems for ATRM and CPO. While the general trend rules out any change in surface areas, NiO particle size, and metal dispersion, the Ag-promoted system did exhibit higher methane conversion, explained in terms of a better redox capacity consequent to the higher CO and CO_2 desorption in CO_2 temperature-programmed desorption (TPD).[393] Recently, more insights into ATR by nanostructured nickel and other noble metals such as Pd, Pt, and Rh were provided by Ismagilov et al., who employed La_2O_3, $Ce_xGd_{1-x}O_y$, and $Ce_xZr_{1-x}O_y$ as supports and correlated the activity to the composition of the catalytic system.[394] Several other studies on ceria-zirconia-based systems have been conducted for the ATRM, including a trend evaluation of CeO_2-ZrO_2-supported platinum catalysts in relation to parameters such as reaction temperature, presence of CO_2 in the feedstock, and H_2O/CH_4 molar ratio, as well as different preparative methods. While increase of H_2O/CH_4 molar ratio has a positive influence, increase of temperature lowers the catalyst activity. Presence of CO_2 results in initial higher methane conversion, but it is associated with a lower stability of the catalyst.[395] An indirect two-step mechanism based on total combustion at lower temperatures followed by methane reforming by CO_2 or steam at higher temperature was

proposed for a Ni/CeO_2-ZrO_2 catalyst with different compositions. The catalysts were also compared with the Al_2O_3-supported analogues as well as mixed oxide supports CeO_2/Al_2O_3 and $Ce_{0.5}Zr_{0.5}O_2/Al_2O_3$, and the chief role of CeO_2-ZrO_2 was identified in providing an alternative available pathway for the adsorption and dissociation of oxygen and steam; thus, the formation of O_2^- and OH^- on the support surface aided to avoid deactivation by reacting with the carbon deposit.[396] Similarly, high activity and stability were observed for a Ni/CeO_2-ZrO_2/θ-Al_2O_3 catalyst and were attributed to the formation of stable NiO_x species rather than free NiO or inactive $NiAl_2O_4$ favored by a CeO_2-ZrO_2 layer precoated on θ-Al_2O_3.[397]

Hydrocarbons other than methane received less although decent attention. A ceria-supported Pt catalyst prepared by combustion method exhibited good stability over several hours for the oxidative steam reforming of propane; the activity was shown to be critically dependent upon the O_2:C_3H_8 and H_2O:C_3H_8 ratios of the feed.[398] CeO_2 was also tested as an additive in the Pt/Al_2O_3 catalyst for the ATR of diesel surrogates, resulting in the inhibition of the formation of the α-phase of the Al_2O_3 substrate and thus improved performances.[399]

Tolerance to sulfur is an important factor to be considered for the design of market-oriented catalysts. A series of Pt/CeO_2–Al_2O_3 catalysts doped with Gd_2O_3 (from 0.8 wt % to 4 wt %) were prepared by stepwise incipient wetness impregnation (IWI) method and employed in the ATR of sulfur-containing (158–500 ppm) gasoline, exhibiting promising performances depending on the preparation method.[400] Bimetallic Rh-Pt supported on several types of supports, among which was CeO_2, were investigated as catalysts for the ATR of low-sulfur diesel fuels, and the authors established an order of conversion RhPt/SiO_2 < RhPt/TiO_2 < RhPt/Al_2O_3 < RhPt/CeO_2 (17.5 wt %)–ZrO_2 (1 wt % Pt and Rh loading), with ceria-zirconia reaching up to 98%, with such activity related to the ability of the support to provide higher reducibility of RhO_x species and better Rh and Pt dispersion.[401]

Iso-octane was investigated as fuel for the ATR catalyzed by Ni-based catalysts in relation to the effect of metal nanoparticle size in the presence of sulfur[402] and the influence of thiophene in the ATR process,[403] while a highly active quaternary RuO–NiO–CeO_2–Al_2O_3 xerogel catalyst prepared by the sol–gel method was lately reported for the ATR of *n*-dodecane.[404]

CeO_2 has been shown to be a good promoter for the ATR of methanol (ATRMe) when incorporated into a Cu/Al_2O_3 catalyst, increasing the metal dispersion and surface area, as well as lowering the temperature of catalyst reduction.[405] On the other hand, Ni-impregnated CeO_2-ZrO_2 supports of different compositions were tested, with activity reaching highest values for Ce-rich materials.[406] Three different CeO_2 washcoats mixed with ZnO-CuO and supported on porous alumina for the ATRMe exhibited a strong Cu-CeO_2 interaction which led to formation of Cu-O-Ce bridges and was held responsible for the high activity.[407]

A comparison between SR, CPO, and ATR processes for H_2 production from ethanol was carried out using a Pt/$Ce_{0.75}Zr_{0.25}O_2$ catalyst; at low temperature, autothermal conditions, under which ethanol decomposition was inhibited, resulted in more efficient conversions, although a lower selectivity toward H_2 was observed. Improved activity also in terms of selectivity was observed at higher temperature. A mechanism based on two different pathways, in which the role of the support as oxygen buffer was clearly confirmed by diffuse reflectance infrared fourier transform spectroscopy (DRIFTS) analyses, was proposed.[408]

The superior behavior of CeO_2-ZrO_2 supports was also recently proved in the ATR of biobutanol raw mixture (butanol/acetone/ethanol = 6/3/1 mass ratio) by bimetallic Co-Ir . The order of performances with different supports was shown to follow the order of OSC and reducibility of the catalyst: CoIr/CeO_2-ZrO_2 > CoIr/ZnO > CoIr/TiO_2.[409]

Autothermal reforming of ethanol (ATRE) was investigated on a Al_2O_3-supported Ni catalyst promoted by $Ce_{0.5}Zr_{0.5}O_2$, which other than enhancing activity by reducing the Ni particle size and dispersion, is crucial to increase the number of surface oxygen species and decrease coke formation.[410]

The addition of CeO_2 to Rh/Al_2O_3 considerably enhanced methanol, ethylene glycol, and glycerol conversion during ATR, with selectivity to H_2 near to the equilibrium, chiefly due to an increase of the surface oxidation rates.[411] The concept of "hydrogen economy" had been exploited by the same group in a milestone work in which ethanol could be directly converted into H_2 simply and with high efficiency (~100% selectivity and > 95% conversion) under ATR conditions using Rh-ceria on a ceramic foam made of low-area alumina or alumina spheres.[412]

7.3.2. Water-Gas Shift Reaction and Preferential Oxidation of CO. From the industrial point-of-view, processes like Fischer–Tropsch synthesis, methanol synthesis, or hydroformylation require well-defined $H_2/CO/CO_2$ ratios to be efficiently operative. For this reason, after being produced, the H_2/CO ratio in the syn-gas must be adjusted to the desired value. On the other hand, in order to be used for ammonia synthesis, for hydrogenation reactions or as possible energy vector in combination with PEMFC, H_2 must contain very low amounts of CO (sometimes below 10 ppm), to avoid poisoning of the various catalysts employed.

The most promising process to purify H_2 stream from CO appears to be a combination of the water gas shift reaction (WGSR) and the preferential oxidation (PROX) of residual CO, in the presence of an excess of H_2, using O_2.[413]

It is important to underline that the WGSR is an exothermic reaction (ΔH^0_{298} = −41 kJ mol^{-1}), and that the equilibrium constant decreases with increasing temperature. Hence, the CO concentration is essentially dictated by the thermodynamic of the reaction at the temperature of the exit of the reactor, and, in order to obtain a high CO removal, the temperature should be as low as possible. The WGSR is usually performed in two consecutive stages: a high-temperature (HT-WGSR, operative between 300 and 450 °C and a low-temperature stage (LT-WGSR, operative between 200 and 300 °C). The HT-WGSR is commonly catalyzed by Fe_2O_3-Cr_2O_3, while the LT-WGSR usually involves Cu/ZnO catalysts. Moreover, the CO oxidation in the final PROX step requires the development of highly selective catalysts, able to promote the removal of CO without a significant loss of H_2.

CeO_2-based catalysts appear to be particularly useful for LT-WGSR and PROX. However, reports are available in which HT-WGSR has been explored. For example, the effect of the preparation method for a Ni:Cu (1:1 mol)/CeO_2 catalyst was determined for the HT-WGSR, indicating the evaporation-induced self-assembly method as the most favorable one.[414] On the other hand, the effect of chlorine was investigated in the PROX by Pt/CeO_2 using two different metal precursors, namely $(Pt(NH_3)_4))(NO_3)_2$ and H_2PtCl_6, and it was established that for low temperature PROX, the chlorine-free

catalyst could perform better.[415] In general, many noble and non-noble metals supported on pure or doped CeO_2 function as active catalysts for H_2 purification. Among them, Pt, Au, and Cu represent certainly the most promising systems and therefore are the most studied in detail.[416,417]

Two reaction mechanisms have been proposed for CeO_2-based catalysts under WGSR or PROX conditions:

•*Formate Route.* The reaction involves the formation of OH groups on Ce ions, which react with CO to form formates. CO_2 and/or H_2 are produced by decomposition of the intermediate species (formates or carbonates adsorbed on the oxide surface). The role of the metal is to allow the adsorption of CO and to promote the cleavage of the C−H bond of formate.[418,419]

•*Redox Route.* Reactive oxygen atoms are transferred from the support to the metal particles, leading to oxygen vacancies on the support surface. Active oxygen reacts with CO adsorbed on the metal particles producing CO_2, while H_2O or O_2 restore surface oxide anions, producing H_2.[102,420−423]

Some variations from the above main mechanisms have also been proposed based on DFT or microkinetic modeling, in particular, when Pt is used as a catalyst. In such alternative mechanisms, the rate-determining step is the formation of a COOH species, with the formate acting mainly as the spectator,[424,425] with the CO reacting with OH rather than water.[426]

Going back to the two main mechanisms, the effective occurrence of the formate mechanism on WGSR catalysts was reviewed a few years ago by Burch and co-workers,[427] highlighting that formate could be the main reaction intermediate only for the catalysts with lower activity (for example, 0.2% Rh/CeO_2 reported by Shido and Iwasawa).[419] In the case of catalysts with high catalytic activity (such as Au/CeO_2-La_2O_3,[428] Pt/CeO_2,[429] and $Au/CeZrO_4$[429]) and of interest for current fuel cell applications, the major contribution of a formate mechanism was not proven, since the formate decomposition rate calculated from IR data accounts for less than 10−15% of the total WGS reaction rate. Moreover, DRIFTS and near ambient pressure-XPS indicated that formates seem not necessarily involved in the main reaction path, at least for Cu- and Pt-based catalysts.[430,431] Recently, using a combination of in situ and operando techniques, Rodriguez et al. showed that both metal (Cu, Au, and Pt) and the oxide support (CeO_2 and CeO_2-TiO_2) undergo important modifications during WGSR. XRD, EXAFS, and pair distribution function (PDF) analyses evidenced the partial reduction of the support, favoring H_2O dissociation that is not active on the metal alone.[430] Key issues still need to be addressed to understand possible reorganization of the surface during catalysis, the nature of the active sites for H_2O activation and the atomic arrangements required to facilitate the formation of intermediates, such as carboxylic groups (HOCO), formates (HCOO), or carbonates. Particular interest should be devoted in developing multitechnique experiments to investigate structural, morphological, and electronic properties of the catalysts and the nature of adsorbates during WGSR.[430]

Pt/CeO_2 catalysts demonstrated promising performance under realistic WGSR conditions (presence of H_2 and CO_2 in the reaction mixture), although they suffer from deactivation by carbonate deposition during start−stop operation.[432] This disadvantage can be limited by doping ZrO_2 in CeO_2, although Pt sintering is observed in this case.[433] WGSR on $Pt/Ce_xZr_{1-x}O_2$ proceeds mainly via the redox mechanism, with activity dependent on reaction temperature, support composition (Ce/Zr ratio), and Pt particle size.[434] Efstathiou and co-workers extensively studied the activity and the mechanism of WGSR on Pt supported on La-doped CeO_2: the best activity was observed for $Ce_{0.8}La_{0.2}O_{2-\delta}$, which had the highest OSC in the 250−550 °C range.[435] Steady state isotopic transient kinetic analysis (SSITKA)-DRIFT and transient isothermal response experiments suggest that WGSR can proceed through both a "redox mechanism" and an "associative formate with −OH regeneration" mechanism.[436]

Pt-based catalysts for WGSR often promote CO methanation, with a considerable loss of H_2 and the production of an undesired byproduct. CH_4 formation can be suppressed by engineering the catalyst at the nanoscale level. "Pt-in-ceria" catalysts prepared by a microemulsion approach to maximize the metal−support interaction, resulted in suppression of CH_4 production.[437]

Au/CeO_2 represents one of the most promising systems studied for H_2 purification, although many aspects are still to be clarified. In particular, the real form of Au particles (size and/or charge) under working conditions is still unclear. Au nanoparticles (less than 5 nm in size)[438,439] or cationic/partially positive gold species ($Au^{\delta+}$)[440−442] are candidates as active phase in Au/CeO_2 catalysts. Other than the nature of the metal phase, the electronic interaction of the metal nanoparticles with the CeO_2 surface (i.e., electron transfer from a reduced ceria to a metal) represents a critical point to obtain active and selective catalysts. When metallic gold clusters are in intimate contact with the CeO_2-based support, the Au atoms at the interface with the support would be expected to carry a small positive charge ($Au^{\delta+}$),[441] providing the active sites for the WGSR. On the other hand, the active sites for the WGSR were reported as involving pure gold nanoparticles in contact with oxygen vacancies.[248,443] Moreover, the activity for the WGSR was strongly related to the morphology at the nanoscale level (e.g., different geometry and exposed crystal planes).[444]

Au-based catalysts have been investigated on a large variety of CeO_2-containing supports as solid solutions or composite materials, including CeO_2-Al_2O_3,[445,446] CeO_2-Fe_2O_3,[447,448] CeO_2-MnO_2,[448] CeO_2-SnO_2,[448] CeO_2-Ga_2O_3,[449] CeO_2-RE_2O_3 (RE = La, Sm, Gd, Yb, Y),[428,450−454] CeO_2-TiO_2,[455−458] and CeO_2-ZrO_2.[429,441,459,460] In most cases, the promotional effect is not dramatic, and the activity is mainly dependent on the preparation method, as exemplified by the work of Tabakova and co-workers.[448]

The situation for Cu/CeO_2 catalysts is very similar. Cu is usually present, in the as-prepared catalysts, as CuO entities. In one example, a series of CuO/CeO_2 catalysts were prepared and tested in the WGSR, with activity strongly influenced by the amount of surface oxygen vacancies.[461] Other authors proposed that metallic Cu interacts in a complex fashion with CeO_2 oxygen vacancies, with water dissociation occurring at the interface between Cu and O vacancies.[462,463] Moreover, the activity of Cu/CeO_2 catalysts can be increased by doping of the support with ZrO_2.[464] Addition of Cu to Ni/CeO_2 catalysts also suppresses CH_4 production thanks to the formation of Ni-Cu alloyed particles.[465]

CO oxidation and, in particular, PROX have been widely studied on CeO_2-supported catalysts. By precisely controlling the size of metal nanoparticles supported on CeO_2, Cargnello et al. clearly demonstrated that the active sites for CO oxidation on Pt/CeO_2, Pd/CeO_2, and Ni/CeO_2 are peripheral metal atoms in contact with CeO_2.[255]

Also in the case of PROX, Pt, Au, and Cu gave the best performance when supported on CeO_2-based oxides.[417,466] The poor selectivity of Pd/CeO_2 compared to Pt/CeO_2 has been related to the formation of Pd β-hydride, which rapidly reacts with activated oxygen (from the gas phase or from the CeO_2 support) forming H_2O and decreasing the selectivity of the process.[467] "Ir-in-ceria" catalysts prepared following a coprecipitation (CP) method showed good activity and selectivity to CO_2 compared to reference materials prepared by deposition-precipitation (DP), even if CO conversion was lower than that which is reported for the most active metals (Figure 23).[468]

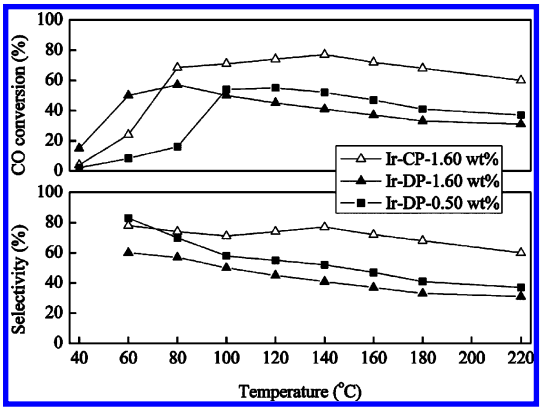

Figure 23. CO conversion and selectivity to CO_2 as a function of reaction temperature in the PROX reaction over 100 mg of the coprecipitated Ir-CeO_2 catalyst (Ir-CP-1.60 wt %) and Ir-CeO_2 catalysts prepared by deposition-precipitation (Ir-DP-1.60 wt % and Ir-DP-0.50 wt %). Reacting gas composition: $CO/O_2/He/H_2$ = 2/1/57/40 (vol %); gas hourly space velocity (GHSV) = 40000 mL h^{-1} g^{-1}. Reproduced with permission from ref 468. Copyright 2008 Elsevier.

CeO_2-based materials are fundamental to promote the activity and to control the reaction mechanism of Pt-based catalysts for the PROX process.[423,469−473] The mechanism of preferential CO oxidation through activated oxygen from CeO_2 has been clearly demonstrated,[470,471] as well as the detrimental effect on the CO oxidation activity by residual chlorides through blocking of oxygen vacancies and hindering O mobility at the Pt-CeO_2 interface.[415,423] Selectivity of Pt/CeO_2 to CO oxidation in the PROX process has been interpreted by a change in the reaction mechanism depending on CO coverage on Pt nanoparticles: at high coverage, reaction proceeds through a Mars-van Krevelen mechanism, while, at low coverage, a Langmuir−Hinshelwood mechanism is operative.[472] CO coverage on Pt is controlled mainly by the CO/O_2 ratio and, at low CO coverage, H_2 oxidation takes place to a considerable extent, decreasing the selectivity of the process.[472] Again, CO oxidation rates well-correlate with the interfacial Pt length, accounting for the importance of the Pt-O-Ce bonds formed at the interface between Pt and CeO_2 for the redox activity.[472] Gao et al. studied the effect of CeO_2 morphology on the CO oxidation in the PROX reaction.[473] The activity order of Pt/CeO_2 was nanorods > cubes > octahedra, in parallel with reducibility of materials and concentration of oxygen vacancies.[473]

Au/CeO_2 catalysts exhibit peculiar properties in the PROX process. The control of the particle size of CeO_2 support is important as well as the control of the dimension of Au nanoparticles. Carrettin et al.[474] evidenced that specific rate of CO oxidation on Au nanoparticles deposited on nanocrystalline CeO_2 is two orders of magnitude higher than that of a catalyst prepared using conventional precipitation. This is reasonably explained in terms of the strong electronic interaction between the two components, at the interface of which CO is adsorbed on Au atoms in close proxmity to highly defective CeO_2 able to activate O_2.[474] With the aim of maximizing Au-CeO_2 electronic interaction (i.e., the possibility of an electron transfer from partially reduced ceria to the metal) and of preventing sintering of Au nanoparticles, Au@CeO_2 catalysts which showed good activity and selectivity as well as remarkable stability under PROX conditions were prepared. The observed deactivation was fully reversible and assigned to carbonate deposition on the active sites.[475] Similarly to Pt/CeO_2, the morphology of CeO_2 in Au/CeO_2 has a peculiar effect on CO oxidation activity, in the order: nanorods > polyhedra > nanocubes.[476,477] Three different synthetic protocols, namely solvated metal atom dispersion (SMAD), deposition-precipitation, and coprecipitation methods were used for the preparation of Au/CeO_2 catalysts for CO oxidation, with the SMAD method turning out to be the most efficient. Rather than being related to the small gold particles obtained via SMAD, the highest activity was due to the strong interaction between ionic gold and ceria, which also enhanced the ceria surface oxygen reducibility.[478]

Among nanocomposite materials, CeO_2 shows a beneficial effect when added to Au/Al_2O_3,[479,480] Au/SiO_2,[481] Au/Co_3O_4,[482−484] and Au-TiO_2.[485] CeO_2 doped with many different cations has been tested for the PROX reaction, including Zr,[486] Fe,[486−490] Zn,[486,491,492] Mn,[487,493] and RE (RE = La, Sm, Gd, and Y).[491,492,494] Also in the case of the PROX reaction, the preparation method of the CeO_2-based support and the technique adopted for the deposition of Au nanoparticles strongly influence the catalytic activity.

Concerning Cu/CeO_2 catalysts, a partial reduction of Cu(II) at the interface CuO-CeO_2 is observed, and the CO conversion well fits with the intensity of the Cu(I)-CO band of IR spectra.[495,496] In-situ XAFS spectroscopy evidenced that partially reduced CuO entities are present when CO oxidation is predominant, while at higher temperature, full reduction of CuO to Cu is responsible for H_2 oxidation.[495,496]

The morphology and the exposed faces of CeO_2 particles also influence the performance of the catalysts. CuO/CeO_2-nanocubes, exposing mainly (100) faces, are more selective in PROX of CO compared to CuO/CeO_2-nanorods and CuO/CeO_2-nanospheres, exposing mainly (111) faces, although the latter catalysts are slightly more active.[497,498] This is due to the strong electronic interaction of CuO entities with CeO_2 (100) faces, resulting in a more difficult reduction of copper to the zerovalent state.[497,498] The successful dispersion of the CuO component within CeO_2 is also an important parameter. Recently, very homogeneous dispersions of CuO_x clusters up to 10% loading on CeO_2 nanorods surface was achieved via deposition-precipitation methods, resulting in excellent activity.[499]

Considering the low cost of Cu-based catalysts, CuO/CeO_2 composites have been prepared in a wide range of compositions, investigating also materials with a high CuO content, the so-called "inverse" CeO_2/CuO catalysts.[500,501] In this type of catalyst, an improvement in CO_2 selectivity is observed when doping ZnO into CuO phase, as a result of the stabilization of CuO against reduction, which in turn enables to extend the temperature window of the catalysts.[502]

Table 2. Most Relevant Results from Studies on Methane Catalytic Combustion

catalyst	preparation method[a]	BET surface area ($m^2\ g^{-1}$)	GHSV ($mL\ g^{-1}\ h^{-1}$)	methane concentration	T_{50}[b] (°C)	ref
$Ce_{0.75}Zr_{0.25}O_2$, calcined at 500 °C	S-G	108.4	60000	2%	545	542
CeO_2 calcined at 500 °C		101.6			675	
ZrO_2 calcined at 500 °C		79.0			721	
$Ce_{0.75}Zr_{0.25}O_2$, calcined at 900 °C		9.2			625	
CeO_2 calcined at 900 °C		4.6			750	
ZrO_2 calcined at 900 °C		12.2			>750	
5 wt % Cu/CeO_2	hydrothermal	22.6	27000	1%	540	543
	S-G	43.8			525	
	TD	68.7			490	
1 wt % Cu/CeO_2	TD	68.7	54000		540	
$Ce_{0.85}Cu_{0.1}Ca_{0.05}O_{2-\delta}$	citric acid complexation-combustion	31.3	30000	1%	478	544
$Ce_{0.9}Cu_{0.1}O_{2-\delta}$		38.9			538	
Co_3O_4-CeO_2	CP	31	60000	0.3%	471	545
CeO_2	S-G	9	13500	0.2%	600	546
Ce(0.6)-La-O	S-G	52.4			505	
CeO_2 flowerlike microspheres (FM)	modified DP	181.4	30000	1%	550	547
La-doped-CeO_2 FM		97.4			525	
10 wt % CeO_2-Mg-Al-oxide	CP	52	16000	1%	561	548
CeO_2		16			635	
Mg-Al-oxide		188			725	
2 wt% $Pt/Ce_{0.67}Zr_{0.33}O_2$	IMP of support, prepared by CP	79	12800	1%	300	536
2 wt% $Pd/Ce_{0.67}Zr_{0.33}O_2$		77			320	
$Pd@CeO_2/SiO_2$-Al_2O_3	bottom-up synthesis	100	200000	0.5%	350	221

[a]CP = coprecipitation, IMP = impregnation, DP = deposition precipitation, MCD = metallic colloid dispersion, TD = thermal decomposition, and S-G = sol−gel. [b]Light-off temperature at which conversion of methane is 50%.

Nanocomposites comprising CuO/CeO_2 active phase have been prepared using Al_2O_3,[503,504] Al-pillared clay,[505] ZrO_2,[503,504] SiO_2,[504,506−508] TiO_2,[503] MnO_2,[503] Co_3O_4,[509] or MWCNT[510] as supports, showing moderate improvements of the performance in comparison with CuO/CeO_2 materials.

An increase in CO conversion is observed on Cu-based catalysts supported on CeO_2-ZrO_2, although the extent of the promotional effect depends on the Cu loading.[511−513] Promotion in activity of CuO/CeO_2 has been reported also for ceria doped with MnO_2,[514−516] TiO_2,[517] Tb_4O_7,[518] and PrO_x,[518] while La_2O_3 doping has a detrimental effect on the activity,[518] although differences among the various dopants are significantly reduced in the presence of H_2O and CO_2 in the reaction feed.[518]

Finally, CeO_2 was used as support for bimetallic catalysts comprising various combinations of Pt, Au, and Cu. Pt-Au/CeO_2 displayed the best catalytic performance compared to the correspondent monometallic catalysts.[519,520] Pt-Cu/CeO_2 catalysts have been prepared by a radiolytic process, and the resulting strong contact between Pt and CuO_x entities led to the formation of new active sites, responsible for a decrease of light-off temperature and an increase of CO_2 selectivity, widening the operative temperature window of the catalysts.[521−525] Au, added by incipient wetness impregnation, acts as a promoter for CuO/CeO_2, even if the particle size of Au was quite large (20−40 nm).[526] A reduction treatment in H_2, resulting in the formation of Au-Cu alloy nanoparticles, increases the performance of Au-Cu/CeO_2 catalysts compared to the parent monometallic materials, regardless of the Au/Cu molar ratio.[527]

7.3.3. Oxidation of Volatile Organic Compounds (VOC). Ceria and ceria-based materials are efficient catalysts for VOCs catalytic combustion (and in general for refractory organic pollutants in industrial wastewaters), thanks to their excellent reducibility and OSC.[528,529] The reaction is considered to follow a Mars-van Krevelen type mechanism, in which ceria supplies oxygen to the reaction and it is reoxidized by gas phase oxygen.[530−532] When ceria is used as high surface area support for noble metals (Pd, Pt, and Au), the catalytic systems are particularly active at low temperature, due to the increased metal dispersion and to CeO_2 participation into the reaction.[528,533−538] An extensive and detailed review on Au-based catalysts for VOCs abatement was recently published by Scirè and Liotta.[539]

Methane (CH_4) is the most difficult VOC to be oxidized and represents an environmental hazard due to its global warming effect and ozone depletion potential.[540,541] Methane combustion over metal free and metal-doped ceria based materials has been deeply investigated as summarized in Table 2. However, the dramatic influence of the GHSV on the light-off temperature makes a proper comparison difficult. The catalytic performances are mostly related to the ability of the systems to release lattice oxygen. Pure ceria or mixed oxides show medium-high temperature methane conversion, while metal-doped systems have significantly lower conversion temperatures. The methane oxidation activity of CeO_2-ZrO_2 solid solution prepared via urea hydrolysis was found to be dependent on the Ce:Zr ratio, with a maximum activity for the $Ce_{0.75}Zr_{0.25}O_2$ composition and a gradual decrease in activity with increasing Zr concentration, as a result of the phase separation and modification of redox properties. Despite the usually good thermal stability of these materials,[99,261] a general deactivation of the catalysts during light off experiments was observed.[542]

In one study, the presence of a strong electronic interaction between Co_3O_4 and CeO_2 (i.e., electron transfer) led to enhanced redox properties and improved methane oxidation.[545] Similarly, when CuO/CeO_2 catalysts were employed, it turned out that optimization of the CuO dispersion, metal loading, and its electronic interaction with ceria led to enhancement of the catalytic activity. Despite the promising performances, presence of H_2O caused a remarkable decrease in activity.[543] The incorporation of Ca in $Ce_{0.9-x}Cu_{0.1}Ca_xO_{2-y}$ solid solutions also favored the formation of oxygen vacancies; although a remarkable enhancement of the catalytic performance was obtained, a loss of activity over time was observed, due to the Ca migration to the surface with consequent formation of calcium carbonate species.[544]

La−Ce−O mixed oxides were also explored, resulting in a general improvement of the reducibility of ceria, together with increased production of oxygen vacancies and surface superoxide ions. It was noted that when the ratio Ce/(Ce + La) was maintained in the range from 1.0 to 0.2, significantly smaller crystal sizes were generated as a result of the formation of $La_xCe_{1-x}O_{2-x/2}$ solid solutions.[546] Similarly, a boost of activity was observed when testing the methane combustion over flowerlike mesoporous microspheres made of $La_xCe_{1-x}O_{2-x/2}$ or $Pr_xCe_{1-x}O_{2-x/2}$ as a result of the more pronounced production of oxygen vacancies and improved oxygen mobility.[547]

Noble metal (NM)-based catalysts, and Pd-based catalysts in particular, show significantly superior performances.[549] Pd oxidation to PdO and PdO decomposition to Pd during methane combustion are very important for the catalytic activity because of the different specific activity of Pd and PdO. The cycling between the two phases depends on many factors, among which the temperature of the catalyst, the oxygen partial pressure, and the support are especially relevant.[537,550] CeO_2 considerably speeds up the Pd reoxidation to PdO, thus reducing the characteristic Pd-PdO hysteresis.[537] Nevertheless, anticipated reoxidation threshold is not enough to enhance catalytic activity, since also PrO_x, La_2O_3, and Tb_4O_7 promote Pd reoxidation, but their effect on activity loss is almost negligible. This confirms the complexity of the role of support on Pd reoxidation, which involves both direct surface interaction, as for ceria-doped catalyst, and indirect control of Pd dispersion, as for Pd supported on zirconia. PrO_x, La_2O_3, Tb_4O_7, and CeO_2-ZrO_2 as well as bare ZrO_2 supports all promote the onset of Pd oxidation upon cooling compared to Pd supported on alumina, with higher oxidation rates for Pd supported on CeO_2-Al_2O_3 and ZrO_2.[538]

An ordered and stable Pd-O-Ce surface superstructure was revealed by DFT calculations on the basis of HR-TEM data on one-step solution combustion synthesis (SCS) of Pd/CeO_2 catalysts (Figure 24). When compared with samples prepared by IWI, the T_{50} temperature for SCS catalysts was lower, with full conversion occurring already at about 100 °C lower temperature. Furthermore, no deactivation was observed after repeated combustion cycles or after aging up to 15 h at 900 °C in all samples investigated.[551]

As revealed by XPS analysis of model Pt/CeO_2 catalysts and recent calculations, CeO_2-NM oxygen transfer requires nanometric contact between the two phases to occur.[254] Optimized contact leads in general to better catalytic performances. For instance, methane complete oxidation was obtained at temperatures lower than 400 °C over nanostructured Pd@CeO_2 catalysts (composed of a Pd nanoparticle core surrounded by a porous CeO_2 shell) deposited on a modified γ-Al_2O_3 support (Figure 25). The remarkably high activity of the core−shell catalysts was rationalized in terms of thermal stabilization of Pd nanoparticles against sintering and optimal contact between Pd and CeO_2, ensured by the bottom-up synthetic approach, which facilitates oxygen transfer from CeO_2 to the active phase.[221]

A main drawback in the use of Pd-based catalysts is their susceptibility to water and sulfur poisoning, which can cause severe and in most cases irreversible deactivation of the catalysts under real conditions.[552−554] Quantitative measurements indicate that $Pd/CeO_2/Al_2O_3$ adsorbs less SO_2 than Pd/Al_2O_3 catalysts under reaction conditions. However, both catalysts are strongly deactivated by SO_2.[550] The addition of Pt

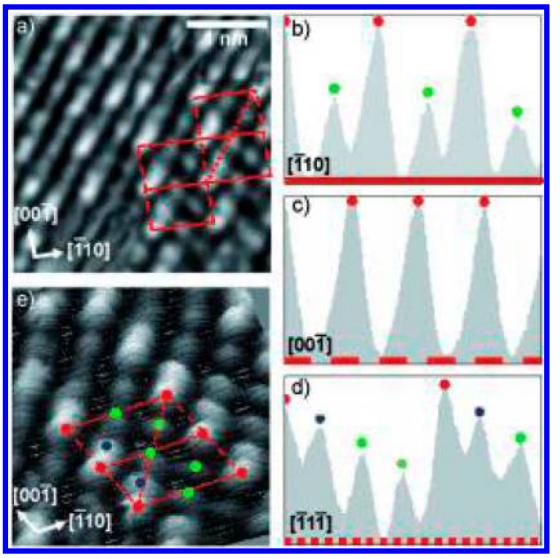

Figure 24. Profile line analysis of the periodic Pd-O-Ce superstructure. (a) HRTEM image of the superstructure. (b−d) Profile line analysis for one of the samples (sample SCS2). All line profiles shown in (b−d) span a distance of 2.2 nm. Colored circles correspond to the atomic rows marked in the computed 3D image shown in (e). Reproduced with permission from ref 551. Copyright 2009 Wiley-VCH.

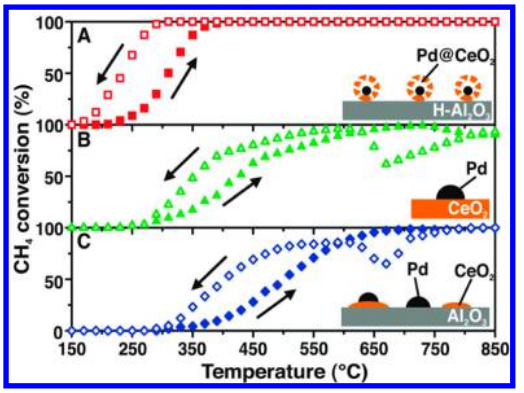

Figure 25. Heating and cooling (10 °C min^{-1}) light-off curves of CH_4 conversion against the temperature for the three catalyst formulations used. (A) Pd@CeO_2/hydrophobic Al_2O_3 (H-Al_2O_3) core−shell catalyst, (B) Pd/CeO_2 prepared by incipient wetness impregnation, and (C) $Pd/CeO_2/Al_2O_3$ prepared by coimpregnation of Pd and Ce precursors. Reproduced with permission from ref 221. Copyright 2012 AAAS.

Table 3. Most Relevant Results from Studies on Non-Methane VOC Catalytic Combustion

catalyst	preparation method[a]	BET surface area (m^2 g^{-1})	VOC	GHSV (mL g^{-1} h^{-1})	VOC concentration	T_{50}[b] (°C)	ref
CeO_2	S-G	3	toluene	200000	1000 ppm	430	528
		28				275	
		32				270	
		55				245	
5 wt % CeO_2/Al_2O_3	IMP	161				425	
90 wt % CeO_2/Al_2O_3		82				250	
5 wt % CeO_2/Al_2O_3	IMP	156	toluene	54000	1400 ppm	275	558
$Ce_{0.9}Zr_{0.1}O_2$	S-G	56	toluene	20000	1000 ppm	221	559
			ethanol		1000 ppm	207	
CeO_2	citric acid complexation	23	benzene	60000	1700 ppm	526	560
$Ce_{0.9}Zr_{0.1}O_2$		37				445	
$Ce_{0.7}Zr_{0.3}O_2$		28				479	
$LaCoO_3$		11.3				330	
20 wt % $LaCoO_3/CeO_2$		15.7				337	
20 wt % $LaCoO_3/Ce_{0.9}Zr_{0.1}O_2$		22.7				333	
20 wt% $LaCoO_3$/ $Ce_{0.7}Zr_{0.3}O_2$		15.1				355	
CeO_2	citric acid complexation	23	toluene	60000	1700 ppm	380	560
$Ce_{0.9}Zr_{0.1}O_2$		37				295	
$Ce_{0.7}Zr_{0.3}O_2$		28				310	
$LaCoO_3$		11.3				244	
20 wt % $LaCoO_3/CeO_2$		15.7				218	
20 wt % $LaCoO_3/Ce_{0.9}Zr_{0.1}O_2$		22.7				192	
20 wt % $LaCoO_3/Ce_{0.7}Zr_{0.3}O_2$		15.1				240	
CuO-CeO_2/γ-Al_2O_3	IMP	156	propane	2300	5.9%	350	561
$Cu_{0.13}Ce_{0.87}O_2$	combustion	27	acetone	60000	1000 ppm	200	562
MnO_x-CeO_2	S-G	22.2	formaldehyde		580 ppm	160	532
	CP	126.3				140	
	modified CP	124.0				90	
MnO_x-CeO_2	modified CP	124	benzene	30000	200 ppm	260	532
Cu/MnO_x-CeO_2	modified CP	118	benzene			200	
3 wt % Ag/MnO_x-CeO_2	DP	124.0	formaldehyde	30000	580 ppm	70	563
3 wt % Pt/MnO_x-CeO_2	IMP	124.0	formaldehyde	30000	580 ppm	20	564
0.5 wt % Pt/CeO_2	IMP	3	toluene	200000	1000 ppm	180	528
1.5 wt % Au/CeO_2	DP	79	propene	35000	1000 ppm	230	533
			toluene	35000	1000 ppm	293	
0.25 wt % Pt/23 wt % CeO_2/Al_2O_3	S-G	95	acetic acid	30000	1000 ppm	175	534
	S-G	3	*n*-butanol	200000	1000 ppm	430	

[a]CP = coprecipitation, IMP = impregnation, DP = deposition precipitation, MCD = metallic colloid dispersion, TD = thermal decomposition, and S-G = sol−gel. [b]Light-off temperature at which conversion of VOC is 50%.

to the formulation of the catalyst leads to increased resistance to both water and SO_2 poisoning.[555,556]

Pt catalysts are also active for methane combustion, but their activity is generally lower than that of Pd.[557] In a series of Pt/$Ce_{1-x}Zr_xO_2$ catalysts with various compositions, $Ce_{0.67}Zr_{0.33}O_2$ exhibited the best thermal stability, the highest oxygen mobility, and the best catalytic activity after aging at 1000 °C. Furthermore, the fresh Pt/$Ce_{0.67}Zr_{0.33}O_2$ catalyst was much more active than the corresponding Pt/Al_2O_3, although a deactivation on stream was observed in the 200−500 °C temperature range, and the promoting effect disappeared after aging at 1000 °C.[535]

The time on stream deactivation was associated with a gradual oxidation of the catalysts, whereas a reduction at 300 °C strongly activates the solids. After the reduction, a large amount of oxygen vacancies were introduced on both Pd- and Pt-based catalysts supported on $Ce_{0.67}Zr_{0.33}O_2$, thus favoring activity because of an electron transfer to the noble metals and an improvement of the lattice oxygen mobility. Consistently, the observed time-on-stream deactivation was accompanied by the slow filling of these vacancies.[536]

Table 3 reports a selection of ceria-based materials investigated for non-methane VOC (NMVOCs) combustion.

Pure CeO_2 catalytic performances depend mostly on the specific surface area and the crystallites size of the oxide,[528] that in turn are affected, for example, by the preparation conditions,[528,565] the calcination temperature,[528] and by the particular VOC chosen as reactant. The presence of defects and the nanostructure of CeO_2 also influence the reducibility of the oxide.[566] As for applications which have been previously mentioned, the modification of ceria with other metal oxides can enhance the catalytic performances of the material in terms of thermal stability, redox properties, and oxygen mobility. Once again, CeO_2-ZrO_2 catalysts have been widely investigated

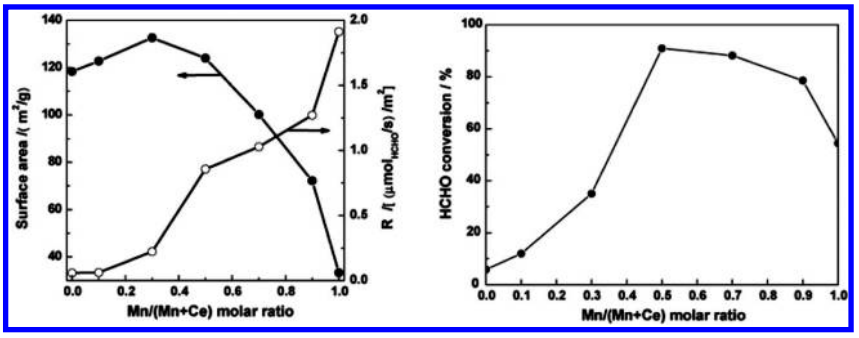

Figure 26. (Left) Surface area (●) and specific activity (○) vs Mn/(Mn+Ce). (Right) Formaldehyde conversion at 90 °C over MnO_x–CeO_2 (HCHO = 580 ppm, O_2 = 20.0 vol %, He balance, GHSV = 30000 mL g^{-1} h^{-1}). Reprinted with permission from ref 564. Copyright 2008 Elsevier.

for the oxidation of VOCs, chlorinated VOCs, and methane oxidation.[567−569]

$Ce_{1-x}Zr_xO_2$ (x = 0−0.3) have been studied as catalysts and as supports for $LaCoO_3$ perovskites in the catalytic combustion of benzene and toluene. $Ce_{1-x}Zr_xO_2$ were all more active than pure CeO_2 in the combustion of benzene and toluene, with a shift to almost 100 °C lower values of the light-off temperature corresponding to 50% of conversion (T_{50}) for $Ce_{0.9}Zr_{0.1}O_2$ catalyst.[560] $Cu_xCe_{1-x}O_{2-y}$ (x = 0.06, 0.13, and 0.23) catalysts prepared by combustion method were studied for the catalytic combustion of acetone. The activity was dependent on the catalyst composition which determines the presence of different CuO species, as revealed by XPS analysis. Among the three catalysts, $Cu_{0.13}Ce_{0.87}O_y$ was found to be the most active. Pulse reaction of pure acetone in the absence of O_2 confirmed the participation of lattice oxygen from the catalyst in the acetone combustion, in accordance with a Mars-van Krevelen type mechanism. XRD analysis of the aged catalyst showed that the segregation of bulk CuO was responsible for the observed deactivation.[562] A synergistic effect between cupric oxide (CuO) and ceria was observed during total oxidation of propane. The activation energies for reduction and reoxidation of the binary metal oxide catalyst are 20 kJ mol^{-1} lower than those obtained on the single CuO- or CeO_2-based catalysts.[561]

MnO_x–CeO_2 mixed oxides tested for ethanol, ethyl acetate, formaldehyde, and toluene oxidation showed higher activity when compared to CeO_2 and MnO_x, even though the specific activity was lower, taking into account the higher surface area resulting from thermal stabilization of the catalysts (Figure 26).[564,570]

Formaldehyde combustion by MnO_x–CeO_2 mixed oxides highlighted a dependence upon the oxides preparation methods. The increased catalytic activity was ascribed to the formation of MnO_x–CeO_2 solid solution, which led to a higher oxidation state of manganese and richer lattice oxygen species on the surface, promoting activation of molecular oxygen through the oxygen transfer mechanism.[532] Copper may have a significant promoting effect on the catalytic activity of the MnO_x–CeO_2, as demonstrated by the increased activity in the oxidation of benzene, with complete conversion taking place at 250 °C over the 2.5 wt % Cu/MnO_x-CeO_2 catalyst, as opposed to 380 °C when the copper-free catalyst was used. XRD and H_2-temperature programmed reduction (TPR) measurements indicated that the copper species were highly dispersed on the surface of the mixed oxide and could improve the redox properties of the catalyst. Through XPS and FTIR analyses, it was established that the improved performance must be ascribed to an increased generation of surface oxygen species by copper and of active sites for benzene adsorption.[514] A promoting effect on MnO_x–CeO_2 mixed oxides activity toward formaldehyde combustion was observed when Ag or Pt were added to the formulation of the catalysts.[563,564]

Among VOCs, chlorinated volatile organic compounds (CVOCs) have drawn special attention on account of their toxicity, high stability, and widespread application in industry.[571] Photocatalytic decomposition, catalytic hydrodechlorination and steam reforming are promising techniques for CVOCs removal but all present critical drawbacks.[571] Catalytic combustion is still an effective technology for reducing the emissions of CVOCs from waste gaseous streams. Among transition metal oxide catalysts, Cr-based catalysts have exhibited the highest activity for CVOCs abatement, but their use is restricted because of leaching of toxic chromium oxychloride.[571] Industrial catalysts are usually based on vanadium and manganese oxides supported on alumina and loaded with noble metals such as palladium or platinum.[572]

The formation of undesired higher chlorinated compounds and of molecular chlorine, due to activity of the catalysts in the Deacon reaction (eq 5) and oxychlorination reaction (eq 6), is a major drawback of CVOCs catalytic oxidation.

$$4HCl + O_2 \rightleftarrows 2Cl_2 + 2H_2O \quad (5)$$

$$C_nH_m + 2HCl + \frac{1}{2}O_2 \rightarrow C_nH_{m+2}Cl_2 + H_2O \quad (6)$$

Chlorination of the metal active sites can occur, leading to deactivation of the catalyst.[573] Therefore, there is still a call for the development of more suitable catalysts for efficiently eliminating CVOCs and overcoming deactivation and selectivity problems.[571] For this reason, in the last years, the abatement of CVOCs has also been studied on many CeO_2-based catalysts, in which ceria was used as an actual catalyst, catalytic support, or additive to other catalysts. In general, thanks to the redox properties of ceria, its addition to the catalyst formulation has led to enhanced complete oxidation activity (less byproducts concentration, higher CO_2 selectivity over unwanted CO) and lower light-off temperatures. However, ceria activity for oxidation can be detrimental in some cases because it can favor Deacon reaction at higher temperature (300−400 °C), leading to Cl_2 formation. Moreover, time-on-stream deactivation problems are still encountered in some cases, depending on reactant, reaction conditions, and catalyst formulation.

CeO_2-based catalysts have been tested in catalytic combustion of model chlorinated compounds found in many industrial off-gases [e.g., trichloroethylene (TCE), 1,2-dichloroethane (DCE), and chlorobenzene (CB)]. Pure ceria was also

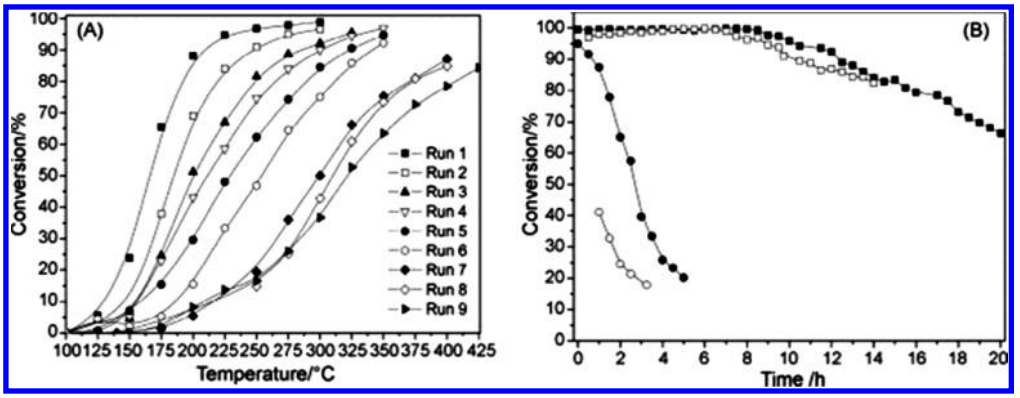

Figure 27. Stability of CeO_2 for triochloroethane catalytic combustion: (A) the reaction runs under dry condition; (B) the reaction under different conditions at constant temperature: (■) 350 °C in dry condition; (□) 350 °C in humid condition; (●) 200 °C in dry condition; (○) 200 °C in humid condition; gas composition: 1000 ppm TCE, air balance; GHSV = 15000 h^{-1}. Reprinted with permission from ref 571. Copyright 2008 Elsevier.

found to be quite active in CVOCs catalytic oxidation.[565,571] The performances of pure CeO_2 catalysts depend on many factors, such as calcination temperature, morphology, and reaction conditions (GHSV, chlorinated compound species, and concentration). For example, nanostructured ceria, in the form of flowerlike microspheres obtained by hydrothermal routes, exhibited much higher activity in catalytic combustion of TCE than CeO_2 obtained by deposition precipitation or thermal decomposition.[574] However, deactivation and poor selectivity are common obstacles with CeO_2 catalysts. Their activity quickly diminishes at temperatures lower than 400 °C due to the strong adsorption of HCl or Cl_2 produced from the decomposition of chlorinated compounds on the active sites of CeO_2 (Figure 27).[571,575]

Deactivation can be avoided at higher temperature by oxidation of dissociatively adsorbed Cl to Cl_2 via the Deacon reaction, but as a result, lower HCl selectivity is observed.[575,576] Slow accumulation of Cl species may result in the formation of higher chlorinated byproducts during steady-state experiments even after hours of running time, as observed for CB combustion over CeO_2 catalysts.[576] Therefore, activity and selectivity of CVOCs catalysts should be monitored in long steady-state experiments at different temperatures in order to evaluate catalysts actual performances.

Introduction of limited amounts of water in the reaction feed (1.5 vol %) can enhance HCl selectivity by hindering the Deacon reaction, without the occurrence of water-related deactivation problems. At higher concentration (3 vol %) water was observed to inhibit TCE oxidation, while at even higher concentration (12 vol %), it enhanced the activity to a certain extent. This complex behavior suggests that TCE destruction occurs via both hydrolysis and oxidation under humid conditions.[571] Sweeping the catalyst with humid air after operation may also remove Cl species, but the removal of chlorine or chloride ions from CeO_2 surface is slow.[571]

Ceria-based mixed oxides generally perform better than pure ceria catalysts in the oxidation of CVOCs because of their different redox properties and acid sites population. $Ce_xZr_{1-x}O_2$ catalysts having different compositions were tested in DCE and TCE combustion, and they proved to be more active than both CeO_2 and ZrO_2 alone. Moreover, the use of the mixed oxide resulted in an increase in selectivity to CO_2 and HCl as well as a lower content of chlorinated byproducts, such as tetrachloroethylene (in the case of TCE) and vinyl chloride (from DCE).[573] The simultaneous oxidation of both chlorinated feeds (TCE and DCE) and *n*-hexane[569] or toluene over these Ce-Zr mixed oxides catalysts revealed that the presence of non-chlorinated VOC could affect the catalysis both in terms of activity and product selectivity.[567] In general, a mutual inhibition was observed, resulting in higher temperatures required for deep combustion of all the reactants. TCE was more affected by the presence of *n*-hexane, while the oxidation of *n*-hexane was inhibited to a larger extent in the presence of DCE. Inhibition effects appeared to be related to competition between VOC molecules for adsorption sites. However, no specific species was able to dominate the adsorption sites, thereby completely preventing the adsorption and reaction of other species. The addition of *n*-hexane considerably promoted the catalyst selectivity to HCl. This effect was ascribed to water produced in situ from *n*-hexane combustion, which would reverse the Deacon reaction.[567] Stability under operating conditions, which is a crucial issue for CVOCs catalytic oxidation, unfortunately was not reported for CeO_2-ZrO_2 systems.[567,569,573] However, the poor stability of ceria-based catalysts at temperatures lower than 400 °C can be dramatically improved by incorporation of praseodymium.[577] The best performances for DCE combustion were observed for $Ce_{0.5}Pr_{0.5}O_2$, which was more active and stable than both CeO_2 and PrO_2 alone thanks to improved reducibility of the material and better resistance to Cl species formation and accumulation. As revealed by XPS and Raman analysis, the chlorination of the best performing mixed oxides was limited to the surface of the material and did not increase considerably after long steady-state aging, while in the case of PrO_2 and Pr-rich oxides chlorination was more extensive and it affected the bulk of the material as well. Remarkably, at 335 °C, 60% DCE conversion was observed over $Ce_{0.5}Pr_{0.5}O_2$ for more than 115 h. Despite these encouraging results, the selectivity to CO_2 and HCl was low (only 25% and 50%, respectively), and vinyl chloride was continuously produced during the test in 100 ppm concentration.[577] Low-temperature catalytic combustion of CB was evaluated over MnO_x-CeO_2 mixed oxide catalysts.[578] The incorporation of MnO_x into CeO_2 greatly improves the activity and stability of the catalyst compared to the pure oxides. During steady-state aging experiments, a deactivation process depending on the amount of Ce in the catalyst was observed, which presumably arises from adsorption of Cl species on Ce active sites.[578]

Ceria was also studied as additive in state-of-the-art catalysts to improve their performance (e.g., with zeolites catalysts,[579,580] V_2O_5-based catalysts,[581] and noble metal based catalysts).[582] Zeolites are catalytically active for the oxidation of CVOCs on account of their strong surface acidity, high internal surface area, and 3D channel system. The activity for DCE catalytic oxidation was tested over a H-ZSM5-type zeolite, both pure and deposited with different amount of CeO_2.[579] Addition of CeO_2 resulted in slightly higher activity than pure H-ZSM5 for DCE oxidation in light-off experiments, reaching peak performances with 11 wt % CeO_2. The product distribution of DCE oxidation was better for CeO_2-added catalysts than for pure H-ZSM5, reaching very high HCl selectivity (>90%) at 350 °C (complete conversion of DCE), even if CO_2 selectivity was low in all cases (30−60%). Notably, methyl chloride and vinyl chloride production was lower and limited to low temperature (<350 °C), and no other carbon compounds were detected. Addition of CeO_2 into the formulation of the catalysts led to a reduced coke deposition, which in turn resulted in better stability in steady-state experiments. The enhanced catalytic performance of CeO_2/H-ZSM5 catalysts was ascribed to the combination of acidic and oxidizing properties of the two components.[579] Similar results in DCE oxidation were observed for USY type zeolite added with CeO_2 and/or CuO.[583] Both CeO_2/USY and CeO_2-CuO/USY catalysts were very active and stable, reaching complete conversion of DCE at 300 °C with no deactivation over time. However, product distribution was not as good as that of CeO_2/H-ZSM5: incomplete oxidation of DCE produced acetaldehyde and acetic acid, while methyl and vinyl chloride were produced up to 450 °C when using CeO_2/USY. Nonetheless, chlorinated byproducts formation during DCE oxidation was much reduced and very limited in the temperature range (200−300 °C) on the CeO_2-CuO/USY catalyst. This was not the case for TCE and DCM combustion over the same catalyst, for which also chlorinated byproducts were obtained in considerable amounts.[583]

Doping TiO_2 supports with ceria resulted in an improvement of activity for V_2O_5-based catalysts in the oxidation of CB.[581] In another study, a series of pure and sulfonated TiO_2 and TiO_2−CeO_2 aerogel supports loaded with 2 wt % V_2O_5 was investigated. The sulfonated and cerium-doped catalyst showed the best catalytic performance thanks to the introduction of acid sites on the surface and to its redox properties. Stable levels of CB conversion were observed in short steady-state experiments (2 h 30 min) between 100 and 400 °C. As for selectivity, CO_2 and CO were the only carbon products observed (up to 30% CO), while HCl/Cl_2 ratio was not reported.[581]

Noble metal catalysts supported on ceria have been studied for CB and DCM and were generally found to promote CeO_2 activity and stability. Ru/CeO_2 catalysts tested for CB oxidation proved to be stable during steady-state experiments at 300 °C, the temperature at which pure CeO_2 rapidly deactivates due to blocking of active sites by Cl species.[576] Ru catalyzes the removal of adsorbed chlorine species from CeO_2 via the Deacon reaction at lower temperature than CeO_2 itself, thus stabilizing the catalyst. However, this causes a sharp decrease in HCl selectivity due to Cl_2 production.[576] Au and Pt deposited on ceria-zirconia mixed oxides were also tested for CB oxidation, leading to a great improvement of activity and carbon selectivity in light-off experiments. Indeed, no CO was detected for the Pt (1 wt %)-loaded catalyst, while it was the only product observed over the pure support.[584] Despite the very promising results reported, neither HCl selectivity nor stability during steady state experiments were addressed for these catalysts.[584] Similar observations were reported for Pt (1 wt %) and Pd (1 wt %) catalysts supported on 25 wt % CeO_2/Al_2O_3 in the oxidation of perchloroethylene (PCE).[582] These catalysts proved to be superior when compared to catalysts based on Rh and V_2O_5 and to ceria-free, Al_2O_3-supported catalysts. Noticeably, in the case of Pt (or Pd)/CeO_2-Al_2O_3 catalysts, the selectivity to CO_2 and HCl was almost complete at every temperature.

For common CVOCs, such as TCE, DCE, and CB in particular, noble metals/CeO_2-based catalysts bear the potential to define new state-of-the-art catalysts in CVOCs oxidation if activity and stability during steady state experiments could be increased to some extent.

7.3.4. Dehalogenation. Exploitation of CeO_2 in the oxidation of HCl is emerging as an interesting strategy, able to become an economic alternative to the costly state-of-the-art RuO_2-based catalysts. HCl oxidation is an important reaction as hydrochloric acid (HCl) is an hazardous byproduct of many processes of growing industrial interest, such as polycarbonates production from dihydroxylated organics and phosgene and organics chlorination reactions. Cl_2 is becoming the most attractive industrial output for HCl disposal.[585] Stable activity for CeO_2-based catalytic systems was reported in O_2-rich feeds ($O_2/HCl > 0.75$), as a consequence of the resistance of cerium oxide against chlorination, which is limited to few surface and subsurface layers, while bulk chlorinated phases that deactivate the catalyst are formed only in stoichiometric or sub-stoichiometric feeds ($O_2/HCl < 0.25$). The negative impact of high Cl coverages on the activity was attributed to the more difficult vacancy formation. The original activity of deactivated samples can be restored by exposure to an excess of oxygen, indicating a reversible deactivation induced by chlorination.[586] Supporting the CeO_2 active phase on ZrO_2 enhances the long-term stability of the catalysts (700 h on stream). The catalyst also showed reduced chlorine uptake in comparison to CeO_2.[587]

7.3.5. Partial Hydrogenation. CeO_2 shows a high activity and selectivity in the gas-phase hydrogenation of alkynes to olefins. This finding has direct impact on the purification of olefin streams and on the manufacturing of fine chemicals, since ceria is less expensive than viable state-of-the-art Pd-based catalysts (Lindlar's catalyst). The use of ceria in hydrogenation reactions has been investigated for years as a promoter or as a carrier of noble metal nanoparticles.[588,589] Activation of hydrogen on CeO_2 is often regarded as the limiting step of the reaction, as also observed for other functional groups, including substituted nitroarenes.[590]

DFT applied to CeO_2{111} was employed to rationalize the applicability of CeO_2 as a catalyst for olefin production. The high selectivity toward formation of alkenes was attributed to the lower activation barrier leading to gas-phase C_2H_4 compared to that for the formation of β-C_2H_4 radical species, which would open up the reaction pathway to alkane formation. The outstanding performance of CeO_2 in comparison with other oxides was tentatively explained on the basis of CeO_2 ability of stabilizing highly reactive β-C_2H_2 radicals on the {111} surface by easily accommodating one electron into Ce 4f states (Figure 28).[591]

TiO_2-, Al_2O_3-, and ZrO_2-supported CeO_2 catalysts with different Ce loadings prepared by simple impregnation of Ce salts were evaluated in the three-phase hydrogenation of

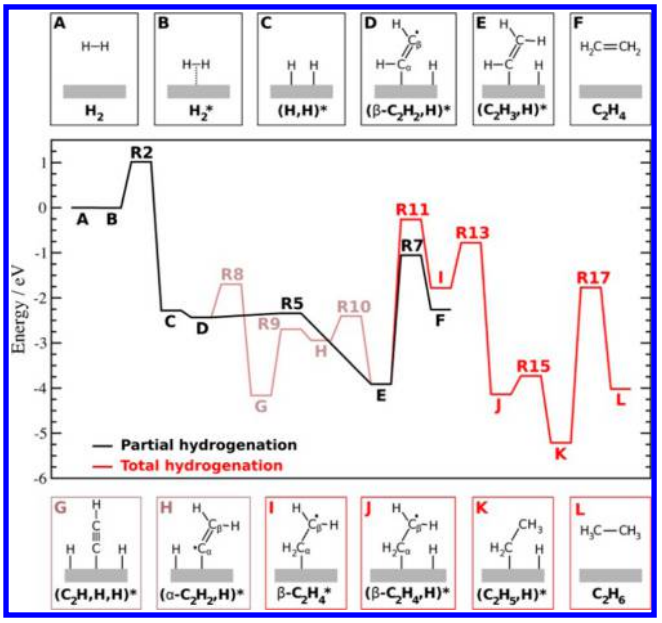

Figure 28. Reaction energy profile for acetylene hydrogenation on CeO_2{111}. All energies are referenced to the total energy of H_2(g), C_2H_2(g), and the clean CeO_2{111} surface (state A). States A–L stand for minima, and their structures are schematically shown in the insets, whereas transition structures are indicated by R2–R17. Colors indicate different pathways: partial hydrogenation of acetylene to ethylene via R5 (black line) or via dissociative acetylene adsorption (light brown), and total hydrogenation to C_2H_6 (red line). Reprinted from ref 591. Copyright 2014 American Chemical Society.

alkynes under continuous-flow conditions at variable temperature (20–140 °C) and H_2 pressure (1–90 bar). A number of acetylenic compounds, possessing terminal or internal triple bonds, conjugated unsaturations, and additional functionalities were systematically assessed. The CeO_2-based catalysts required demanding conditions of temperature and pressure (140 °C, 90 bar) because of the intrinsic inability of ceria to activate hydrogen. However, selectivity-wise, supported ceria outperformed the state-of-the art Lindlar catalyst. The results revealed the full stereo- and chemoselective character of the ceria catalysts, which was not influenced by the type of carrier and the Ce loading. These results enabled the use of a cheap metal oxide for the production of olefinic compounds in fine chemical and pharmaceutical applications.[592]

7.3.6. Photocatalysis. In the past decade, cerium-based materials have gained increasing attention as photocatalysts alternative to the more conventional TiO_2, both for wastewater treatment[593−597] and water splitting.[598−600]

CeO_2 is a wide band gap semiconductor (3.2–3.4 eV), and therefore, photogeneration of charge carriers is obtained under UV light. Mesoporous ceria nanorods have been shown to possess a lower band gap (~2.75 eV), thanks to the presence of Ce(III).[601] More recently, an electron beam irradiation approach was proposed to narrow the band gap of pristine CeO_2 nanostructures to enhance their visible light activity through defect engineering.[602] The resulting modified CeO_2 exhibits superior photocatalytic activities in the degradation of 4-nitrophenol and methylene blue in the presence of visible light (λ > 400 nm) compared to the pristine CeO_2. Surface defects such as oxygen vacancies can prevent hole–electron recombination working as electron traps and can also act as strong binding and dissociation sites for adsorbates. Therefore, the introduction of oxygen vacancies in an oxide can improve its photocatalytic activity, as recently shown.[603]

Doping CeO_2 with 3d transition metal ions has been indicated as a suitable way to enhance the mobility of excitons, thus facilitating its surface reaction. Accordingly, CeO_2 nanoparticles doped with different transition metal cations such as Fe, Mn, and Co showed improved optical activity as well as enhanced capability in methylene blue (MB) degradation.[604] Recently, exciton diffusion visualization in tetracene molecular crystal via time and space-resolved fluorescence spectroscopy demonstrated that on the archetypical thin film the mechanism of exciton transport depends strongly on the nanoscale morphology. This imaging technique can be a powerful tool to investigate and lead the design of systems that rely on exciton transport, comprising photocatalytic materials.[605]

Most of the photocatalytic experiments reported in the literature are conducted at room temperature, testing the catalyst performances when irradiated with the UV and visible window of the solar spectrum. However, higher temperatures can favor mobility of oxygen vacancies, improving photocatalytic activity, as revealed by a recent study on mesoporous nanorod-like ceria in the temperature range of 160–240 °C.[601] Similarly, the photocatalytic efficiency of the Y-doped ceria (YDC) systems in dyes degradation was much higher (20-fold increase) at 100 °C than at room temperature.[603]

The factors governing photocatalytic activity of CeO_2 in the degradation of dyes are not yet fully understood, but there is an evident dependence of activity on the textural and crystallinity properties of the oxide. Many different preparation methods have been explored, leading to CeO_2 microspheres,[594] lamellar ceria crystallites,[595] nanorods,[606] and nanoparticles.[593,606] The promising performances of CeO_2 were attributed to the good adsorption capacity and to the 4f electron configuration that enhanced electron transfer from the adsorbed dye to oxygen species.[593]

Doping of metal oxides is a common strategy for changing their electronic properties. Both MB and naphthol blue black (NBB) catalytic photodegradation was enhanced on transition metal doped CeO_2. A significant increase in the photocatalytic activity of CeO_2 was observed by substitution of Mn(IV) in CeO_2 crystal lattice (up to 30 mol %)[607] and upon CeO_2 doping with 5 mol % Co.[604] This effect was ascribed to the reduction of the CeO_2 band gap thanks to the empty 3d states of the dopant ions, lying at energy lower than the 4f states of Ce.[604]

CeO_2-doped TiO_2 and CeO_2-ZrO_2 codoped TiO_2 have been studied for the photodegradation of MB in comparison with TiO_2, showing that the addition of CeO_2 improved the catalytic performances of the catalysts.[608−610] Well-dispersed CeO_2 nanoparticles loaded on reduced graphene oxide (RGO) nanosheets were tested for the degradation of MB under simulated sunlight irradiation, outperforming bare CeO_2 nanoparticles. The enhanced activity was attributed to the improved separation of electron–hole pairs and improved adsorption due to the presence of RGO.[611] CeO_2–Bi_2O_3 composites were also investigated showing increased photocatalytic activity for the degradation of RhB as compared to pure Bi_2O_3 or CeO_2. The results were discussed in terms of suppression of charge recombination in CeO_2–Bi_2O_3.[612] The role of interface contact between CeO_2 and TiO_2 was found to be crucial for the photocatalytic elimination of toluene.[613] Similarly, solar light-driven elimination of benzene was achieved

by the use of a nanocomposite consisting of CeO_2-TiO_2, with a much superior activity than those of the individual oxides. In this instance, however, the authors assigned the photocatalytic ability to the TiO_2 phase, while the CeO_2 would thermochemically assist the process thanks to a promotion of the reduction of CeO_2 by the titania catalyst.[614] In another report, CeO_2/Fe_2O_3 nanospindles synthesized by the coprecipitation method displayed an improved efficiency for the degradation of eosin yellow (EY) under visible light (Figure 29), as a result of the intercrossing of both photogenerated holes and electrons between the conduction band and valence band of the two oxides.[615]

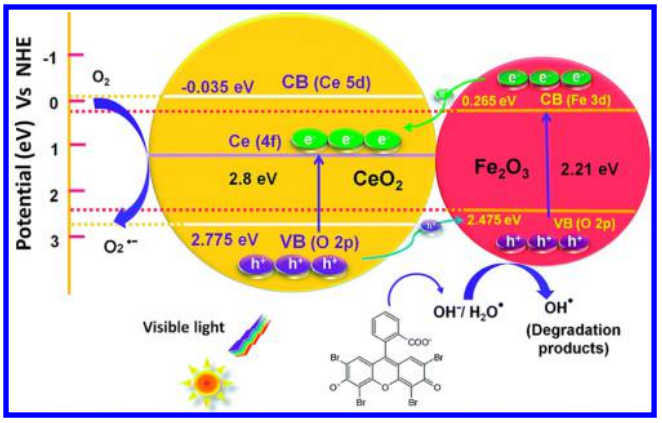

Figure 29. Proposed photodegradation mechanism of CeO_2/Fe_2O_3 composite nanospindles in degrading eosin yellow dye under visible light irradiation. Reprinted with permission from ref 615. Copyright 2015 Royal Society of Chemistry.

The reduction of the health-hazardous Cr(VI) to the less toxic and more easily precipitated Cr(III) was made photochemically viable upon utilization of CeO_2 nanotubes. In addition to the nanostructured morphology of the ceria, the key to this experiment is the presence of oxalic acid, which is responsible for the light-induced ligand-to-metal electron transfer to surface Ce atoms, which in turn causes the reduction of Cr(VI).[616]

7.3.7. Thermochemical Water Splitting. Over the past decade, ceria has been gaining an accelerated popularity as a non-stoichiometric catalyst component for the production of H_2 fuel from the thermochemical splitting of water, which was first demonstrated in 2006 for fuel cell applications.[617] Later studies indicated that the addition of other cations such as Zr would favor the reduction step of ceria.[618] CeO_2-ZrO_2 indeed appear to be the most promising materials for the thermochemical water splitting, as the presence of Zr severely affects the OSC and in turn the oxygen release during the reduction step. In function of variable amounts of Zr, the reduction step was shown to proceed with yield as high as 27% when operating at 1200 °C. Other dopants such as Y, La, Pr, and Gd cations may affect very poorly the reducibility, while they do improve the thermal stability over repeated cycling.[619] The effect of dopants was evaluated also in other investigations. In particular, Ta(V) considerably increased the reduction yield but also caused some structural changes after high-temperature thermal treatment which compromised H_2 yields. On the other hand, lanthanide elements such as La, Sm, and Gd can improve the thermal stability but overall do not affect the performance in comparison with pure ceria. In contrast, lanthanide-doped CeO_2-ZrO_2 generates higher activity than the corresponding CeO_2-ZrO_2.[620]

Despite the fact that a good deal of reports is available on thermochemical water splitting by CeO_2, most efforts have been focused on the production of syngas (H_2 and CO) by coupling the water splitting with the CO_2 thermochemical splitting. If concentrated solar energy is used as a source of heat, high solar-to-fuel energy conversion efficiencies are attained. Ceria has rapidly gained the role as state-of-the-art catalyst due to its rapid redox kinetics. For example, solar-to-fuel efficiencies as high as 0.8% were reported in a seminal work by Steinfeld et al., which demonstrated the benefit of directly exposing CeO_2 to the concentrated solar irradiation by building a scalable reactor (Figure 30).[621]

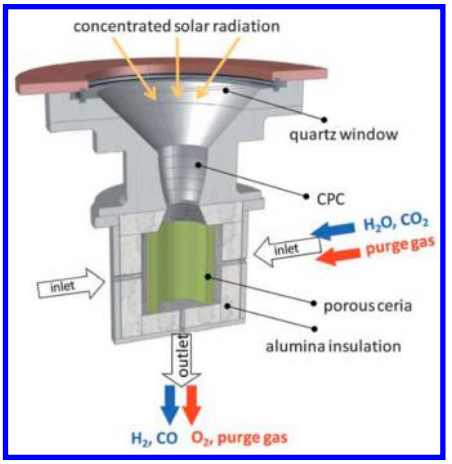

Figure 30. Schematic of the solar reactor for the two-step, solar-driven thermochemical production of fuels. It consists of a thermally insulated cavity receiver containing a porous monolithic ceria cylinder. Concentrated solar radiation enters through a windowed aperture and impinges on the ceria inner walls. Reacting gases flow radially across the porous ceria toward the cavity inside, whereas product gases exit the cavity through an axial outlet port at the bottom. Blue arrows indicate ceria reduction; red arrows indicate oxidation. CPC: compound parabolic concentrator. Adapted with permission from ref 622. Copyright 2012 Royal Society of Chemistry.

As a common depiction, the solar thermochemical redox cycles are described in terms of two separate reduction/oxidation steps with ceria as reactive intermediate:

$$\text{reduction at } T_{high}\text{: } CeO_2 \rightarrow CeO_{2-\delta} + \delta/2O_2 \quad (7)$$

$$\text{oxidation at } T_{low}\text{: } CeO_{2-\delta} + \alpha H_2O + \beta CO_2 \rightarrow CeO_2 + \alpha H_2 + \beta CO \quad (8)$$

with $\alpha + \beta = \delta$. Temperature for the reduction process are generally above 1200 °C, while for the oxidation step they are considerably lower. The temperature becomes an important parameter to consider as it can affect the thermodynamic of the oxidation step, in which either H_2O or CO_2 is reduced first. It is also important that the reaction proceeds at T below the melting point of the catalyst, which makes CeO_2 a less problematic candidate than iron oxide based catalysts, the other benchmark catalyst class for the thermochemical H_2O and CO_2 splitting, and which further mitigate the relatively lower OSC of ceria as compared to other redox metal oxides.[623]

As for the pure water splitting, an attractive feature for the H_2O and CO_2 simultaneous splitting is CeO_2 doping, which

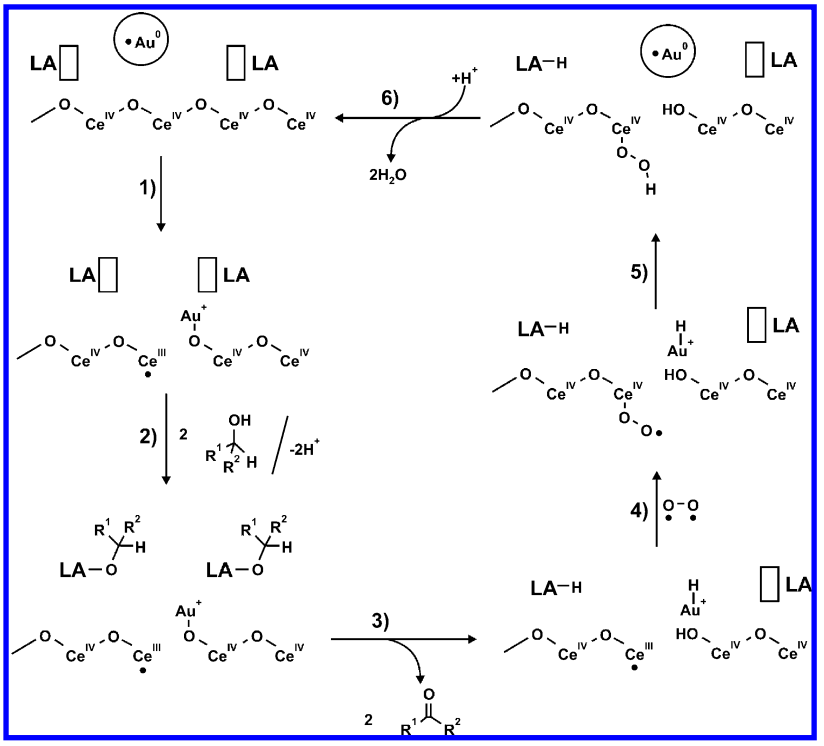

Figure 31. Proposed mechanism for the oxidation of alcohols in the presence of Au/CeO_2 prepared using nanoparticulated support. LA = Lewis acid. Reproduced with permission from ref 632. Copyright 2005 Wiley-VCH.

further improves the thermodynamic and kinetic properties of ceria compared to the thermochemical redox cycle. A careful evaluation of Zr(IV)-doped CeO_2 in function of the Zr(IV) content underlined the higher reduction extent of the doped ceria in the two-step H_2O and CO_2 splitting. The different thermodynamic properties of the Zr-doped derivative were also described and compared to those of pure CeO_2.[624] In another study, the thermodynamic characteristics were investigated by increasing the Zr content up to 20%, and it was shown how the benefit of including Zr can be especially pronounced if isothermal or near-isothermal conditions are applied, in contrast with the two-temperature cycling, in which the system pays a price in terms of steam-to-hydrogen conversion efficiency.[625]

Another important parameter to consider is the H_2O:CO_2 molar ratio in order to have control on the syngas molar ratio. This aspect was most prominently investigated by varying the H_2O:CO_2 molar ratio in the range from 0.8 to 7.7, resulting in the formation of syngas with H_2:CO molar ratio that could be varied from 0.25 to 2.34.[15] An aspect that is still under debate is the solar-to-fuel maximum efficiency that can be reached, as several studies seem to produce varying results. Moreover, in some cases the theoretical maximum efficiency under realistic conditions was not reported for both solar and mechanical work. Very recently, this feature was analyzed in the presence of an inert sweep gas in order to facilitate reduction. A robust model was built based on a mixed flow method for chemical equilibrium. The model proved that the efficiency needed are strongly dependent on oxidation temperature, and a maximum efficiency of 11% was predicted under these conditions.[626]

The pure thermochemical CO_2 splitting has also been investigated using pure ceria as a catalyst. Superior performances were disclosed when using a dual-scale porosity ceria reticulated porous ceramic, with solar-to-fuel energy conversion efficiency of 1.72%.[627]

7.3.8. Organic Reactions. Organic synthesis is one of the most prominent areas of chemistry research. Reports on CeO_2 used as catalyst or catalytic support for organic transformations are being released at an increasing rate, witnessing the versatility of this material in catalytic applications. The range and scope of organocatalytic reactions is wide and has been well-reviewed.[8] Only few representative examples will be provided here. Other than partial hydrogenation, already discussed, CeO_2-based catalysts have been employed for the hydrogenation of olefins and carbonyl bonds. For instance, 1,3-butadiene could be reduced to 1-butene with good yield by a Pd/CeO_2 catalyst supported on alumina. Thanks to the presence of ceria, the selectivity toward 1-butene was excellent, much higher than that of the alumina-supported Pd catalyst.[628] On the other hand, crotonaldehyde has served as a model compound to test the selectivity of Pt/CeO_2 catalysts toward C═C or C═O bonds. Temperature can have a pronounced effect on the evolution of the reduction; in one study, selectivity toward crotyl alcohol was promoted by the ceria support for the high-temperature condition, while a 100% butanal was obtained for hydrogenation conducted at 200 °C,[629] in agreement with another report in which $PtZn/CeO_2$ was employed as the catalyst.[630] Remarkably, hydrogenation of benzene is also a viable process, especially if cyclohexane is obtained as the selective product, as observed when using a catalyst consisting of nickel clusters adsorbed on ceria, which displayed high catalytic activity and selectivity toward this product.[631] One more obvious use of CeO_2 resides in its exploitation as an oxidant, owing to its powerful ability to store and supply oxygen. Oxidation of alcohol is a typical application, and very good selectivity can be achieved. This was the case in the oxidation of a series of alcohols by Au/CeO_2 in the presence of

a Lewis acid (Figure 31), for which selectivity in many reactions overcame 99% with high Turn Over Frequencies (TOFs). The results were related to an extra stabilization of the positive oxidation states of Au due to the nanometric electronic interaction with the ceria surface.[632]

Higher activities for CeO_2-supported Au were also found during a study of the mechanism of the oxidation of alcohols using different supports, in which also other parameters such as Au particle size and gold content were screened. The authors could hypothesize a mechanism based on a metal-alcoholate, β-hydride shift from carbon to metal, and the oxidation of the resulting M-H (metal-hydride).[633]

Beyond oxidations and hydrogenations, CeO_2 is proving its value in other more complex organic reactions, in both traditional and advanced synthesis, projecting CeO_2 as a very versatile and attractive catalyst. In one of the latest investigations on the ability of several metal oxides in catalyzing the low-temperature conversion of alcohols and amines into imines, CeO_2 exhibited excellent activity, as high as 96%, on account of its redox properties, while no other oxide was capable of catalyzing the reaction. Furthermore, the catalyst could be reused three more times without loss of any activity.[634] The reusability of the catalyst is indeed being pursued quite extensively, leading also to the assembly of very efficient functional systems. Magnetic recyclability has been exploited by combining CeO_2 with magnetic Fe_3O_4 in the one pot multicomponent synthesis of dihydropyridines under environmental friendly conditions.[635]

Classic coupling reactions such as aldol condensation,[636,637] Knoevenagel condensation,[638] Mannich reaction,[639] Suzuki-Miyaura,[640] or Sonogashira cross couplings[641] have also been reported, although in various cases ceria-zirconia is used as support.

7.3.9. Biomedical Applications. Ceria shows tremendous potentialities in a large variety of biomedical applications, in superoxide dismutase mimetic activity, catalase mimetic activity, hydroxyl radical scavenging, nitric oxide radical scavenging, peroxidase mimetic activity, oxidase mimetic activity, and phosphatase-mimetic activity, as recently overviewed by Xu and Qu.[642] Indeed, nanoceria, which is apparently well-tolerated by the organism, might fight chronic inflammation and the pathologies associated with oxidative stress, which include cancer and neurodegeneration, and this promises a revolution in pharmacology to improve or create ex novo therapies.[643,644] Here, only some key applications will be briefly highlighted.

The very promising biomedical performances are mostly related to ceria redox capability and the possibility to engineer its vacancies by making nanostructured materials. Thanks to this flexibility, ceria can effectively interact with many radicals or superoxides, and therefore, it has been tested in both animal and cell culture models to determine its ability to protect against oxidative stress.[645−647]

As a consequence of the reduced oxidative stress induced by ceria, treatment of adult rat neurons with 10 nm nanoceria resulted in a significant decrease in cellular senescence after 30 days.[648] Among several factors including size/surface area and oxygen vacancy sites, the oxidation state of cerium have been shown to play a key role that may be responsible for the effectiveness of nanoceria in catalyzing superoxide dismutase (SOD) activity.[649] Nanoceria has been shown to be able to protect primary cells from the detrimental effects of radiation therapy[647] and to prevent retinal degeneration induced by intracellular peroxides.[650] Furthermore, nanoceria has been implicated as a critical mediator of inflammation reactive oxygen species (ROS) production in states of inflammation and therefore it serves as a novel therapy for chronic inflammation.[651] The excellent biocompatibility and free radical scavenging properties of ceria has recently stimulated studies on its application in orthobiologic materials. Consistently, cytotoxicity measurements showed that mesoporous ceria foams were non-toxic and no significant inflammatory response was measured when monocytic cells were cultured with the ceria foam.[652] More so, hybrid ceramic polymeric bioactive scaffolds loaded with ceria hold great potential for tissue engineering applications.[12] Remarkably, ceria nanoparticles have also shown protective effects against ischemic stroke in living animals.[13] Polymer-coated ceria nanoparticles have been shown to be robust and water-soluble redox catalysts with excellent oxidase-like activity, as they can facilitate the fast oxidation of organic dyes and small molecules in slightly acidic conditions without the need of hydrogen peroxide.[653] CeO_2 nanomaterials were also proposed as potential drug delivery systems.[654] Yb(III) and Er(III) codoped cerium oxide nanoparticles exhibited strong upconversion properties that were found to kill lung cancer cells by inducing apoptosis, thereby demonstrating the potential to be used as clinical contrast agents for imaging and as therapeutic agents for treatment of cancer.[655]

CeO_2 nanoparticles, coupling UV shielding with biological and genetic protection, appear to be ideal candidates for next-generation sun shields. In fact, irradiated CeO_2 nanoparticles exerted impressive protection on UV-treated cells, by buffering oxidation, preserving viability and proliferation, reducing DNA damage, and accelerating repair; strikingly, they almost eliminated mutagenesis, thus acting as an important tool to prevent skin cancer.[656]

8. CONCLUSION AND OUTLOOK

In the last 40 years, ceria, first thought to be an "inert" support able to well-disperse and stabilize catalytically active metal nanoparticles, has become first a non-innocent support, that directly participate to the reaction with lattice oxygen, then a cocatalyst, and more recently a catalyst itself. In this process, two major directions have been followed to boost the applications of ceria-based materials in catalysis.

First, the increase of surface area and the enhancement of its thermal stability was a mandatory target for application in car converters, which happens to be the most relevant industrial application of ceria. Formation of solid solutions with transition and/or rare earth metals, zirconium in particular, gained this goal, with the additional benefit to boost also redox properties as the introduction of cations with different ionic radii into the ceria lattice induces structural disorder that facilitates oxygen release. These successful approaches allowed for the development of closed coupled catalysts CCC that can cope with a working temperature higher than 1000 °C, making modern ceria-zirconia-based TWCs the most relevant example of environmental catalysts. This application is mature, the materials are mostly optimized and widely adopted in current car converters, and improvements are essentially limited to the reduction of the amount of active components and to changes of formulation needed to cope with fluctuation in cost and availability. However, still, intriguing is the ongoing debate on the importance of compositional phase homogeneity of these doped/nanocomposites materials. In particular, besides the use of neutron diffraction in combination with XRD and Raman

spectroscopy, very stimulating is the recent and still poorly applied use of Eu luminescence as a structural probe to analyze compositional heterogeneity.[59,60]

Second, the advent of nanotechnology allowed for the obtainment of well-controlled nanomaterials in shape and size. Despite some limitations due to the thermal instability of nanostructures in general, this opened the perspective of understanding the different reactivity of exposed facets, and in combination with today's state-of-the-art computational simulations allowed for the clear correlation of structural parameters and reactivity. This approach has proven to be successful in demonstrating how OSC depends on nanostructure,[204] the surface dependence of soot combustion,[280] or the effect of ceria crystal plane on CO and propane oxidation.[657]

Impressive catalytic improvements have been achieved by modulating metal support interaction in ceria-based systems, opening new directions for boosting existing materials. Very sensitive is the case of gold supported on ceria-based systems, in which CO chemisorbed capability of gold was significantly perturbed by mild reduction treatments.[658] The possibility to tune the metal support interface by making core−shell, embedded catalysts is a suitable and successful strategy that is finding more and more applications.[221,468] Very challenging is also the investigation of highly dispersed metal ions on ceria, which qualify as single-atom catalysts and hold a promise of radical reduction of precious metal load in critical large-scale catalytic systems.[659] The intrinsic difficulties in characterizing these materials highlights the importance of a multidisciplinary approach, which shall take advantage of state-of-the-art characterization techniques, including synchrotron radiation facilities, coupled with state-of-the-art computational capabilities.

While oxidation reactions, including those involved in organic reactions,[8] are effectively promoted by ceria-based materials, and emerging applications are proposed, such as in fuel cells, halogen production, or dimethyl carbonate synthesis, there is still plenty of room for applications under reducing conditions.

Increasing attention is dedicated to ceria-based photocatalysts, due to the observation of UV photoinduced processes. While these studies are relevant from an intellectual point of view, the observed performances are still much less promising with respect to those of many visible light photocatalysts, limiting the interest for photoelectro applications mainly in the field of solar fuels. Finally, nanostructures ceria-based materials are extremely promising for biomedical applications,[642] in which the structural and reactivity data derived from materials science and catalytic studies are extremely useful for understanding interactions with biologically relevant species such as radicals or H_2O_2.

Summarizing, CeO_2 is a very versatile and robust catalytic material with surface acid−base properties and structure that can be nicely tuned by doping with transition or rare earth metals. As recently proposed by Pérez-Ramírez and co-workers, a suitable interpretation and prediction of the catalytic behavior of ceria-based material can be made by the identification of descriptors, that can be derived either experimentally or computationally.[660] This new approach can inspire the development of new and more active/selective heterogeneous catalysts.

AUTHOR INFORMATION

Corresponding Author

*E-mail: pfornasiero@units.it.

Notes

The authors declare no competing financial interest.

Biographies

Tiziano Montini obtained his degree in Chemistry in 2002 and his Ph.D. in 2006 at the University of Trieste (Italy). After a postdoctoral fellowship, he was appointed as an assistant professor in 2014 with a "tenure track" at the University of Trieste. His major research interests are in design and characterization of heterogeneous catalysts with applications to environmental protection and sustainable energy production. In 2012, he was awarded with the "Alfredo Di Braccio" prize by the Accademia Nazionale dei Lincei and the 4th Junior Research Award by the European Rare-Earth and Actinide Society, both assigned to a researcher younger than 35 years old.

Michele Melchionna completed his Ph.D. in Chemistry at the University of Edinburgh in 2007. He then carried out postdoctoral research both in academia (University of Helsinki, Finland, and Palacky University, Czech Republic) and industry (Advanced Molecular Technologies, Australia) focusing on organic synthesis and catalysis. He currently holds a position as a senior postdoctoral fellow at the University of Trieste, working on carbon nanostructure-based catalysts for energy applications.

Matteo Monai graduated in Chemistry in 2013 and is now a Ph.D. candidate in the Graduate School of Chemistry at the University of Trieste (Italy). His research project concerns the design, synthesis, and characterization of nanostructured heterogeneous catalysts. He spent various periods in synchrotron facilities.

Paolo Fornasiero obtained his degree in Chemistry in 1992 and his Ph.D. in 1997 at the University of Trieste (Italy). After a postdoctoral fellowship at the University of Reading (UK), he was appointed as an assistant professor in 1998 and an associate professor of inorganic chemistry in 2006 at the University of Trieste. Since 2008, he has been the scientist responsible for the CNR research unit associated with the Institute of Chemistry of OrganoMetallic Compounds (ICCOM-CNR) of Florence. In 2015, he became an associate editor of the journal, *ACS Catalysis*. He received the Nasini Gold medal in 2005 for his contribution in Inorganic Chemistry and the Chiusoli Gold medal in 2013 for his studies in catalysis by the Italian Chemical Society. In 2016, he received the Heinz Heinemann Award for his contribution to catalyst science and technology from the International Association of Catalysis Societies.

ACKNOWLEDGMENTS

The authors acknowledge University of Trieste, ICCOM-CNR, INSTM Consortium, MIUR, Italy, through the project HIPHUTURE (protocol 2010N3T9M4) and European Community through the project FP7-NMP-2012-SMALL-6 (project ID 310651) for financial support.

REFERENCES

(1) Haxel, G. B.; Hedrick, J. B.; Orris, G. J. Supporting Sound Management of Our Mineral Resourses: Rare Earth Elements—Critical Resources for High Technology; *United States Geological Survey Fact Sheet*; 087−02; USGS: Reston, VA, 2002; p 4.

(2) *Critical Materials Strategy*; DOE/PI-0009; U.S. Department of Energy: Washington, D.C., 2011; pp 1−196.

(3) Paier, J.; Penschke, C.; Sauer, J. Oxygen Defects and Surface Chemistry of Ceria: Quantum Chemical Studies Compared to Experiment. *Chem. Rev.* **2013**, *113*, 3949−3985.
(4) Mogensen, M.; Sammes, N. M.; Tompsett, G. A. Physical, Chemical and Electrochemical Properties of Pure and Doped Ceria. *Solid State Ionics* **2000**, *129*, 63−94.
(5) Fan, L.; Wang, C.; Chen, M.; Zhu, B. Recent Development of Ceria-Based (nano)composite Materials for Low Temperature Ceramic Fuel Cells and Electrolyte-Free Fuel Cells. *J. Power Sources* **2013**, *234*, 154−174.
(6) Sun, C.; Li, H.; Chen, L. Nanostructured Ceria-Based Materials: Synthesis, Properties, and Applications. *Energy Environ. Sci.* **2012**, *5*, 8475−8505.
(7) Huang, W.; Gao, Y. Morphology-Dependent Surface Chemistry and Catalysis of CeO_2 Nanocrystals. *Catal. Sci. Technol.* **2014**, *4*, 3772−3784.
(8) Vivier, L.; Duprez, D. Ceria-Based Solid Catalysts for Organic Chemistry. *ChemSusChem* **2010**, *3*, 654−678.
(9) Zhang, D.; Du, X.; Shi, L.; Gao, R. Shape-Controlled Synthesis and Catalytic Application of Ceria Nanomaterials. *Dalton Trans.* **2012**, *41*, 14455−14475.
(10) Trovarelli, A. Catalytic Properties of Ceria and CeO_2-Containing Materials. *Catal. Rev.: Sci. Eng.* **1996**, *38*, 439−520.
(11) Xu, C.; Lin, Y.; Wang, J.; Wu, L.; Wei, W.; Ren, J.; Qu, X. Nanoceria-Triggered Synergetic Drug Release Based on CeO_2-Capped Mesoporous Silica Host-Guest Interactions and Switchable Enzymatic Activity and Cellular Effects of CeO_2. *Adv. Healthcare Mater.* **2013**, *2*, 1591−1599.
(12) Mandoli, C.; Pagliari, F.; Pagliari, S.; Forte, G.; Di Nardo, P.; Licoccia, S.; Traversa, E. Stem Cell Aligned Growth Induced by CeO_2 Nanoparticles in PLGA Scaffolds with Improved Bioactivity for Regenerative Medicine. *Adv. Funct. Mater.* **2010**, *20*, 1617−1624.
(13) Kim, C. K.; Kim, T.; Choi, I.-Y.; Soh, M.; Kim, D.; Kim, Y.-J.; Jang, H.; Yang, H.-S.; Kim, J. Y.; Park, H.-K.; Park, S. P.; Park, S.; Yu, T.; Yoon, B.-W.; Lee, S.-H.; Hyeon, T. Ceria Nanoparticles That Can Protect against Ischemic Stroke. *Angew. Chem., Int. Ed.* **2012**, *51*, 11039−11043.
(14) Scheffe, J. R.; Welte, M.; Steinfeld, A. Thermal Reduction of Ceria within an Aerosol Reactor for H_2O and CO_2 Splitting. *Ind. Eng. Chem. Res.* **2014**, *53*, 2175−2182.
(15) Furler, P.; Scheffe, J. R.; Steinfeld, A. Syngas Production by Simultaneous Splitting of H_2O and CO_2 via Ceria Redox Reactions in a High-Temperature Solar Reactor. *Energy Environ. Sci.* **2012**, *5*, 6098−6103.
(16) Furler, P.; Scheffe, J.; Gorbar, M.; Moes, L.; Vogt, U.; Steinfeld, A. Solar Thermochemical CO_2 Splitting Utilizing a Reticulated Porous Ceria Redox System. *Energy Fuels* **2012**, *26*, 7051−7059.
(17) Adachi, G.; Imanaka, N. The Binary Rare Earth Oxides. *Chem. Rev.* **1998**, *98*, 1479−1514.
(18) Yashima, M.; Ishimura, D.; Yamaguchi, Y.; Ohoyama, K.; Kawachi, K. High-Temperature Neutron Powder Diffraction Study of Cerium Dioxide up to 1770 K. *Chem. Phys. Lett.* **2003**, *372*, 784−787.
(19) Yashima, M.; Kobayashi, S. Positional Disorder of Oxygen Ions in Ceria at High Temperatures. *Appl. Phys. Lett.* **2004**, *84*, 526−528.
(20) Knappe, P.; Eyring, L. Preparation and Electron Microscopy of Intermediate Phases in the Interval Ce_7O_{12} - $Ce_{11}O_{20}$. *J. Solid State Chem.* **1985**, *58*, 312−324.
(21) Brauer, G.; Gingerich, K. A. Über Die Oxyde Des cers—V. *J. Inorg. Nucl. Chem.* **1960**, *16*, 87−99.
(22) Shannon, R. D.; Prewitt, C. T. Effective Ionic Radii in Oxides and Fluorides. *Acta Crystallogr., Sect. B: Struct. Crystallogr. Cryst. Chem.* **1969**, *25*, 925−946.
(23) Zinkevich, M.; Djurovic, D.; Aldinger, F. Thermodynamic Modelling of the Cerium - Oxygen System. *Solid State Ionics* **2006**, *177*, 989−1001.
(24) Sørensen, O. T. Thermodynamic Studies of the Phase Relationships of Nonstoichiometric Cerium Oxides at Higher Temperatures. *J. Solid State Chem.* **1976**, *18*, 217−233.
(25) Kümmerle, E.; Heger, G. The Structures of C−$Ce_2O_{3+\delta}$, Ce_7O_{12}, and $Ce_{11}O_{20}$. *J. Solid State Chem.* **1999**, *147*, 485−500.
(26) Ray, S. P.; Nowick, A. S.; Cox, D. E. X-Ray and Neutron Diffraction Study of Intermediate Phases in Nonstoichiometric Cerium Dioxide. *J. Solid State Chem.* **1975**, *15*, 344−351.
(27) Ray, S. P.; Cox, D. E. Neutron Diffraction Determination of the Crystal Structure of Ce_7O_{12}. *J. Solid State Chem.* **1975**, *15*, 333−343.
(28) Tsunekawa, S.; Sivamohan, R.; Ito, S.; Kasuya, A.; Fukuda, T. Structural Study on Monosize CeO_{2-X} Nano-Particles. *Nanostruct. Mater.* **1999**, *11*, 141−147.
(29) Bevan, D. J. M. Ordered Intermediate Phases in the System CeO_2-Ce_2O_3. *J. Inorg. Nucl. Chem.* **1955**, *1*, 49−59.
(30) Perrichon, V.; Laachir, A.; Bergeret, G.; Fréty, R.; Tournayan, L.; Touret, O. Reduction of Cerias with Different Textures by Hydrogen and Their Reoxidation by Oxygen. *J. Chem. Soc., Faraday Trans.* **1994**, *90*, 773−781.
(31) Bärnighausen, H.; Schiller, G. The Crystal Structure of A-Ce_2O_3. *J. Less-Common Met.* **1985**, *110*, 385−390.
(32) Conesa, J. Computer Modeling of Surfaces and Defects on Cerium Dioxide. *Surf. Sci.* **1995**, *339*, 337−352.
(33) Kim, D.-J. Lattice Parameters, Ionic Conductivities, and Solubility Limits in Fluorite-Structure MO_2 Oxide [M = Hf^{4+}, Zr^{4+}, Ce^{4+}, Th^{4+}, U^{4+}] Solid Solutions. *J. Am. Ceram. Soc.* **1989**, *72*, 1415−1421.
(34) Hong, S. J.; Virkar, A. V. Lattice Parameters and Densities of Rare-Earth Oxide Doped Ceria Electrolytes. *J. Am. Ceram. Soc.* **1995**, *78*, 433−439.
(35) Nakamura, A. New Defect-Crystal-Chemical Approach to Non-Vegardianity and Complex Defect Structure of Fluorite-Based MO_2−$LnO_{1.5}$ Solid Solutions (M^{4+} = Ce, Th; Ln^{3+} = Lanthanide) Part I: Model Description and Lattice-Parameter Data Analysis. *Solid State Ionics* **2010**, *181*, 1543−1564.
(36) Nakamura, A. New Defect-Crystal-Chemical Approach to Non-Vegardianity and Complex Defect Structure of Fluorite-Based MO_2−$LnO_{1.5}$ Solid Solutions (M^{4+} = Ce, Th; Ln^{3+} = lanthanide)Part II: Detailed Local-Structure and Ionic-Conductivity Analysis. *Solid State Ionics* **2010**, *181*, 1631−1653.
(37) Di Monte, R.; Kaspar, J. Nanostructured CeO_2-ZrO_2 Mixed Oxides. *J. Mater. Chem.* **2005**, *15*, 633−648.
(38) Etsell, T. H.; Flengas, S. N. Electrical Properties of Solid Oxide Electrolytes. *Chem. Rev.* **1970**, *70*, 339−376.
(39) Duwez, P.; Odell, F. Phase Relationships in the System Zirconia-Ceria. *J. Am. Ceram. Soc.* **1950**, *33*, 274−283.
(40) Yoshimura, M.; Tani, E.; Somiya, S. The Confirmation of Phase Equilibria in the System ZrO_2-CeO_2 below 1400°C. *Solid State Ionics* **1981**, *3*−*4*, 477−481.
(41) Duran, P.; Gonzalez, M.; Moure, C.; Jurado, J. R.; Pascual, C. A New Tentative Phase Equilibrium Diagram for the ZrO_2-CeO_2 System in Air. *J. Mater. Sci.* **1990**, *25*, 5001−5006.
(42) Yashima, M.; Takashina, H.; Kakihana, M.; Yoshimura, M. Low-Temperature Phase Equilibria by the Flux Method and the Metastable-Stable Phase Diagram in the ZrO_2-CeO_2 System. *J. Am. Ceram. Soc.* **1994**, *77*, 1869−1874.
(43) Yashima, M. Invited Review: Some Recent Developments in the Atomic-Scale Characterization of Structural and Transport Properties of Ceria-Based Catalysts and Ionic Conductors. *Catal. Today* **2015**, *253*, 3−19.
(44) Du, Y.; Yashima, M.; Koura, T.; Kakihana, M.; Yoshimura, M. Thermodynamic Evaluation of the ZrO_2-CeO_2 System. *Scr. Metall. Mater.* **1994**, *31*, 327−332.
(45) Yashima, M.; Arashi, H.; Kakihana, M.; Yoshimura, M. Raman Scattering Study of Cubic-Tetragonal Phase Transition in $Zr_{1-x}Ce_xO_2$ Solid Solution. *J. Am. Ceram. Soc.* **1994**, *77*, 1067−1071.
(46) Yashima, M.; Morimoto, K.; Ishizawa, N.; Yoshimura, M. Zirconia-Ceria Solid Solution Synthesis and the Temperature-Time-Transformation Diagram for the 1:1 Composition. *J. Am. Ceram. Soc.* **1993**, *76*, 1745−1750.
(47) Yashima, M.; Sasaki, S.; Yamaguchi, Y.; Kakihana, M.; Yoshimura, M.; Mori, T. Internal Distortion in ZrO_2−CeO_2 Solid

Solutions: Neutron and High-Resolution Synchrotron X-Ray Diffraction Study. *Appl. Phys. Lett.* **1998**, *72*, 182.
(48) Yashima, M.; Mitsuhashi, T.; Takashina, H.; Kakihana, M.; Ikegami, T.; Yoshimura, M. Tetragonal-Monoclinic Phase Transition Enthalpy and Temperature of ZrO_2-CeO_2 Solid Solutions. *J. Am. Ceram. Soc.* **1995**, *78*, 2225−2228.
(49) Yashima, M.; Hirose, T.; Katano, S.; Suzuki, Y.; Kakihana, M.; Yoshimura, M. Structural Changes of ZrO_2-CeO_2 Solid Solutions around the Monoclinic-Tetragonal Phase Boundary. *Phys. Rev. B: Condens. Matter Mater. Phys.* **1995**, *51*, 8018−8025.
(50) Thomson, J. B.; Armstrong, A. R.; Bruce, P. G. An Interstitial Pyrochlore Formed by Chemical Intercalation of Oxygen. *Chem. Commun.* **1996**, 10, 1165−1166.10.1039/cc9960001165.
(51) Thomson, J. B.; Armstrong, A. R.; Bruce, P. G. A New Class of Pyrochlore Solid Solution Formed by Chemical Intercalation of Oxygen. *J. Am. Chem. Soc.* **1996**, *118*, 11129−11133.
(52) Kishimoto, H.; Omata, T.; Otsuka-Yao-Matsuo, S.; Ueda, K.; Hosono, H.; Kawazoe, H. Crystal Structure of Metastable κ-$CeZrO_4$ Phase Possessing an Ordered Arrangement of Ce and Zr Ions. *J. Alloys Compd.* **2000**, *312*, 94−103.
(53) Otsuka-Yao-Matsuo, S.; Omata, T.; Izu, N.; Kishimoto, H. Oxygen Release Behavior of $CeZrO_4$ Powders and Appearance of New Compounds κ and t*. *J. Solid State Chem.* **1998**, *138*, 47−54.
(54) Yashima, M.; Kakihana, M.; Yoshimura, M. Metastable-Stable Phase Diagrams in the Zirconia-Containing Systems Utilized in Solid-Oxide Fuel Cell Application. *Solid State Ionics* **1996**, *86−88*, 1131−1149.
(55) Vlaic, G.; Fornasiero, P.; Geremia, S.; Kašpar, J.; Graziani, M. Relationship between the Zirconia-Promoted Reduction in the Rh-Loaded $Ce_{0.5}Zr_{0.5}O_2$ Mixed Oxide and the Zr−O Local Structure. *J. Catal.* **1997**, *168*, 386−392.
(56) Fornasiero, P.; Fonda, E.; Di Monte, R.; Vlaic, G.; Kašpar, J.; Graziani, M. Relationships between Structural/Textural Properties and Redox Behavior in $Ce_{0.6}Zr_{0.4}O_2$ Mixed Oxides. *J. Catal.* **1999**, *187*, 177−185.
(57) Lemaux, S.; Bensaddik, A.; van der Eerden, A. M. J.; Bitter, J. H.; Koningsberger, D. C. Understanding of Enhanced Oxygen Storage Capacity in $Ce_{0.5}Zr_{0.5}O_2$: The Presence of an Anharmonic Pair Distribution Function in the Zr−O_2 Subshell as Analyzed by XAFS Spectroscopy. *J. Phys. Chem. B* **2001**, *105*, 4810−4815.
(58) Omata, T.; Kishimoto, H.; Otsuka-Yao-Matsuo, S.; Ohtori, N.; Umesaki, N. Vibrational Spectroscopic and X-Ray Diffraction Studies of Cerium Zirconium Oxides with Ce/Zr Composition Ratio = 1 Prepared by Reduction and Successive Oxidation of t′-$(Ce_{0.5}Zr_{0.5})O_2$ Phase. *J. Solid State Chem.* **1999**, *147*, 573−583.
(59) Montini, T.; Speghini, A.; De Rogatis, L.; Lorenzut, B.; Bettinelli, M.; Graziani, M.; Fornasiero, P. Identification of the Structural Phases of $Ce_xZr_{1-x}O_2$ by Eu(III) Luminescence Studies. *J. Am. Chem. Soc.* **2009**, *131*, 13155−13160.
(60) Tiseanu, C.; Parvulescu, V.; Avram, D.; Cojocaru, B.; Boutonnet, M.; Sanchez-Dominguez, M. Local Structure and Nanoscale Homogeneity of CeO_2-ZrO_2: Differences and Similarities to Parent Oxides Revealed by Luminescence with Temporal and Spectral Resolution. *Phys. Chem. Chem. Phys.* **2014**, *16*, 703−710.
(61) Parvulescu, V. I.; Tiseanu, C. Local Structure in CeO_2 and CeO_2−ZrO_2 Nanoparticles Probed by Eu Luminescence. *Catal. Today* **2015**, *253*, 33−39.
(62) Montini, T.; Speghini, A.; Fornasiero, P.; Bettinelli, M.; Graziani, M. Effect of the Thermal Pre-Treatments on Ceria−zirconia Redox Properties: An Eu^{3+} Luminescence Study. *J. Alloys Compd.* **2008**, *451*, 617−620.
(63) Tiseanu, C.; Parvulescu, V. I.; Sanchez-Dominguez, M.; Boutonnet, M. Temperature Induced Conversion from Surface to "Bulk" Sites in Eu^{3+}-Impregnated CeO_2 Nanocrystals. *J. Appl. Phys.* **2012**, *112*, 013521.
(64) Avram, D.; Gheorghe, C.; Rotaru, C.; Cojocaru, B.; Florea, M.; Parvulescu, V.; Tiseanu, C. Lanthanide−Lanthanide and Lanthanide−Defect Interactions in Co-Doped Ceria Revealed by Luminescence Spectroscopy. *J. Alloys Compd.* **2014**, *616*, 535−541.
(65) Avram, D.; Sanchez-Dominguez, M.; Cojocaru, B.; Florea, M.; Parvulescu, V.; Tiseanu, C. Toward a Unified Description of Luminescence−Local Structure Correlation in Ln Doped CeO_2 Nanoparticles: Roles of Ln Ionic Radius, Ln Concentration, and Oxygen Vacancies. *J. Phys. Chem. C* **2015**, *119*, 16303−16313.
(66) Fornasiero, P.; Speghini, A.; Di Monte, R.; Bettinelli, M.; Kašpar, J.; Bigotto, A.; Sergo, V.; Graziani, M. Laser-Excited Luminescence of Trivalent Lanthanide Impurities and Local Structure in CeO_2−ZrO_2 Mixed Oxides. *Chem. Mater.* **2004**, *16*, 1938−1944.
(67) Vanpoucke, D. E. P.; Cottenier, S.; Van Speybroeck, V.; Van Driessche, I.; Bultinck, P. Tetravalent Doping of CeO_2: The Impact of Valence Electron Character on Group IV Dopant Influence. *J. Am. Ceram. Soc.* **2014**, *97*, 258−266.
(68) Chen, W.; Hong, J.; Li, H.; Li, Y. Fabrication and Ultraviolet-Shielding Properties of Silica-Coated Titania-Doped Ceria Nanoparticles. *J. Rare Earths* **2011**, *29*, 810−814.
(69) Fu, M.; Wei, L.; Li, Y.; Zhou, X.; Hao, S.; Li, Y. Surface Charge Tuning of Ceria Particles by Titanium Doping: Towards Significantly Improved Polishing Performance. *Solid State Sci.* **2009**, *11*, 2133−2137.
(70) Reddy, B. M.; Khan, A.; Lakshmanan, P.; Aouine, M.; Loridant, S.; Volta, J.-C. Structural Characterization of Nanosized CeO_2-SiO_2, CeO_2-TiO_2, and CeO_2-ZrO_2 Catalysts by XRD, Raman, and HREM Techniques. *J. Phys. Chem. B* **2005**, *109*, 3355−3363.
(71) Martos, M.; Julián-López, B.; Folgado, J. V.; Cordoncillo, E.; Escribano, P. Sol−Gel Synthesis of Tunable Cerium Titanate Materials. *Eur. J. Inorg. Chem.* **2008**, *2008*, 3163−3171.
(72) Kępiński, L.; Wołcyrz, M.; Marchewka, M. Structure Evolution of Nanocrystalline CeO_2 Supported on Silica: Effect of Temperature and Atmosphere. *J. Solid State Chem.* **2002**, *168*, 110−118.
(73) van Hal, H. A. M.; Hintzen, H. T. Compound Formation in the Ce_2O_3-SiO_2 System. *J. Alloys Compd.* **1992**, *179*, 77−85.
(74) Zec, S.; Bošković, S.; Bogdanov, Ž.; Popović, N. Low Temperature $Ce_2Si_2O_7$ Polymorph Formed by Mechanical Activation. *Mater. Chem. Phys.* **2006**, *95*, 150−153.
(75) Rocchini, E.; Vicario, M.; Llorca, J.; de Leitenburg, C.; Dolcetti, G.; Trovarelli, A. Reduction and Oxygen Storage Behavior of Noble Metals Supported on Silica-Doped Ceria. *J. Catal.* **2002**, *211*, 407−421.
(76) Rocchini, E.; Trovarelli, A.; Llorca, J.; Graham, G. W.; Weber, W. H.; Maciejewski, M.; Baiker, A. Relationships between Structural/Morphological Modifications and Oxygen Storage−Redox Behavior of Silica-Doped Ceria. *J. Catal.* **2000**, *194*, 461−478.
(77) Chavan, S. V.; Tyagi, A. K. Investigations on Ceria−Hafnia System for Phase Analysis, and HT-XRD Studies on a Few Cubic Compositions. *Mater. Sci. Eng., A* **2006**, *433*, 203−207.
(78) Fujimori, H.; Yashima, M.; Sasaki, S.; Kakihana, M.; Mori, T.; Tanaka, M.; Yoshimura, M. Internal Distortion in Ceria-Doped Hafnia Solid Solutions: High-Resolution X-Ray Diffraction and Raman Scattering. *Phys. Rev. B: Condens. Matter Mater. Phys.* **2001**, *64*, 134104.
(79) Reddy, B. M.; Bharali, P.; Thrimurthulu, G.; Saikia, P.; Katta, L.; Park, S.-E. Catalytic Efficiency of Ceria−Zirconia and Ceria−Hafnia Nanocomposite Oxides for Soot Oxidation. *Catal. Lett.* **2008**, *123*, 327−333.
(80) Khder, A. E. R. S.; Hassan, H. M. A.; Betiha, M. A.; Khairou, K. S.; Ibrahim, A. A. CO Oxidation over Au and Pd Nanoparticles Supported on Ceria − Hafnia Mixed Oxides. *React. Kinet., Mech. Catal.* **2014**, *112*, 61−75.
(81) Harshini, D.; Lee, D. H.; Jeong, J.; Kim, Y.; Nam, S. W.; Ham, H. C.; Han, J. H.; Lim, T.-H.; Yoon, C. W. Enhanced Oxygen Storage Capacity of $Ce_{0.65}Hf_{0.25}M_{0.1}O_{2-\delta}$ (M = Rare Earth Elements): Applications to Methane Steam Reforming with High Coking Resistance. *Appl. Catal., B* **2014**, *148−149*, 415−423.
(82) Zhou, G.; Gorte, R. J. Thermodynamic Investigation of the Redox Properties for Ceria-Hafnia, Ceria-Terbia, and Ceria-Praseodymia Solid Solutions. *J. Phys. Chem. B* **2008**, *112*, 9869−9875.
(83) Brauer, G.; Gradinger, H. Über Heterotype Mischphasen Bei Seltenerdoxyden. I. *Z. Anorg. Allg. Chem.* **1954**, *276*, 209−226.

(84) Brauer, G.; Gradinger, H. Über Anomale Mischkristalle Im Bereiche Des Fluoritgittertyps. *Naturwissenschaften* **1951**, *38*, 559−560.
(85) Zintl, E.; Croatto, U. Fluoritgitter Mit Leeren Anionenplätzen. *Zeitschrift für Anorg. und Allg. Chemie* **1939**, *242*, 79−86.
(86) McCullough, J. D. An X-Ray Study of the Rare-Earth Oxide Systems: Ce^{IV}-Nd^{III}, Cr^{IV}-Pr^{III}, Ce^{IV}-Pr^{IV} and Pr^{IV}-Nd^{III}. *J. Am. Chem. Soc.* **1950**, *72*, 1386−1390.
(87) McCullough, J. D.; Britton, J. D. X-Ray Studies of Rare Earth Oxide Systems. II. The Oxide Systems Ce^{IV}-Sm^{III}, Ce^{IV}-Gd^{III}, Ce^{IV}-Y^{III}, Pr^{IV}-Y^{III} and Pr^{III}-Y^{III}. *J. Am. Chem. Soc.* **1952**, *74*, 5225−5227.
(88) Chandrashekhar, G. V.; Mehrotra, P. N.; Rao, G. V. S.; Subbarao, E. C.; Rao, C. N. R. Semiconduction in Non-Stoichiometric Rare Earth Oxides. *Trans. Faraday Soc.* **1967**, *63*, 1295−1301.
(89) Eguchi, K.; Setoguchi, T.; Inoue, T.; Arai, H. Electrical Properties of Ceria-Based Oxides and Their Application to Solid Oxide Fuel Cells. *Solid State Ionics* **1992**, *52*, 165−172.
(90) Chavan, S.; Tyagi, A. Sub-Solidus Phase Equilibria in CeO_2−SrO System. *Thermochim. Acta* **2002**, *390*, 79−82.
(91) Truffault, L.; Ta, M.-T.; Devers, T.; Konstantinov, K.; Harel, V.; Simmonard, C.; Andreazza, C.; Nevirkovets, I. P.; Pineau, A.; Veron, O.; Blondeau, J.-P. Application of Nanostructured Ca-Doped CeO_2 for Ultraviolet Filtration. *Mater. Res. Bull.* **2010**, *45*, 527−535.
(92) Yan, M.; Mori, T.; Ye, F.; Ou, D. R.; Zou, J.; Drennan, J. Effects of Dopant Concentration and Calcination Temperature on the Microstructure of Ca-Doped Ceria Nanopowders. *J. Eur. Ceram. Soc.* **2008**, *28*, 2709−2716.
(93) Yan, M.; Mori, T.; Zou, J.; Drennan, J. Effect of Grain Growth on Densification and Conductivity of Ca-Doped CeO_2 Electrolyte. *J. Am. Ceram. Soc.* **2009**, *92*, 2745−2750.
(94) Wu, Y.-C.; Lin, C.-C. The Microstructures and Property Analysis of Aliovalent Cations (Sm^{3+}, Mg^{2+}, Ca^{2+}, Sr^{2+}, Ba^{2+}) Co-Doped Ceria-Base Electrolytes after an Aging Treatment. *Int. J. Hydrogen Energy* **2014**, *39*, 7988−8001.
(95) Kreuer, K. D. Proton-Conducting Oxides. *Annu. Rev. Mater. Res.* **2003**, *33*, 333−359.
(96) Bi, L.; Boulfrad, S.; Traversa, E. Steam Electrolysis by Solid Oxide Electrolysis Cells (SOECs) with Proton-Conducting Oxides. *Chem. Soc. Rev.* **2014**, *43*, 8255−8270.
(97) Danielson, E.; Devenney, M.; Giaquinta, D. M.; Golden, J. H.; Haushalter, R. C.; McFarland, E. W.; Poojary, D. M.; Reaves, C. M.; Weinberg, W. H.; Wu, X. D. A Rare-Earth Phosphor Containing One-Dimensional Chains Identified Through Combinatorial Methods. *Science* **1998**, *279*, 837−839.
(98) Yao, H.; Yu Yao, Y. Ceria in Automotive Exhaust Catalysts I. Oxygen Storage. *J. Catal.* **1984**, *86*, 254−265.
(99) Kašpar, J.; Fornasiero, P.; Graziani, M. Use of CeO_2-Based Oxides in the Three-Way Catalysis. *Catal. Today* **1999**, *50*, 285−298.
(100) Craciun, R.; Shereck, B.; Gorte, R. J. Kinetic Studies of Methane Steam Reforming on Ceria-Supported Pd. *Catal. Lett.* **1998**, *51*, 149−153.
(101) Wang, X.; Gorte, R. J. Steam Reforming of N-Butane on Pd/Ceria. *Catal. Lett.* **2001**, *73*, 15−19.
(102) Bunluesin, T.; Gorte, R. J.; Graham, G. W. Studies of the Water-Gas-Shift Reaction on Ceria-Supported Pt, Pd, and Rh: Implications for Oxygen-Storage Properties. *Appl. Catal., B* **1998**, *15*, 107−114.
(103) Duprez, D.; Descorme, C.; Birchem, T.; Rohart, E. Oxygen Storage and Mobility on Model Three-Way Catalysts. *Top. Catal.* **2001**, *16−17*, 49−56.10.1023/A:1016622612521.
(104) Su, E. C.; Montreuil, C. N.; Rothschild, W. G. Oxygen Storage Capacity of Monolith Three-Way Catalysts. *Appl. Catal.* **1985**, *17*, 75−86.
(105) Kummer, J. T. Catalysts for Automobile Emission Control. *Prog. Energy Combust. Sci.* **1980**, *6*, 177−199.
(106) Madier, Y.; Descorme, C.; Le Govic, A. M.; Duprez, D. Oxygen Mobility in CeO_2 and $Ce_xZr_{(1-x)}O_2$ Compounds: Study by CO Transient Oxidation and $^{18}O/^{16}O$ Isotopic Exchange. *J. Phys. Chem. B* **1999**, *103*, 10999−11006.
(107) Fornasiero, P.; Dimonte, R.; Rao, G. R.; Kaspar, J.; Meriani, S.; Trovarelli, A.; Graziani, M. Rh-Loaded CeO_2-ZrO_2 Solid-Solutions as Highly Efficient Oxygen Exchangers: Dependence of the Reduction Behavior and the Oxygen Storage Capacity on the Structural-Properties. *J. Catal.* **1995**, *151*, 168−177.
(108) Murota, T.; Hasegawa, T.; Aozasa, S.; Matsui, H.; Motoyama, M. Production Method of Cerium Oxide with High Storage Capacity of Oxygen and Its Mechanism. *J. Alloys Compd.* **1993**, *193*, 298−299.
(109) Miki, T.; Ogawa, T.; Haneda, M.; Kakuta, N.; Ueno, A.; Tateishi, S.; Matsuura, S.; Sato, M. Enhanced Oxygen Storage Capacity of Cerium Oxides in $CeO_2/La_2O_3/Al_2O_3$ Containing Precious Metals. *J. Phys. Chem.* **1990**, *94*, 6464−6467.
(110) Maillet, T.; Madier, Y.; Taha, R.; Barbier, J.; Duprez, D. Spillover of Oxygen Species in the Steam Reforming of Propane on Ceria-Containing Catalysts. *Stud. Surf. Sci. Catal.* **1997**, *112*, 267−275.
(111) Cho, B. Chemical Modification of Catalyst Support for Enhancement of Transient Catalytic Activity: Nitric Oxide Reduction by Carbon Monoxide over Rhodium. *J. Catal.* **1991**, *131*, 74−87.
(112) Rossignol, S.; Madier, Y.; Duprez, D. Preparation of Zirconia−Ceria Materials by Soft Chemistry. *Catal. Today* **1999**, *50*, 261−270.
(113) Trovarelli, A.; Zamar, F.; Llorca, J.; Leitenburg, C.; Dolcetti, G.; Kiss, J. T. Nanophase Fluorite-Structured CeO_2−ZrO_2 Catalysts Prepared by High-Energy Mechanical Milling. *J. Catal.* **1997**, *169*, 490−502.
(114) Kacimi, S.; Barbier, J.; Taha, R.; Duprez, D. Oxygen Storage Capacity of Promoted Rh/CeO_2 Catalysts. Exceptional Behavior of $RhCu/CeO_2$. *Catal. Lett.* **1993**, *22*, 343−350.
(115) Gorte, R. J. Ceria in Catalysis: From Automotive Applications to the Water-Gas Shift Reaction. *AIChE J.* **2010**, *56*, 1126−1135.
(116) Bedrane, S.; Descorme, C.; Duprez, D. Investigation of the Oxygen Storage Process on Ceria- and Ceria−Zirconia-Supported Catalysts. *Catal. Today* **2002**, *75*, 401−405.
(117) Descorme, C.; Taha, R.; Mouaddib-Moral, N.; Duprez, D. Oxygen Storage Capacity Measurements of Three-Way Catalysts under Transient Conditions. *Appl. Catal., A* **2002**, *223*, 287−299.
(118) Martin, D.; Taha, R.; Duprez, D. Effects of Sintering and of Additives on the Oxygen Storage Capacity of PtRh Catalysts. *Stud. Surf. Sci. Catal.* **1995**, *96*, 801−811.
(119) Taha, R.; Duprez, D.; Mouaddib-Moral, N.; Gauthier, C. Oxygen Storage Capacity of Three-Way Catalysts: A Global Test for Catalyst Deactivation. *Stud. Surf. Sci. Catal.* **1998**, *116*, 549−558.
(120) Taha, R.; Martin, D.; Kacimi, S.; Duprez, D. Exchange and Oxidation of $C^{16}O$ on ^{18}O-Predosed Rh/Al_2O_3 and Rh/CeO_2 Catalysts. *Catal. Today* **1996**, *29*, 89−92.
(121) Holmgren, A.; Andersson, B. Oxygen Storage Dynamics in $Pt/CeO_2/Al_2O_3$ Catalysts. *J. Catal.* **1998**, *178*, 14−25.
(122) Descorme, C.; Duprez, D. Oxygen Surface Mobility and Isotopic Exchange on Oxides: Role of the Nature and the Structure of Metal Particles. *Appl. Catal., A* **2000**, *202*, 231−241.
(123) Duprez, D. Study of Surface Mobility by Isotopic Exchange: Recent Developments and Perspectives. *Stud. Surf. Sci. Catal.* **1997**, *112*, 13−28.
(124) Descorme, C.; Madier, Y.; Duprez, D. Infrared Study of Oxygen Adsorption and Activation on Cerium−Zirconium Mixed Oxides. *J. Catal.* **2000**, *196*, 167−173.
(125) Martínez-Arias, A.; Fernández-García, M.; Salamanca, L. N.; Valenzuela, R. X.; Conesa, J. C.; Soria, J. Structural and Redox Properties of Ceria in Alumina-Supported Ceria Catalyst Supports. *J. Phys. Chem. B* **2000**, *104*, 4038−4046.
(126) Hepburn, J. S.; Dobson, D. A.; Gandhi, H. S. A New Test for Catalyst Oxygen Storage Which Correlates with Catalyst Performance on the Vehicle. *International Fuels and Lubricants Meeting and Exposition*, Baltimore, MD, Oct 17−20, 1994; SAE International, 1994, 942071.
(127) Larese, C.; Cabello Galisteo, F.; López Granados, M.; Mariscal López, R.; Fierro, J. L.; Lambrou, P.; Efstathiou, A. Effects of Calcination Temperature on the Stability of $CePO_4$ Detected in Vehicle-Aged Commercial Three-Way Catalysts. *Appl. Catal., B* **2004**, *48*, 113−123.

(128) Christou, S. Y.; Efstathiou, A. M. The Effects of P-Poisoning of $Ce_xZr_{1-x}O_2$ on the Transient Oxygen Storage and Release Kinetics. *Top. Catal.* **2013**, *56*, 232−238.
(129) Christou, S. Y.; Álvarez-Galván, M. C.; Fierro, J. L. G.; Efstathiou, A. M. Suppression of the Oxygen Storage and Release Kinetics in $Ce_{0.5}Zr_{0.5}O_2$ Induced by P, Ca and Zn Chemical Poisoning. *Appl. Catal., B* **2011**, *106*, 103−113.
(130) Luo, T.; Gorte, R. J. A Mechanistic Study of Sulfur Poisoning of the Water-Gas-Shift Reaction over Pd/Ceria. *Catal. Lett.* **2003**, *85*, 139−146.
(131) Zhou, G.; Shah, P. R.; Montini, T.; Fornasiero, P.; Gorte, R. J. Oxidation Enthalpies for Reduction of Ceria Surfaces. *Surf. Sci.* **2007**, *601*, 2512−2519.
(132) Shah, P. R.; Kim, T.; Zhou, G.; Fornasiero, P.; Gorte, R. J. Evidence for Entropy Effects in the Reduction of Ceria−Zirconia Solutions. *Chem. Mater.* **2006**, *18*, 5363−5369.
(133) Kim, T.; Vohs, J. M.; Gorte, R. J. Thermodynamic Investigation of the Redox Properties of Ceria−Zirconia Solid Solutions. *Ind. Eng. Chem. Res.* **2006**, *45*, 5561−5565.
(134) Zhou, G.; Shah, P. R.; Kim, T.; Fornasiero, P.; Gorte, R. J. Oxidation Entropies and Enthalpies of Ceria−Zirconia Solid Solutions. *Catal. Today* **2007**, *123*, 86−93.
(135) Novotny, Z.; Netzer, F. P.; Dohnálek, Z. Cerium Oxide Nanoclusters on Graphene/Ru(0001): Intercalation of Oxygen via Spillover. *ACS Nano* **2015**, *9*, 8617−8626.
(136) Vecchietti, J.; Bonivardi, A.; Xu, W.; Stacchiola, D.; Delgado, J. J.; Calatayud, M.; Collins, S. E. Understanding the Role of Oxygen Vacancies in the Water Gas Shift Reaction on Ceria-Supported Platinum Catalysts. *ACS Catal.* **2014**, *4*, 2088−2096.
(137) Ganduglia-Pirovano, M. V.; Da Silva, J. L. F.; Sauer, J. Density-Functional Calculations of the Structure of Near-Surface Oxygen Vacancies and Electron Localization on CeO_2(111). *Phys. Rev. Lett.* **2009**, *102*, 026101.
(138) Li, H.-Y.; Wang, H.-F.; Gong, X.-Q.; Guo, Y.-L.; Guo, Y.; Lu, G.; Hu, P. Multiple Configurations of the Two Excess 4f Electrons on Defective CeO_2(111): Origin and Implications. *Phys. Rev. B: Condens. Matter Mater. Phys.* **2009**, *79*, 193401.
(139) Jerratsch, J.-F.; Shao, X.; Nilius, N.; Freund, H.-J.; Popa, C.; Ganduglia-Pirovano, M. V.; Burow, A. M.; Sauer, J. Electron Localization in Defective Ceria Films: A Study with Scanning-Tunneling Microscopy and Density-Functional Theory. *Phys. Rev. Lett.* **2011**, *106*, 246801.
(140) Esch, F.; Fabris, S.; Zhou, L.; Montini, T.; Africh, C.; Fornasiero, P.; Comelli, G.; Rosei, R. Electron Localization Determines Defect Formation on Ceria Substrates. *Science* **2005**, *309*, 752−755.
(141) Kullgren, J.; Wolf, M. J.; Castleton, C. W. M.; Mitev, P.; Briels, W. J.; Hermansson, K. Oxygen Vacancies versus Fluorine at CeO_2(111): A Case of Mistaken Identity? *Phys. Rev. Lett.* **2014**, *112*, 156102.
(142) Pieper, H. H.; Derks, C.; Zoellner, M. H.; Olbrich, R.; Tröger, L.; Schroeder, T.; Neumann, M.; Reichling, M. Morphology and Nanostructure of CeO_2(111) Surfaces of Single Crystals and Si(111) Supported Ceria Films. *Phys. Chem. Chem. Phys.* **2012**, *14*, 15361−15368.
(143) Wu, X.-P.; Gong, X.-Q. Clustering of Oxygen Vacancies at CeO_2(111): Critical Role of Hydroxyls. *Phys. Rev. Lett.* **2016**, *116*, 086102.
(144) Fabris, S.; de Gironcoli, S.; Baroni, S.; Vicario, G.; Balducci, G. Taming Multiple Valency with Density Functionals: A Case Study of Defective Ceria. *Phys. Rev. B: Condens. Matter Mater. Phys.* **2005**, *71*, 041102.
(145) Becke, A. D. Density-Functional Thermochemistry. III. The Role of Exact Exchange. *J. Chem. Phys.* **1993**, *98*, 5648.
(146) Branda, M. M.; Castellani, N. J.; Grau-Crespo, R.; de Leeuw, N. H.; Hernandez, N. C.; Sanz, J. F.; Neyman, K. M.; Illas, F. On the Difficulties of Present Theoretical Models to Predict the Oxidation State of Atomic Au Adsorbed on Regular Sites of CeO_2(111). *J. Chem. Phys.* **2009**, *131*, 094702.
(147) Dholabhai, P. P.; Adams, J. B.; Crozier, P.; Sharma, R. Oxygen Vacancy Migration in Ceria and Pr-Doped Ceria: A DFT+U Study. *J. Chem. Phys.* **2010**, *132*, 094104.
(148) Dholabhai, P. P.; Adams, J. B.; Crozier, P.; Sharma, R. A Density Functional Study of Defect Migration in Gadolinium Doped Ceria. *Phys. Chem. Chem. Phys.* **2010**, *12*, 7904−7910.
(149) Feng, X.; Sayle, D. C.; Wang, Z. L.; Paras, M. S.; Santora, B.; Sutorik, A. C.; Sayle, T. X. T.; Yang, Y.; Ding, Y.; Wang, X.; Her, Y.-S. Converting Ceria Polyhedral Nanoparticles into Single-Crystal Nanospheres. *Science* **2006**, *312*, 1504−1508.
(150) Sayle, D. C.; Feng, X.; Ding, Y.; Wang, Z. L.; Sayle, T. X. T. "Simulating Synthesis": Ceria Nanosphere Self-Assembly into Nanorods and Framework Architectures. *J. Am. Chem. Soc.* **2007**, *129*, 7924−7935.
(151) Zhang, C.; Michaelides, A.; Jenkins, S. J. Theory of Gold on Ceria. *Phys. Chem. Chem. Phys.* **2011**, *13*, 22−33.
(152) Zhang, C.; Michaelides, A.; King, D. A.; Jenkins, S. J. Structure of Gold Atoms on Stoichiometric and Defective Ceria Surfaces. *J. Chem. Phys.* **2008**, *129*, 194708.
(153) Branda, M. M.; Hernández, N. C.; Sanz, J. F.; Illas, F. Density Functional Theory Study of the Interaction of Cu, Ag, and Au Atoms with the Regular CeO_2 (111) Surface. *J. Phys. Chem. C* **2010**, *114*, 1934−1941.
(154) Luches, P.; Pagliuca, F.; Valeri, S.; Illas, F.; Preda, G.; Pacchioni, G. Nature of Ag Islands and Nanoparticles on the CeO_2(111) Surface. *J. Phys. Chem. C* **2012**, *116*, 1122−1132.
(155) Yang, Z.; Luo, G.; Lu, Z.; Hermansson, K. Oxygen Vacancy Formation Energy in Pd-Doped Ceria: A DFT+U Study. *J. Chem. Phys.* **2007**, *127*, 074704.
(156) Vayssilov, G. N.; Migani, A.; Neyman, K. Density Functional Modeling of the Interactions of Platinum Clusters with CeO_2 Nanoparticles of Different Size. *J. Phys. Chem. C* **2011**, *115*, 16081−16086.
(157) Alfredsson, M.; Catlow, C. R. A. A Comparison between Metal Supported c-ZrO_2 and CeO_2. *Phys. Chem. Chem. Phys.* **2002**, *4*, 6100−6108.
(158) Kim, H. Y.; Lee, H. M.; Henkelman, G. CO Oxidation Mechanism on CeO_2-Supported Au Nanoparticles. *J. Am. Chem. Soc.* **2012**, *134*, 1560−1570.
(159) Chen, Y.; Cheng, J.; Hu, P.; Wang, H. Examining the Redox and Formate Mechanisms for Water−Gas Shift Reaction on Au/CeO_2 Using Density Functional Theory. *Surf. Sci.* **2008**, *602*, 2828−2834.
(160) Sharma, S.; Hu, Z.; Zhang, P.; McFarland, E. W.; Metiu, H. CO_2 Methanation on Ru-Doped Ceria. *J. Catal.* **2011**, *278*, 297−309.
(161) Yang, Z.; Woo, T. K.; Hermansson, K. Strong and Weak Adsorption of CO on CeO_2 Surfaces from First Principles Calculations. *Chem. Phys. Lett.* **2004**, *396*, 384−392.
(162) Fronzi, M.; Piccinin, S.; Delley, B.; Traversa, E.; Stampfl, C. Water Adsorption on the Stoichiometric and Reduced CeO_2(111) Surface: A First-Principles Investigation. *Phys. Chem. Chem. Phys.* **2009**, *11*, 9188−9199.
(163) Kumar, S.; Schelling, P. K. Density Functional Theory Study of Water Adsorption at Reduced and Stoichiometric Ceria (111) Surfaces. *J. Chem. Phys.* **2006**, *125*, 204704.
(164) Chen, H.-T.; Choi, Y.; Liu, M.; Lin, M. C. A First-Principles Analysis for Sulfur Tolerance of CeO_2 in Solid Oxide Fuel Cells. *J. Phys. Chem. C* **2007**, *111*, 11117−11122.
(165) Marrocchelli, D.; Yildiz, B. First-Principles Assessment of H_2S and H_2O Reaction Mechanisms and the Subsequent Hydrogen Absorption on CeO_2(111) Surface. *J. Phys. Chem. A* **2012**, *116*, 2411−2424.
(166) Nolan, M.; Parker, S. C.; Watson, G. W. Reduction of NO_2 on Ceria Surfaces. *J. Phys. Chem. B* **2006**, *110*, 2256−2262.
(167) Rodriguez, J. A.; Jirsak, T.; Sambasivan, S.; Fischer, D.; Maiti, A. Chemistry of NO_2 on CeO_2 and MgO: Experimental and Theoretical Studies on the Formation of NO_3. *J. Chem. Phys.* **2000**, *112*, 9929.

(168) Müller, C.; Hermansson, K.; Paulus, B. Electron Correlation Contribution to the N_2O/Ceria(111) Interaction. *Chem. Phys.* **2009**, *362*, 91−96.
(169) Lu, Z.; Müller, C.; Yang, Z.; Hermansson, K.; Kullgren, J. SO_x on Ceria from Adsorbed SO_2. *J. Chem. Phys.* **2011**, *134*, 184703.
(170) Hu, Z.; Metiu, H. Halogen Adsorption on CeO_2: The Role of Lewis Acid−Base Pairing. *J. Phys. Chem. C* **2012**, *116*, 6664−6671.
(171) Preda, G.; Migani, A.; Neyman, K. M.; Bromley, S. T.; Illas, F.; Pacchioni, G. Formation of Superoxide Anions on Ceria Nanoparticles by Interaction of Molecular Oxygen with Ce^{3+} Sites. *J. Phys. Chem. C* **2011**, *115*, 5817−5822.
(172) Capdevila-Cortada, M.; García-Melchor, M.; López, N. Unraveling the Structure Sensitivity in Methanol Conversion on CeO_2: A DFT+U Study. *J. Catal.* **2015**, *327*, 58−64.
(173) Zabilskiy, M.; Djinović, P.; Tchernychova, E.; Tkachenko, O. P.; Kustov, L. M.; Pintar, A. Nanoshaped CuO/CeO_2 Materials: Effect of the Exposed Ceria Surfaces on Catalytic Activity in N_2O Decomposition Reaction. *ACS Catal.* **2015**, *5*, 5357−5365.
(174) Zhou, K.; Wang, X.; Sun, X.; Peng, Q.; Li, Y. Enhanced Catalytic Activity of Ceria Nanorods from Well-Defined Reactive Crystal Planes. *J. Catal.* **2005**, *229*, 206−212.
(175) Wang, S.; Zhao, L.; Wang, W.; Zhao, Y.; Zhang, G.; Ma, X.; Gong, J. Morphology Control of Ceria Nanocrystals for Catalytic Conversion of CO_2 with Methanol. *Nanoscale* **2013**, *5*, 5582−5588.
(176) Asahina, S.; Takami, S.; Otsuka, T.; Adschiri, T.; Terasaki, O. Exploitation of Surface-Sensitive Electrons in Scanning Electron Microscopy Reveals the Formation Mechanism of New Cubic and Truncated Octahedral CeO_2 Nanoparticles. *ChemCatChem* **2011**, *3*, 1038−1044.
(177) Agarwal, S.; Lefferts, L.; Mojet, B. L.; Ligthart, D. A. J. M.; Hensen, E. J. M.; Mitchell, D. R. G.; Erasmus, W. J.; Anderson, B. G.; Olivier, E. J.; Neethling, J. H.; Datye, A. K. Exposed Surfaces on Shape-Controlled Ceria Nanoparticles Revealed through AC-TEM and Water-Gas Shift Reactivity. *ChemSusChem* **2013**, *6*, 1898−1906.
(178) Yamashita, M.; Kameyama, K.; Yabe, S.; Yoshida, S.; Fujishiro, Y.; Kawai, T.; Sato, T. Synthesis and Microstructure of Calcia Doped Ceria as UV Filters. *J. Mater. Sci.* **2002**, *37*, 683−687.
(179) Tsai, M.-S. Powder Synthesis of Nano Grade Cerium Oxide via Homogenous Precipitation and Its Polishing Performance. *Mater. Sci. Eng., B* **2004**, *110*, 132−134.
(180) Zhou, X.-D.; Huebner, W.; Anderson, H. U. Room-Temperature Homogeneous Nucleation Synthesis and Thermal Stability of Nanometer Single Crystal CeO_2. *Appl. Phys. Lett.* **2002**, *80*, 3814−3816.
(181) Wang, Z. L.; Feng, X. Polyhedral Shapes of CeO_2 Nanoparticles. *J. Phys. Chem. B* **2003**, *107*, 13563−13566.
(182) Wang, G.; Mu, Q.; Chen, T.; Wang, Y. Synthesis, Characterization and Photoluminescence of CeO_2 Nanoparticles by a Facile Method at Room Temperature. *J. Alloys Compd.* **2010**, *493*, 202−207.
(183) Chaudhary, Y. S.; Panigrahi, S.; Nayak, S.; Satpati, B.; Bhattacharjee, S.; Kulkarni, N. Facile Synthesis of Ultra-Small Monodisperse Ceria Nanocrystals at Room Temperature and Their Catalytic Activity under Visible Light. *J. Mater. Chem.* **2010**, *20*, 2381.
(184) Li, C. R.; Cui, M. Y.; Sun, Q. T.; Dong, W. J.; Zheng, Y. Y.; Tsukamoto, K.; Chen, B. Y.; Tang, W. H. Nanostructures and Optical Properties of Hydrothermal Synthesized $CeOHCO_3$ and Calcined CeO_2 with PVP Assistance. *J. Alloys Compd.* **2010**, *504*, 498−502.
(185) Yang, S.; Gao, L. Controlled Synthesis and Self-Assembly of CeO_2 Nanocubes. *J. Am. Chem. Soc.* **2006**, *128*, 9330−9331.
(186) Taniguchi, T.; Katsumata, K.; Omata, S.; Okada, K.; Matsushita, N. Tuning Growth Modes of Ceria-Based Nanocubes by a Hydrothermal Method. *Cryst. Growth Des.* **2011**, *11*, 3754−3760.
(187) Wu, Q.; Zhang, F.; Xiao, P.; Tao, H.; Wang, X.; Hu, Z.; Lü, Y. Great Influence of Anions for Controllable Synthesis of CeO_2 Nanostructures: From Nanorods to Nanocubes. *J. Phys. Chem. C* **2008**, *112*, 17076−17080.
(188) Mai, H.-X.; Sun, L.-D.; Zhang, Y.-W.; Si, R.; Feng, W.; Zhang, H.-P.; Liu, H.-C.; Yan, C.-H. Shape-Selective Synthesis and Oxygen Storage Behavior of Ceria Nanopolyhedra, Nanorods, and Nanocubes. *J. Phys. Chem. B* **2005**, *109*, 24380−24385.
(189) Du, X.; Zhang, D.; Shi, L.; Gao, R.; Zhang, J. Morphology Dependence of Catalytic Properties of Ni/CeO_2 Nanostructures for Carbon Dioxide Reforming of Methane. *J. Phys. Chem. C* **2012**, *116*, 10009−10016.
(190) Kuiry, S. C.; Patil, S. D.; Deshpande, S.; Seal, S. Spontaneous Self-Assembly of Cerium Oxide Nanoparticles to Nanorods through Supraaggregate Formation. *J. Phys. Chem. B* **2005**, *109*, 6936−6939.
(191) Sun, C.; Li, H.; Wang, Z.; Chen, L.; Huang, X. Synthesis and Characterization of Polycrystalline CeO_2 Nanowires. *Chem. Lett.* **2004**, *33*, 662−663.
(192) Sun, C.; Li, H.; Zhang, H.; Wang, Z.; Chen, L. Controlled Synthesis of CeO_2 Nanorods by a Solvothermal Method. *Nanotechnology* **2005**, *16*, 1454−1463.
(193) Ho, C.; Yu, J. C.; Kwong, T.; Mak, A. C.; Lai, S. Morphology-Controllable Synthesis of Mesoporous CeO_2 Nano- and Microstructures. *Chem. Mater.* **2005**, *17*, 4514−4522.
(194) Yu, K.-L.; Ruan, G.-L.; Ben, Y.-H.; Zou, J.-J. Convenient Synthesis of CeO_2 Nanotubes. *Mater. Sci. Eng., B* **2007**, *139*, 197−200.
(195) Melchionna, M.; Marchesan, S.; Prato, M.; Fornasiero, P. Carbon Nanotubes and Catalysis: The Many Facets of a Successful Marriage. *Catal. Sci. Technol.* **2015**, *5*, 3859−3875.
(196) Zhang, D.; Fu, H.; Shi, L.; Fang, J.; Li, Q. Carbon Nanotube Assisted Synthesis of CeO_2 Nanotubes. *J. Solid State Chem.* **2007**, *180*, 654−660.
(197) Zhang, D.; Pan, C.; Shi, L.; Huang, L.; Fang, J.; Fu, H. A Highly Reactive Catalyst for CO Oxidation: CeO_2 Nanotubes Synthesized Using Carbon Nanotubes as Removable Templates. *Microporous Mesoporous Mater.* **2009**, *117*, 193−200.
(198) Cargnello, M.; Grzelczak, M.; Rodríguez-González, B.; Syrgiannis, Z.; Bakhmutsky, K.; La Parola, V.; Liz-Marzán, L. M.; Gorte, R. J.; Prato, M.; Fornasiero, P. Multiwalled Carbon Nanotubes Drive the Activity of Metal@Oxide Core-Shell Catalysts in Modular Nanocomposites. *J. Am. Chem. Soc.* **2012**, *134*, 11760−11766.
(199) Beltram, A.; Melchionna, M.; Montini, T.; Nasi, L.; Gorte, R. J.; Prato, M.; Fornasiero, P. Improved Activity and Stability of Pd@CeO_2 Core−shell Catalysts Hybridized with Multi-Walled Carbon Nanotubes in the Water Gas Shift Reaction. *Catal. Today* **2015**, *253*, 142−148.
(200) Feng, Y.; Liu, L.; Wang, X. Hydrothermal Synthesis and Automotive Exhaust Catalytic Performance of CeO_2 Nanotube Arrays. *J. Mater. Chem.* **2011**, *21*, 15442−15448.
(201) Lu, X.; Zhai, T.; Cui, H.; Shi, J.; Xie, S.; Huang, Y.; Liang, C.; Tong, Y. Redox Cycles Promoting Photocatalytic Hydrogen Evolution of CeO_2 Nanorods. *J. Mater. Chem.* **2011**, *21*, 5569−5572.
(202) Chen, J.; Zhong, S.; Liu, Q.; Wang, Y.; Wang, S.; Xu, R.; Luo, L.; Wang, S. Cerium Sulfate Microdisks Prepared by a Solvothermal Method and Their Conversion to Ceria Microdisks. *Powder Technol.* **2010**, *197*, 136−139.
(203) Guo, X.-H.; Mao, C.-C.; Zhang, J.; Huang, J.; Wang, W.-N.; Deng, Y.-H.; Wang, Y.-Y.; Cao, Y.; Huang, W.-X.; Yu, S.-H. Cobalt-Doping-Induced Synthesis of Ceria Nanodisks and Their Significantly Enhanced Catalytic Activity. *Small* **2012**, *8*, 1515−1520.
(204) Wang, D.; Kang, Y.; Doan-Nguyen, V.; Chen, J.; Küngas, R.; Wieder, N. L.; Bakhmutsky, K.; Gorte, R. J.; Murray, C. B. Synthesis and Oxygen Storage Capacity of Two-Dimensional Ceria Nanocrystals. *Angew. Chem., Int. Ed.* **2011**, *50*, 4378−4381.
(205) Wang, Z.-L.; Li, G.-R.; Ou, Y.-N.; Feng, Z.-P.; Qu, D.-L.; Tong, Y.-X. Electrochemical Deposition of Eu^{3+}-Doped CeO_2 Nanobelts with Enhanced Optical Properties. *J. Phys. Chem. C* **2011**, *115*, 351−356.
(206) Titirici, M.-M.; Antonietti, M.; Thomas, A. A Generalized Synthesis of Metal Oxide Hollow Spheres Using a Hydrothermal Approach. *Chem. Mater.* **2006**, *18*, 3808−3812.
(207) Strandwitz, N. C.; Stucky, G. D. Hollow Microporous Cerium Oxide Spheres Templated By Colloidal Silica. *Chem. Mater.* **2009**, *21*, 4577−4582.

(208) Sun, C.; Sun, J.; Xiao, G.; Zhang, H.; Qiu, X.; Li, H.; Chen, L. Mesoscale Organization of Nearly Monodisperse Flowerlike Ceria Microspheres. *J. Phys. Chem. B* **2006**, *110*, 13445−13452.
(209) Xiao, G.; Li, S.; Li, H.; Chen, L. Synthesis of Doped Ceria with Mesoporous Flowerlike Morphology and Its Catalytic Performance for CO Oxidation. *Microporous Mesoporous Mater.* **2009**, *120*, 426−431.
(210) Xian, C. N.; Li, H.; Chen, L. Q.; Lee, J. S. Morphological and Catalytic Stability of Mesoporous Peony-like Ceria. *Microporous Mesoporous Mater.* **2011**, *142*, 202−207.
(211) Sun, J.; Wang, Y.; Li, J.; Xiao, G.; Zhang, L.; Li, H.; Cheng, Y.; Sun, C.; Cheng, Z.; Dong, Z. H_2 Production from Stable Ethanol Steam Reforming over Catalyst of NiO Based on Flowerlike CeO_2 Microspheres. *Int. J. Hydrogen Energy* **2010**, *35*, 3087−3091.
(212) Sun, C.; Xie, Z.; Xia, C.; Li, H.; Chen, L. Investigations of Mesoporous CeO_2−Ru as a Reforming Catalyst Layer for Solid Oxide Fuel Cells. *Electrochem. Commun.* **2006**, *8*, 833−838.
(213) Xiao, G.; Jiang, Z.; Li, H.; Xia, C.; Chen, L. Studies on Composite Cathode with Nanostructured $Ce_{0.9}Sm_{0.1}O_{1.95}$ for Intermediate Temperature Solid Oxide Fuel Cells. *Fuel Cells* **2009**, *9*, 650−656.
(214) Hirano, M.; Fukuda, Y.; Iwata, H.; Hotta, Y.; Inagaki, M. Preparation and Spherical Agglomeration of Crystalline Cerium(IV) Oxide Nanoparticles by Thermal Hydrolysis. *J. Am. Ceram. Soc.* **2000**, *83*, 1287−1289.
(215) Zhou, F.; Zhao, X.; Xu, H.; Yuan, C. CeO_2 Spherical Crystallites: Synthesis, Formation Mechanism, Size Control, and Electrochemical Property Study. *J. Phys. Chem. C* **2007**, *111*, 1651−1657.
(216) Xia, B.; Lenggoro, I. W.; Okuyama, K. Synthesis of CeO_2 Nanoparticles by Salt-Assisted Ultrasonic Aerosol Decomposition. *J. Mater. Chem.* **2001**, *11*, 2925−2927.
(217) Zhang, D.; Qian, Y.; Shi, L.; Mai, H.; Gao, R.; Zhang, J.; Yu, W.; Cao, W. Cu-Doped CeO_2 Spheres: Synthesis, Characterization, and Catalytic Activity. *Catal. Commun.* **2012**, *26*, 164−168.
(218) Lu, X.; Li, X.; Chen, F.; Ni, C.; Chen, Z. Hydrothermal Synthesis of Prism-like Mesocrystal CeO_2. *J. Alloys Compd.* **2009**, *476*, 958−962.
(219) Yu, T.; Joo, J.; Park, Y. Il; Hyeon, T. Large-Scale Nonhydrolytic Sol-Gel Synthesis of Uniform-Sized Ceria Nanocrystals with Spherical, Wire, and Tadpole Shapes. *Angew. Chem., Int. Ed.* **2005**, *44*, 7411−7414.
(220) Cargnello, M.; Wieder, N. L.; Montini, T.; Gorte, R. J.; Fornasiero, P. Synthesis of Dispersible Pd@CeO_2 Core-Shell Nanostructures by Self-Assembly. *J. Am. Chem. Soc.* **2010**, *132*, 1402−1409.
(221) Cargnello, M.; Delgado Jaén, J. J.; Hernández Garrido, J. C.; Bakhmutsky, K.; Montini, T.; Calvino Gámez, J. J.; Gorte, R. J.; Fornasiero, P. Exceptional Activity for Methane Combustion over Modular Pd@CeO_2 Subunits on Functionalized Al_2O_3. *Science* **2012**, *337*, 713−717.
(222) Monai, M.; Montini, T.; Chen, C.; Fonda, E.; Gorte, R. J.; Fornasiero, P. Methane Catalytic Combustion over Hierarchical Pd@CeO_2/Si-Al_2O_3: Effect of the Presence of Water. *ChemCatChem* **2015**, *7*, 2038−2046.
(223) Zhang, S.; Chen, C.; Cargnello, M.; Fornasiero, P.; Gorte, R. J.; Graham, G. W.; Pan, X. Dynamic Structural Evolution of Supported Palladium-Ceria Core-Shell Catalysts Revealed by in Situ Electron Microscopy. *Nat. Commun.* **2015**, *6*, 7778.
(224) Kim, J. E.; Carroll, P. J.; Schelter, E. J. Bidentate Nitroxide Ligands Stable toward Oxidative Redox Cycling and Their Complexes with Cerium and Lanthanum. *Chem. Commun.* **2015**, *51*, 15047−15050.
(225) Mitsudome, T.; Mikami, Y.; Matoba, M.; Mizugaki, T.; Jitsukawa, K.; Kaneda, K. Design of a Silver-Cerium Dioxide Core-Shell Nanocomposite Catalyst for Chemoselective Reduction Reactions. *Angew. Chem., Int. Ed.* **2012**, *51*, 136−139.
(226) Qi, J.; Chen, J.; Li, G.; Li, S.; Gao, Y.; Tang, Z. Facile Synthesis of Core−shell Au@CeO_2 Nanocomposites with Remarkably Enhanced Catalytic Activity for CO Oxidation. *Energy Environ. Sci.* **2012**, *5*, 8937.
(227) Saada, R.; Kellici, S.; Heil, T.; Morgan, D.; Saha, B. Greener Synthesis of Dimethyl Carbonate Using a Novel Ceria−Zirconia Oxide/Graphene Nanocomposite Catalyst. *Appl. Catal., B* **2015**, *168*−*169*, 353−362.
(228) Yamada, Y.; Tsung, C.-K.; Huang, W.; Huo, Z.; Habas, S. E.; Soejima, T.; Aliaga, C. E.; Somorjai, G. A.; Yang, P. Nanocrystal Bilayer for Tandem Catalysis. *Nat. Chem.* **2011**, *3*, 372−376.
(229) Freund, H.-J.; Pacchioni, G. Oxide Ultra-Thin Films on Metals: New Materials for the Design of Supported Metal Catalysts. *Chem. Soc. Rev.* **2008**, *37*, 2224−2242.
(230) Faisal, F.; Toghan, A.; Khalakhan, I.; Vorokhta, M.; Matolin, V.; Libuda, J. Characterization of Thin CeO_2 Films Electrochemically Deposited on HOPG. *Appl. Surf. Sci.* **2015**, *350*, 142−148.
(231) Wang, A. Q.; Golden, T. D. Anodic Electrodeposition of Cerium Oxide Thin Films. *J. Electrochem. Soc.* **2003**, *150*, C616.
(232) Luo, Y.; Li, J.; Zhu, J.; Zhao, Y.; Gao, X. Fabrication of Condensate Microdrop Self-Propelling Porous Films of Cerium Oxide Nanoparticles on Copper Surfaces. *Angew. Chem., Int. Ed.* **2015**, *54*, 4876−4879.
(233) Gritschneder, S.; Reichling, M. Structural Elements of CeO_2(111) Surfaces. *Nanotechnology* **2007**, *18*, 044024.
(234) Molinari, M.; Parker, S. C.; Sayle, D. C.; Islam, M. S. Water Adsorption and Its Effect on the Stability of Low Index Stoichiometric and Reduced Surfaces of Ceria. *J. Phys. Chem. C* **2012**, *116*, 7073−7082.
(235) Mullins, D. R.; Albrecht, P. M.; Chen, T.-L.; Calaza, F. C.; Biegalski, M. D.; Christen, H. M.; Overbury, S. H. Water Dissociation on CeO_2(100) and CeO_2(111) Thin Films. *J. Phys. Chem. C* **2012**, *116*, 19419−19428.
(236) Matolín, V.; Matolínová, I.; Dvořák, F.; Johánek, V.; Mysliveček, J.; Prince, K. C.; Skála, T.; Stetsovych, O.; Tsud, N.; Václavů, M.; Šmíd, B. Water Interaction with CeO_2(111)/Cu(111) Model Catalyst Surface. *Catal. Today* **2012**, *181*, 124−132.
(237) Lykhach, Y.; Johánek, V.; Aleksandrov, H. A.; Kozlov, S. M.; Happel, M.; Skála, T.; Petkov, P., St.; Tsud, N.; Vayssilov, G. N.; Prince, K. C.; Neyman, K. M.; Matolín, V.; Libuda, J. Water Chemistry on Model Ceria and Pt/Ceria Catalysts. *J. Phys. Chem. C* **2012**, *116*, 12103−12113.
(238) Lykhach, Y.; Happel, M.; Johánek, V.; Skála, T.; Kollhoff, F.; Tsud, N.; Dvořák, F.; Prince, K. C.; Matolín, V.; Libuda, J. Adsorption and Decomposition of Formic Acid on Model Ceria and Pt/Ceria Catalysts. *J. Phys. Chem. C* **2013**, *117*, 12483−12494.
(239) Staudt, T.; Lykhach, Y.; Tsud, N.; Skála, T.; Prince, K. C.; Matolín, V.; Libuda, J. Ceria Reoxidation by CO_2: A Model Study. *J. Catal.* **2010**, *275*, 181−185.
(240) Happel, M.; Mysliveček, J.; Johánek, V.; Dvořák, F.; Stetsovych, O.; Lykhach, Y.; Matolín, V.; Libuda, J. Adsorption Sites, Metal-Support Interactions, and Oxygen Spillover Identified by Vibrational Spectroscopy of Adsorbed CO: A Model Study on Pt/Ceria Catalysts. *J. Catal.* **2012**, *289*, 118−126.
(241) Lykhach, Y.; Staudt, T.; Lorenz, M. P. A.; Streber, R.; Bayer, A.; Steinrück, H.-P.; Libuda, J. Microscopic Insights into Methane Activation and Related Processes on Pt/Ceria Model Catalysts. *ChemPhysChem* **2010**, *11*, 1496−1504.
(242) Happel, M.; Lykhach, Y.; Tsud, N.; Skála, T.; Johánek, V.; Prince, K. C.; Matolín, V.; Libuda, J. SO_2 Decomposition on Pt/CeO_2(111) Model Catalysts: On the Reaction Mechanism and the Influence of H_2 and CO. *J. Phys. Chem. C* **2012**, *116*, 10959−10967.
(243) Stetsovych, V.; Pagliuca, F.; Dvořák, F.; Duchoň, T.; Vorokhta, M.; Aulická, M.; Lachnitt, J.; Schernich, S.; Matolínová, I.; Veltruská, K.; Skála, T.; Mazur, D.; Mysliveček, J.; Libuda, J.; Matolín, V. Epitaxial Cubic Ce_2O_3 Films via Ce−CeO_2 Interfacial Reaction. *J. Phys. Chem. Lett.* **2013**, *4*, 866−871.
(244) Senanayake, S. D.; Gordon, W. O.; Overbury, S. H.; Mullins, D. R. Adsorption and Reaction of Acetone over CeO_x (111) Thin Films. *J. Phys. Chem. C* **2009**, *113*, 6208−6214.

(245) James, T. E.; Hemmingson, S. L.; Ito, T.; Campbell, C. T. Energetics of Cu Adsorption and Adhesion onto Reduced CeO_2 (111) Surfaces by Calorimetry. *J. Phys. Chem. C* **2015**, *119*, 17209−17217.
(246) James, T. E.; Hemmingson, S. L.; Campbell, C. T. Energy of Supported Metal Catalysts: From Single Atoms to Large Metal Nanoparticles. *ACS Catal.* **2015**, *5*, 5673−5678.
(247) Rodríguez, J. A.; Hrbek, J. Inverse Oxide/Metal Catalysts: A Versatile Approach for Activity Tests and Mechanistic Studies. *Surf. Sci.* **2010**, *604*, 241−244.
(248) Rodriguez, J. A.; Ma, S.; Liu, P.; Hrbek, J.; Evans, J.; Pérez, M. Activity of CeO_x and TiO_x Nanoparticles Grown on Au(111) in the Water-Gas Shift Reaction. *Science* **2007**, *318*, 1757−1760.
(249) Senanayake, S. D.; Stacchiola, D.; Rodriguez, J. A. Unique Properties of Ceria Nanoparticles Supported on Metals: Novel Inverse Ceria/Copper Catalysts for CO Oxidation and the Water-Gas Shift Reaction. *Acc. Chem. Res.* **2013**, *46*, 1702−1711.
(250) Luches, P.; Pagliuca, F.; Valeri, S. Morphology, Stoichiometry, and Interface Structure of CeO_2 Ultrathin Films on Pt(111). *J. Phys. Chem. C* **2011**, *115*, 10718−10726.
(251) Fiala, R.; Vaclavu, M.; Rednyk, A.; Khalakhan, I.; Vorokhta, M.; Lavkova, J.; Potin, V.; Matolinova, I.; Matolin, V. Pt−CeO_x Thin Film Catalysts for PEMFC. *Catal. Today* **2015**, *240*, 236−241.
(252) Alessandri, I.; Zucca, M.; Ferroni, M.; Bontempi, E.; Depero, L. E. Tailoring the Pore Size and Architecture of CeO_2/TiO_2 Core/Shell Inverse Opals by Atomic Layer Deposition. *Small* **2009**, *5*, 336−340.
(253) Hartmann, P.; Brezesinski, T.; Sann, J.; Lotnyk, A.; Eufinger, J.-P.; Kienle, L.; Janek, J. Defect Chemistry of Oxide Nanomaterials with High Surface Area: Ordered Mesoporous Thin Films of the Oxygen Storage Catalyst CeO_2-ZrO_2. *ACS Nano* **2013**, *7*, 2999−3013.
(254) Vayssilov, G. N.; Lykhach, Y.; Migani, A.; Staudt, T.; Petrova, G. P.; Tsud, N.; Skála, T.; Bruix, A.; Illas, F.; Prince, K. C.; Matolín, V.; Neyman, K. M.; Libuda, J. Support Nanostructure Boosts Oxygen Transfer to Catalytically Active Platinum Nanoparticles. *Nat. Mater.* **2011**, *10*, 310−315.
(255) Cargnello, M.; Doan-Nguyen, V. V. T.; Gordon, T. R.; Diaz, R. E.; Stach, E. A.; Gorte, R. J.; Fornasiero, P.; Murray, C. B. Control of Metal Nanocrystal Size Reveals Metal-Support Interface Role for Ceria Catalysts. *Science* **2013**, *341*, 771−773.
(256) Wu, Z.; Li, M.; Overbury, S. H. On the Structure Dependence of CO Oxidation over CeO_2 Nanocrystals with Well-Defined Surface Planes. *J. Catal.* **2012**, *285*, 61−73.
(257) Torrente-Murciano, L.; Gilbank, A.; Puertolas, B.; Garcia, T.; Solsona, B.; Chadwick, D. Shape-Dependency Activity of Nanostructured CeO_2 in the Total Oxidation of Polycyclic Aromatic Hydrocarbons. *Appl. Catal., B* **2013**, *132*−*133*, 116−122.
(258) Brezesinski, T.; Wang, J.; Senter, R.; Brezesinski, K.; Dunn, B.; Tolbert, S. H. On the Correlation between Mechanical Flexibility, Nanoscale Structure, and Charge Storage in Periodic Mesoporous CeO_2 Thin Films. *ACS Nano* **2010**, *4*, 967−977.
(259) Bruix, A.; Lykhach, Y.; Matolínová, I.; Neitzel, A.; Skála, T.; Tsud, N.; Vorokhta, M.; Stetsovych, V.; Ševčíková, K.; Myslivecek, J.; Fiala, R.; Václavů, M.; Prince, K. C.; Bruyère, S.; Potin, V.; Illas, F.; Matolín, V.; Libuda, J.; Neyman, K. M. Maximum Noble-Metal Efficiency in Catalytic Materials: Atomically Dispersed Surface Platinum. *Angew. Chem., Int. Ed.* **2014**, *53*, 10525−10530.
(260) Costa-Nunes, O.; Ferrizz, R. M.; Gorte, R. J.; Vohs, J. M. Structure and Thermal Stability of Ceria Films Supported on YSZ(100) and α-Al_2O_3(0001). *Surf. Sci.* **2005**, *592*, 8−17.
(261) Kašpar, J.; Fornasiero, P.; Hickey, N. Automotive Catalytic Converters: Current Status and Some Perspectives. *Catal. Today* **2003**, *77*, 419−449.
(262) Shelef, M.; McCabe, R. Twenty-Five Years after Introduction of Automotive Catalysts: What Next? *Catal. Today* **2000**, *62*, 35−50.
(263) Kim, G. Ceria-Promoted Three-Way Catalysts for Auto Exhaust Emission Control. *Ind. Eng. Chem. Prod. Res. Dev.* **1982**, *21*, 267−274.
(264) Usmen, R. K.; McCabe, R. W.; Graham, G. W.; Weber, W. H.; Peters, C. R.; Gandhi, H. S. Techniques for Analyzing Thermal Deactivation of Automotive Catalysts. *International Fuels and Lubricants Meeting and Exposition*, San Francisco, CA, Oct 19−22, 1992; SAE International, 1992, 92233610.4271/922336.
(265) Kaspar, J.; Fornasiero, P.; Balducci, G.; Di Monte, R.; Hickey, N.; Sergo, V. Effect of ZrO_2 Content on Textural and Structural Properties of CeO_2−ZrO_2 Solid Solutions Made by Citrate Complexation Route. *Inorg. Chim. Acta* **2003**, *349*, 217−226.
(266) Di Monte, R.; Fornasiero, P.; Kašpar, J.; Graziani, M.; Gatica, J. M.; Bernal, S.; Gómez-Herrero, A. Stabilisation of Nanostructured $Ce_{0.2}Zr_{0.8}O_2$ Solid Solution by Impregnation on Al_2O_3: A Suitable Method for the Production of Thermally Stable Oxygen Storage/Release Promoters for Three-Way Catalysts. *Chem. Commun.* **2000**, *2000*, 2167−2168.
(267) Di Monte, R.; Fornasiero, P.; Desinan, S.; Kašpar, J.; Gatica, J. M.; Calvino, J. J.; Fonda, E. Thermal Stabilization of $Ce_xZr_{1-x}O_2$ Oxygen Storage Promoters by Addition of Al_2O_3: Effect of Thermal Aging on Textural, Structural, and Morphological Properties. *Chem. Mater.* **2004**, *16*, 4273−4285.
(268) Mamontov, E.; Egami, T. Structural Defects in a Nano-Scale Powder of CeO_2 Studied by Pulsed Neutron Diffraction. *J. Phys. Chem. Solids* **2000**, *61*, 1345−1356.
(269) Mamontov, E.; Egami, T.; Brezny, R.; Koranne, M.; Tyagi, S. Lattice Defects and Oxygen Storage Capacity of Nanocrystalline Ceria and Ceria-Zirconia. *J. Phys. Chem. B* **2000**, *104*, 11110−11116.
(270) Ciambelli, P.; Palma, V.; Russo, P.; Vaccaro, S. Performances of a Catalytic Foam Trap for Soot Abatement. *Catal. Today* **2002**, *75*, 471−478.
(271) Bueno-López, A. Diesel Soot Combustion Ceria Catalysts. *Appl. Catal., B* **2014**, *146*, 1−11.
(272) Liu, S.; Wu, X.; Weng, D.; Ran, R. Ceria-Based Catalysts for Soot Oxidation: A Review. *J. Rare Earths* **2015**, *33*, 567−590.
(273) Liu, J.; Zhao, Z.; Wang, J.; Xu, C.; Duan, A.; Jiang, G.; Yang, Q. The Highly Active Catalysts of Nanometric CeO_2-Supported Cobalt Oxides for Soot Combustion. *Appl. Catal., B* **2008**, *84*, 185−195.
(274) Krishna, K.; Bueno-López, A.; Makkee, M.; Moulijn, J. A. Potential Rare Earth Modified CeO_2 Catalysts for Soot Oxidation. *Appl. Catal., B* **2007**, *75*, 189−200.
(275) Aneggi, E.; de Leitenburg, C.; Dolcetti, G.; Trovarelli, A. Diesel Soot Combustion Activity of Ceria Promoted with Alkali Metals. *Catal. Today* **2008**, *136*, 3−10.
(276) Atribak, I.; Bueno-López, A.; García-García, A. Combined Removal of Diesel Soot Particulates and NO_x over CeO_2−ZrO_2 Mixed Oxides. *J. Catal.* **2008**, *259*, 123−132.
(277) Neyertz, C. A.; Banús, E. D.; Miró, E. E.; Querini, C. A. Potassium-Promoted $Ce_{0.65}Zr_{0.35}O_2$ Monolithic Catalysts for Diesel Soot Combustion. *Chem. Eng. J.* **2014**, *248*, 394−405.
(278) Aneggi, E.; de Leitenburg, C.; Dolcetti, G.; Trovarelli, A. Promotional Effect of Rare Earths and Transition Metals in the Combustion of Diesel Soot over CeO_2 and CeO_2−ZrO_2. *Catal. Today* **2006**, *114*, 40−47.
(279) dos Santos Xavier, L. P.; Rico-Pérez, V.; Hernández-Giménez, A. M.; Lozano-Castelló, D.; Bueno-López, A. Simultaneous Catalytic Oxidation of Carbon Monoxide, Hydrocarbons and Soot with Ce−Zr−Nd Mixed Oxides in Simulated Diesel Exhaust Conditions. *Appl. Catal., B* **2015**, *162*, 412−419.
(280) Aneggi, E.; Wiater, D.; de Leitenburg, C.; Llorca, J.; Trovarelli, A. Shape-Dependent Activity of Ceria in Soot Combustion. *ACS Catal.* **2014**, *4*, 172−181.
(281) Aneggi, E.; de Leitenburg, C.; Llorca, J.; Trovarelli, A. Higher Activity of Diesel Soot Oxidation over Polycrystalline Ceria and Ceria−Zirconia Solid Solutions from More Reactive Surface Planes. *Catal. Today* **2012**, *197*, 119−126.
(282) Fornasiero, P.; Montini, T.; Graziani, M.; Zilio, S.; Succi, M. Development of Functionalized Fe−Al−Cr Alloy Fibers as Innovative Catalytic Oxidation Devices. *Catal. Today* **2008**, *137*, 475−482.
(283) Boaro, M.; Vicario, M.; de Leitenburg, C.; Dolcetti, G.; Trovarelli, A. The Use of Temperature-Programmed and Dynamic/Transient Methods in Catalysis: Characterization of Ceria-Based, Model Three-Way Catalysts. *Catal. Today* **2003**, *77*, 407−417.

(284) Bassou, B.; Guilhaume, N.; Lombaert, K.; Mirodatos, C.; Bianchi, D. Experimental Microkinetic Approach of the Catalytic Oxidation of Diesel Soot by Ceria Using Temperature-Programmed Experiments. Part 2: Kinetic Modeling of the Impact of the Ceria/Soot Contacts on the Rate of Oxidation. *Energy Fuels* **2010**, *24*, 4781−4792.
(285) Kumar, P. A.; Tanwar, M. D.; Bensaid, S.; Russo, N.; Fino, D. Soot Combustion Improvement in Diesel Particulate Filters Catalyzed with Ceria Nanofibers. *Chem. Eng. J.* **2012**, *207*−*208*, 258−266.
(286) Peralta, M.; Milt, V.; Cornaglia, L.; Querini, C. Stability of Ba,K/CeO_2 Catalyst during Diesel Soot Combustion: Effect of Temperature, Water, and Sulfur Dioxide. *J. Catal.* **2006**, *242*, 118−130.
(287) Hernández-Giménez, A. M.; Lozano-Castelló, D.; Bueno-López, A. Effect of CO_2, H_2O and SO_2 in the Ceria-Catalyzed Combustion of Soot under Simulated Diesel Exhaust Conditions. *Appl. Catal., B* **2014**, *148*−*149*, 406−414.
(288) Sudarsanam, P.; Hillary, B.; Deepa, D. K.; Amin, M. H.; Mallesham, B.; Reddy, B. M.; Bhargava, S. K. Highly Efficient Cerium Dioxide Nanocube-Based Catalysts for Low Temperature Diesel Soot Oxidation: The Cooperative Effect of Cerium- and Cobalt-Oxides. *Catal. Sci. Technol.* **2015**, *5*, 3496−3500.
(289) Yang, Q.; Gu, F.; Tang, Y.; Zhang, H.; Liu, Q.; Zhong, Z.; Su, F. A Co_3O_4−CeO_2 Functionalized SBA-15 Monolith with a Three-Dimensional Framework Improves NO_x-Assisted Soot Combustion. *RSC Adv.* **2015**, *5*, 26815−26822.
(290) Takahashi, T. *Physics of Electrolytes*; Hladik, J., Ed.; Academic Press: London, 1972.
(291) Mogensen, M. Physical Properties of Mixed Conductor Solid Oxide Fuel Cell Anodes of Doped CeO_2. *J. Electrochem. Soc.* **1994**, *141*, 2122−2128.
(292) Marina, O. A.; Bagger, C.; Primdahl, S.; Mogensen, M. A Solid Oxide Fuel Cell with a Gadolinia-Doped Ceria Anode: Preparation and Performance. *Solid State Ionics* **1999**, *123*, 199−208.
(293) Park, S.; Vohs, J.; Gorte, R. Direct Oxidation of Hydrocarbons in a Solid-Oxide Fuel Cell. *Nature* **2000**, *404*, 265−267.
(294) Gorte, R. J.; Vohs, J. M. Nanostructured Anodes for Solid Oxide Fuel Cells. *Curr. Opin. Colloid Interface Sci.* **2009**, *14*, 236−244.
(295) Murray, E. P.; Tsai, T.; Barnett, S. A. A Direct-Methane Fuel Cell with a Ceria-Based Anode. *Nature* **1999**, *400*, 649−651.
(296) Adijanto, L.; Sampath, A.; Yu, A. S.; Cargnello, M.; Fornasiero, P.; Gorte, R. J.; Vohs, J. M. Synthesis and Stability of Pd@CeO_2 Core−Shell Catalyst Films in Solid Oxide Fuel Cell Anodes. *ACS Catal.* **2013**, *3*, 1801−1809.
(297) Zhan, Z.; Barnett, S. A. An Octane-Fueled Solid Oxide Fuel Cell. *Science* **2005**, *308*, 844−847.
(298) He, H.; Gorte, R. J.; Vohs, J. M. Highly Sulfur Tolerant Cu-Ceria Anodes for SOFCs. *Electrochem. Solid-State Lett.* **2005**, *8*, A279−A280.
(299) Kurokawa, H.; Sholklapper, T. Z.; Jacobson, C. P.; De Jonghe, L. C.; Visco, S. J. Ceria Nanocoating for Sulfur Tolerant Ni-Based Anodes of Solid Oxide Fuel Cells. *Electrochem. Solid-State Lett.* **2007**, *10*, B135−B138.
(300) Lee, Y.-H.; Sumi, H.; Muroyama, H.; Matsui, T.; Eguchi, K. Influence of Ni-Oxide Anode Thickness on Performance Stability in Internal Reforming of Methane for Solid Oxide Fuel Cells. *J. Electrochem. Soc.* **2013**, *160*, F579−F584.
(301) Inaba, H.; Tagawa, H. Ceria-Based Solid Electrolytes. *Solid State Ionics* **1996**, *83*, 1−16.
(302) Tuller, H. Ionic Conduction in Nanocrystalline Materials. *Solid State Ionics* **2000**, *131*, 143−157.
(303) Guo, X.; Sigle, W.; Fleig, J.; Maier, J. Role of Space Charge in the Grain Boundary Blocking Effect in Doped Zirconia. *Solid State Ionics* **2002**, *154*−*155*, 555−561.
(304) Zhu, B.; Mat, M. D. Studies on Dual Phase Ceria-Based Composites in Electrochemistry. *Int. J. Electrochem. Sci.* **2006**, *1*, 383−402.
(305) Zhu, B. Functional Ceria−Salt-Composite Materials for Advanced ITSOFC Applications. *J. Power Sources* **2003**, *114*, 1−9.
(306) Wang, X.; Ma, Y.; Li, S.; Kashyout, A.-H.; Zhu, B.; Muhammed, M. Ceria-Based Nanocomposite with Simultaneous Proton and Oxygen Ion Conductivity for Low-Temperature Solid Oxide Fuel Cells. *J. Power Sources* **2011**, *196*, 2754−2758.
(307) Ferreira, A. S. V.; Soares, C. M. C.; Figueiredo, F. M. H. L. R.; Marques, F. M. B. Intrinsic and Extrinsic Compositional Effects in Ceria/Carbonate Composite Electrolytes for Fuel Cells. *Int. J. Hydrogen Energy* **2011**, *36*, 3704−3711.
(308) Jain, V.; Bobade, S.; Gulwade, D.; Gopalan, P. Role of the Salt Phase in GDC and Alumina-Based Composites. *Ionics* **2010**, *16*, 487−496.
(309) Li, X.; Xiao, G.; Huang, K. Effective Ionic Conductivity of a Novel Intermediate-Temperature Mixed Oxide-Ion and Carbonate-Ion Conductor. *J. Electrochem. Soc.* **2011**, *158*, B225−B232.
(310) Benamira, M.; Ringuedé, A.; Albin, V.; Vannier, R.-N.; Hildebrandt, L.; Lagergren, C.; Cassir, M. Gadolinia-Doped Ceria Mixed with Alkali Carbonates for Solid Oxide Fuel Cell Applications: I. A Thermal, Structural and Morphological Insight. *J. Power Sources* **2011**, *196*, 5546−5554.
(311) Wang, X.; Ma, Y.; Raza, R.; Muhammed, M.; Zhu, B. Novel Core−Shell SDC/Amorphous Na_2CO_3 Nanocomposite Electrolyte for Low-Temperature SOFCs. *Electrochem. Commun.* **2008**, *10*, 1617−1620.
(312) Zhu, B.; Liu, X.; Schober, T. Novel Hybrid Conductors Based on Doped Ceria and BCY20 for ITSOFC Applications. *Electrochem. Commun.* **2004**, *6*, 378−383.
(313) Raza, R.; Abbas, G.; Wang, X.; Ma, Y.; Zhu, B. Electrochemical Study of the Composite Electrolyte Based on Samaria-Doped Ceria and Containing Yttria as a Second Phase. *Solid State Ionics* **2011**, *188*, 58−63.
(314) Raza, R.; Abbas, G.; Imran, S. K.; Patel, I.; Zhu, B. GDC-Y_2O_3 Oxide Based Two Phase Nanocomposite Electrolyte. *J. Fuel Cell Sci. Technol.* **2011**, *8*, 041012.
(315) Hu, J.; Tosto, S.; Guo, Z.; Wang, Y. Dual-Phase Electrolytes for Advanced Fuel Cells. *J. Power Sources* **2006**, *154*, 106−114.
(316) Liu, X. R.; Zhu, B.; Xu, J. R.; Sun, J. C.; Mao, Z. Q. Sulphate-Ceria Composite Ceramics for Energy Environmental Co-Generation Technology. *Key Eng. Mater.* **2005**, *280*−*283*, 425−430.
(317) Zhu, B.; Liu, X.; Zhou, P.; Zhu, Z.; Zhu, W.; Zhou, S. Cost-Effective Yttrium Doped Ceria-Based Composite Ceramic Materials for Intermediate Temperature Solid Oxide Fuel Cell Applications. *J. Mater. Sci. Lett.* **2001**, *20*, 591−594.
(318) Faur Ghenciu, A. Review of Fuel Processing Catalysts for Hydrogen Production in PEM Fuel Cell Systems. *Curr. Opin. Solid State Mater. Sci.* **2002**, *6*, 389−399.
(319) *Handbook of Fuel Cells: Fundamentals, Technology, Applications*; Vielstich, W., Lamm, A., Gasteiger, H. A., Eds.; Wiley, 2003.
(320) Xu, H.; Hou, X. Synergistic Effect of CeO_2 Modified Pt/C Electrocatalysts on the Performance of PEM Fuel Cells. *Int. J. Hydrogen Energy* **2007**, *32*, 4397−4401.
(321) Lei, M.; Yang, T. Z.; Wang, W. J.; Huang, K.; Zhang, R.; Fu, X. L.; Yang, H. J.; Wang, Y. G.; Tang, W. H. Self-Assembled Mesoporous Carbon Sensitized with Ceria Nanoparticles as Durable Catalyst Support for PEM Fuel Cell. *Int. J. Hydrogen Energy* **2013**, *38*, 205−211.
(322) Bambagioni, V.; Bianchini, C.; Chen, Y.; Filippi, J.; Fornasiero, P.; Innocenti, M.; Lavacchi, A.; Marchionni, A.; Oberhauser, W.; Vizza, F. Energy Efficiency Enhancement of Ethanol Electrooxidation on Pd-CeO_2/C in Passive and Active Polymer Electrolyte-Membrane Fuel Cells. *ChemSusChem* **2012**, *5*, 1266−1273.
(323) Feng, Z. A.; El Gabaly, F.; Ye, X.; Shen, Z.-X.; Chueh, W. C. Fast Vacancy-Mediated Oxygen Ion Incorporation across the Ceria-Gas Electrochemical Interface. *Nat. Commun.* **2014**, *5*, 4374.
(324) Feng, Z. A.; Machala, M. L.; Chueh, W. C. Surface Electrochemistry of CO_2 Reduction and CO Oxidation on Sm-Doped CeO_{2-X}: Coupling between Ce^{3+} and Carbonate Adsorbates. *Phys. Chem. Chem. Phys.* **2015**, *17*, 12273−12281.
(325) Seo, Y.-S.; Shirley, A.; Kolaczkowski, S. Evaluation of Thermodynamically Favourable Operating Conditions for Production of Hydrogen in Three Different Reforming Technologies. *J. Power Sources* **2002**, *108*, 213−225.

(326) Kusakabe, K.; Sotowa, K.-I.; Eda, T.; Iwamoto, Y. Methane Steam Reforming over Ce−ZrO_2-Supported Noble Metal Catalysts at Low Temperature. *Fuel Process. Technol.* **2004**, *86*, 319−326.
(327) Laosiripojana, N.; Chadwick, D.; Assabumrungrat, S. Effect of High Surface Area CeO_2 and Ce-ZrO_2 Supports over Ni Catalyst on CH_4 Reforming with H_2O in the Presence of O_2, H_2, and CO_2. *Chem. Eng. J.* **2008**, *138*, 264−273.
(328) Halabi, M. H.; de Croon, M. H. J. M.; van der Schaaf, J.; Cobden, P. D.; Schouten, J. C. Low Temperature Catalytic Methane Steam Reforming over Ceria−Zirconia Supported Rhodium. *Appl. Catal., A* **2010**, *389*, 68−79.
(329) Roh, H.-S.; Eum, I.-H.; Jeong, D.-W. Low Temperature Steam Reforming of Methane over Ni−$Ce_{1-x}Zr_xO_2$ Catalysts under Severe Conditions. *Renewable Energy* **2012**, *42*, 212−216.
(330) Roh, H.-S.; Koo, K. Y.; Yoon, W. L. Combined Reforming of Methane over Co-Precipitated Ni−CeO_2, Ni−ZrO_2 and Ni−$Ce_{0.8}Zr_{0.2}O_2$ Catalysts to Produce Synthesis Gas for Gas to Liquid (GTL) Process. *Catal. Today* **2009**, *146*, 71−75.
(331) Xu, J.; Yeung, C. M. Y.; Ni, J.; Meunier, F.; Acerbi, N.; Fowles, M.; Tsang, S. C. Methane Steam Reforming for Hydrogen Production Using Low Water-Ratios without Carbon Formation over Ceria Coated Ni Catalysts. *Appl. Catal., A* **2008**, *345*, 119−127.
(332) Ramírez-Cabrera, E.; Atkinson, A.; Chadwick, D. Catalytic Steam Reforming of Methane over $Ce_{0.9}Gd_{0.1}O_{2-x}$. *Appl. Catal., B* **2004**, *47*, 127−131.
(333) Zhao, S.; Gorte, R. J. The Effect of Oxide Dopants in Ceria on n-Butane Oxidation. *Appl. Catal., A* **2003**, *248*, 9−18.
(334) Krumpelt, M. Fuel Processing for Fuel Cell Systems in Transportation and Portable Power Applications. *Catal. Today* **2002**, *77*, 3−16.
(335) Wang, X.; Gorte, R. J. A Study of Steam Reforming of Hydrocarbon Fuels on Pd/Ceria. *Appl. Catal., A* **2002**, *224*, 209−218.
(336) Alphonse, P.; Ansart, F. Catalytic Coatings on Steel for Low-Temperature Propane Prereforming to Solid Oxide Fuel Cell (SOFC) Application. *J. Colloid Interface Sci.* **2009**, *336*, 658−666.
(337) Laosiripojana, N.; Sangtongkitcharoen, W.; Assabumrungrat, S. Catalytic Steam Reforming of Ethane and Propane over CeO_2-Doped Ni/Al_2O_3 at SOFC Temperature: Improvement of Resistance toward Carbon Formation by the Redox Property of Doping CeO_2. *Fuel* **2006**, *85*, 323−332.
(338) Thormann, J.; Maier, L.; Pfeifer, P.; Kunz, U.; Deutschmann, O.; Schubert, K. Steam Reforming of Hexadecane over a Rh/CeO_2 Catalyst in Microchannels: Experimental and Numerical Investigation. *Int. J. Hydrogen Energy* **2009**, *34*, 5108−5120.
(339) Liu, Y.; Hayakawa, T.; Suzuki, K.; Hamakawa, S.; Tsunoda, T.; Ishii, T.; Kumagai, M. Highly Active Copper/Ceria Catalysts for Steam Reforming of Methanol. *Appl. Catal., A* **2002**, *223*, 137−145.
(340) Oguchi, H.; Nishiguchi, T.; Matsumoto, T.; Kanai, H.; Utani, K.; Matsumura, Y.; Imamura, S. Steam Reforming of Methanol over Cu/CeO_2/ZrO_2 Catalysts. *Appl. Catal., A* **2005**, *281*, 69−73.
(341) Mastalir, A.; Frank, B.; Szizybalski, A.; Soerijanto, H.; Deshpande, A.; Niederberger, M.; Schomäcker, R.; Schlögl, R.; Ressler, T. Steam Reforming of Methanol over Cu/ZrO_2/CeO_2 Catalysts: A Kinetic Study. *J. Catal.* **2005**, *230*, 464−475.
(342) Huang, T.-J.; Chen, H.-M. Hydrogen Production via Steam Reforming of Methanol over Cu/(Ce,Gd)O_{2-x} Catalysts. *Int. J. Hydrogen Energy* **2010**, *35*, 6218−6226.
(343) Liu, Y.; Hayakawa, T.; Tsunoda, T.; Suzuki, K.; Hamakawa, S.; Murata, K.; Shiozaki, R.; Ishii, T.; Kumagai, M. Steam Reforming of Methanol Over Cu/CeO_2 Catalysts Studied in Comparison with Cu/ZnO and Cu/Zn(Al)O Catalysts. *Top. Catal.* **2003**, *22*, 205−213.
(344) Yi, N.; Si, R.; Saltsburg, H.; Flytzani-Stephanopoulos, M. Steam Reforming of Methanol over Ceria and Gold-Ceria Nanoshapes. *Appl. Catal., B* **2010**, *95*, 87−92.
(345) Yi, N.; Si, R.; Saltsburg, H.; Flytzani-Stephanopoulos, M. Active Gold Species on Cerium Oxide Nanoshapes for Methanol Steam Reforming and the Water Gas Shift Reactions. *Energy Environ. Sci.* **2010**, *3*, 831−837.
(346) Pojanavaraphan, C.; Nakaranuwattana, W.; Luengnaruemitchai, A.; Gulari, E. Effect of Support Composition and Metal Loading on Au/$Ce_{1-x}Zr_xO_2$ Catalysts for the Oxidative Steam Reforming of Methanol. *Chem. Eng. J.* **2014**, *240*, 99−108.
(347) Haryanto, A.; Fernando, S.; Murali, N.; Adhikari, S. Current Status of Hydrogen Production Techniques by Steam Reforming of Ethanol: A Review. *Energy Fuels* **2005**, *19*, 2098−2106.
(348) Roh, H.-S.; Wang, Y.; King, D. L.; Platon, A.; Chin, Y.-H. Low Temperature and H_2 Selective Catalysts for Ethanol Steam Reforming. *Catal. Lett.* **2006**, *108*, 15−19.
(349) Montini, T.; De Rogatis, L.; Gombac, V.; Fornasiero, P.; Graziani, M. Rh(1%)@$Ce_xZr_{1-x}O_2$−Al_2O_3 Nanocomposites: Active and Stable Catalysts for Ethanol Steam Reforming. *Appl. Catal., B* **2007**, *71*, 125−134.
(350) De Rogatis, L.; Montini, T.; Casula, M. F.; Fornasiero, P. Design of Rh@$Ce_{0.2}Zr_{0.8}O_2$−Al_2O_3 Nanocomposite for Ethanol Steam Reforming. *J. Alloys Compd.* **2008**, *451*, 516−520.
(351) Birot, A.; Epron, F.; Descorme, C.; Duprez, D. Ethanol Steam Reforming over Rh/$Ce_xZr_{1-x}O_2$ Catalysts: Impact of the CO−CO_2−CH_4 Interconversion Reactions on the H_2 Production. *Appl. Catal., B* **2008**, *79*, 17−25.
(352) Romero-Sarria, F.; Vargas, J. C.; Roger, A.-C.; Kiennemann, A. Hydrogen Production by Steam Reforming of Ethanol. *Catal. Today* **2008**, *133*−*135*, 149−153.
(353) Jalowiecki-Duhamel, L.; Pirez, C.; Capron, M.; Dumeignil, F.; Payen, E. Hydrogen Production from Ethanol in Presence of Water over Cerium and Nickel Mixed Oxides. *Catal. Today* **2010**, *157*, 456−461.
(354) Zhou, G.; Barrio, L.; Agnoli, S.; Senanayake, S. D.; Evans, J.; Kubacka, A.; Estrella, M.; Hanson, J. C.; Martínez-Arias, A.; Fernández-García, M.; Rodriguez, J. A. High Activity of $Ce_{1-x}Ni_xO_{2-Y}$ for H_2 Production through Ethanol Steam Reforming: Tuning Catalytic Performance through Metal-Oxide Interactions. *Angew. Chem., Int. Ed.* **2010**, *49*, 9680−9684.
(355) Carbajal-Ramos, I. A.; Montini, T.; Lorenzut, B.; Troiani, H.; Gennari, F. C.; Graziani, M.; Fornasiero, P. Hydrogen Production from Ethanol Steam Reforming on M/CeO_2/YSZ (M = Ru, Pd, Ag) Nanocomposites. *Catal. Today* **2012**, *180*, 96−104.
(356) Ribeiro, M. C.; Jacobs, G.; Davis, B. H.; Mattos, L. V.; Noronha, F. B. Ethanol Steam Reforming: Higher Dehydrogenation Selectivities Observed by Tuning Oxygen-Mobility and Acid/Base Properties with Mn in CeO_2·MnO_x·SiO_2 Catalysts. *Top. Catal.* **2013**, *56*, 1634−1643.
(357) Palma, V.; Castaldo, F.; Ciambelli, P.; Iaquaniello, G. CeO_2-Supported Pt/Ni Catalyst for the Renewable and Clean H_2 Production via Ethanol Steam Reforming. *Appl. Catal., B* **2014**, *145*, 73−84.
(358) Moretti, E.; Storaro, L.; Talon, A.; Chitsazan, S.; Garbarino, G.; Busca, G.; Finocchio, E. Ceria−Zirconia Based Catalysts for Ethanol Steam Reforming. *Fuel* **2015**, *153*, 166−175.
(359) Jacobs, G.; Keogh, R.; Davis, B. Steam Reforming of Ethanol over Pt/Ceria with Co-Fed Hydrogen. *J. Catal.* **2007**, *245*, 326−337.
(360) de Lima, S. M.; da Silva, A. M.; Jacobs, G.; Davis, B. H.; Mattos, L. V.; Noronha, F. B. New Approaches to Improving Catalyst Stability over Pt/Ceria during Ethanol Steam Reforming: Sn Addition and CO_2 Co-Feeding. *Appl. Catal., B* **2010**, *96*, 387−398.
(361) Song, H.; Ozkan, U. Ethanol Steam Reforming over Co-Based Catalysts: Role of Oxygen Mobility. *J. Catal.* **2009**, *261*, 66−74.
(362) Song, H.; Ozkan, U. S. Changing the Oxygen Mobility in Co/Ceria Catalysts by Ca Incorporation: Implications for Ethanol Steam Reforming. *J. Phys. Chem. A* **2010**, *114*, 3796−3801.
(363) Soykal, I. I.; Bayram, B.; Sohn, H.; Gawade, P.; Miller, J. T.; Ozkan, U. S. Ethanol Steam Reforming over Co/CeO_2 Catalysts: Investigation of the Effect of Ceria Morphology. *Appl. Catal., A* **2012**, *449*, 47−58.
(364) Song, H.; Mirkelamoglu, B.; Ozkan, U. S. Effect of Cobalt Precursor on the Performance of Ceria-Supported Cobalt Catalysts for Ethanol Steam Reforming. *Appl. Catal., A* **2010**, *382*, 58−64.

(365) Soykal, I. I.; Sohn, H.; Ozkan, U. S. Effect of Support Particle Size in Steam Reforming of Ethanol over Co/CeO_2 Catalysts. *ACS Catal.* **2012**, *2*, 2335−2348.
(366) da Silva, A. M.; de Souza, K. R.; Mattos, L. V.; Jacobs, G.; Davis, B. H.; Noronha, F. B. The Effect of Support Reducibility on the Stability of Co/CeO_2 for the Oxidative Steam Reforming of Ethanol. *Catal. Today* **2011**, *164*, 234−239.
(367) de Lima, S. M.; da Silva, A. M.; da Costa, L. O. O.; Graham, U. M.; Jacobs, G.; Davis, B. H.; Mattos, L. V.; Noronha, F. B. Study of Catalyst Deactivation and Reaction Mechanism of Steam Reforming, Partial Oxidation, and Oxidative Steam Reforming of Ethanol over Co/CeO_2 Catalyst. *J. Catal.* **2009**, *268*, 268−281.
(368) Zhang, B.; Tang, X.; Li, Y.; Cai, W.; Xu, Y.; Shen, W. Steam Reforming of Bio-Ethanol for the Production of Hydrogen over Ceria-Supported Co, Ir and Ni Catalysts. *Catal. Commun.* **2006**, *7*, 367−372.
(369) Wang, F.; Cai, W.; Provendier, H.; Schuurman, Y.; Descorme, C.; Mirodatos, C.; Shen, W. Hydrogen Production from Ethanol Steam Reforming over Ir/CeO_2 Catalysts: Enhanced Stability by PrO_x Promotion. *Int. J. Hydrogen Energy* **2011**, *36*, 13566−13574.
(370) Rioche, C.; Kulkarni, S.; Meunier, F. C.; Breen, J. P.; Burch, R. Steam Reforming of Model Compounds and Fast Pyrolysis Bio-Oil on Supported Noble Metal Catalysts. *Appl. Catal., B* **2005**, *61*, 130−139.
(371) Vagia, E. C.; Lemonidou, A. A. Investigations on the Properties of Ceria−Zirconia-Supported Ni and Rh Catalysts and Their Performance in Acetic Acid Steam Reforming. *J. Catal.* **2010**, *269*, 388−396.
(372) Zheng, X.; Yan, C.; Hu, R.; Li, J.; Hai, H.; Luo, W.; Guo, C.; Li, W.; Zhou, Z. Hydrogen from Acetic Acid as the Model Compound of Biomass Fast-Pyrolysis Oil over Ni Catalyst Supported on Ceria−Zirconia. *Int. J. Hydrogen Energy* **2012**, *37*, 12987−12993.
(373) Zhang, B.; Tang, X.; Li, Y.; Xu, Y.; Shen, W. Hydrogen Production from Steam Reforming of Ethanol and Glycerol over Ceria-Supported Metal Catalysts. *Int. J. Hydrogen Energy* **2007**, *32*, 2367−2373.
(374) Montini, T.; Singh, R.; Das, P.; Lorenzut, B.; Bertero, N.; Riello, P.; Benedetti, A.; Giambastiani, G.; Bianchini, C.; Zinoviev, S.; Miertus, S.; Fornasiero, P. Renewable H_2 from Glycerol Steam Reforming: Effect of La_2O_3 and CeO_2 Addition to Pt/Al_2O_3 Catalysts. *ChemSusChem* **2010**, *3*, 619−628.
(375) Gallegos-Suárez, E.; Guerrero-Ruiz, A.; Fernández-García, M.; Rodríguez-Ramos, I.; Kubacka, A. Efficient and Stable Ni−Ce Glycerol Reforming Catalysts: Chemical Imaging Using X-Ray Electron and Scanning Transmission Microscopy. *Appl. Catal., B* **2015**, *165*, 139−148.
(376) Yan, C.-F.; Cheng, F.-F.; Hu, R.-R. Hydrogen Production from Catalytic Steam Reforming of Bio-Oil Aqueous Fraction over Ni/CeO_2−ZrO_2 Catalysts. *Int. J. Hydrogen Energy* **2010**, *35*, 11693−11699.
(377) Shotipruk, A.; Assabumrungrat, S.; Pavasant, P.; Laosiripojana, N. Reactivity of and toward Steam Reforming of Palm Fatty Acid Distilled (PFAD) with Co-Fed Oxygen and Hydrogen. *Chem. Eng. Sci.* **2009**, *64*, 459−466.
(378) Laosiripojana, N.; Assabumrungrat, S. Catalytic Dry Reforming of Methane over High Surface Area Ceria. *Appl. Catal., B* **2005**, *60*, 107−116.
(379) Laosiripojana, N.; Sutthisripok, W.; Assabumrungrat, S. Synthesis Gas Production from Dry Reforming of Methane over CeO_2 Doped Ni/Al_2O_3: Influence of the Doping Ceria on the Resistance toward Carbon Formation. *Chem. Eng. J.* **2005**, *112*, 13−22.
(380) Damyanova, S.; Pawelec, B.; Arishtirova, K.; Huerta, M. V. M; Fierro, J. L. G. The Effect of CeO_2 on the Surface and Catalytic Properties of Pt/CeO_2−ZrO_2 Catalysts for Methane Dry Reforming. *Appl. Catal., B* **2009**, *89*, 149−159.
(381) Chen, J.; Yao, C.; Zhao, Y.; Jia, P. Synthesis Gas Production from Dry Reforming of Methane over $Ce_{0.75}Zr_{0.25}O_2$-Supported Ru Catalysts. *Int. J. Hydrogen Energy* **2010**, *35*, 1630−1642.
(382) Kambolis, A.; Matralis, H.; Trovarelli, A.; Papadopoulou, C. Ni/CeO_2-ZrO_2 Catalysts for the Dry Reforming of Methane. *Appl. Catal., A* **2010**, *377*, 16−26.
(383) Gonzalez-Delacruz, V. M.; Ternero, F.; Pereñíguez, R.; Caballero, A.; Holgado, J. P. Study of Nanostructured Ni/CeO_2 Catalysts Prepared by Combustion Synthesis in Dry Reforming of Methane. *Appl. Catal., A* **2010**, *384*, 1−9.
(384) Luisetto, I.; Tuti, S.; Di Bartolomeo, E. Co and Ni Supported on CeO_2 as Selective Bimetallic Catalyst for Dry Reforming of Methane. *Int. J. Hydrogen Energy* **2012**, *37*, 15992−15999.
(385) Djinović, P.; Osojnik Črnivec, I. G.; Erjavec, B.; Pintar, A. Influence of Active Metal Loading and Oxygen Mobility on Coke-Free Dry Reforming of Ni−Co Bimetallic Catalysts. *Appl. Catal., B* **2012**, *125*, 259−270.
(386) Paksoy, A. I.; Caglayan, B. S.; Aksoylu, A. E. A Study on Characterization and Methane Dry Reforming Performance of Co−Ce/ZrO_2 Catalyst. *Appl. Catal., B* **2015**, *168−169*, 164−174.
(387) Wang, N.; Chu, W.; Zhang, T.; Zhao, X.-S. Manganese Promoting Effects on the Co−Ce−Zr−Ox Nano Catalysts for Methane Dry Reforming with Carbon Dioxide to Hydrogen and Carbon Monoxide. *Chem. Eng. J.* **2011**, *170*, 457−463.
(388) Zhou, G.; Shah, P. R.; Gorte, R. J. A Study of Cerium−Manganese Mixed Oxides for Oxidation Catalysis. *Catal. Lett.* **2008**, *120*, 191−197.
(389) da Silva, A. M.; de Souza, K. R.; Jacobs, G.; Graham, U. M.; Davis, B. H.; Mattos, L. V.; Noronha, F. B. Steam and CO_2 Reforming of Ethanol over Rh/CeO_2 Catalyst. *Appl. Catal., B* **2011**, *102*, 94−109.
(390) Hotz, N.; Osterwalder, N.; Stark, W. J.; Bieri, N. R.; Poulikakos, D. Disk-Shaped Packed Bed Micro-Reactor for Butane-to-Syngas Processing. *Chem. Eng. Sci.* **2008**, *63*, 5193−5201.
(391) Feio, L. S. F.; Hori, C. E.; Mattos, L. V.; Zanchet, D.; Noronha, F. B.; Bueno, J. M. C. Partial Oxidation and Autothermal Reforming of Methane on Pd/CeO_2−Al_2O_3 Catalysts. *Appl. Catal., A* **2008**, *348*, 183−192.
(392) Cao, L.; Ni, C.; Yuan, Z.; Wang, S. Autothermal Reforming of Methane Over CeO_2−ZrO_2−La_2O_3 Supported Rh Catalyst. *Catal. Lett.* **2009**, *131*, 474−479.
(393) Dantas, S. C.; Escritori, J. C.; Soares, R. R.; Hori, C. E. Effect of Different Promoters on Ni/$CeZrO_2$ Catalyst for Autothermal Reforming and Partial Oxidation of Methane. *Chem. Eng. J.* **2010**, *156*, 380−387.
(394) Ismagilov, I. Z.; Matus, E. V.; Kuznetsov, V. V.; Mota, N.; Navarro, R. M.; Kerzhentsev, M. A.; Ismagilov, Z. R.; Fierro, J. L. G. Nanoscale Control during Synthesis of Me/La_2O_3, Me/$Ce_xGd_{1-x}O_y$ and Me/$Ce_xZr_{1-x}O_y$ (Me = Ni, Pt, Pd, Rh) Catalysts for Autothermal Reforming of Methane. *Catal. Today* **2013**, *210*, 10−18.
(395) Ruiz, J. A. C.; Passos, F. B.; Bueno, J. M. C.; Souza-Aguiar, E. F.; Mattos, L. V.; Noronha, F. B. Syngas Production by Autothermal Reforming of Methane on Supported Platinum Catalysts. *Appl. Catal., A* **2008**, *334*, 259−267.
(396) Escritori, J. C.; Dantas, S. C.; Soares, R. R.; Hori, C. E. Methane Autothermal Reforming on Nickel−Ceria−Zirconia Based Catalysts. *Catal. Commun.* **2009**, *10*, 1090−1094.
(397) Roh, H.; Jun, K. W.; Park, S. E. Methane-Reforming Reactions over Ni/Ce-ZrO_2/θ-Al_2O_3 Catalysts. *Appl. Catal., A* **2003**, *251*, 275−283.
(398) Pino, L.; Vita, A.; Cipitì, F.; Laganà, M.; Recupero, V. Performance of Pt/CeO_2 Catalyst for Propane Oxidative Steam Reforming. *Appl. Catal., A* **2006**, *306*, 68−77.
(399) Alvarez-Galvan, M. C.; Navarro, R. M.; Rosa, F.; Briceño, Y.; Ridao, M. A.; Fierro, J. L. G. Hydrogen Production for Fuel Cell by Oxidative Reforming of Diesel Surrogate: Influence of Ceria and/or Lanthana over the Activity of Pt/Al_2O_3 Catalysts. *Fuel* **2008**, *87*, 2502−2511.
(400) Xue, Q.; Gao, L.; Lu, Y. Sulfur-Tolerant Pt/Gd_2O_3−CeO_2−Al_2O_3 Catalyst for High Efficiency H_2 Production from Autothermal Reforming of Retail Gasoline. *Catal. Today* **2009**, *146*, 103−109.
(401) Karatzas, X.; Jansson, K.; González, A.; Dawody, J.; Pettersson, L. J. Autothermal Reforming of Low-Sulfur Diesel over Bimetallic RhPt Supported on Al_2O_3, CeO_2−ZrO_2, SiO_2 and TiO_2. *Appl. Catal., B* **2011**, *106*, 476−487.

(402) Mayne, J. M.; Dahlberg, K. A.; Westrich, T. A.; Tadd, A. R.; Schwank, J. W. Effect of Metal Particle Size on Sulfur Tolerance of Ni Catalysts during Autothermal Reforming of Isooctane. *Appl. Catal., A* **2011**, *400*, 203−214.
(403) Mayne, J. M.; Tadd, A. R.; Dahlberg, K. A.; Schwank, J. W. Influence of Thiophene on the Isooctane Reforming Activity of Ni-Based Catalysts. *J. Catal.* **2010**, *271*, 140−152.
(404) Guggilla, V. S.; Mangalampalli, V. P. S.; Akyurtlu, J. F.; Akyurtlu, A. H_2 Production by Autothermal Reforming of n-Dodecane over Highly Active Ru−Ni−Ce−Al_2O_3 Catalyst. *Ind. Eng. Chem. Res.* **2012**, *52*, 338−345.
(405) Patel, S.; Pant, K. K. Hydrogen Production by Oxidative Steam Reforming of Methanol Using Ceria Promoted Copper−Alumina Catalysts. *Fuel Process. Technol.* **2007**, *88*, 825−832.
(406) Pérez-Hernández, R.; Gutiérrez-Martínez, A.; Palacios, J.; Vega-Hernández, M.; Rodríguez-Lugo, V. Hydrogen Production by Oxidative Steam Reforming of Methanol over Ni/CeO_2−ZrO_2 Catalysts. *Int. J. Hydrogen Energy* **2011**, *36*, 6601−6608.
(407) Lin, K.-S.; Chowdhury, S.; Yeh, H.-P.; Hong, W.-T.; Yeh, C.-T. Preparation and Characterization of CuO/ZnO−Al_2O_3 Catalyst Washcoats with CeO_2 Sols for Autothermal Reforming of Methanol in a Microreactor. *Catal. Today* **2011**, *164*, 251−256.
(408) de Lima, S. M.; Dacruz, I.; Jacobs, G.; Davis, B. H.; Mattos, L.; Noronha, F. B. Steam Reforming, Partial Oxidation, and Oxidative Steam Reforming of Ethanol over Pt/$CeZrO_2$ Catalyst. *J. Catal.* **2008**, *257*, 356−368.
(409) Cai, W.; de la Piscina, P. R.; Gabrowska, K.; Homs, N. Hydrogen Production from Oxidative Steam Reforming of Bio-Butanol over CoIr-Based Catalysts: Effect of the Support. *Bioresour. Technol.* **2013**, *128*, 467−471.
(410) Srisiriwat, N.; Therdthianwong, S.; Therdthianwong, A. Oxidative Steam Reforming of Ethanol over Ni/Al_2O_3 Catalysts Promoted by CeO_2, ZrO_2 and CeO_2−ZrO_2. *Int. J. Hydrogen Energy* **2009**, *34*, 2224−2234.
(411) Dauenhauer, P.; Salge, J.; Schmidt, L. Renewable Hydrogen by Autothermal Steam Reforming of Volatile Carbohydrates. *J. Catal.* **2006**, *244*, 238−247.
(412) Deluga, G. A.; Salge, J. R.; Schmidt, L. D.; Verykios, X. E. Renewable Hydrogen from Ethanol by Autothermal Reforming. *Science* **2004**, *303*, 993−997.
(413) Trimm, D. L. Minimisation of Carbon Monoxide in a Hydrogen Stream for Fuel Cell Application. *Appl. Catal., A* **2005**, *296*, 1−11.
(414) Jha, A.; Jeong, D.-W.; Jang, W.-J.; Lee, Y.-L.; Roh, H.-S. Hydrogen Production from Water−Gas Shift Reaction over Ni−Cu−CeO_2 Oxide Catalyst: The Effect of Preparation Methods. *Int. J. Hydrogen Energy* **2015**, *40*, 9209−9216.
(415) Jardim, E. O.; Rico-Francés, S.; Coloma, F.; Anderson, J. A.; Silvestre-Albero, J.; Sepúlveda-Escribano, A. Influence of the Metal Precursor on the Catalytic Behavior of Pt/Ceria Catalysts in the Preferential Oxidation of CO in the Presence of H_2 (PROX). *J. Colloid Interface Sci.* **2015**, *443*, 45−55.
(416) Ratsanamy, C.; Wagner, J. P. Water Gas Shift Catalysis. *Catal. Rev.: Sci. Eng.* **2009**, *51*, 325−440.
(417) Bion, N.; Epron, F.; Moreno, M.; Mariño, F.; Duprez, D. Preferential Oxidation of Carbon Monoxide in the Presence of Hydrogen (PROX) over Noble Metals and Transition Metal Oxides: Advantages and Drawbacks. *Top. Catal.* **2008**, *51*, 76−88.
(418) Shido, T.; Iwasawa, Y. Regulation of Reaction Intermediate by Reactant in the Water-Gas Shift Reaction on CeO_2, in Relation to Reactant-Promoted Mechanism. *J. Catal.* **1992**, *136*, 493−503.
(419) Shido, T.; Iwasawa, Y. Reactant-Promoted Reaction Mechanism for Water-Gas Shift Reaction on Rh-Doped CeO_2. *J. Catal.* **1993**, *141*, 71−81.
(420) Zafiris, G. Evidence for Low-Temperature Oxygen Migration from Ceria to Rh. *J. Catal.* **1993**, *139*, 561−567.
(421) Zafiris, G.; Gorte, R. J. Evidence for a Second CO Oxidation Mechanism on Rh/Ceria. *J. Catal.* **1993**, *143*, 86−91.
(422) Li, Y.; Fu, Q.; Flytzani-Stephanopoulos, M. Low-Temperature Water-Gas Shift Reaction over Cu- and Ni-Loaded Cerium Oxide Catalysts. *Appl. Catal., B* **2000**, *27*, 179−191.
(423) Wootsch, A.; Descorme, C.; Duprez, D. Preferential Oxidation of Carbon Monoxide in the Presence of Hydrogen (PROX) over Ceria-Zirconia and Alumina-Supported Pt Catalysts. *J. Catal.* **2004**, *225*, 259−266.
(424) Carrasquillo-Flores, R.; Gallo, J. M. R.; Hahn, K.; Dumesic, J. A.; Mavrikakis, M. Density Functional Theory and Reaction Kinetics Studies of the Water-Gas Shift Reaction on Pt-Re Catalysts. *ChemCatChem* **2013**, *5*, 3690−3699.
(425) Mhadeshwar, A. B.; Vlachos, D. G. Is the Water−Gas Shift Reaction on Pt Simple?: Computer-Aided Microkinetic Model Reduction, Lumped Rate Expression, and Rate-Determining Step. *Catal. Today* **2005**, *105*, 162−172.
(426) Mhadeshwar, A. B.; Vlachos, D. G. Microkinetic Modeling for Water-Promoted CO Oxidation, Water−Gas Shift, and Preferential Oxidation of CO on Pt. *J. Phys. Chem. B* **2004**, *108*, 15246−15258.
(427) Burch, R.; Goguet, A.; Meunier, F. C. A Critical Analysis of the Experimental Evidence for and against a Formate Mechanism for High Activity Water-Gas Shift Catalysts. *Appl. Catal., A* **2011**, *409−410*, 3−12.
(428) Meunier, F.; Reid, D.; Goguet, A.; Shekhtman, S.; Hardacre, C.; Burch, R.; Deng, W.; Flytzani-Stephanopoulos, M. Quantitative Analysis of the Reactivity of Formate Species Seen by DRIFTS over a Au/Ce(La)O_2 Water−Gas Shift Catalyst: First Unambiguous Evidence of the Minority Role of Formates as Reaction Intermediates. *J. Catal.* **2007**, *247*, 277−287.
(429) Meunier, F.; Goguet, A.; Hardacre, C.; Burch, R.; Thompsett, D. Quantitative DRIFTS Investigation of Possible Reaction Mechanisms for the Water−Gas Shift Reaction on High-Activity Pt- and Au-Based Catalysts. *J. Catal.* **2007**, *252*, 18−22.
(430) Rodriguez, J. A.; Hanson, J. C.; Stacchiola, D.; Senanayake, S. D. In Situ/Operando Studies for the Production of Hydrogen through the Water-Gas Shift on Metal Oxide Catalysts. *Phys. Chem. Chem. Phys.* **2013**, *15*, 12004−12025.
(431) Mudiyanselage, K.; Senanayake, S. D.; Feria, L.; Kundu, S.; Baber, A. E.; Graciani, J.; Vidal, A. B.; Agnoli, S.; Evans, J.; Chang, R.; Axnanda, S.; Liu, Z.; Sanz, J. F.; Liu, P.; Rodriguez, J. A.; Stacchiola, D. J. Importance of the Metal-Oxide Interface in Catalysis: In Situ Studies of the Water-Gas Shift Reaction by Ambient-Pressure X-Ray Photoelectron Spectroscopy. *Angew. Chem., Int. Ed.* **2013**, *52*, 5101−5105.
(432) Liu, X.; Ruettinger, W.; Xu, X.; Farrauto, R. Deactivation of Pt/CeO_2 Water-Gas Shift Catalysts due to Shutdown/Startup Modes for Fuel Cell Applications. *Appl. Catal., B* **2005**, *56*, 69−75.
(433) Ruettinger, W.; Liu, X.; Farrauto, R. J. Mechanism of Aging for a Pt/CeO_2-ZrO_2 Water Gas Shift Catalyst. *Appl. Catal., B* **2006**, *65*, 135−141.
(434) Kalamaras, C. M.; Dionysiou, D. D.; Efstathiou, A. M. Mechanistic Studies of the Water−Gas Shift Reaction over Pt/$Ce_xZr_{1-x}O_2$ Catalysts: The Effect of Pt Particle Size and Zr Dopant. *ACS Catal.* **2012**, *2*, 2729−2742.
(435) Petallidou, K. C.; Efstathiou, A. M. Low-Temperature Water-Gas Shift on Pt/$Ce_{1-x}La_xO_{2-\delta}$: Effect of Ce/La Ratio. *Appl. Catal., B* **2013**, *140−141*, 333−347.
(436) Kalamaras, C. M.; Petallidou, K. C.; Efstathiou, A. M. The Effect of La^{3+}-Doping of CeO_2 Support on the Water-Gas Shift Reaction Mechanism and Kinetics over Pt/$Ce_{1-x}La_xO_{2-\delta}$. *Appl. Catal., B* **2013**, *136−137*, 225−238.
(437) Yeung, C. M. Y.; Yu, K. M. K.; Fu, Q. J.; Thompsett, D.; Petch, M. I.; Tsang, S. C. Engineering Pt in Ceria for a Maximum Metal-Support Interaction in Catalysis. *J. Am. Chem. Soc.* **2005**, *127*, 18010−18011.
(438) Hickey, N.; Arneodo Larochette, P.; Gentilini, C.; Sordelli, L.; Olivi, L.; Polizzi, S.; Montini, T.; Fornasiero, P.; Pasquato, L.; Graziani, M. Monolayer Protected Gold Nanoparticles on Ceria for an Efficient CO Oxidation Catalyst. *Chem. Mater.* **2007**, *19*, 650−651.

(439) Sakurai, H.; Akita, T.; Tsubota, S.; Kiuchi, M.; Haruta, M. Low-Temperature Activity of Au/CeO_2 for Water Gas Shift Reaction, and Characterization by ADF-STEM, Temperature-Programmed Reaction, and Pulse Reaction. *Appl. Catal., A* **2005**, *291*, 179−187.
(440) Fu, Q.; Saltsburg, H.; Flytzani-Stephanopoulos, M. Active Nonmetallic Au and Pt Species on Ceria-Based Water-Gas Shift Catalysts. *Science* **2003**, *301*, 935−938.
(441) Tibiletti, D.; Fonseca, A. A.; Burch, R.; Chen, Y.; Fisher, J. M.; Goguet, A.; Hardacre, C.; Hu, P.; Thompsett, D. DFT and in Situ EXAFS Investigation of Gold/Ceria-Zirconia Low-Temperature Water Gas Shift Catalysts: Identification of the Nature of the Active Form of Gold. *J. Phys. Chem. B* **2005**, *109*, 22553−22559.
(442) Farnesi Camellone, M.; Fabris, S. Reaction Mechanisms for the CO Oxidation on Au/CeO_2 Catalysts: Activity of Substitutional Au^{3+}/Au^{+} Cations and Deactivation of Supported Au^{+} Adatoms. *J. Am. Chem. Soc.* **2009**, *131*, 10473−10483.
(443) Rodriguez, J. A.; Wang, X.; Liu, P.; Wen, W.; Hanson, J. C.; Hrbek, J.; Pérez, M.; Evans, J. Gold Nanoparticles on Ceria: Importance of O Vacancies in the Activation of Gold. *Top. Catal.* **2007**, *44*, 73−81.
(444) Si, R.; Flytzani-Stephanopoulos, M. Shape and Crystal-Plane Effects of Nanoscale Ceria on the Activity of $Au\text{-}CeO_2$ Catalysts for the Water-Gas Shift Reaction. *Angew. Chem., Int. Ed.* **2008**, *47*, 2884−2887.
(445) Andreeva, D.; Ivanov, I.; Ilieva, L.; Abrashev, M. V. Gold Catalysts Supported on Ceria and Ceria−Alumina for Water-Gas Shift Reaction. *Appl. Catal., A* **2006**, *302*, 127−132.
(446) Andreeva, D.; Ivanov, I.; Ilieva, L.; Sobczak, J. W.; Avdeev, G.; Tabakova, T. Nanosized Gold Catalysts Supported on Ceria and Ceria-Alumina for WGS Reaction: Influence of the Preparation Method. *Appl. Catal., A* **2007**, *333*, 153−160.
(447) Tabakova, T.; Manzoli, M.; Paneva, D.; Boccuzzi, F.; Idakiev, V.; Mitov, I. CO-Free Hydrogen Production over $Au/CeO_2-Fe_2O_3$ Catalysts: Part 2. Impact of the Support Composition on the Performance in the Water-Gas Shift Reaction. *Appl. Catal., B* **2011**, *101*, 266−274.
(448) Tabakova, T.; Ilieva, L.; Ivanov, I.; Zanella, R.; Sobczak, J. W.; Lisowski, W.; Kaszkur, Z.; Andreeva, D. Influence of the Preparation Method and Dopants Nature on the WGS Activity of Gold Catalysts Supported on Doped by Transition Metals Ceria. *Appl. Catal., B* **2013**, *136−137*, 70−80.
(449) Vecchietti, J.; Collins, S.; Delgado, J. J.; Małecka, M.; del Rio, E.; Chen, X.; Bernal, S.; Bonivardi, A. Gold Catalysts Supported on Cerium−Gallium Mixed Oxide for the Carbon Monoxide Oxidation and Water Gas Shift Reaction. *Top. Catal.* **2011**, *54*, 201−209.
(450) Andreeva, D.; Kantcheva, M.; Ivanov, I.; Ilieva, L.; Sobczak, J. W.; Lisowski, W. Gold Supported on Ceria Doped by Me^{3+} (Me = Al and Sm) for Water Gas Shift Reaction: Influence of Dopant and Preparation Method. *Catal. Today* **2010**, *158*, 69−77.
(451) Fu, Q.; Kudriavtseva, S.; Saltsburg, H.; Flytzani-Stephanopoulos, M. Gold−Ceria Catalysts for Low-Temperature Water-Gas Shift Reaction. *Chem. Eng. J.* **2003**, *93*, 41−53.
(452) Fu, Q.; Deng, W.; Saltsburg, H.; Flytzani-Stephanopoulos, M. Activity and Stability of Low-Content Gold−Cerium Oxide Catalysts for the Water−Gas Shift Reaction. *Appl. Catal., B* **2005**, *56*, 57−68.
(453) Deng, W.; Jesus, J. De; Saltsburg, H.; Flytzani-Stephanopoulos, M. Low-Content Gold-Ceria Catalysts for the Water−Gas Shift and Preferential CO Oxidation Reactions. *Appl. Catal., A* **2005**, *291*, 126−135.
(454) Andreeva, D.; Ivanov, I.; Ilieva, L.; Abrashev, M. V.; Zanella, R.; Sobczak, J. W.; Lisowski, W.; Kantcheva, M.; Avdeev, G.; Petrov, K. Gold Catalysts Supported on Ceria Doped by Rare Earth Metals for Water Gas Shift Reaction: Influence of the Preparation Method. *Appl. Catal., A* **2009**, *357*, 159−169.
(455) Si, R.; Tao, J.; Evans, J.; Park, J. B.; Barrio, L.; Hanson, J. C.; Zhu, Y.; Hrbek, J.; Rodriguez, J. A. Effect of Ceria on Gold−Titania Catalysts for the Water−Gas Shift Reaction: Fundamental Studies for $Au/CeO_x/TiO_2(110)$ and $Au/CeO_x/TiO_2$ Powders. *J. Phys. Chem. C* **2012**, *116*, 23547−23555.
(456) González, I. D.; Navarro, R. M.; Wen, W.; Marinkovic, N.; Rodriguéz, J. A.; Rosa, F.; Fierro, J. L. G. A Comparative Study of the Water Gas Shift Reaction over Platinum Catalysts Supported on CeO_2, TiO_2 and Ce-Modified TiO_2. *Catal. Today* **2010**, *149*, 372−379.
(457) Park, J. B.; Graciani, J.; Evans, J.; Stacchiola, D.; Senanayake, S. D.; Barrio, L.; Liu, P.; Fdez Sanz, J.; Hrbek, J.; Rodriguez, J. A. Gold, Copper, and Platinum Nanoparticles Dispersed on $CeO_x/TiO_2(110)$ Surfaces: High Water-Gas Shift Activity and the Nature of the Mixed-Metal Oxide at the Nanometer Level. *J. Am. Chem. Soc.* **2010**, *132*, 356−363.
(458) Manzoli, M.; Vindigni, F.; Chiorino, A.; Tabakova, T.; Idakiev, V.; Boccuzzi, F. New Gold Catalysts Supported on Mixed Ceria-Titania Oxides for Water-Gas Shift and Preferential CO Oxidation Reactions. *React. Kinet. Catal. Lett.* **2007**, *91*, 213−221.
(459) Amieiro Fonseca, A.; Fisher, J. M.; Ozkaya, D.; Shannon, M. D.; Thompsett, D. Ceria-Zirconia Supported Au as Highly Active Low Temperature Water-Gas Shift Catalysts. *Top. Catal.* **2007**, *44*, 223−235.
(460) Goguet, A.; Burch, R.; Chen, Y.; Hardacre, C.; Hu, P.; Joyner, R. W.; Meunier, F. C.; Mun, B. S.; Thompsett, D.; Tibiletti, D. Deactivation Mechanism of a $Au/CeZrO_4$ Catalyst During a Low-Temperature Water Gas Shift Reaction. *J. Phys. Chem. C* **2007**, *111*, 16927−16933.
(461) Li, L.; Zhan, Y.; Zheng, Q.; Zheng, Y.; Chen, C.; She, Y.; Lin, X.; Wei, K. Water−Gas Shift Reaction over CuO/CeO_2 Catalysts: Effect of the Thermal Stability and Oxygen Vacancies of CeO_2 Supports Previously Prepared by Different Methods. *Catal. Lett.* **2009**, *130*, 532−540.
(462) Wang, X.; Rodriguez, J. A.; Hanson, J. C.; Gamarra, D.; Martínez-Arias, A.; Fernández-García, M. In Situ Studies of the Active Sites for the Water Gas Shift Reaction over $Cu\text{-}CeO_2$ Catalysts: Complex Interaction between Metallic Copper and Oxygen Vacancies of Ceria. *J. Phys. Chem. B* **2006**, *110*, 428−434.
(463) Rodriguez, J. A.; Liu, P.; Wang, X.; Wen, W.; Hanson, J.; Hrbek, J.; Pérez, M.; Evans, J. Water-Gas Shift Activity of Cu Surfaces and Cu Nanoparticles Supported on Metal Oxides. *Catal. Today* **2009**, *143*, 45−50.
(464) Pradhan, S.; Reddy, A. S.; Devi, R. N.; Chilukuri, S. Copper-Based Catalysts for Water Gas Shift Reaction: Influence of Support on Their Catalytic Activity. *Catal. Today* **2009**, *141*, 72−76.
(465) Saw, E. T.; Oemar, U.; Tan, X. R.; Du, Y.; Borgna, A.; Hidajat, K.; Kawi, S. Bimetallic Ni−Cu Catalyst Supported on CeO_2 for High-Temperature Water−Gas Shift Reaction: Methane Suppression via Enhanced CO Adsorption. *J. Catal.* **2014**, *314*, 32−46.
(466) Mariño, F.; Descorme, C.; Duprez, D. Supported Base Metal Catalysts for the Preferential Oxidation of Carbon Monoxide in the Presence of Excess Hydrogen (PROX). *Appl. Catal., B* **2005**, *58*, 175−183.
(467) Pozdnyakova, O.; Teschner, D.; Wootsch, A.; Krohnert, J.; Steinhauer, B.; Sauer, H.; Toth, L.; Jentoft, F.; Knopgericke, A.; Paal, Z. Preferential CO Oxidation in Hydrogen (PROX) on Ceria-Supported Catalysts, Part II: Oxidation States and Surface Species on Pd/CeO_2 under Reaction Conditions, Suggested Reaction Mechanism. *J. Catal.* **2006**, *237*, 17−28.
(468) Huang, Y.; Wang, A.; Li, L.; Wang, X.; Su, D.; Zhang, T. "Ir-in-Ceria": A Highly Selective Catalyst for Preferential CO Oxidation. *J. Catal.* **2008**, *255*, 144−152.
(469) Wang, F.; Lu, G. High Performance Rare Earth Oxides LnO_x (Ln = La, Ce, Nd, Sm and Dy)-Modified Pt/SiO_2 Catalysts for CO Oxidation in the Presence of H_2. *J. Power Sources* **2008**, *181*, 120−126.
(470) Teschner, D.; Wootsch, A.; Pozdnyakova-Tellinger, O.; Kröhnert, J.; Vass, E.; Hävecker, M.; Zafeiratos, S.; Schnörch, P.; Jentoft, P.; Knop-Gericke, A. Partial Pressure Dependent in Situ Spectroscopic Study on the Preferential CO Oxidation in Hydrogen (PROX) over Pt/Ceria Catalysts. *J. Catal.* **2007**, *249*, 318−327.
(471) Mariño, F.; Descorme, C.; Duprez, D. Noble Metal Catalysts for the Preferential Oxidation of Carbon Monoxide in the Presence of Hydrogen (PROX). *Appl. Catal., B* **2004**, *54*, 59−66.

(472) Polster, C. S.; Zhang, R.; Cyb, M. T.; Miller, J. T.; Baertsch, C. D. Selectivity Loss of Pt/CeO_2 PROX Catalysts at Low CO Concentrations: Mechanism and Active Site Study. *J. Catal.* **2010**, *273*, 50−58.
(473) Gao, Y.; Wang, W.; Chang, S.; Huang, W. Morphology Effect of CeO_2 Support in the Preparation, Metal-Support Interaction, and Catalytic Performance of Pt/CeO_2 Catalysts. *ChemCatChem* **2013**, *5*, 3610−3620.
(474) Carrettin, S.; Concepción, P.; Corma, A.; López Nieto, J. M.; Puntes, V. F. Nanocrystalline CeO_2 Increases the Activity of Au for CO Oxidation by Two Orders of Magnitude. *Angew. Chem., Int. Ed.* **2004**, *43*, 2538−2540.
(475) Cargnello, M.; Gentilini, C.; Montini, T.; Fonda, E.; Mehraeen, S.; Chi, M.; Herrera-Collado, M.; Browning, N. D.; Polizzi, S.; Pasquato, L.; Fornasiero, P. Active and Stable Embedded $Au@CeO_2$ Catalysts for Preferential Oxidation of CO. *Chem. Mater.* **2010**, *22*, 4335−4345.
(476) Yi, G.; Xu, Z.; Guo, G.; Tanaka, K.; Yuan, Y. Morphology Effects of Nanocrystalline CeO_2 on the Preferential CO Oxidation in H_2-Rich Gas over Au/CeO_2 Catalyst. *Chem. Phys. Lett.* **2009**, *479*, 128−132.
(477) Yi, G.; Yang, H.; Li, B.; Lin, H.; Tanaka, K.; Yuan, Y. Preferential CO Oxidation in a H_2-Rich Gas by Au/CeO_2 Catalysts: Nanoscale CeO_2 Shape Effect and Mechanism Aspect. *Catal. Today* **2010**, *157*, 83−88.
(478) Venezia, A. M.; Pantaleo, G.; Longo, A.; Di Carlo, G.; Casaletto, M. P.; Liotta, F. L.; Deganello, G. Relationship between Structure and CO Oxidation Activity of Ceria-Supported Gold Catalysts. *J. Phys. Chem. B* **2005**, *109*, 2821−2827.
(479) Fonseca, J.; Royer, S.; Bion, N.; Pirault-Roy, L.; Rangel, M. d. C.; Duprez, D.; Epron, F. Preferential CO Oxidation over Nanosized Gold Catalysts Supported on Ceria and Amorphous Ceria−Alumina. *Appl. Catal., B* **2012**, *128*, 10−20.
(480) Storaro, L.; Lenarda, M.; Moretti, E.; Talon, A.; Porta, F.; Moltrasio, B.; Canton, P. Gold Stabilized Aqueous Sols Immobilized on Mesoporous CeO_2-Al_2O_3 as Catalysts for the Preferential Oxidation of Carbon Monoxide. *J. Colloid Interface Sci.* **2010**, *350*, 435−442.
(481) Zepeda, T. A.; Martinez-Hernández, A.; Guil-López, R.; Pawelec, B. Preferential CO Oxidation in Excess of Hydrogen over Au/HMS Catalysts Modified by Ce, Fe and Ti Oxides. *Appl. Catal., B* **2010**, *100*, 450−462.
(482) Liu, Y.; Liu, B.; Wang, Q.; Li, C.; Hu, W.; Liu, Y.; Jing, P.; Zhao, W.; Zhang, J. Three-Dimensionally Ordered Macroporous Au/CeO_2−Co_3O_4 Catalysts with Mesoporous Walls for Enhanced CO Preferential Oxidation in H_2-Rich Gases. *J. Catal.* **2012**, *296*, 65−76.
(483) Wang, H.; Zhu, H.; Qin, Z.; Liang, F.; Wang, G.; Wang, J. Deactivation of a Au/CeO_2−Co_3O_4 Catalyst during CO Preferential Oxidation in H_2-Rich Stream. *J. Catal.* **2009**, *264*, 154−162.
(484) Wang, H.; Zhu, H.; Qin, Z.; Wang, G.; Liang, F.; Wang, J. Preferential Oxidation of CO in H_2 Rich Stream over Au/CeO_2−Co_3O_4 Catalysts. *Catal. Commun.* **2008**, *9*, 1487−1492.
(485) Sangeetha, P.; Chen, Y.-W. Preferential Oxidation of CO in H_2 Stream on Au/CeO_2−TiO_2 Catalysts. *Int. J. Hydrogen Energy* **2009**, *34*, 7342−7347.
(486) Laguna, O. H.; Romero Sarria, F.; Centeno, M. A.; Odriozola, J. A. Gold Supported on Metal-Doped Ceria Catalysts (M = Zr, Zn and Fe) for the Preferential Oxidation of CO (PROX). *J. Catal.* **2010**, *276*, 360−370.
(487) Ilieva, L.; Pantaleo, G.; Ivanov, I.; Maximova, A.; Zanella, R.; Kaszkur, Z.; Venezia, A. M.; Andreeva, D. Preferential Oxidation of CO in H_2 Rich Stream (PROX) over Gold Catalysts Supported on Doped Ceria: Effect of Preparation Method and Nature of Dopant. *Catal. Today* **2010**, *158*, 44−55.
(488) Arzamendi, G.; Uriz, I.; Diéguez, P. M.; Laguna, O. H.; Hernández, W. Y.; Álvarez, A.; Centeno, M. A.; Odriozola, J. A.; Montes, M.; Gandía, L. M. Selective CO Removal over Au/CeFe and CeCu Catalysts in Microreactors Studied through Kinetic Analysis and CFD Simulations. *Chem. Eng. J.* **2011**, *167*, 588−596.
(489) Tabakova, T.; Avgouropoulos, G.; Papavasiliou, J.; Manzoli, M.; Boccuzzi, F.; Tenchev, K.; Vindigni, F.; Ioannides, T. CO-Free Hydrogen Production over Au/CeO_2−Fe_2O_3 Catalysts: Part 1. Impact of the Support Composition on the Performance for the Preferential CO Oxidation Reaction. *Appl. Catal., B* **2011**, *101*, 256−265.
(490) Liao, X.; Chu, W.; Dai, X.; Pitchon, V. Promoting Effect of Fe in Preferential Oxidation of Carbon Monoxide Reaction (PROX) on Au/CeO_2. *Appl. Catal., A* **2012**, *449*, 131−138.
(491) Avgouropoulos, G.; Manzoli, M.; Boccuzzi, F.; Tabakova, T.; Papavasiliou, J.; Ioannides, T.; Idakiev, V. Catalytic Performance and Characterization of Au/Doped-Ceria Catalysts for the Preferential CO Oxidation Reaction. *J. Catal.* **2008**, *256*, 237−247.
(492) Manzoli, M.; Avgouropoulos, G.; Tabakova, T.; Papavasiliou, J.; Ioannides, T.; Boccuzzi, F. Preferential CO Oxidation in H_2-Rich Gas Mixtures over Au/Doped Ceria Catalysts. *Catal. Today* **2008**, *138*, 239−243.
(493) Chang, L.-H.; Sasirekha, N.; Chen, Y.-W.; Wang, W.-J. Preferential Oxidation of CO in H_2 Stream over Au/MnO_2−CeO_2 Catalysts. *Ind. Eng. Chem. Res.* **2006**, *45*, 4927−4935.
(494) Ilieva, L.; Pantaleo, G.; Ivanov, I.; Zanella, R.; Venezia, A. M.; Andreeva, D. A Comparative Study of Differently Prepared Rare Earths-Modified Ceria-Supported Gold Catalysts for Preferential Oxidation of CO. *Int. J. Hydrogen Energy* **2009**, *34*, 6505−6515.
(495) Gamarra, D.; Belver, C.; Fernandez-García, M.; Martínez-Arias, A. Selective CO Oxidation in Excess H_2 over Copper-Ceria Catalysts: Identification of Active Entities/Species. *J. Am. Chem. Soc.* **2007**, *129*, 12064−12065.
(496) Gamarra, D.; Munuera, G.; Hungria, A. B.; Fernandez-Garcia, M.; Conesa, J. C.; Midgley, P. A.; Wang, X. Q.; Hanson, J. C.; Rodriguez, J. A.; Martinez-Arias, A. Structure-Activity Relationship in Nanostructured Copper-Ceria-Based Preferential CO Oxidation Catalysts. *J. Phys. Chem. C* **2007**, *111*, 11026−11038.
(497) Gamarra, D.; Cámara, A. L.; Monte, M.; Rasmussen, S. B.; Chinchilla, L. E.; Hungría, A. B.; Munuera, G.; Gyorffy, N.; Schay, Z.; Corberán, V. C.; Conesa, J. C.; Martínez-Arias, A. Preferential Oxidation of CO in Excess H_2 over CuO/CeO_2 Catalysts: Characterization and Performance as a Function of the Exposed Face Present in the CeO_2 Support. *Appl. Catal., B* **2013**, *130*−*131*, 224−238.
(498) Monte, M.; Gamarra, D.; López Cámara, A.; Rasmussen, S. B.; Gyorffy, N.; Schay, Z.; Martínez-Arias, A.; Conesa, J. C. Preferential Oxidation of CO in Excess H_2 over CuO/CeO_2 Catalysts: Performance as a Function of the Copper Coverage and Exposed Face Present in the CeO_2 Support. *Catal. Today* **2014**, *229*, 104−113.
(499) Wang, W.-W.; Du, P.-P.; Zou, S.-H.; He, H.-Y.; Wang, R.-X.; Jin, Z.; Shi, S.; Huang, Y.-Y.; Si, R.; Song, Q.-S.; Jia, C.-J.; Yan, C.-H. Highly Dispersed Copper Oxide Clusters as Active Species in Copper-Ceria Catalyst for Preferential Oxidation of Carbon Monoxide. *ACS Catal.* **2015**, *5*, 2088−2099.
(500) Zeng, S.; Zhang, W.; Śliwa, M.; Su, H. Comparative Study of CeO_2/CuO and CuO/CeO_2 Catalysts on Catalytic Performance for Preferential CO Oxidation. *Int. J. Hydrogen Energy* **2013**, *38*, 3597−3605.
(501) Zeng, S.; Wang, Y.; Ding, S.; Sattler, J. J. H. B.; Borodina, E.; Zhang, L.; Weckhuysen, B. M.; Su, H. Active Sites over CuO/CeO_2 and Inverse CeO_2/CuO Catalysts for Preferential CO Oxidation. *J. Power Sources* **2014**, *256*, 301−311.
(502) López Cámara, A.; Cortés Corberán, V.; Barrio, L.; Zhou, G.; Si, R.; Hanson, J. C.; Monte, M.; Conesa, J. C.; Rodriguez, J. A.; Martínez-Arias, A. Improving the CO-PROX Performance of Inverse CeO_2/CuO Catalysts: Doping of the CuO Component with Zn. *J. Phys. Chem. C* **2014**, *118*, 9030−9041.
(503) Kosmambetova, G. R.; Moroz, E. M.; Guralsky, A. V.; Pakharukova, V. P.; Boronin, A. I.; Ivashchenko, T. S.; Gritsenko, V. I.; Strizhak, P. E. Low Temperature Hydrogen Purification from CO for Fuel Cell Application over Copper−Ceria Catalysts Supported on Different Oxides. *Int. J. Hydrogen Energy* **2011**, *36*, 1271−1275.
(504) Águila, G.; Gracia, F.; Araya, P. CuO and CeO_2 Catalysts Supported on Al_2O_3, ZrO_2, and SiO_2 in the Oxidation of CO at Low Temperature. *Appl. Catal., A* **2008**, *343*, 16−24.

(505) Ramaswamy, V.; Malwadkar, S.; Chilukuri, S. Cu−Ce Mixed Oxides Supported on Al-Pillared Clay: Effect of Method of Preparation on Catalytic Activity in the Preferential Oxidation of Carbon Monoxide. *Appl. Catal., B* **2008**, *84*, 21−29.
(506) Tang, C.; Sun, J.; Yao, X.; Cao, Y.; Liu, L.; Ge, C.; Gao, F.; Dong, L. Efficient Fabrication of Active CuO-CeO_2/SBA-15 Catalysts for Preferential Oxidation of CO by Solid State Impregnation. *Appl. Catal., B* **2014**, *146*, 201−212.
(507) Moretti, E.; Storaro, L.; Talon, A.; Moreno-Tost, R.; Rodríguez-Castellón, E.; Jiménez-López, A.; Lenarda, M. CO Preferential Oxidation Activity of CuO/CeO_2 Supported on Zirconium Doped Mesoporous MSU Type Silica. *Catal. Lett.* **2009**, *129*, 323−330.
(508) Reyes-Carmona, Á.; Arango-Díaz, A.; Moretti, E.; Talon, A.; Storaro, L.; Lenarda, M.; Jiménez-López, A.; Rodríguez-Castellón, E. CuO/CeO_2 Supported on Zr Doped SBA-15 as Catalysts for Preferential CO Oxidation (CO-PROX). *J. Power Sources* **2011**, *196*, 4382−4387.
(509) Chen, Y.; Liu, D.; Yang, L.; Meng, M.; Zhang, J.; Zheng, L.; Chu, S.; Hu, T. Ternary Composite Oxide Catalysts CuO/Co_3O_4−CeO_2 with Wide Temperature-Window for the Preferential Oxidation of CO in H_2-Rich Stream. *Chem. Eng. J.* **2013**, *234*, 88−98.
(510) Gao, Y.; Xie, K.; Wang, W.; Mi, S.; Liu, N.; Pan, G.; Huang, W. Structural Features and Catalytic Performance in CO Preferential Oxidation of CuO−CeO_2 Supported on Multi-Walled Carbon Nanotubes. *Catal. Sci. Technol.* **2015**, *5*, 1568−1579.
(511) Ratnasamy, P.; Srinivas, D.; Satyanarayana, C. V. V; Manikandan, P.; Senthil Kumaran, R. S.; Sachin, M.; Shetti, V. N. Influence of the Support on the Preferential Oxidation of CO in Hydrogen-Rich Steam Reformates over the CuO−CeO_2−ZrO_2 System. *J. Catal.* **2004**, *221*, 455−465.
(512) Moretti, E.; Storaro, L.; Talon, A.; Lenarda, M.; Riello, P.; Frattini, R.; de Yuso, M.; del, V. M.; Jiménez-López, A.; Rodríguez-Castellón, E. Effect of Thermal Treatments on the Catalytic Behaviour in the CO Preferential Oxidation of a CuO−CeO_2−ZrO_2 Catalyst with a Flower-like Morphology. *Appl. Catal., B* **2011**, *102*, 627−637.
(513) Moretti, E.; Lenarda, M.; Riello, P.; Storaro, L.; Talon, A.; Frattini, R.; Reyes-Carmona, A.; Jiménez-López, A.; Rodríguez-Castellón, E. Influence of Synthesis Parameters on the Performance of CeO_2−CuO and CeO_2−ZrO_2−CuO Systems in the Catalytic Oxidation of CO in Excess of Hydrogen. *Appl. Catal., B* **2013**, *129*, 556−565.
(514) Tang, X.; Xu, Y.; Shen, W. Promoting Effect of Copper on the Catalytic Activity of MnO_x−CeO_2 Mixed Oxide for Complete Oxidation of Benzene. *Chem. Eng. J.* **2008**, *144*, 175−180.
(515) Gong, L.; Huang, Z.; Luo, L.; Zhang, N. Promoting Effect of MnO_x on the Performance of CuO/CeO_2 Catalysts for Preferential Oxidation of CO in H_2-Rich Gases. *React. Kinet., Mech. Catal.* **2014**, *111*, 489−504.
(516) Peng, C.-T.; Lia, H.-K.; Liaw, B.-J.; Chen, Y.-Z. Removal of CO in Excess Hydrogen over $CuO/Ce_{1-x}Mn_xO_2$ Catalysts. *Chem. Eng. J.* **2011**, *172*, 452−458.
(517) Wu, Z.; Zhu, H.; Qin, Z.; Wang, H.; Huang, L.; Wang, J. Preferential Oxidation of CO in H_2-Rich Stream over $CuO/Ce_{1-x}Ti_xO_2$ Catalysts. *Appl. Catal., B* **2010**, *98*, 204−212.
(518) Cecilia, J. A.; Arango-Díaz, A.; Rico-Pérez, V.; Bueno-López, A.; Rodríguez-Castellón, E. The Influence of Promoters (Zr, La, Tb, Pr) on the Catalytic Performance of CuO-CeO_2 Systems for the Preferential Oxidation of CO in the Presence of CO_2 and H_2O. *Catal. Today* **2015**, *253*, 115−125.
(519) Monyanon, S.; Pongstabodee, S.; Luengnaruemitchai, A. Catalytic Activity of Pt−Au/CeO_2 Catalyst for the Preferential Oxidation of CO in H_2-Rich Stream. *J. Power Sources* **2006**, *163*, 547−554.
(520) Liu, Y.; Liu, B.; Liu, Y.; Wang, Q.; Hu, W.; Jing, P.; Liu, L.; Yu, S.; Zhang, J. Improvement of Catalytic Performance of Preferential Oxidation of CO in H_2-Rich Gases on Three-Dimensionally Ordered Macro- and Meso-Porous Pt−Au/CeO_2 Catalysts. *Appl. Catal., B* **2013**, *142*−*143*, 615−625.
(521) Kugai, J.; Moriya, T.; Seino, S.; Nakagawa, T.; Ohkubo, Y.; Nitani, H.; Daimon, H.; Yamamoto, T. A. CeO_2-Supported Pt−Cu Alloy Nanoparticles Synthesized by Radiolytic Process for Highly Selective CO Oxidation. *Int. J. Hydrogen Energy* **2012**, *37*, 4787−4797.
(522) Kugai, J.; Moriya, T.; Seino, S.; Nakagawa, T.; Ohkubo, Y.; Nitani, H.; Mizukoshi, Y.; Yamamoto, T. A. Effect of Support for PtCu Bimetallic Catalysts Synthesized by Electron Beam Irradiation Method on Preferential CO Oxidation. *Appl. Catal., B* **2012**, *126*, 306−314.
(523) Kugai, J.; Moriya, T.; Seino, S.; Nakagawa, T.; Ohkubo, Y.; Nitani, H.; Yamamoto, T. A. Comparison of Structure and Catalytic Performance of Pt−Co and Pt−Cu Bimetallic Catalysts Supported on Al_2O_3 and CeO_2 Synthesized by Electron Beam Irradiation Method for Preferential CO Oxidation. *Int. J. Hydrogen Energy* **2013**, *38*, 4456−4465.
(524) Kugai, J.; Moriya, T.; Seino, S.; Nakagawa, T.; Ohkubo, Y.; Nitani, H.; Akita, T.; Mizukoshi, Y.; Yamamoto, T. A. Effect of CeO_2 Support Properties on Structure of Pt−Cu Nanoparticles Synthesized by Electron Beam Irradiation Method for Preferential CO Oxidation. *Chem. Eng. J.* **2013**, *223*, 347−355.
(525) Kugai, J.; Moriya, T.; Seino, S.; Nakagawa, T.; Ohkubo, Y.; Nitani, H.; Yamamoto, T. A. Active Metal−Oxide Interfaces in Supported Pt−Cu/CeO_2 and Mechanically Mixed Pt−Cu+CeO_2 Catalysts Synthesized by an Electron Beam Irradiation Method for Selective CO Oxidation. *Catal. Lett.* **2013**, *143*, 1182−1187.
(526) Gamboa-Rosales, N. K.; Ayastuy, J. L.; González-Marcos, M. P.; Gutiérrez-Ortiz, M. A. Effect of Au Promoter in CuO/CeO_2 Catalysts for the Oxygen-Assisted WGS Reaction. *Catal. Today* **2011**, *176*, 63−71.
(527) Liao, X.; Chu, W.; Dai, X.; Pitchon, V. Bimetallic Au−Cu Supported on Ceria for PROX Reaction: Effects of Cu/Au Atomic Ratios and Thermal Pretreatments. *Appl. Catal., B* **2013**, *142*−*143*, 25−37.
(528) Saqer, S. M.; Kondarides, D. I.; Verykios, X. E. Catalytic Activity of Supported Platinum and Metal Oxide Catalysts for Toluene Oxidation. *Top. Catal.* **2009**, *52*, 517−527.
(529) Kim, K.-H.; Ihm, S.-K. Heterogeneous Catalytic Wet Air Oxidation of Refractory Organic Pollutants in Industrial Wastewaters: A Review. *J. Hazard. Mater.* **2011**, *186*, 16−34.
(530) Aneggi, E.; Boaro, M.; Leitenburg, C. de; Dolcetti, G.; Trovarelli, A. Insights into the Redox Properties of Ceria-Based Oxides and Their Implications in Catalysis. *J. Alloys Compd.* **2006**, *408*−*412*, 1096−1102.
(531) Scirè, S.; Minicò, S.; Crisafulli, C.; Satriano, C.; Pistone, A. Catalytic Combustion of Volatile Organic Compounds on Gold/Cerium Oxide Catalysts. *Appl. Catal., B* **2003**, *40*, 43−49.
(532) Tang, X.; Li, Y.; Huang, X.; Xu, Y.; Zhu, H.; Wang, J.; Shen, W. MnO_x−CeO_2 Mixed Oxide Catalysts for Complete Oxidation of Formaldehyde: Effect of Preparation Method and Calcination Temperature. *Appl. Catal., B* **2006**, *62*, 265−273.
(533) Ousmane, M.; Liotta, L. F.; Carlo, G. D.; Pantaleo, G.; Venezia, A. M.; Deganello, G.; Retailleau, L.; Boreave, A.; Giroir-Fendler, A. Supported Au Catalysts for Low-Temperature Abatement of Propene and Toluene, as Model VOCs: Support Effect. *Appl. Catal., B* **2011**, *101*, 629−637.
(534) Sedjame, H.-J.; Fontaine, C.; Lafaye, G.; Barbier, J., Jr On the Promoting Effect of the Addition of Ceria to Platinum Based Alumina Catalysts for VOCs Oxidation. *Appl. Catal., B* **2014**, *144*, 233−242.
(535) Bozo, C.; Guilhaume, N.; Garbowski, E.; Primet, M. Combustion of Methane on CeO_2−ZrO_2 Based Catalysts. *Catal. Today* **2000**, *59*, 33−45.
(536) Bozo, C.; Guilhaume, N.; Herrmann, J.-M. Role of the Ceria−Zirconia Support in the Reactivity of Platinum and Palladium Catalysts for Methane Total Oxidation under Lean Conditions. *J. Catal.* **2001**, *203*, 393−406.
(537) Colussi, S.; Trovarelli, A.; Vesselli, E.; Baraldi, A.; Comelli, G.; Groppi, G.; Llorca, J. Structure and Morphology of Pd/Al_2O_3 and $Pd/CeO_2/Al_2O_3$ Combustion Catalysts in Pd−PdO Transformation Hysteresis. *Appl. Catal., A* **2010**, *390*, 1−10.

(538) Colussi, S.; Trovarelli, A.; Cristiani, C.; Lietti, L.; Groppi, G. The Influence of Ceria and Other Rare Earth Promoters on Palladium-Based Methane Combustion Catalysts. *Catal. Today* **2012**, *180*, 124−130.
(539) Scirè, S.; Liotta, L. F. Supported Gold Catalysts for the Total Oxidation of Volatile Organic Compounds. *Appl. Catal., B* **2012**, *125*, 222−246.
(540) Shindell, D. T.; Faluvegi, G.; Koch, D. M.; Schmidt, G. A.; Unger, N.; Bauer, S. E. Improved Attribution of Climate Forcing to Emissions. *Science* **2009**, *326*, 716−718.
(541) Myhre, G.; Shindell, D.; Bréon, F.-M.; Collins, W.; Fuglestvedt, J.; Huang, J.; Koch, D.; Lamarque, J.-F.; Lee, D.; Mendoza, B.; Nakajima, T.; Robock, A.; Stephens, G.; Takemura, T.; Zhang, H. Anthropogenic and Natural Radiative Forcing Supplementary Material. In *Climate Change 2013: The Physical Science Basis. Contribution of Working Group I to the Fifth Assessment Report of the Intergovernmental Panel on Climate Change*; Stocker, T. F., Qin, D., Plattner, G.-K., Tignor, M., Allen, S. K., Boschung, J., Nauels, A., Xia, Y., Bex, V., Midgley, P. M., Eds.; 2013; pp 659−740.
(542) Pengpanich, S.; Meeyoo, V.; Rirksomboon, T.; Bunyakiat, K. Catalytic Oxidation of Methane over CeO_2-ZrO_2 Mixed Oxide Solid Solution Catalysts Prepared via Urea Hydrolysis. *Appl. Catal., A* **2002**, *234*, 221−233.
(543) Yang, W.; Li, D.; Xu, D.; Wang, X. Effect of CeO_2 Preparation Method and Cu Loading on CuO/CeO_2 Catalysts for Methane Combustion. *J. Nat. Gas Chem.* **2009**, *18*, 458−466.
(544) Qiao, D.; Lu, G.; Mao, D.; Liu, X.; Li, H.; Guo, Y.; Guo, Y. Effect of Ca Doping on the Catalytic Performance of $CuO-CeO_2$ Catalysts for Methane Combustion. *Catal. Commun.* **2010**, *11*, 858−861.
(545) Liotta, L. F.; Di Carlo, G.; Pantaleo, G.; Venezia, A. M.; Deganello, G. Co_3O_4/CeO_2 Composite Oxides for Methane Emissions Abatement: Relationship between $Co_3O_4-CeO_2$ Interaction and Catalytic Activity. *Appl. Catal., B* **2006**, *66*, 217−227.
(546) Zhang, B.; Li, D.; Wang, X. Catalytic Performance of La−Ce−O Mixed Oxide for Combustion of Methane. *Catal. Today* **2010**, *158*, 348−353.
(547) Li, H.; Lu, G.; Wang, Y.; Guo, Y.; Guo, Y. Synthesis of Flower-like La or Pr-Doped Mesoporous Ceria Microspheres and Their Catalytic Activities for Methane Combustion. *Catal. Commun.* **2010**, *11*, 946−950.
(548) Urdă, A.; Popescu, I.; Cacciaguerra, T.; Tanchoux, N.; Tichit, D.; Marcu, I.-C. Total Oxidation of Methane over Rare Earth Cation-Containing Mixed Oxides Derived from LDH Precursors. *Appl. Catal., A* **2013**, *464*−*465*, 20−27.
(549) Gélin, P.; Primet, M. Complete Oxidation of Methane at Low Temperature over Noble Metal Based Catalysts: A Review. *Appl. Catal., B* **2002**, *39*, 1−37.
(550) Colussi, S.; Arosio, F.; Montanari, T.; Busca, G.; Groppi, G.; Trovarelli, A. Study of Sulfur Poisoning on Pd/Al_2O_3 and $Pd/CeO_2/Al_2O_3$ Methane Combustion Catalysts. *Catal. Today* **2010**, *155*, 59−65.
(551) Colussi, S.; Gayen, A.; Farnesi Camellone, M.; Boaro, M.; Llorca, J.; Fabris, S.; Trovarelli, A. Nanofaceted Pd-O Sites in Pd-Ce Surface Superstructures: Enhanced Activity in Catalytic Combustion of Methane. *Angew. Chem., Int. Ed.* **2009**, *48*, 8481−8484.
(552) Persson, K.; Pfefferle, L. D.; Schwartz, W.; Ersson, A.; Järås, S. G. Stability of Palladium-Based Catalysts during Catalytic Combustion of Methane: The Influence of Water. *Appl. Catal., B* **2007**, *74*, 242−250.
(553) Gao, D.; Wang, S.; Zhang, C.; Yuan, Z.; Wang, S. Methane Combustion over Pd/Al_2O_3 Catalyst: Effects of Chlorine Ions and Water on Catalytic Activity. *Chinese J. Catal.* **2008**, *29*, 1221−1225.
(554) Hurtado, P.; Ordonez, S.; Sastre, H.; Diez, F. V. Combustion of Methane over Palladium Catalyst in the Presence of Inorganic Compounds: Inhibition and Deactivation Phenomena. *Appl. Catal., B* **2004**, *47*, 85−93.
(555) Corro, G.; Cano, C.; Fierro, J. L. G. A Study of $Pt-Pd/\gamma-Al_2O_3$ Catalysts for Methane Oxidation Resistant to Deactivation by Sulfur Poisoning. *J. Mol. Catal. A: Chem.* **2010**, *315*, 35−42.
(556) Narui, K.; Yata, H.; Furuta, K.; Nishida, A.; Kohtoku, Y.; Matsuzaki, T. Effects of Addition of Pt to PdO/Al_2O_3 Catalyst on Catalytic Activity for Methane Combustion and TEM Observations of Supported Particles. *Appl. Catal., A* **1999**, *179*, 165−173.
(557) Gélin, P.; Urfels, L.; Primet, M.; Tena, E. Complete Oxidation of Methane at Low Temperature over Pt and Pd Catalysts for the Abatement of Lean-Burn Natural Gas Fuelled Vehicles Emissions: Influence of Water and Sulphur Containing Compounds. *Catal. Today* **2003**, *83*, 45−57.
(558) Del Angel, G.; Padilla, J. M.; Cuauhtémoc, I.; Navarrete, J. Toluene Combustion on $\gamma-Al_2O_3-CeO_2$ Catalysts Prepared from Boehmite and Cerium Nitrate. *J. Mol. Catal. A: Chem.* **2008**, *281*, 173−178.
(559) Gaálová, J.; Topka, P.; Kaluža, L.; Šolcová, O. Gold versus Platinum on Ceria−Zirconia Mixed Oxides in Oxidation of Ethanol and Toluene. *Catal. Today* **2011**, *175*, 231−237.
(560) Alifanti, M.; Florea, M.; Pârvulescu, V. I. Ceria-Based Oxides as Supports for $LaCoO_3$ Perovskite; Catalysts for Total Oxidation of VOC. *Appl. Catal., B* **2007**, *70*, 400−405.
(561) Heynderickx, P. M.; Thybaut, J. W.; Poelman, H.; Poelman, D.; Marin, G. B. The Total Oxidation of Propane over Supported Cu and Ce Oxides: A Comparison of Single and Binary Metal Oxides. *J. Catal.* **2010**, *272*, 109−120.
(562) Hu, C.; Zhu, Q.; Jiang, Z.; Chen, L.; Wu, R. Catalytic Combustion of Dilute Acetone over Cu-Doped Ceria Catalysts. *Chem. Eng. J.* **2009**, *152*, 583−590.
(563) Tang, X.; Chen, J.; Li, Y.; Li, Y.; Xu, Y.; Shen, W. Complete Oxidation of Formaldehyde over Ag/MnO_x-CeO_2 Catalysts. *Chem. Eng. J.* **2006**, *118*, 119−125.
(564) Tang, X.; Chen, J.; Huang, X.; Xu, Y.; Shen, W. Pt/MnO_x-CeO_2 Catalysts for the Complete Oxidation of Formaldehyde at Ambient Temperature. *Appl. Catal., B* **2008**, *81*, 115−121.
(565) Li, H.; Lu, G.; Dai, Q.; Wang, Y.; Guo, Y.; Guo, Y. Hierarchical Organization and Catalytic Activity of High-Surface-Area Mesoporous Ceria Microspheres Prepared via Hydrothermal Routes. *ACS Appl. Mater. Interfaces* **2010**, *2*, 838−846.
(566) Sayle, T. X. T.; Cantoni, M.; Bhatta, U. M.; Parker, S. C.; Hall, S. R.; Möbus, G.; Molinari, M.; Reid, D.; Seal, S.; Sayle, D. C. Strain and Architecture-Tuned Reactivity in Ceria Nanostructures; Enhanced Catalytic Oxidation of CO to CO_2. *Chem. Mater.* **2012**, *24*, 1811−1821.
(567) de Rivas, B.; Gutiérrez-Ortiz, J. I.; López-Fonseca, R.; González-Velasco, J. R. Analysis of the Simultaneous Catalytic Combustion of Chlorinated Aliphatic Pollutants and Toluene over Ceria-Zirconia Mixed Oxides. *Appl. Catal., A* **2006**, *314*, 54−63.
(568) Díaz, E.; de Rivas, B.; López-Fonseca, R.; Ordóñez, S.; Gutiérrez-Ortiz, J. I. Characterization of Ceria-Zirconia Mixed Oxides as Catalysts for the Combustion of Volatile Organic Compounds Using Inverse Gas Chromatography. *J. Chromatogr. A* **2006**, *1116*, 230−239.
(569) Gutiérrez-Ortiz, J. I.; de Rivas, B.; López-Fonseca, R.; González-Velasco, J. R. Effect of the Presence of n-Hexane on the Catalytic Combustion of Chlororganics over Ceria−Zirconia Mixed Oxides. *Catal. Today* **2005**, *107*−*108*, 933−941.
(570) Delimaris, D.; Ioannides, T. VOC Oxidation over MnO_x-CeO_2 Catalysts Prepared by a Combustion Method. *Appl. Catal., B* **2008**, *84*, 303−312.
(571) Dai, Q.; Wang, X.; Lu, G. Low-Temperature Catalytic Combustion of Trichloroethylene over Cerium Oxide and Catalyst Deactivation. *Appl. Catal., B* **2008**, *81*, 192−202.
(572) Finocchio, E.; Ramis, G.; Busca, G. A Study on Catalytic Combustion of Chlorobenzenes. *Catal. Today* **2011**, *169*, 3−9.
(573) Gutiérrez-Ortiz, J. I.; de Rivas, B.; López-Fonseca, R.; González-Velasco, J. R. Catalytic Purification of Waste Gases Containing VOC Mixtures with Ce/Zr Solid Solutions. *Appl. Catal., B* **2006**, *65*, 191−200.

(574) Gutiérrez-Ortiz, J. I.; de Rivas, B.; López-Fonseca, R.; González-Velasco, J. R. Combustion of Aliphatic C_2 Chlorohydrocarbons over Ceria−Zirconia Mixed Oxides Catalysts. *Appl. Catal., A* **2004**, *269*, 147−155.
(575) Yu, D.; Xingyi, W.; Dao, L.; Qiguang, D. Catalytic Combustion of Chlorobenzene over Mn-Ce-La-O Mixed Oxide Catalysts. *J. Hazard. Mater.* **2011**, *188*, 132−139.
(576) Dai, Q.; Bai, S.; Wang, X.; Lu, G. Catalytic Combustion of Chlorobenzene over Ru-Doped Ceria Catalysts: Mechanism Study. *Appl. Catal., B* **2013**, *129*, 580−588.
(577) de Rivas, B.; Guillén-Hurtado, N.; López-Fonseca, R.; Coloma-Pascual, F.; García-García, A.; Gutiérrez-Ortiz, J. I.; Bueno-López, A. Activity, Selectivity and Stability of Praseodymium-Doped CeO_2 for Chlorinated VOCs Catalytic Combustion. *Appl. Catal., B* **2012**, *121−122*, 162−170.
(578) Wang, X.; Kang, Q.; Li, D. Low-Temperature Catalytic Combustion of Chlorobenzene over MnO_x−CeO_2 Mixed Oxide Catalysts. *Catal. Commun.* **2008**, *9*, 2158−2162.
(579) de Rivas, B.; Sampedro, C.; López-Fonseca, R.; Gutiérrez-Ortiz, M. Á.; Gutiérrez-Ortiz, J. I. Low-Temperature Combustion of Chlorinated Hydrocarbons over CeO_2/H-ZSM5 Catalysts. *Appl. Catal., A* **2012**, *417−418*, 93−101.
(580) Huang, Q.; Meng, Z.; Zhou, R. The Effect of Synergy between Cr_2O_3-CeO_2 and USY Zeolite on the Catalytic Performance and Durability of Chromium and Cerium Modified USY Catalysts for Decomposition of Chlorinated Volatile Organic Compounds. *Appl. Catal., B* **2012**, *115−116*, 179−189.
(581) Gannoun, C.; Delaigle, R.; Debecker, D. P.; Eloy, P.; Ghorbel, A.; Gaigneaux, E. M. Effect of Support on V_2O_5 Catalytic Activity in Chlorobenzene Oxidation. *Appl. Catal., A* **2012**, *447−448*, 1−6.
(582) Pitkäaho, S.; Matejova, L.; Ojala, S.; Gaalova, J.; Keiski, R. L. Oxidation of Perchloroethylene—Activity and Selectivity of Pt, Pd, Rh, and V_2O_5 Catalysts Supported on Al_2O_3, Al_2O_3-TiO_2 and Al_2O_3-CeO_2. *Appl. Catal., B* **2012**, *113−114*, 150−159.
(583) Huang, Q.; Xue, X.; Zhou, R. Catalytic Behavior and Durability of CeO_2 or/and CuO Modified USY Zeolite Catalysts for Decomposition of Chlorinated Volatile Organic Compounds. *J. Mol. Catal. A: Chem.* **2011**, *344*, 74−82.
(584) Matějová, L.; Topka, P.; Kaluža, L.; Pitkäaho, S.; Ojala, S.; Gaálová, J.; Keiski, R. L. Total Oxidation of Dichloromethane and Ethanol over Ceria−Zirconia Mixed Oxide Supported Platinum and Gold Catalysts. *Appl. Catal., B* **2013**, *142−143*, 54−64.
(585) Amrute, A. P.; Mondelli, C.; Moser, M.; Novell-Leruth, G.; López, N.; Rosenthal, D.; Farra, R.; Schuster, M. E.; Teschner, D.; Schmidt, T.; Pérez-Ramírez, J. Performance, Structure, and Mechanism of CeO_2 in HCl Oxidation to Cl_2. *J. Catal.* **2012**, *286*, 287−297.
(586) Farra, R.; Eichelbaum, M.; Schlögl, R.; Szentmiklósi, L.; Schmidt, T.; Amrute, A. P.; Mondelli, C.; Pérez-Ramírez, J.; Teschner, D. Do Observations on Surface Coverage-Reactivity Correlations Always Describe the True Catalytic Process? A Case Study on Ceria. *J. Catal.* **2013**, *297*, 119−127.
(587) Moser, M.; Mondelli, C.; Schmidt, T.; Girgsdies, F.; Schuster, M. E.; Farra, R.; Szentmiklósi, L.; Teschner, D.; Pérez-Ramírez, J. Supported CeO_2 Catalysts in Technical Form for Sustainable Chlorine Production. *Appl. Catal., B* **2013**, *132−133*, 123−131.
(588) Segura, Y.; Lopez, N.; Perez-Ramirez, J. Origin of the Superior Hydrogenation Selectivity of Gold Nanoparticles in Alkyne + Alkene Mixtures: Triple- versus Double-Bond Activation. *J. Catal.* **2007**, *247*, 383−386.
(589) Azizi, Y.; Petit, C.; Pitchon, V. Formation of Polymer-Grade Ethylene by Selective Hydrogenation of Acetylene over Au/CeO_2 Catalyst. *J. Catal.* **2008**, *256*, 338−344.
(590) Zhu, H.-Z.; Lu, Y.-M.; Fan, F.-J.; Yu, S.-H. Selective Hydrogenation of Nitroaromatics by Ceria Nanorods. *Nanoscale* **2013**, *5*, 7219−7223.
(591) Carrasco, J.; Vilé, G.; Fernández-Torre, D.; Pérez, R.; Pérez-Ramírez, J.; Ganduglia-Pirovano, M. V. Molecular-Level Understanding of CeO_2 as a Catalyst for Partial Alkyne Hydrogenation. *J. Phys. Chem. C* **2014**, *118*, 5352−5360.
(592) Vilé, G.; Wrabetz, S.; Floryan, L.; Schuster, M. E.; Girgsdies, F.; Teschner, D.; Pérez-Ramírez, J. Stereo- and Chemoselective Character of Supported CeO_2 Catalysts for Continuous-Flow Three-Phase Alkyne Hydrogenation. *ChemCatChem* **2014**, *6*, 1928−1934.
(593) Ji, P.; Zhang, J.; Chen, F.; Anpo, M. Study of Adsorption and Degradation of Acid Orange 7 on the Surface of CeO_2 under Visible Light Irradiation. *Appl. Catal., B* **2009**, *85*, 148−154.
(594) Feng, T.; Wang, X.; Feng, G. Synthesis of Novel CeO_2 Microspheres with Enhanced Solar Light Photocatalyic Properties. *Mater. Lett.* **2013**, *100*, 36−39.
(595) Chen, F.; Cao, Y.; Jia, D. Preparation and Photocatalytic Property of CeO_2 Lamellar. *Appl. Surf. Sci.* **2011**, *257*, 9226−9231.
(596) Sabari Arul, N.; Mangalaraj, D.; Kim, T. W.; Chen, P. C.; Ponpandian, N.; Meena, P.; Masuda, Y. Synthesis of CeO_2 Nanorods with Improved Photocatalytic Activity: Comparison between Precipitation and Hydrothermal Process. *J. Mater. Sci.: Mater. Electron.* **2013**, *24*, 1644−1650.
(597) Chan, S. H. S.; Yeong Wu, T.; Juan, J. C.; Teh, C. Y. Recent Developments of Metal Oxide Semiconductors as Photocatalysts in Advanced Oxidation Processes (AOPs) for Treatment of Dye Waste-Water. *J. Chem. Technol. Biotechnol.* **2011**, *86*, 1130−1158.
(598) Bamwenda, G. R.; Arakawa, H. Cerium Dioxide as a Photocatalyst for Water Decomposition to O_2 in the Presence of Ce_{aq}^{4+} and Fe_{aq}^{3+} Species. *J. Mol. Catal. A: Chem.* **2000**, *161*, 105−113.
(599) Bamwenda, G. R.; Uesigi, T.; Abe, Y.; Sayama, K.; Arakawa, H. The Photocatalytic Oxidation of Water to O_2 over Pure CeO_2, WO_3, and TiO_2 Using Fe^{3+} and Ce^{4+} as Electron Acceptors. *Appl. Catal., A* **2001**, *205*, 117−128.
(600) Primo, A.; Marino, T.; Corma, A.; Molinari, R.; García, H. Efficient Visible-Light Photocatalytic Water Splitting by Minute Amounts of Gold Supported on Nanoparticulate CeO_2 Obtained by a Biopolymer Templating Method. *J. Am. Chem. Soc.* **2011**, *133*, 6930−6933.
(601) Li, Y.; Sun, Q.; Kong, M.; Shi, W.; Huang, J.; Tang, J.; Zhao, X. Coupling Oxygen Ion Conduction to Photocatalysis in Mesoporous Nanorod-like Ceria Significantly Improves Photocatalytic Efficiency. *J. Phys. Chem. C* **2011**, *115*, 14050−14057.
(602) Khan, M. M.; Ansari, S. A.; Pradhan, D.; Han, D. H.; Lee, J.; Cho, M. H. Defect-Induced Band Gap Narrowed CeO_2 Nanostructures for Visible Light Activities. *Ind. Eng. Chem. Res.* **2014**, *53*, 9754−9763.
(603) Liyanage, A. D.; Perera, S. D.; Tan, K.; Chabal, Y.; Balkus, K. J. Synthesis, Characterization, and Photocatalytic Activity of Y-Doped CeO_2 Nanorods. *ACS Catal.* **2014**, *4*, 577−584.
(604) Yue, L.; Zhang, X.-M. Structural Characterization and Photocatalytic Behaviors of Doped CeO_2 Nanoparticles. *J. Alloys Compd.* **2009**, *475*, 702−705.
(605) Akselrod, G. M.; Deotare, P. B.; Thompson, N. J.; Lee, J.; Tisdale, W. A.; Baldo, M. A.; Menon, V. M.; Bulović, V. Visualization of Exciton Transport in Ordered and Disordered Molecular Solids. *Nat. Commun.* **2014**, *5*, 3646.
(606) Li, H.; Wang, G.; Zhang, F.; Cai, Y.; Wang, Y.; Djerdj, I. Surfactant-Assisted Synthesis of CeO_2 Nanoparticles and Their Application in Wastewater Treatment. *RSC Adv.* **2012**, *2*, 12413−12423.
(607) Borker, P.; Salker, A. V. Solar Assisted Photocatalytic Degradation of Naphthol Blue Black Dye Using $Ce_{1-x}Mn_xO_2$. *Mater. Chem. Phys.* **2007**, *103*, 366−370.
(608) Li, G.; Zhang, D.; Yu, J. C. Thermally Stable Ordered Mesoporous CeO_2/TiO_2 Visible-Light Photocatalysts. *Phys. Chem. Chem. Phys.* **2009**, *11*, 3775−3782.
(609) Li, M.; Zhang, S.; Lv, L.; Wang, M.; Zhang, W.; Pan, B. A Thermally Stable Mesoporous ZrO_2−CeO_2−TiO_2 Visible Light Photocatalyst. *Chem. Eng. J.* **2013**, *229*, 118−125.
(610) Aman, N.; Satapathy, P. K.; Mishra, T.; Mahato, M.; Das, N. N. Synthesis and Photocatalytic Activity of Mesoporous Cerium Doped TiO_2 as Visible Light Sensitive Photocatalyst. *Mater. Res. Bull.* **2012**, *47*, 179−183.

(611) Ji, Z.; Shen, X.; Li, M.; Zhou, H.; Zhu, G.; Chen, K. Synthesis of Reduced Graphene Oxide/CeO_2 Nanocomposites and Their Photocatalytic Properties. *Nanotechnology* **2013**, *24*, 115603.
(612) Li, L.; Yan, B. CeO_2−Bi_2O_3 Nanocomposite: Two Step Synthesis, Microstructure and Photocatalytic Activity. *J. Non-Cryst. Solids* **2009**, *355*, 776−779.
(613) Muñoz-Batista, M. J.; Gómez-Cerezo, M. N.; Kubacka, A.; Tudela, D.; Fernández-García, M. Role of Interface Contact in CeO_2−TiO_2 Photocatalytic Composite Materials. *ACS Catal.* **2014**, *4*, 63−72.
(614) Zeng, M.; Li, Y.; Mao, M.; Bai, J.; Ren, L.; Zhao, X. Synergetic Effect between Photocatalysis on TiO_2 and Thermocatalysis on CeO_2 for Gas-Phase Oxidation of Benzene on TiO_2/CeO_2 Nanocomposites. *ACS Catal.* **2015**, *5*, 3278−3286.
(615) Sabari Arul, N.; Mangalaraj, D.; Ramachandran, R.; Grace, A. N.; Han, J. I. Fabrication of CeO_2/Fe_2O_3 Composite Nanospindles for Enhanced Visible Light Driven Photocatalysts and Supercapacitor Electrodes. *J. Mater. Chem. A* **2015**, *3*, 15248−15258.
(616) Wu, J.; Wang, J.; Du, Y.; Li, H.; Yang, Y.; Jia, X. Chemically Controlled Growth of Porous CeO_2 Nanotubes for Cr(VI) Photoreduction. *Appl. Catal., B* **2015**, *174*−*175*, 435−444.
(617) Abanades, S.; Flamant, G. Thermochemical Hydrogen Production from a Two-Step Solar-Driven Water-Splitting Cycle Based on Cerium Oxides. *Sol. Energy* **2006**, *80*, 1611−1623.
(618) Abanades, S.; Legal, A.; Cordier, A.; Peraudeau, G.; Flamant, G.; Julbe, A. Investigation of Reactive Cerium-Based Oxides for H_2 Production by Thermochemical Two-Step Water-Splitting. *J. Mater. Sci.* **2010**, *45*, 4163−4173.
(619) Le Gal, A.; Abanades, S.; Bion, N.; Le Mercier, T.; Harlé, V. Reactivity of Doped Ceria-Based Mixed Oxides for Solar Thermochemical Hydrogen Generation via Two-Step Water-Splitting Cycles. *Energy Fuels* **2013**, *27*, 6068−6078.
(620) Le Gal, A.; Abanades, S. Dopant Incorporation in Ceria for Enhanced Water-Splitting Activity during Solar Thermochemical Hydrogen Generation. *J. Phys. Chem. C* **2012**, *116*, 13516−13523.
(621) Chueh, W. C.; Falter, C.; Abbott, M.; Scipio, D.; Furler, P.; Haile, S. M.; Steinfeld, A. High-Flux Solar-Driven Thermochemical Dissociation of CO_2 and H_2O Using Nonstoichiometric Ceria. *Science* **2010**, *330*, 1797−1801.
(622) Romero, M.; Steinfeld, A. Concentrating Solar Thermal Power and Thermochemical Fuels. *Energy Environ. Sci.* **2012**, *5*, 9234−9245.
(623) Panlener, R. J.; Blumenthal, R. N.; Garnier, J. E. A Thermodynamic Study of Nonstoichiometric Cerium Dioxide. *J. Phys. Chem. Solids* **1975**, *36*, 1213−1222.
(624) Takacs, M.; Scheffe, J. R.; Steinfeld, A. Oxygen Nonstoichiometry and Thermodynamic Characterization of Zr Doped Ceria in the 1573−1773 K Temperature Range. *Phys. Chem. Chem. Phys.* **2015**, *17*, 7813−7822.
(625) Hao, Y.; Yang, C.-K.; Haile, S. M. Ceria−Zirconia Solid Solutions ($Ce_{1-x}Zr_xO_{2-\delta}$, $x \leq 0.2$) for Solar Thermochemical Water Splitting: A Thermodynamic Study. *Chem. Mater.* **2014**, *26*, 6073−6082.
(626) Krenzke, P. T.; Davidson, J. H. On the Efficiency of Solar H_2 and CO Production via the Thermochemical Cerium Oxide Redox Cycle: The Option of Inert-Swept Reduction. *Energy Fuels* **2015**, *29*, 1045−1054.
(627) Furler, P.; Scheffe, J.; Marxer, D.; Gorbar, M.; Bonk, A.; Vogt, U.; Steinfeld, A. Thermochemical CO_2 Splitting via Redox Cycling of Ceria Reticulated Foam Structures with Dual-Scale Porosities. *Phys. Chem. Chem. Phys.* **2014**, *16*, 10503−10511.
(628) Monteiro, R. de S.; Noronha, F. B.; Dieguez, L. C.; Schmal, M. Characterization of Pd-CeO_2 Interaction on Alumina Support and Hydrogenation of 1,3-Butadiene. *Appl. Catal., A* **1995**, *131*, 89−106.
(629) Sepúlveda-Escribano, A.; Coloma, F.; Rodríguez-Reinoso, F. Promoting Effect of Ceria on the Gas Phase Hydrogenation of Crotonaldehyde over Platinum Catalysts. *J. Catal.* **1998**, *178*, 649−657.
(630) Silvestre-Albero, J.; Coloma, F.; Sepúlveda-Escribano, A.; Rodríguez-Reinoso, F. Effect of the Presence of Chlorine in Bimetallic PtZn/CeO_2 Catalysts for the Vapor-Phase Hydrogenation of Crotonaldehyde. *Appl. Catal., A* **2006**, *304*, 159−167.
(631) Chettibi, S.; Wojcieszak, R.; Boudjennad, E. H.; Belloni, J.; Bettahar, M. M.; Keghouche, N. Ni−Ce Intermetallic Phases in CeO_2-Supported Nickel Catalysts Synthesized by γ-Radiolysis. *Catal. Today* **2006**, *113*, 157−165.
(632) Abad, A.; Concepción, P.; Corma, A.; García, H. A Collaborative Effect between Gold and a Support Induces the Selective Oxidation of Alcohols. *Angew. Chem., Int. Ed.* **2005**, *44*, 4066−4069.
(633) Abad, A.; Corma, A.; García, H. Catalyst Parameters Determining Activity and Selectivity of Supported Gold Nanoparticles for the Aerobic Oxidation of Alcohols: The Molecular Reaction Mechanism. *Chem. - Eur. J.* **2008**, *14*, 212−222.
(634) Tamura, M.; Tomishige, K. Redox Properties of CeO_2 at Low Temperature: The Direct Synthesis of Imines from Alcohol and Amine. *Angew. Chem., Int. Ed.* **2015**, *54*, 864−867.
(635) Gawande, M. B.; Bonifácio, V. D. B.; Varma, R. S.; Nogueira, I. D.; Bundaleski, N.; Ghumman, C. A. A.; Teodoro, O. M. N. D.; Branco, P. S. Magnetically Recyclable Magnetite−Ceria (Nanocat-Fe-Ce) Nanocatalyst − Applications in Multicomponent Reactions under Benign Conditions. *Green Chem.* **2013**, *15*, 1226.
(636) Kunkes, E. L.; Gürbüz, E. I.; Dumesic, J. A. Vapour-Phase C−C Coupling Reactions of Biomass-Derived Oxygenates over Pd/$CeZrO_x$ Catalysts. *J. Catal.* **2009**, *266*, 236−249.
(637) Gürbüz, E. I.; Kunkes, E. L.; Dumesic, J. A. Integration of C−C Coupling Reactions of Biomass-Derived Oxygenates to Fuel-Grade Compounds. *Appl. Catal., B* **2010**, *94*, 134−141.
(638) Postole, G.; Chowdhury, B.; Karmakar, B.; Pinki, K.; Banerji, J.; Auroux, A. Knoevenagel Condensation Reaction over Acid−Base Bifunctional Nanocrystalline $Ce_xZr_{1-x}O_2$ Solid Solutions. *J. Catal.* **2010**, *269*, 110−121.
(639) Reddy, B. M.; Sreekanth, P. M.; Lakshmanan, P.; Khan, A. Synthesis, Characterization and Activity Study of SO_4^{2-}/$Ce_xZr_{1-x}O_2$ Solid Superacid Catalyst. *J. Mol. Catal. A: Chem.* **2006**, *244*, 1−7.
(640) Amoroso, F.; Colussi, S.; Del Zotto, A.; Llorca, J.; Trovarelli, A. An Efficient and Reusable Catalyst Based on Pd/CeO_2 for the Room Temperature Aerobic Suzuki−Miyaura Reaction in Water/Ethanol. *J. Mol. Catal. A: Chem.* **2010**, *315*, 197−204.
(641) González-Arellano, C.; Abad, A.; Corma, A.; García, H.; Iglesias, M.; Sánchez, F. Catalysis by Gold(I) and Gold(III): A Parallelism between Homo- and Heterogeneous Catalysts for Copper-Free Sonogashira Cross-Coupling Reactions. *Angew. Chem., Int. Ed.* **2007**, *46*, 1536−1538.
(642) Xu, C.; Qu, X. Cerium Oxide Nanoparticle: A Remarkably Versatile Rare Earth Nanomaterial for Biological Applications. *NPG Asia Mater.* **2014**, *6*, e90.
(643) Celardo, I.; Pedersen, J. Z.; Traversa, E.; Ghibelli, L. Pharmacological Potential of Cerium Oxide Nanoparticles. *Nanoscale* **2011**, *3*, 1411−1420.
(644) Celardo, I.; Traversa, E.; Ghibelli, L. Cerium Oxide Nanoparticles: A Promise for Applications in Therapy. *J. Exp. Ther. Oncol.* **2011**, *9*, 47−51.
(645) Niu, J.; Azfer, A.; Rogers, L. M.; Wang, X.; Kolattukudy, P. E. Cardioprotective Effects of Cerium Oxide Nanoparticles in a Transgenic Murine Model of Cardiomyopathy. *Cardiovasc. Res.* **2007**, *73*, 549−559.
(646) Schubert, D.; Dargusch, R.; Raitano, J.; Chan, S.-W. Cerium and Yttrium Oxide Nanoparticles Are Neuroprotective. *Biochem. Biophys. Res. Commun.* **2006**, *342*, 86−91.
(647) Tarnuzzer, R. W.; Colon, J.; Patil, S.; Seal, S. Vacancy Engineered Ceria Nanostructures for Protection from Radiation-Induced Cellular Damage. *Nano Lett.* **2005**, *5*, 2573−2577.
(648) Das, M.; Patil, S.; Bhargava, N.; Kang, J.-F.; Riedel, L. M.; Seal, S.; Hickman, J. J. Auto-Catalytic Ceria Nanoparticles Offer Neuroprotection to Adult Rat Spinal Cord Neurons. *Biomaterials* **2007**, *28*, 1918−1925.

(649) Heckert, E. G.; Karakoti, A. S.; Seal, S.; Self, W. T. The Role of Cerium Redox State in the SOD Mimetic Activity of Nanoceria. *Biomaterials* **2008**, *29*, 2705−2709.
(650) Chen, J.; Patil, S.; Seal, S.; McGinnis, J. F. Rare Earth Nanoparticles Prevent Retinal Degeneration Induced by Intracellular Peroxides. *Nat. Nanotechnol.* **2006**, *1*, 142−150.
(651) Hirst, S. M.; Karakoti, A. S.; Tyler, R. D.; Sriranganathan, N.; Seal, S.; Reilly, C. M. Anti-Inflammatory Properties of Cerium Oxide Nanoparticles. *Small* **2009**, *5*, 2848−2856.
(652) Ball, J. P.; Mound, B. A.; Monsalve, A. G.; Nino, J. C.; Allen, J. B. Biocompatibility Evaluation of Porous Ceria Foams for Orthopedic Tissue Engineering. *J. Biomed. Mater. Res., Part A* **2015**, *103*, 8−15.
(653) Asati, A.; Santra, S.; Kaittanis, C.; Nath, S.; Perez, J. M. Oxidase-like Activity of Polymer-Coated Cerium Oxide Nanoparticles. *Angew. Chem., Int. Ed.* **2009**, *48*, 2308−2312.
(654) Patil, S.; Reshetnikov, S.; Haldar, M. K.; Seal, S.; Mallik, S. Surface-Derivatized Nanoceria with Human Carbonic Anhydrase II Inhibitors and Fluorophores: A Potential Drug Delivery Device. *J. Phys. Chem. C* **2007**, *111*, 8437−8442.
(655) Babu, S.; Cho, J.-H.; Dowding, J. M.; Heckert, E.; Komanski, C.; Das, S.; Colon, J.; Baker, C. H.; Bass, M.; Self, W. T.; Seal, S. Multicolored Redox Active Upconverter Cerium Oxide Nanoparticle for Bio-Imaging and Therapeutics. *Chem. Commun.* **2010**, *46*, 6915−6917.
(656) Caputo, F.; De Nicola, M.; Sienkiewicz, A.; Giovanetti, A.; Bejarano, I.; Licoccia, S.; Traversa, E.; Ghibelli, L. Cerium Oxide Nanoparticles, Combining Antioxidant and UV Shielding Properties, Prevent UV-Induced Cell Damage and Mutagenesis. *Nanoscale* **2015**, *7*, 15643−15656.
(657) Hu, Z.; Liu, X.; Meng, D.; Guo, Y.; Guo, Y.; Lu, G. Effect of Ceria Crystal Plane on the Physicochemical and Catalytic Properties of Pd/Ceria for CO and Propane Oxidation. *ACS Catal.* **2016**, *6*, 2265−2279.
(658) López-Haro, M.; Cíes, J. M.; Trasobares, S.; Pérez-Omil, J. A.; Delgado, J. J.; Bernal, S.; Bayle-Guillemaud, P.; Stéphan, O.; Yoshida, K.; Boyes, E. D.; Gai, P. L.; Calvino, J. J. Imaging Nanostructural Modifications Induced by Electronic Metal-Support Interaction Effects at Au/Cerium-Based Oxide Nanointerfaces. *ACS Nano* **2012**, *6*, 6812−6820.
(659) Dvořák, F.; Farnesi Camellone, M.; Tovt, A.; Tran, N.-D.; Negreiros, F. R.; Vorokhta, M.; Skála, T.; Matolínová, I.; Mysliveček, J.; Matolín, V.; Fabris, S. Creating Single-Atom Pt-Ceria Catalysts by Surface Step Decoration. *Nat. Commun.* **2016**, *7*, 10801.
(660) Capdevila-Cortada, M.; Vilé, G.; Teschner, D.; Pérez-Ramírez, J.; López, N. Reactivity Descriptors for Ceria in Catalysis. *Appl. Catal. B: Environ.* **2016**, DOI: 10.1016/j.apcatb.2016.02.035.